MANCHESTER 1824

The University of Manchester

Self-Assembling Peptide Hydrogel for Intervertebral Disc Tissue Engineering

A thesis submitted to the University of Manchester
for the degree of Doctor of Philosophy
in the Faculty of Engineering and Physical Sciences

2015

SIMON WAN

School of Materials

CONTENTS

WORD COUNT – 71122 (entire document).

LIST OF FIGURES

LIST OF TABLES

LIST OF ABBREVIATIONS

µl	Microlitre
µm	Micrometre
β-sheet	Beta-sheet
2D	Two dimensional
3D	Three dimensional
ACAN	Aggrecan gene
ADR	Artificial disc replacement
AF	Annulus fibrosus
AFM	Atomic Force Microscopy
ANOVA	Analysis of variance
bNPC	Bovine nucleus pulposus cell
BSA	Bovine serum albumin
CA12	Carbonic anhydrase 12 gene
CO_2	Carbon dioxide
CEP	Cartilage end plate
cm	Centimetre
COL1A2	Type I collagen gene
COL2A1	Type II collagen gene
CS	Chondroitin sulphate
DAPI	4’,6-diamidino-2-phenylindole
DDD	Degenerative disc disease
DEAE	Diethylaminoethyl
DMEM	Dulbecco’s modified Eagles medium
DMMB	Dimethylmethylene blue
DNA	Deoxyribonucleic acid
EDTA	Ethylenediaminetetraacetic acid
ECM	Extracellular matrix
EthD-1	Ethidium homodimer-1
FBS	Fetal bovine serum

Fmoc	Fluorenylmethyloxycarbonyl
FOXF1	Forkhead Box F1 gene
FTIR	Fourier transform infrared spectroscopy
G’	Elastic modulus / storage modulus
G’’	Viscous modulus / loss modulus
GAG	Glycosaminoglycan
GAPDH	Glyceraldehyde 3-phosphate dehydrogenase gene
GDF	Growth differentiation factor
Glu or E	Glutamic acid
H_2O	Water
HA	Hyaluronic acid
h-BMMSC	Human bone marrow derived mesenchymal stem cell
Hz	Hertz
ICC	Immunocytochemistry
IR	Infrared
IVD	Intervertebral disc
kPa	Kilopascal
KRT8	Keratin 8 gene
KRT18	Keratin 18 gene
KRT19	Keratin 19 gene
KS	Keratan sulphate
LBP	Lower back pain
LDH	Lactate dehydrogenase
Lys or K	Lysine
mg	Milligram
ml	Millilitre
MPa	Megapascal
mM	Millimolar
MMP	Matrix metalloproteinase
MSC	Mesenchymal stem cell

NaCl	Sodium chloride
NaOH	Sodium hydroxide
nm	Nanometre
NP	Nucleus pulposus
O_2	Oxygen
P	Calculated probability
Pa	Pascal
PBS	Phosphate buffered saline
PCR	Polymerase chain reaction
PG	Proteoglycan
Phe or F	Phenylalanine
rpm	Revolutions per minute
RNA	Ribonucleic acid
RT	Room temperature
SAPH	Self-assembling peptide hydrogel
s-GAG	Sulphated glycosaminoglycan
SOX9	Transcription factor SOX-9 gene
TFA	Trifluoroacetic acid
TGF-β	Transforming growth factor beta

ABSTRACT

The intervertebral disc (IVD), situated between adjoining vertebrae, consists of the gelatinous nucleus pulposus (NP) in the centre surrounded by the tougher annulus fibrosus (AF). Its main roles are to distribute loads and to act as joints. With aging, degenerative disc disease (DDD) occurs due to an imbalance in anabolic and catabolic events in the IVD, which results in a loss of function. Lower back pain (LBP) affects 84% of people at some point in their lifetime and is strongly associated with DDD. Current LBP treatments have limited long term efficacy and are symptomatic rather than curative. Cell-based therapies are regarded to hold great potential for the treatment of DDD as it has been hypothesised that they could regenerate the damaged tissue and alleviate LBP. A number of natural and synthetic biomaterials have been investigated as NP tissue engineering scaffolds with varying results.

In this study, a self assembling peptide hydrogel (SAPH) was investigated for its potential as a cell carrier and/or scaffold for NP tissue engineering. SAPHs display the advantages of natural polymer hydrogels such as biocompatibility and biodegradability whilst combining the advantages of synthetic materials such as controlled structural and mechanical properties

Characterisation determined that the SAPH nanofibrous architecture had features that were of similar scale to extracellular matrix (ECM) components of the human NP. The mechanical properties of the SAPH could be optimised to closely match the native tissue. The system could shear thin and self-heal making the system ideally suited to delivery via minimally invasive procedure.

The three dimensional (3D) culture of bovine NP cells (bNPCs) in the SAPH demonstrated that the NP phenotype could be restored after de-differentiation during monolayer culture. Gene expression results demonstrated that ‘traditional’ and ‘novel’ NP markers were highly expressed throughout *in vitro* culture. Cell viability was high, cell population remained stable and bNPCs adopted the characteristic rounded morphology of native NPCs. Finally, type II collagen and aggrecan, the main ECM components of the NP, were deposited with increasing production over culture period.

Growth differentiation factor 6 (GDF-6) has been identified as the most promising current growth factor for inducing discogenic differentiation from human bone marrow mesenchymal stem cell (h-BMMSCs). After samples were stimulated with GDF-6, gene expression results confirmed that a NP-like phenotype could be induced with high expression of ‘traditional’ and ‘novel’ NP markers. Cell viability was high, cell population remained stable and NP associated ECM components were deposited with cells displaying a rounded morphology.

Interestingly, when h-BMMSCs were cultured without GDF-6, it was strongly suggested that spontaneous discogenic differentiation occurred after culture in the SAPHs as ‘traditional’ and ‘novel’ NP markers were highly expressed, morphology was comparable to native NPCs and type II collagen and aggrecan were deposited extracellularly. If these findings were accurate then this is the first study to demonstrate that a NP-like phenotype could be induced from MSCs without use of an exogenous growth factor or a discogenic bioactive motif. Despite exciting and novel results, further work is required to confirm the potential of SAPHs for NP tissue engineering scaffolds.

DECLARATION

No portion of the work referred to in this thesis has been submitted in support of an application for another degree or qualification of this or any other university or other institute of learning.

COPYRIGHT STATEMENT

i. The author of this thesis (including any appendices and/or schedules to this thesis) owns certain copyright or related rights in it (the “Copyright”) and s/he has given The University of Manchester certain rights to use such Copyright, including for administrative purposes.

ii. Copies of this thesis, either in full or in extracts and whether in hard or electronic copy, may be made only in accordance with the Copyright, Designs and Patents Act 1988 (as amended) and regulations issued under it or, where appropriate, in accordance with licensing agreements which the University has from time to time. This page must form part of any such copies made.

iii. The ownership of certain Copyright, patents, designs, trade marks and other intellectual property (the “Intellectual Property”) and any reproductions of copyright works in the thesis, for example graphs and tables (“Reproductions”), which may be described in this thesis, may not be owned by the author and may be owned by third parties. Such Intellectual Property and Reproductions cannot and must not be made available for use without the prior written permission of the owner(s) of the relevant Intellectual Property and/or Reproductions.

iv. Further information on the conditions under which disclosure, publication and commercialisation of this thesis, the Copyright and any Intellectual Property and/or Reproductions described in it may take place is available in the University IP Policy (see http://documents.manchester.ac.uk/DocuInfo.aspx?DocID=487), in any relevant Thesis restriction declarations deposited in the University Library, The University Library’s regulations (see http://www.manchester.ac.uk/library/aboutus/regulations) and in The University’s policy on Presentation of Theses

ACKNOWLEDGMENTS

I would like to thank Prof Julie Gough, Dr Stephen Richardson and Dr Alberto Saiani for their guidance, advice and supervision throughout my PhD. I have thoroughly enjoyed this project so thank you for giving me the opportunity to learn new techniques, to greatly expand my understanding of the biomedical materials field and finally allowing me to present my work at numerous international conferences.

I want to express my gratitude to the technical staff, Dr. Louise Carney and Dr Sonal Patel for their contribution and support. A warm thanks to Dr Nigel Hodson for assisting me with AFM work as well as Sam Borland and Sadia Haq for carrying out the specific GAG assay.

Thank you to the members of the E13 office, the Biomaterials Group and the Polymers & Peptide group for being great colleagues, helping me with my work and making my PhD more enjoyable.

I would like to thank all my nearest and dearest friends in Manchester and from Wales (especially the 502 crew old and new) who have kept me sane throughout the past 4 years and have allowed me to play hard as well as work hard.

Many thanks to my mother, father and brother for supporting me throughout my PhD and my time in Manchester, you're the best.

Finally, I would like to thank the funding body, EPRSC, for financially supporting this research.

Chapter 1. *Introduction.*

1.1. OVERVIEW

Lower back pain (LBP) affects 84% of people in their lifetime [1] and according to the most recent statistics has been estimated to cost the UK economy £12 billion per annum [2]. The aetiology of LBP varies and is multifactorial with aging [3], genetics [4] and mechanical injury all contributing to the condition [5]. However, intervertebral disc (IVD) degeneration is strongly associated with LBP in over 40% of cases [6] as loss of IVD integrity causes destabilisation of the spinal motion segment resulting in pain and disability [7]. Freemont *et al.* stated that 'in almost every case when IVD tissue has been examined from patients with LBP, it has shown the features typical of discal degeneration' [8].

IVDs are located in between adjacent vertebrae of the spine. Each IVD consists of 3 distinct but interdependent tissues; the gel-like nucleus pulposus (NP) in the centre which is surrounded by the tougher fibrous annulus fibrosus (AF) [9] with superior and inferior cartilage endplates (CEPs) restricting the AF and NP axially [10]. The main role of the NP is to transmit loads from body weight and muscle activity to the AF whilst IVDs allow a degree of motion in the back and act as shock absorbing systems [11].

IVD degeneration, also known as degenerative disc disease (DDD), occurs when there is an imbalance between catabolic and anabolic events in the IVD extracellular matrix (ECM) [12]. DDD is a cell driven process with changes in IVD cell phenotype and biochemistry inducing abnormal matrix production. An increase in pro-inflammatory cytokine production levels stimulates increased matrix degrading enzyme expression [13] leading to accelerated ECM degradation. DDD is directly linked to age [6, 14]; as a person ages, the NP dehydrates and becomes fibrous whilst the AF become disorganised and weakens [15]. Nerves can in-grow into the IVD and cell apoptosis occurs. Due to the avascular nature of IVDs [16] there is limited ability for tissue self-repair which means that DDD is irreversible. These degeneration events cause IVDs to lose normal function and often leads to LBP [17].

Current treatments for LBP management range from conservative therapies to surgical intervention which is normally reserved for chronic LBP [7]. However there are doubts over efficacy of surgical procedures [18] and current treatments have limited long term outcomes [5]. Crucially, all current strategies are symptomatic and not curative [19].

Due to the prevalence of LBP which is only going to increase due to an aging population [20] coupled with the ineffectiveness of current treatments, there needs to be an entirely new

approach for DDD treatment that restores the IVD structure and function to potentially alleviate LBP [15].

Cell-based therapies are considered to hold particular promise in regards to the treatment of DDD [5, 15, 21]. Tissue engineered constructs potentially have the ability to restore both the native NP tissue and function whilst preserving the capacity of the IVD to remodel in response to external stimuli [22]. The ultimate goal would be to develop a therapy that leads to mechanical stability of the IVD with the formation of neo-tissue resembling the native organ. There are numerous studies investigating cell-based therapies for the AF and NP. DDD originates within the NP [8] so it has been hypothesised that if a healthy AF was present, then replacement of a degenerated NP with an injectable implant or a tissue engineered construct may slow DDD, reduce pain and also restore mobility of the back [10,15]. Therefore a wide variety of biomaterials have been investigated for potential use as NP tissue engineering constructs.

Scaffolds made from natural biomaterials, such as hyaluronic acid (HA) [23], demonstrate good biocompatibility, although can suffer from batch to batch variation [10]. Also material properties like degradation or gelation time can prove difficult to modify. Synthetic biomaterials, like poly(ethylene glycol) [24] allow greater control over manufacture and final hydrogel properties but can lack the inherent bioactivity of natural biomaterials [25] and might not be of appropriate scale for 3D cell culture due to micro-sized features [26]

Due to the disadvantages of current biomaterials, self-assembling peptide hydrogels (SAPHs) were chosen for investigation as potential scaffolds and/or cell carriers for NP tissue engineering. SAPHs are a relatively new class of biomaterial that have the inherent ability to self-assemble into complex supramolecular structures after exposure to the appropriate stimuli [27, 28]. The simple self-assembly mechanism produces self-supporting hydrogels suitable for cell culture [29, 30]. In theory, SAPHs combine the advantages of natural and synthetic biomaterials whilst overcoming their deficiencies [26, 31]. For example, the peptide sequence can be easily modified to control the final hydrogel mechanical and chemical properties [30] whilst SAPHs should be biocompatible due to amino acids being present *in vivo*. A number of papers have investigated SAPHs for NP tissue engineering as the systems are injectable, biodegradable and biocompatible. However studies did not investigate the rheological behaviour of the SAPHs [32, 33] and only utilised the culture of animal cells [34].

Mesenchymal stem cells (MSCs) are regarded to hold great potential as a cell source in regards to cell-based therapies for DDD [21, 35]. MSCs have high *ex vivo* expansion capability, are readily available and crucially have shown the ability to differentiate towards a NP-like phenotype after the appropriate stimulation [19, 36]. Crucially, a randomised clinical trial demonstrated that after injection of MSCs into degenerate human NPs, increases in pain relief and disc hydration were recorded [37]. Previous studies have used TGF-β [38] or GDF-5 [39] to induce a NP-like phenotype from MSCs. However GDF-6 has recently been identified

as a potentially more promising discogenic differentiating growth factor due to it upregulating ‘traditional’ and ‘novel’ NP markers to a significantly higher level than either TGF-β or GDF-5 as well as stimulating higher deposition of appropriate NP ECM components [40]. To the knowledge of the author only one paper has investigated the culture of human MSCs in SAPHs for NP tissue engineering applications [34].

The overall objective of this study was to;

- Characterise the octapeptide SAPH then optimise the system so mechanical properties closely match the native NP (*chapter 4*).
- Analyse the 3D culture of bNPCs in octapeptide SAPH to determine whether healthy cell population was maintained, if NPCs retained their phenotype and to determine if cells are stimulated into producing appropriate NP associated ECM components (*chapter 5*).
- Analyse the 3D culture of human bone marrow MSCs (h-BMMSCs), stimulated with and without GDF-6, to assess the cell phenotype, viability and ECM component production to determine whether a NP-like phenotype could be induced from MSCs with and without an induction factor following encapsulation in the SAPH (*chapter 6*).

1.2. REFERENCES

1. **Stewart W, Ricci J, Chee E, Morganstein D, Lipton R** 'Lost productive time and cost due to common pain conditions in the US workforce' JAM (2003); Vol.290 No.18 pp.2443–54.
2. **Maniadakis N, Gray A** '*The economic burden of back pain in the UK*' Pain (2000); Vol.84 pp.95-103
3. **Hoy D, Bain C, Williams G, March L, Brooks P, Blyth F, Woolf A, Vos T, Buchbinder R** '*A systematic review of the global prevalence of low back pain*' Arthritis & Rheumatism (2012); Vol.64 No.6 pp.2028-2037
4. **Williams F, Bansal A, Meurs J, Bell J, Meulenbelt I, Suri P, Rivadeneira, Sambrook P, Hofman A, Bierma-Zeinstra S, Menni C, Kloppenburg M, Slagboom P, Hunter D, MacGregor, Uitterlinden A, Spector T** *'Novel genetic variants associated with lumbar disc degeneration in northern Europeans: a meta-analysis of 4600 subjects'* Clinical and epidemiological research (2012); doi:10.1136/annrheumdis-2012-201551
5. **Kandel R, Roberts S, Urban J** '*Tissue engineering and the intervertebral disc: the challenges*' Eur Spine J (2008); Vol.17 pp.480-491
6. **Cheung K, Karppinen J, Chan D, Ho D, Song Y-Q, Sham P, Cheah K, Leong J, Luk K** *'Prevalence and pattern of lumbar magnetic resonance imaging changes in a population study of one thousand forty-three individuals'* Spine (2009); Vol.34 No.9 pp.934-940
7. **Gilbert H, Hoyland J, Richardson S** '*Stem cell regeneration of degenerated intervertebral discs: Current status*' Curr Pain Headache Rep (2013); Vol.17 pp.1-9
8. **Freemont A, Watkins A, Le Maitre C, Jeziorska M, Hoyland J** '*Current understanding of cellular and molecular events in intervertebral disc degeneration: implications for therapy'* Journal of Pathology (2002); Vol.196 Iss.4 pp.374-379
9. **Humzah M, Soames R** '*Human intervertebral disc: Structure and function*' Antatomical Record (1988); Vol.220 pp.337-356
10. **Cloyd J, Malhotra N, Weng L, Chen W, Mauck R, Elliott D** *'Material properties in unconfined compression of human nucleus pulposus, injectable hyaluronic acid-based hydrogels and tissue engineering scaffolds'* Eur Spine J (2007); Vol.16 pp.1892-1898
11. **Adams M** '*Biomechanics of back pain*' Acupuncture in Medicine (2004); Vol.22 No.4 pp.178-188
12. **Le Maitre C, Freemont A, Hoyland J** '*The role of interleukin-1 in the pathogenesis of human intervertebral disc degeneration*' Arthritis Research & Therapy (2005); Vol.7 No.4 pp.732-744
13. **Le Maitre C, Pockert A, Buttle D, Freemont A, Hoyland J** *'Matrix synthesis and degradation in human intervertebral disc degeneration'* Biochemical Society Transactions (2007); Vol.35 pp.652-656
14. **Waris E, Eskelin M, Hermunen H, Kiviluoto O, Paajen H** '*Disc degeneration in low back pain*' Spine (2007); Vol.32 No.6 pp.681-684
15. **Urban J, Roberts S** '*Degeneration of the intervertebral disc*' Arthritis Research & Therapy (2003); Vol.3 pp.120-131
16. **Grunhagen T, Wilde G, Soukane D, Shirazi S, Urban J** '*Nutrient supply and intervertebral disc metabolism*' J of Bone and Joint Surgery (2006); Vol.88 pp.30-35
17. **Luoma K, Riihiamki H, Luukkonen R, Raininko R, Juntura E, Lamminen A** '*Low back pain in relation to lumbar disc degeneration*' Spine (2000); Vol.25 pp.487-492
18. **Park P, Garton H, Gala V, Hoff J, McGillicuddy J** *'Adjacent segment disease after lumbar or lumbosacral fusion: review of literature'* Spine (2004); Vol.29 p.1938
19. **Richardson S, Hoyland J** *'Stem cell regeneration of degenerated intervertebral discs: Current status'* Curr Pain Headache Rep (2008); Vol.12 pp.83-88
20. **Freburger J, Holmes G, Agans R, Jackman A, Darter J, Wallace A, Castel L, Kalsbeek W, Carey T** '*The rising prevalence of chronic low back pain'* Arch Intern Med (2009); Vol.169 No.3 pp.251-258
21. **Sakai D, Grad S** '*Advancing the cellular and molecular therapy for intervertebral disc disease*' Advanced Drug Delivery Reviews (2014); Vol.84 pp.159-171
22. **Hudson K, Alini M, Grunert P, Hartl R, Bonassar L** '*Recent advances in biological therapies for disc degeneration: tissue engineering of the annulus fibrosus, nucleus pulposus and whole intervertebral disc*' Biotechnology (2013); Vol.24 pp.1-8
23. **Calderon L, Collin E, Velasco-Bayon D, Murphy M, O'Halloran D, Pandit A** *'Type II collagen-hyaluronan hydrogel- a step towards a scaffold for intervertebral disc tissue engineering'* European Cells and Materials (2010); Vol.20 pp.134-148
24. **Francisco A, Mancino R, Bowles R, Brunger J, Tainter D, Chen Y, Richardson W, Guilak F, Setton L** *'Injectable laminin-functionalised hydrogel for nucleus pulposus regeneration'* Biomaterials (2013); Vol.34 pp.7381-7388
25. **Chan B, Leong K** '*Scaffolding in tissue engineering: general approaches and tissue-specific considerations*' Eur Spine J (2008); Vol.17 pp.467-479

26. **Zhang S, Yokoi H, Gelain F, Horii A** *'Designer self-assembling peptide nanofibre scaffolds'* Nanotechnology for Biology and Medicine: At the Building Block Level (2012); pp.123-147
27. **Boothroyd S, Saiani A, Miller A** *'Formation of mixed ionic complementary peptide fibrils'* Macromol Symp (2008); Vol.273 pp.139-145
28. **Saiani A, Mohammed A, Frielinghaus N, Collins R, Hodson N, Kielty C, Sherratt M, Miller A** *'Self-assembly and gelation properties of α-helix versus β-sheet forming peptides'* Soft Matter (2009); Vol.4 pp.193-202
29. **Diaz L, Saiani A, Gough J, Miller A** '*Human osteoblasts within soft peptide hydrogels promote mineralisation in vitro*' J of Tissue Engineering (2014); Vol.5 pp.1-12
30. **Miller A, Saiani A** '*Engineering peptide based biomaterials: Structure, properties and application'* Chemistry Today (2010); Vol.28 No.1 pp.34-38
31. **Nune M, Kumaraswamy P, Krishnan U, Sethuraman S** *'Self-assembling peptide nanofibrous scaffolds for tissue engineering: Novel approaches and strategies for effective functional regeneration'* Current Protein and Peptide Science (2013); Vol.14 pp.70-84
32. **Wang B, Wu Y, Shao Z, Yang S, Che B, Sun C, Ma Z, Zhang Y** *'Functionalized self-assembling peptide nanofiber hydrogel as a scaffold for rabbit nucleus pulposus cells'* Journal of Biomedical Materials Research (2012); Vol.100 Iss.3 pp.643-653
33. **Sun J, Zheng Q, Wu Y, Liu Y, Guo X, Wu W** *'Culture of nucleus pulposus cells from intervertebral disc on self-assembling KLD 12 peptide hydrogel scaffold'* Materials Science and Engineering (2010); Vol.30 pp975-980
34. **Wang B, Sun C, Shao Z, Yang S, Che B, Wu Q, Liu J** 'Designer self-assembling peptide nanofibre scaffolds containg link protein N-terminal peptide to induce chondrogenesis of rabbit bone marrow stem cells' Biomed Research (2014); pp.1-10
35. **Ludwinski F, Gnanalingham K, Richardson S, Hoyland J** '*Understanding the native nucleus pulposus cell phenotype has important implications for intervertebral disc regeneration strategies*' Regenerative Medicine (2013); Vol.8 pp.75-87
36. **Minogue B, Richardson S, Zeef L, Freemont A, Hoyland J** '*Characterisation of the human nucleus pulposus cell phenotype and evaluation of novel marker gene expression to define adult stem cell differentiation*' Arthritis & Rheumatism (2010); Vol.62 pp.3695-3705
37. **Orozco L, Soler R, Morena C, Alberca M, Sanchez A, Sancho J** *'Intervertebral disc repair by autologous mesenchymal bone marrow cells: A pilot study'* Clinical and Translational Research (2011); Vol.92 pp.822-829
38. **Risbud M, Shapiro I, Vaccaro A, Albert T** '*Stem cell regeneration of the nucleus pulposus*' Spine J (2004); pp.348-353
39. **Stoyanov J, Gantenbein-Ritter B, Bertolo A, Aebli N, Baur M, Alini M, Grad S** '*Role of hypoxia and growth and differentiation factor-5 on differentiation of human mesenchymal stem cells towards intervertebral nucleus pulposus-like cells'* European Cells and Materials (2011); Vol. 21 pp.533-547
40. **Clarke L, McConnell J, Sherratt M, Derby B, Richardson S, Hoyland J** *'Growth differentiation factor 6 and transforming growth factor-beta differentially mediate mesenchymal stem cell differentiation, composition, and micromechanical properties of nucleus pulposus constructs'* Arthritis & Research (2014); Vol.16 pp.1-13

.

Chapter 2. *Literature Review*.

2.1. REGENERATIVE MEDICINE & TISSUE ENGINEERING

2.1.1. Overview

Regenerative medicine comprises a combination of technological approaches with the central focus on human cells but also encompasses tissue engineering, gene therapy, stem cell transplantation and cloning [1, 2]. The ultimate goal of regenerative medicine is to 'replace or regenerate human cells, tissue or organs to restore or establish normal function' [1]. Tissue engineering is a major component of regenerative medicine and is a multidisciplinary field that involves cell biology, engineering and material techniques to 'restore, maintain or enhance tissue and/or organ function' [3]. Tissue engineering utilises scaffolds as a framework to guide cell growth and support three-dimensional (3D) tissue regeneration [4].

The objective of tissue engineering is to overcome the constraints of conventional treatments which are based upon the implantation of prosthesis to replace body parts or organ transplantation [2]. Current treatments have a number of disadvantages including the body eliciting an immune response to implanted prosthesis or organs. Likelihood of organ transplant rejection can be reduced by the use of immunosuppressant drugs however this leaves the patient more susceptible to infections and can cause other undesired side effects [5]. In theory, engineered tissues and organs can be constructed using autologous cells or stem cells which would likely decrease the immune response. A main driving force behind the increased interest, funding and research into tissue engineering is the lack of organ availability for transplant. According to National Health Service (NHS) statistics for 2013/2014, there were 7026 people on the transplant list with 3505 transplants being carried out (*figure 2.1*).

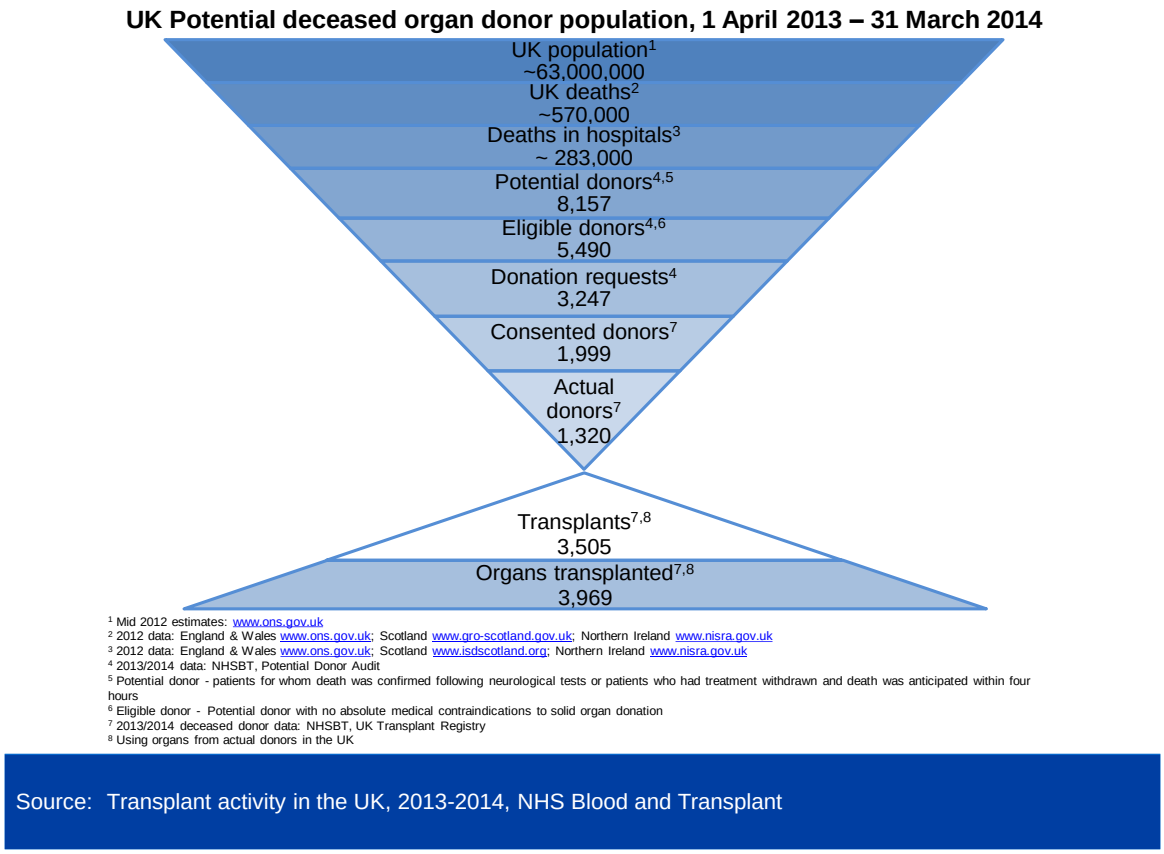

Figure 2.1. Recent statistics showing the eligibility of donors, the actual donors and the number of transplants carried out in the UK from April 2013 to March 2014. *Taken from http://www.organdonation.nhs.uk/statistics/transplant_activity_report/*

2.1.2. Approaches & roles of scaffolds

Tissue engineering strategies can be divided into two categories; acellular scaffolds which rely on the body's ability to regenerate for correct orientation of new tissue or scaffolds with seeded cells [2, 6]. *In vitro* tissue engineering requires the mimicking of microenvironment *ex vivo* so the generation of tissue-like constructs can be produced then implanted into the body [7]. Similarly, *in vivo* tissue engineering needs to mimic the native tissue so recruited or encapsulated cells produce the appropriate extracellular matrix (ECM). Without a scaffold, cells cannot expand into the desired 3D orientations [8].

Two-dimensional (2D) cell culture is in sharp contrast to 3D culture as the *in vivo* environment allows cell to cell interactions and interaction with the extracellular ECM in all directions. In 2D culture only part of the cell is attached to a surface. The transport phenomena (growth factors, cytokines etc.) of 2D and 3D systems are highly different [9]. Cells cultured in 2D can de-differentiate [10]. A successful scaffold needs to be biocompatible, where the biomaterial does not have a toxic effect in the body and performs with an 'appropriate host response in a specific application' [11]. The scaffold needs to be biodegradable so that it breaks down over

time with the degradation products being absorbed by the body or excreted [8] negating the need for additional surgery to remove the biomaterial. Ideally the rate of degradation should be in equilibrium with the rate of new tissue formation by the body.

Traditional tissue engineering strategies require the extraction of autologous cells or the use of cells from another suitable source [2]. The cells need to be expanded in culture and seeded onto the scaffold before implantation. A more relevant and contemporary approach to tissue engineering utilises stem cells seeded within a biomimetic scaffold which encourages the stem cells to differentiate into the required lineage [12]. A well-defined biomimetic milieu should promote specific cell interactions which allows control over cell behaviour and leads to production of a matrix that resembles the native environment [4].

2.1.3. Hydrogels

Hydrogels are a class of scaffold made from either synthetic or natural hydrophilic polymer chains [13] that can be cross-linked chemically or physically [14]. Hydrogels have a high water (H_2O) content which makes diffusion of nutrients and cells, and the removal of waste products easier [9, 14]. However the diffusion and solubility of oxygen and nutrients through a hydrogel is still low which creates diffusion gradients [15]. Stimuli responsive hydrogels are used in tissue engineering as scaffolds, biosensors and for drug delivery [9, 13]. They can assemble or degrade after initiation by an external environmental change which could be physical (temperature) [16], chemical (pH) [17] or biochemical (enzyme action) [18]. For tissue engineering applications, a hydrogel can be administered via minimally invasive procedure to fill an irregularly shaped tissue defect [14, 19]. Hydrogels should also retain cells, protect cells from harsh *in vivo* environments and provide initial support for cell growth [20, 21].

2.2. INTERVERTEBRAL DISC

2.2.1. Morphology

In the spinal column, IVDs are situated in between the vertebrae of the spine [23]. Each IVD is approximately 7-10 mm thick and 40 mm in diameter [24].

The IVD consists of 3 morphologically distinct but interdependent regions (*figure 2.2*); the fibrous AF surrounds the gelatinous NP in the centre with (CEPs) on the superior and inferior surfaces attaching the IVD to the vertebrae [23]. A network of collagen fibres connects the NP to the AF and also to the CEPs [24]. This ensures that the three distinct tissues are linked together to form one structure.

The NP is a gel-like isotropic tissue that consists of a randomly organised type II collagen fibre and radially organised elastin fibre network, embedded in a highly hydrated proteoglycan (PG)-H_2O gel [25]. The cell density within the NP is low with around 4000 cells per mm^3 [26]. NP cells (NPCs) are similar to chondrocytes [27] in terms of morphology and the ECM components produced although the ratio of type II collagen to aggrecan is different [28] and cells have distinct phenotypic markers [29].

The AF surrounds the NP and consists of a series of 15 to 25 concentric rings of type I collagen fibre bundles (lamellae) [23, 30]. The AF is split into 2 distinct regions; inner and outer [31]. Highly organised collagen fibres are directionally oriented with fibres in adjacent lamellae running at alternating 30^o angles to the long axis of the spine [32]. Elastin fibres are found in between the lamellae to return the IVD to its original shape after distortion and to bind lamellae together. Type I collagen makes up approximately 70% of the AFs dry weight [30]. The cell density of the AF is low with 9000 cells per mm^3 [26]. Cells in the outer AF are elongated, thin and similar to fibroblasts whilst cells found closer to the NP (inner AF) are rounded and chondrocyte-like [32]. Cells are aligned parallel to the collagen fibres [25]. The AF behaves in a non-linear anisotropic manner whilst also displaying rate dependent viscoelastic properties [33].

CEP consists of a 1 mm thick horizontal layer of hyaline cartilage. It attaches the IVD to the vertebral bodies via collagen fibres which run horizontally and vertically throughout the structure and into the IVD [24].

A healthy IVD has limited blood supply; the AF is slightly vascularised in the outermost layer whilst the NP is avascular [20, 34]. Therefore cellular activity relies on diffusion of nutrients from capillaries of the vertebrae and the outer AF [20]. Nerves are present in the superficial layers of the AF [35] although extensive innervation is associated with DDD [36].

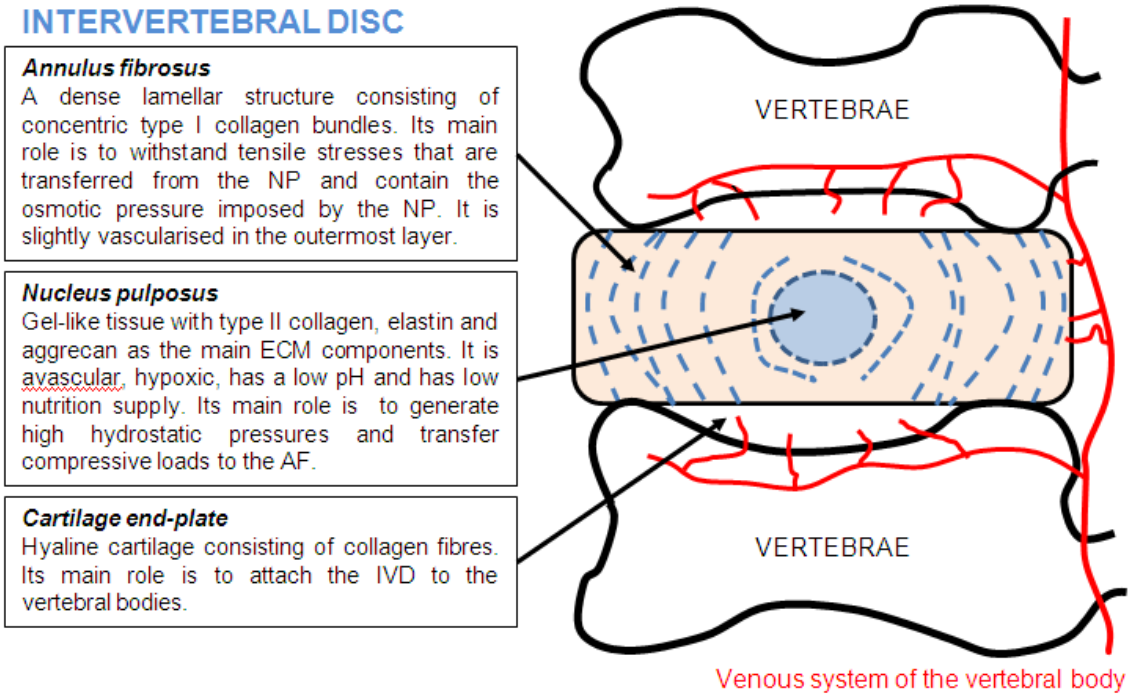

Figure 2.2. The structure and characteristics of the IVD and the vertebral bodies viewed along the sagittal plane. The tough fibrous AF surrounds the gel-like NP in the centre. The CEPs attach the IVD to the vertebral bodies. The IVD has limited blood supply therefore nutrients and metabolites have to diffuse through the CEPs and AF to reach the NP. *Adapted from [20].*

2.2.2. Function

IVDs act as cartilaginous joints linking the vertebral bodies [23]. Their two main functions are to allow a degree of movement in the spine (bending, torsion and flexion) and to act as shock absorbers, dissipating the loads and stresses that the spine is subjected to [24].

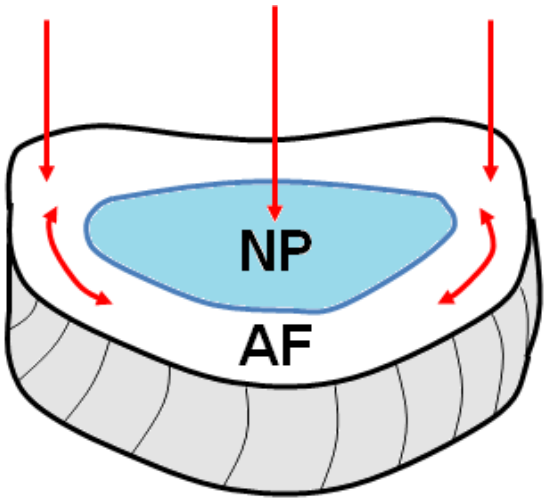

Figure 2.3. Schematic demonstrating how the NP dissipates loads from the spine. Spinal compression generates hydrostatic pressure in the NP which is then transferred to the tougher AF which experiences tensile 'hoop' stresses. *Adapted from [38].*

Spinal compression generates hydrostatic pressure in the central NP and tensile stresses in the AF (*figure 2.3*) [37]. The NP is restricted axially by the CEPs and circumferentially by the surrounding AF. When a compressive load is administered, the NP distends radially and the force is transferred to the tougher AF [38]. Therefore the NP behaves physiologically in an environment that is neither completely confined nor completely unconfined [39].

2.2.3. Physiology

NP ECM is a dynamic structure with homeostasis of the tissue depending on the equilibrium between catabolic and anabolic events [40]. NPCs constantly synthesise ECM components and remodel the tissue [41] whilst matrix metalloproteinases (MMP) and aggrecanases break it down [42]. Tissue inhibitors of matrix proteinases (TIMPs) mediate the action of matrix degrading enzymes [43]. NP cell survival, matrix synthesis and apoptosis are governed by the transcription factor hypoxia inducible factor (HIF) [44]. The NP microenvironment is harsh due to significantly reduced oxygen tension at the centre of the IVD. Cells are adapted to anaerobic metabolism and are reliant on diffusion of nutrients and metabolites which leads to high concentrations of lactic acid build-up and hence low pH [20].

2.2.4. Biochemistry

The function of healthy IVDs is reliant on NP ECM; in particular type II collagen and aggrecan [37, 45]. Type II collagen makes up around 20% of the NPs dry weight [30] with the collagen network providing form and tensile strength to the structure [31]. There is a high concentration of PGs in the NP [47] with aggrecan the most prevalent. Aggrecan is a highly negatively charged molecule due to chondroitin sulphate (CS) and keratan sulphate (KS) glycosaminoglycan (GAG) chains attached to the protein core. Positive ions are attracted to the large negative charges of the sulphate groups within the GAGs. The high concentration of ions leads to an osmotic imbalance which causes H_2O to be drawn into the NP [47]. PGs also play a role in the transport of salts, waste products and gases through the IVD [48]. At a young age, the H_2O content of the tissue ranges from 80 to 88% but the amount decreases with age [23]. The ability of the NP to absorb and release H_2O is directly related to the capacity to transfer loads to the AF [32]. Various other minor ECM components are present in varying amounts such as types III, V, VI, IX, X, XI, XII and XIV collagen [26]. These molecules are thought to play a role in coordinating the assembly, transport and incorporation of collagen fibrils in the IVD [49]. HA is another GAG that is richly present in the NP and is thought to have a role in stimulating ECM biosynthesis and cell proliferation [15].

2.3. LOWER BACK PAIN & DEGENERATIVE DISC DISEASE

2.3.1. Overview

A report released by National Institute for Health and Clinical Excellence in 2009, estimated that the direct cost of LBP treatment in the UK was in excess of £1 billion but including insurance, lost production and other factors the cost could be as high as £12 billion per annum [50]. It is estimated that 84% of people will suffer from LBP at least once in their lifetime [51] with around 10% becoming chronically disabled [25].

Aetiology of the condition is multi-factorial; however IVD degeneration, also known as DDD, is strongly associated with LBP in over 40% of cases (*figure 2.4A*) [52, 53]. DDD occurs when IVD cells fail to maintain a functional tissue matrix. Degradation of the ECM outweighs synthesis as there is an increase in matrix-degrading enzyme activity over natural inhibitors [54] which causes an inflammatory reaction [20]. The exact aetiology of DDD is unclear; it is widely accepted that a combination of factors (genetic, biomechanical and biochemical) cause changes in the IVD ECM which starts a cascade effect leading to DDD and eventually LBP [38].

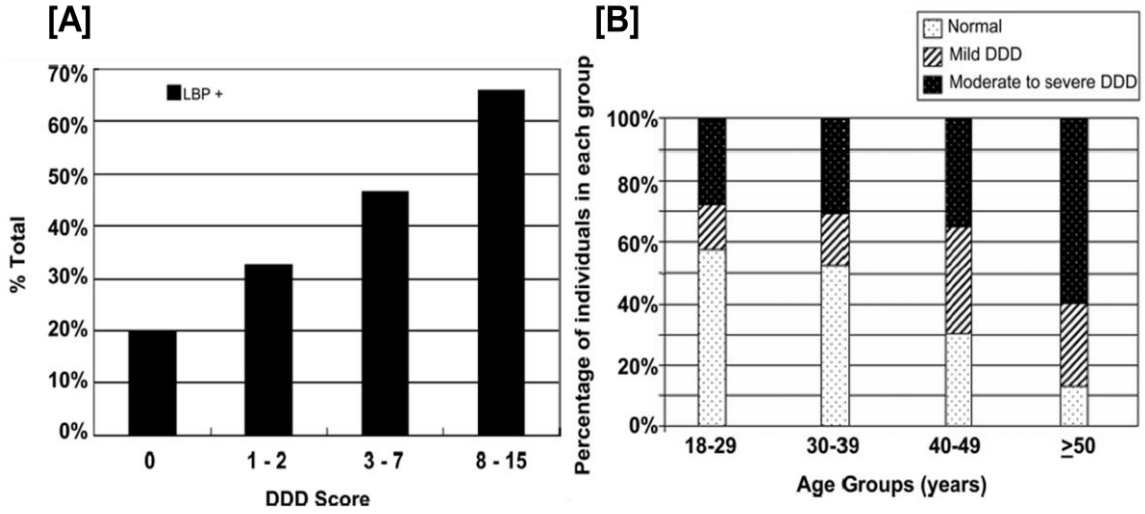

Figure 2.4. [A] The relationship between Schneiderman's grade for severity of degeneration and percentage LBP sufferers. The higher the DDD score then the more severe degeneration. Results show that the more degenerated the IVD then the more likely that the subject suffered from LBP [B] The strong correlation between age of subject and severity of DDD. *Copyright clearance number 3660810574237 from [52].*

The older the person then the more likely that they will suffer from the DDD [55]. Cheung *et al* discovered that severity and prevalence of DDD strongly correlated with age of the subject (*figure 2.4B*) and determined that 100% of subjects over the age of 60 showed some form of DDD [52].

2.3.2. Structure of degenerated discs

Degenerated IVDs have different morphology to healthy ones (*figure 2.5*). The boundary between the AF and NP becomes less distinct with the AF becoming more disorganised and the NP turning more fibrous and dehydrating [56] which causes the disc space to collapse as the inner region cannot pressurise effectively to resist applied load [57]. The NP is not able to transfer stresses to the AF as efficiently whilst the weakened AF cannot dissipate loads as effectively [38]. DDD causes increased vascularisation and innervation of peripheral tissue, high amounts of vascular endothelial growth factor (VEGF) expression has been recorded in degenerated IVDs [58]. Angiogenesis likely occurs due to the body attempting to repair the tissue by increasing nutrient supply and waste product removal. In turn, angiogenesis drives nerve in-growth which exacerbates LBP [54]. Cell apoptosis also occurs during DDD via various signal transduction pathways including autocrine and paracrine Fas Ligand mechanisms [59]. These transduction pathways can be induced by a number of different factors including mechanical loading, biochemical stimuli [60] or acute trauma force [61].

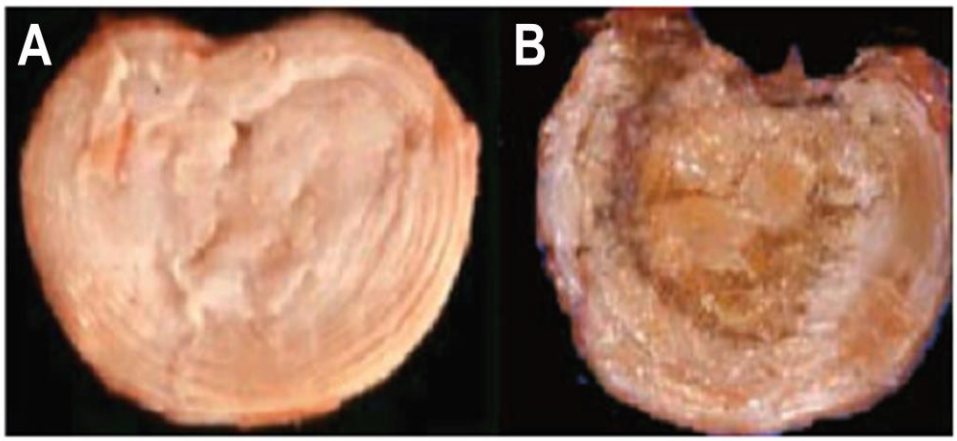

Figure 2.5 Comparison of a [A] healthy IVD and [B] a severely degenerated IVD. In the healthy IVD, the lamellae of the AF are clearly visible and the boundary between the AF and NP is clearly defined. In the severely degenerated IVD, the NP is dehydrated and fibrous whilst the AF is disorganised and weakened. This weakens the whole IVD structure and hinders its mechanical role. *Arthritis Research & Therapy and BioMed Central does not require copyright licence, from email correspondence with BioMed Central customer services on 17.11.15. Taken from [25].*

Disc herniation can occur due to loss of hydration and disc collapse causing increased strain on AF fibres leading to the AF tearing [62]. Herniated discs may come into contact with spinal nerves and cause significant pain to be experienced. Cheung *et al.* classified disc herniation as either disc bulging, protruding or extruding. Disc protrusion or extrusion was when the NP was displaced beyond the confines of the AF [52]. However it is evident that disc herniation induced pressure on the nerve root is not the singular cause of LBP as approximately 70% of people with disc hernitations are asymptomatic for LBP [63].

2.3.3. Biochemistry of degenerated IVDs

During matrix development, turnover and degeneration, NPCs and AFCs produce a variety of MMPs [43]. In a healthy IVD, there is equilibrium between matrix synthesis and breakdown. However in degenerated IVDs, this balance is disrupted with an increase in catabolic events leading to matrix degradation. The change in matrix composition that occurs with DDD is caused by changes in cell physiology [42].

Cytokines regulate nerve and vessel in growth, connective tissue degradation and macrophage accumulation [44]. During DDD there is an increase in pro-inflammatory cytokine expression such as IL-1β [40] and TNF-α [42]. It has been hypothesised that an increase in the expression of catabolic cytokine IL (interleukin)-1α drives DDD as the cytokines stimulate expression of matrix degrading enzymes. Le Maitre *et al.* demonstrated that after IVD cells were treated with IL-1α the balance of anabolic and catabolic events was disrupted [40]. Treatment of human IVD cells with IL-1 caused an increase in MMP and ADAMTS expression and a decrease in matrix gene expression [42]. MMP-1 and MMP-13 are responsible for the breakdown of the helical regions of the fibrillar collagens present in the disc (types I, II and III) which weakens the structure [65]. There is a rise in levels of degradative enzymes such as MMP -1, -3 and -13 as DDD worsens [43]. A disintegrin and metalloprotease thrombospondin type I motif 4 and 5 (ADAMTS) are responsible for specifically cleaving aggrecan. It has been demonstrated that expression of ADAMTS correlated with age so it was hypothesised that it plays a crucial role in DDD [66]. Other studies have shown that IL-1α and IL-1β increases PG leaching from the disc [64] and increased expression of pain mediators such as prostaglandin E2 [67].

The main biochemical change during DDD is the loss of PGs from the NP as aggrecan molecules degrade and leach out of the tissue. In turn this causes the GAG loss, resulting in a decrease of osmotic pressure [54]. H_2O loss from the IVD also causes a reduction in disc height which subjects abnormal loads onto the apophyseal joints and other IVDs in the spine [38]. A decrease in PGs allows large uncharged molecules such as serum proteins and cytokines to enter the IVD and potentially accelerate a degeneration cascade. Typically the high concentration and charge of aggrecan prevents this from occurring [56].

The amount of collagen in the IVD decreases but not by a significant amount, instead the type and distribution varies [25]. There is an increase in type I and III collagen production in the NP making it more fibrous [37, 54]. In conjunction, type II procollagen production decreases and type II collagen denaturation increases [68]. IVD dehydration and loss of disc height directly hinders the NPs ability to absorb and transfer loads [32]. The AF weakens during DDD due to the total amount of type I collagen decreasing [48].

2.3.4. Aetiology of IVD degeneration

DDD aetiology varies and is multifactorial; the main contributors are thought to be mechanical, nutritional and genetic [25]. It was hypothesised that a combination of factors, that weaken the IVD or impair its healing process plays the most important role [38].

A probable main contributor to DDD is lack of nutrient supply to IVD cells. The IVD is virtually avascular so relies on diffusion for nutrient supply and waste removal [34]. A change in oxygen tension or pH in the tissue due to a decrease in nutrient supply could affect IVD cells' ability to synthesise and maintain the ECM [25]. The loss of nutrients also causes a fall in glucose levels and subsequent build up of lactic acid which is likely to contribute to DDD [69].

It is thought that abnormal mechanical loads can initiate a pathway that leads to DDD and eventually LBP [38]. High mechanical loads on the IVD, which can lead to injury, almost certainly exacerbates DDD [25]

Genetics has been determined to play an important role in DDD [70]. Some people will have strong familial predisposition to DDD and disc herniation [71]. For example, a study conducted in Finland found that mutations of two type IX collagen genes, COL9A2 and COL9A3 were strongly associated with DDD and sciatica [72]. It is thought that genetic influences have the most apparent effect on IVD height and structural changes [70]. A meta-analysis of 4600 subjects provided evidence of the association of the parkin RBR E3 ubiquitin protein ligase (PARK2) gene with the pathogenesis of DDD. It was hypothesised that the methylation of the PARK2 gene occurs in people suffering from LBP [73].

2.3.5. Current treatments for LBP & DDD

The majority of LBP sufferers recover without medical intervention. There are conflicting reports but one study found that 30 - 70% of LBP sufferers recover within 3 weeks and 90% are back to work within 2 months [74]. Chronic LBP, where pain exceeds 7-12 weeks or expected healing time, requires more serious intervention [75].

Conservative treatments are non-operative and include exercise, analgesics and spinal manipulation. Exercise is first suggested for the management of LBP [76] however a Finnish study concluded that LBP sufferers who continued normal day to day activities recovered quicker than sufferers who were treated with bed rest or back-mobilising activities [77]. Non-steroidal anti-inflammatory drugs (NSAIDs) provide analgesic, antipyretic and anti-inflammatory effects. Long term use of NSAIDs can lead to gastrointestinal problems as inhibition of COX-1 causes damage to the mucous layer in the stomach. Keller *et al.* analysed a number of randomised controlled trials for non-operative LBP treatments and calculated the effect sizes (using Standardised Mean Differences and Relative Risk). For acute LBP, NSAIDs and manipulation had modest positive affect whilst exercise had minimal effect. For chronic

LBP, NSAIDs, exercise and behavioural therapy all had moderate effect. The study concluded that current non-operative treatments had only a small to medium positive result on alleviating LBP [76].

When conservative treatments fail to alleviate LBP, surgery is the next option. Discectomy is used to remove part of a herniated IVD and laminectomy involves the removal of part or all of the lamina to enlarge the spinal canal to prevent tissue compressing the nerve. These procedures can relieve pain but do not restore lost disc height or recover original load bearing capacity [69]. The current 'gold standard' treatment is spinal fusion which involves fusing 2 or more vertebrae together so the degenerated IVDs are removed and movement is limited in a certain portion of the spine. The fusion process can take up to 18 months to complete and there are concerns over cost and efficacy as spinal fusion has been shown to accelerate DDD in adjacent IVDs [78].

Artificial disc replacements (ADRs) are designed to mimic the complex range of motion that natural IVDs display. Most current ADRs, for example the SB Charité™ or ProDisc®-L, have a similar design consisting of a moving core between 2 metal endplates. ADRs do not have the shock absorbing qualities of natural IVDs, cannot remodel the tissue and are prone to wear [31]. The whole IVD, despite the health of the AF or CEPs, needs to be removed before ADR implantation [79]. A large scale meta-analysis concluded that ADRs failed to show significant superiority for the treatment of DDD compared with spinal fusion [80].

2.4. CELL-BASED THERAPIES FOR DEGENERATIVE DISC DISEASE

2.4.1. Current treatments versus cell-based therapies

Cell-based therapies are regarded to hold particular promise for the future treatment of DDD and LBP [25, 31, 69]. Cell-based therapies include NP tissue engineering, gene therapy and injection of growth factors. Current treatments (*section 2.3.5*) are symptomatic whilst cell-based approaches have the potential to be curative. Current treatments have poor long-term efficacy [82] whilst cell-based approaches have the potential to restore IVD function, encourage formation of neo-tissue and preserve normal biomechanics [83] in the long-term. Cell-based treatments may also restore disc height which has been highlighted as an essential factor for relieving DDD [83, 84, 85]. Finally, most cell-based therapies are designed to be administered by minimally invasive procedure so would negate major surgery [31].

2.4.2. Cell sources for NP tissue engineering

A randomised clinical trial that injected autologous NPCs into degenerated IVDs showed evidence of clinically significant pain relief and retention of disc hydration after a 2-year follow up [85]. Despite promising results, the drawback of using autologous NPCs is that only a finite amount of cells can be extracted. Degenerated IVDs have low cell numbers that might display senescence and extraction of NPCs causes donor site morbidity therefore use of autologous cells is not feasible [69]. In another human trial, allogenic juvenile chondrocytes in a fibrin carrier were injected into the NPs of LBP sufferers. The 1-year follow up demonstrated an improvement in pain relief with the majority of patients having more hydrated NPs [86]. However as the ECM produced by chondrocytes and NPCs differs [28] an alternative cell source better suited to the application was required.

MSCs have been identified as the most promising current cell source [20, 87, 88]. Bone marrow derived (BMMSCs) and adipose derived MSCs (AdMSCs) are readily available, multipotent and have high *ex vivo* expansion potential [89]. Crucially, BMMSCs and AdMSCs have the ability to differentiate into cells with a NP-like phenotype [29, 81]. Originally it was shown that by co-culturing MSCs with NPs and ensuring cell to cell contact, BMMSCs differentiated into cells with a NP-like phenotype with upregulation of SOX9, type II collagen and aggrecan genes [90, 91]. Cell-to-cell contact method requires sufficient amounts of healthy NPCs to stimulate differentiation whilst differentiation of large amount of MSCs could prove difficult. There were no significant changes in NP marker gene expression without cell-to-cell contact which suggested that contact was essential for inducing MSCs towards a NP-like phenotype [92].

More recent studies have demonstrated that by utilising appropriate scaffolds that mimicked the native NP ECM [79, 93], MSCs can be directed towards a NP-like phenotype after

stimulation with discogenic induction growth factors. The appropriate growth factors (TGF-β, GDF-5, GDF-6) play a key role in determining stem cell fate and stimulate synthesis of NP associated proteins [81, 94]. When Feng *et al*. implanted nanofibrous and solid walled PLLA scaffolds into rat caudal discs, results demonstrated that nanofibrous scaffolds had accumulated significantly higher amounts of type II collagen and s-GAG compared to the solid walled scaffolds. The solid-walled scaffolds stained brightly for type I collagen [79] which is produced by NPCs during DDD or after NPC de-differentiation [54, 95]. Results strongly suggested that scaffolds with micro-sized features are unable to mimic the native NP environment [9].

MSCs can be expanded in culture as progenitor cells then injected into a degenerated NP where the microenvironment will provide the appropriate signalling and niche to differentiate MSCs towards a NP-like phenotype [82]. Another approach involves differentiation of MSCs *in vitro* towards a NP-like phenotype before injection into the IVD [93]. A potential disadvantage of injecting MSCs without a scaffold or cell carrier is the risk of leakage from the site. A study injected rabbit MSCs directly into rabbit IVDs where no signs of NP regeneration were observed. It was speculated that MSCs had migrated outside of the NP due to osteophyte formation in the AF and CEPs [21]. It has also been suggested that undifferentiated MSCs may not be suitable for direct implantation into a degenerate IVD due to the harsh conditions [20, 82]. A solution would be differentiating MSCs before implantation or pre-conditioning cells to improve survival chances. Another option is the use of a hydrogel to protect the MSCs and prevent cell leakage from injection site. Retention of NPCs encapsulated in laminin functionalised PEG hydrogel was significantly higher than when NPCs were delivered in PBS after 14 days [96].

Numerous animal trials have produced promising results following injection of MSCs into degenerated NPs, with evidence of cell proliferation, differentiation of MSCs into NP-like cells and increased PG and type II collagen synthesis detected [97, 98]. Despite encouraging animal trial results, the loading in quadriplegic animals and bipedal humans is very different therefore it can be difficult to predict how MSCs and potential scaffolds would respond *in vivo* for humans.

The advantages and outcomes of cell-based NP tissue engineering treatments are based on educated predictions as human studies are still in the early stages and long term trials have yet to be concluded. When an *in vivo* human study grafted collagen sponges seeded with autologous MSCs into the NPs of LBP sufferers, the 2 year follow up demonstrated that there was high H_2O content in the NP with alleviation of LBP symptoms and lower leg numbness for both subjects. The Visual Analog Scale scores for pain significantly decreased [99]. A pilot *in vivo* human study injected MSCs directly into the NPs of 10 patients with chronic LBP and compared the cell-based therapy to the efficacy of current LBP treatments (*figure 2.6*) [83].

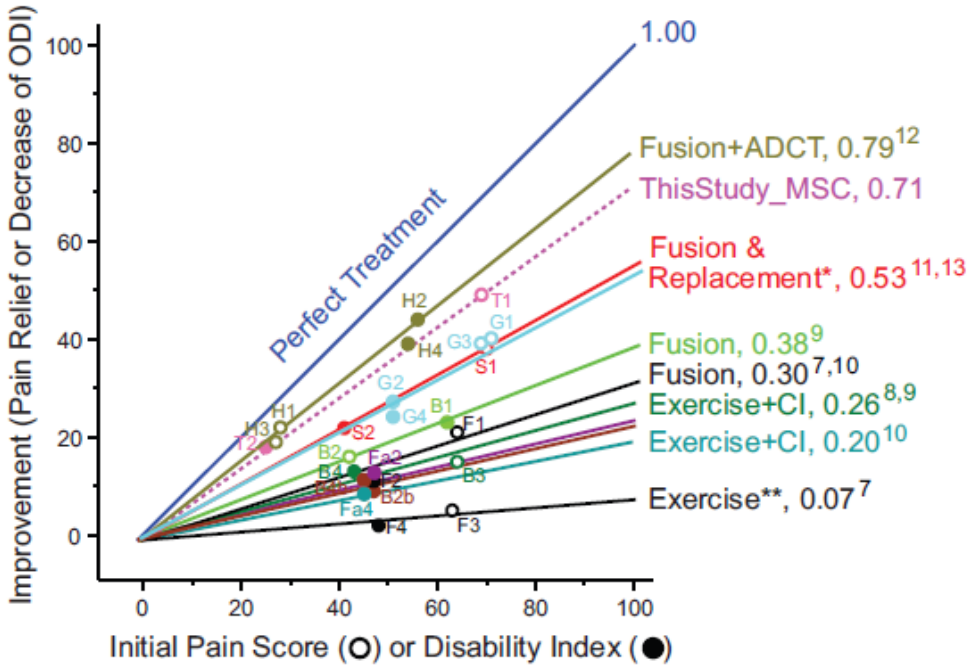

Figure 2.6. The efficacy of various current treatments for LBP in comparison to MSC therapy. The efficacy of the treatment was shown by the gradient of its line, so the perfect treatment, which would entail complete pain relief, had a gradient of 1. 'ThisStudy_MSC' represents pain relief after the injection of MSCs into degenerated NPs. The Visual Analog Scale (open circle) and Oswestry Disability Index (filled circle) are represented as pain relief vs. initial pain score. CI is cognitive intervention, ADCT is autologous disc cell transplantation. *Copyright clearance number 3751400985292 from [83].*

Orozco *et al*. compiled current treatment results from 7 'high-quality' recent clinical trials and expressed the evolution of pain as a percentage [83]. Data was quantified using Visual Analog Scale and the Oswestry Disability Index which are considered to be the 'gold-standard' of LBP functional outcome tools [100]. *Figure 2.6* demonstrated that conservative non-surgical treatment had the lowest efficacy of 0.07. Spinal fusion and ADRs were the most effective treatments according to the gathered data with efficacy ranging from 0.3 to 0.79. The cell-based therapy had the second best efficacy (0.71) without the need for major surgery. The analgesic effects of MSC intervention were faster acting than current treatments [83]. Results of this pilot study supported the hypothesis that cell-based therapies hold great potential in the treatment of LBP and DDD and deserved further extensive investigation.

2.4.3. Review of cell-based strategies for NP tissue engineering

Due to the IVD being a specialised and complex structure with the AF and NP having differing roles and properties, research into tissue engineering strategies usually focus on one tissue. Some studies have investigated biphasic scaffolds to mimic both tissues. Strategies have included using an electrospun poly(L-lactic) acid scaffold [101] and nonwoven mesh

polyglycolic scaffolds [102] for AF tissue engineering and HA hydrogel [101] and alginate gels [102] for NP tissue engineering therefore utilising a tougher polymer scaffold for the AF which surrounded a hydrogel for the NP. Both studies recorded increases in type II collagen and PG content in NP scaffolds and production of type I collagen in the AF scaffolds however still marginal amounts compared to the native tissue [101, 102]. Gebhard *et al.* determined that after implantation of a collagen (to mimic the AF) and alginate (to mimic the NP) composite scaffold into rat tails, results indicated that disc space was maintained and type II collagen and PG was produced after a 1 month follow up [103].

DDD originates in the NP [24, 36] therefore it has been hypothesised that slowing NP degradation could improve overall IVD health [39]. There are typically 2 approaches to cell-based therapies; the first focuses on using the biomaterial as a mechanical replacement for the NP, the second involves cellular therapies with less focus biomechanical properties [57, 85]. However recent studies are investigating both mechanical properties and cellular behaviour in systems due to their important roles in DDD [104, 105]. Current NP tissue engineering strategies have focused on hydrogels for cell encapsulation due to the NP being described as a ‘hydrogel-like’ structure [31].

Natural biomaterials (*table 2.1)*, such as fibrin [105] or alginate [104], should have inherent biocompatibility due to them being present *in vivo* [19, 31] Bovine NPCs cultured in alginate gels displayed the characteristic rounded morphology of native cells and deposited PGs [104]. Human NPCs seeded in fibrin clots produced significant amounts of s-GAG with *COL2A1* and *ACAN* gene expression detected. However *COL1A2*, which is associated with NP de-differentiation and DDD, was expressed almost to the same level [95, 105]. A disadvantage of natural biomaterials is that they suffer from batch to batch variability, for example the mechanical properties of alginate hydrogels vary greatly depending source of material, how it was stored and what cross-linking agent was used [39]. Another disadvantage is that natural biomaterials can contain residual growth factors or impurities which could affect reproducibility and accuracy of results [9]. Finally, it is difficult to modify degradation rate or control the gelation process of natural biomaterials. For example, HA hydrogels have relatively fast degradation times and can display poor cell migration into the structure [107]. Similarly, alginate and fibrin scaffolds lose structural integrity during long term culture [104, 108]. Composite scaffolds have been researched to overcome the limitations of using natural biomaterials. To improve mechanical properties and degradation rates typically the natural biomaterial is cross-linked with a material that displays superior mechanical and degradative resistance properties, such as type II collagen [107, 108]. A HA-type II collagen system observed increases in cell number from day 1 to 7 and increases in aggrecan gene expression with superior mechanical properties to the controls [107].

Synthetic biomaterial scaffolds allow for greater control over mechanical and chemical properties and should produce more consistent final products with less concern over impurities

and sterilisation in comparison to natural biomaterials [8, 9, 109]. A crucial disadvantage of using synthetic biomaterials are that features can be hundreds of nanometres or micrometres in diameter which is not of appropriate scale for 3D cell culture as cells would attach to the architecture [9]. For example, a poly(methyl methacrylate - methacrylic acid - ethyleneglycol dimethylacrylate) - glycidyl methacrylate (DX microgel) used as an injectable microgel to improve the mechanical properties of a degenerated NP encouraged human NPCs to spread and attach to the scaffold [110]. Fibroblastic NPC morphology in an indicator of cellular de-differentiation [41, 95]. To overcome this limitation nanofibrous polymer scaffolds can be manufactured as demonstrated by Feng *et al.* where rat NPCs encapsulated within a nanofibrous polylactic acid gel maintained NP phenotype and produced appropriate ECM components [79]. Synthetic biomaterials are likely to lack the inherent biocompatibility exhibited by natural biomaterials [8]. These limitations can be overcome by introducing bioactive functional groups to the material or by amalgamating synthetic and natural biomaterials [96, 101]. Rheology for a functionalised poly(ethylene glycol) (PEG) hydrogel with laminin determined that the shear modulus was around 0.9 kPa to 1.5 kPa therefore weaker that the 5.39 kPa [39] or 11 kPa [111] for native NP modulus. According to the study, the scaffold stiffness could be manipulated by adjusting the amount of PEG. From a biocompatibility perspective, the addition of laminin allowed retention of porcine notochordal cells after injection into a rat model [96]. Another approach to improving the biocompatibility of synthetic hydrogels is by producing composites with natural biomaterials. After combining a nanofibrous PLLA scaffold and HA hydrogel, encapsulated human BMMSCs were shown to produce types I and II collagen as well as aggrecan after culture with the chondrogenic inducing growth factor TGF-β1 [101].

NP scaffold material	Reference	Mechanical properties	Cell type	Animal study	ECM components	Gene expression
Alginate	Chou *et al.* 2009 [10]	0.59±0.2 to 8.82±0.6 kPa	Bovine NPCs	No	Chondroitin sulphate	N/A
Chitosan-gelatin-glycerolphosphate	Cheng *et al.* 2009[112]	0.05 to 1.2 kPa	Rabbit NPCs	No	Sulphated GAGs	*ACAN* and *COL2A1* upregulation
Fibrin-HA	Li *et al.* 2014 [108]	0.02 to 0.3 kPa	Bovine NPCs	No	Sulphated GAGs	*ACAN* and *COL2A1* downregulation
Hyaluronic acid	Kim *et al.* 2015 [113]	$\|G^*\|$ 1.5 to 2 MPa	Bovine NPCs	No	Sulphated GAGs and type II collagen	*ACAN*, *COL2A1* and NP-specific genes *KRT8*, *KRT18*, *KRT19* upregulation
PEG-HA-pentosan polysulphate	Frith *et al.* 2013 [105]	3.9 to 5.5 kPa	Mesenchymal precursor cells	Rat	Sulphated GAGs and type II collagen	N/A
PEG-laminin	Francisco *et al.* 2013 [96]	0.9 to 1.4 kPa	Porcine NPCs	Rat	N/A	N/A
Poly(D, L-lactide-co-glycolide)	Fraylich *et al.* 2010[114]	<0.1 kPa	Bovine NPCs	No	N/A	N/A
Type II collagen - hyaluronan	Calderon *et al.* 2010[107]	High swelling properties	Rat BMMSCs	No	Sulphated GAGs	*ACAN* and *COL2A1* upregulation
Type I collagen	Clarke *et al.* 2014 [82]	N/A	Human BMMSCs & AdMSCs	No	Sulphated GAGs	*ACAN*, *COL2A1* and NP-specific genes *KRT8*, *KRT18*, *KRT19*, *CA12*, *FOXF1 expressed*

Table 2.1. Summary of various NP tissue engineering strategies using a wide range of natural and synthetic biomaterials. The cell line, mechanical properties of the system, gene expression of encapsulated cells and ECM production are listed.

2.5. SELF-ASSEMBLY

2.5.1. Overview

Self-assembly is defined as ‘the autonomous organisation of components into patterns or structures without human intervention’ [115]. Self-assembly is seen as the main bottom-up approach in nanotechnology and is regarded to be a powerful method for fabricating supramolecular architectures [116, 117]. The bottom-up approach describes techniques that use smaller components to produce larger and more complex structures. Bottom-up approach is regarded to have greater control manipulation at the nanoscale compared with the top-down approach which involves removing material from a bulk material [4]. In nature, proteins and polysaccharides display complex self-assembling behaviour which inspired research into molecular self-assembly [13].

2.5.2. Forces involved in self-assembly

Molecular self-assembly is mediated by non-covalent bonds including hydrogen bonds, van der Waals interactions and hydrophobic interactions [117]. Hydrogen bonding occurs between hydrogen donors and hydrogen acceptors or electronegative atoms. [118]. Electrostatic interactions occur between polar groups, for example a positively charged amide group and a negatively charged carbonyl group. Van der Waals forces are weak interactions that are formed in a non-directional manner between 2 atoms that are in close proximity. There is an attraction between the two nuclei when temporary electrical dipoles are produced by the electron clouds [119]. Individually these bonds are relatively insignificant but when combined together they ‘govern the structural conformation of all biological macromolecules and influence their interaction with other molecules’ [120].

2.6. SELF-ASSEMBLING PEPTIDES

2.6.1. Amino acids

Amino acids, sugars and nucleic acids are the major biological building blocks. Amino acids offer the widest variety for functionality and cell signalling capacity with rapid and relatively simple synthesis of complex molecules [13]. Amino acids consist of an amine group (-NH2), carboxylic group (-COOH) and a specific side chain (-R) (*figure 2.7*). There are 20 different naturally occurring amino acids and a huge amount of artificial amino acids can be manufactured so there are almost infinite amino acid combinations available for the production of engineered peptides.

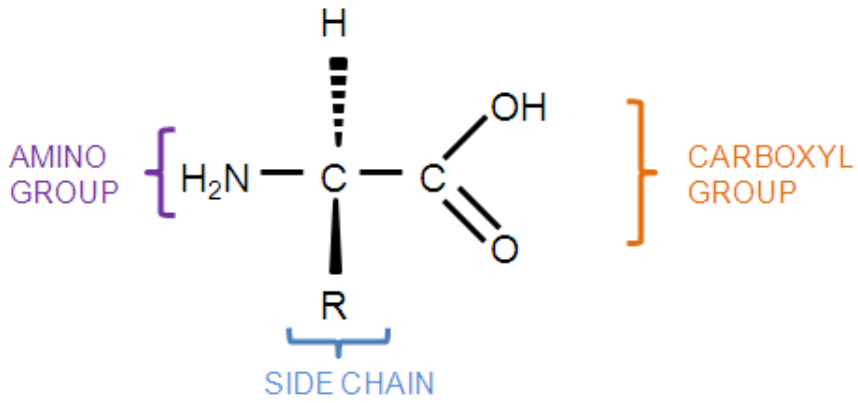

Figure 2.7. General chemical structure of an amino acid. The chiral carbon atom is covalently bonded to the amino group, the carboxyl group, hydrogen atom and the R-group. The R-group is a side-chain specific for each amino acid.

Amino acids covalently bond to one another through a peptide bond which involves a condensation process (*figure 2.8*) where the amino group ($-NH^{3+}$) of one amino acid molecule reacts with the carboxyl group ($-COO^{-}$) of another with the elimination of H_2O [119].

Protein structure is classified into 4 categories according to their degree of complexity.

1. Primary structure refers to the sequence of amino acids in the polypeptide chain.
2. Secondary structure defines the protein sub-structure; the three most common are *α*-helices, *β*-sheets and random coils. Di-sulphide bonds and weak hydrogen bonds are involved in bonding [119].
3. Tertiary structure is the 3D arrangement of the whole protein. Hydrophobic interactions and ionic bonds stabilise the structure [121].
4. Quaternary structure describes the assembly of a number of protein sub-units into oligomers.

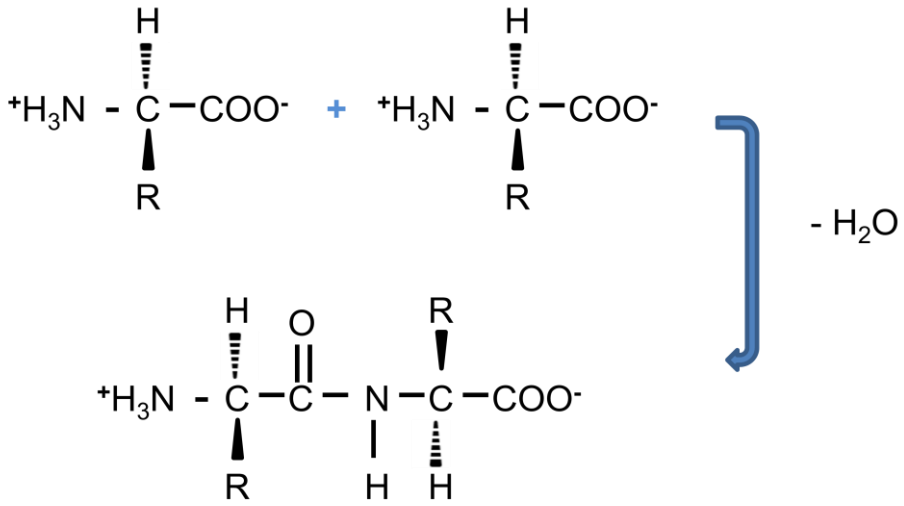

Figure 2.8. Schematic showing the formation of a peptide bond between two amino acids. *Adapted from http://www.peptideguide.com/peptide-bond.html.*

2.6.2. Classes of self-assembling peptide

There are two approaches to the design of non-naturally occurring self-assembling peptides (SAPs). The first method produces peptide amphiphiles which consist of amino acids in the peptide backbone that are covalently linked to an alkyl chain. The second approach involves producing aromatic peptides which have a covalently linked aromatic group [122]. By using peptide secondary structure motifs, peptide sequences can be designed to self-assemble into a variety of supramolecular nanostructures [13].

Amphiphilic peptides are similar to conventional surfactants and have both hydrophobic and hydrophilic segments with a non-polar aliphatic tail [123]. Stupp *et al*. investigated amphiphilic peptides extensively including designing sequences which produced nanostructured fibrous scaffolds reminiscent of ECM. They observed pH triggered assembly of the peptide amphiphiles into cylindrical structures that produced a fibrillar network [124]. In amphiphilic peptide systems, the hydrophobic tail drove aggregation whilst the peptide promoted solubility in H_2O and formation of nanofibres [125].

α-helix forming peptides adopt α-helical conformations and can form fibres with controlled morphologies. Saiani *et al.* demonstrated that alanine based peptides adopted α-helical structures with fibres having a ‘pearl-necklace’ morphology however no gelation occurred in the 0 to 100 mg ml^{-1} concentration range. The reasoning was that the two side chains, the lysine and glutamic acid residues, were present on the same side of the helix which resulted in the repulsion of side chains disrupting self-assembly [123]. In contrast, Banwell *et al.* researched *α*-helix forming peptides that formed self-supporting hydrogels which supported cell growth and MSC differentiation. The system had two peptide components that only gelled upon mixing [126].

β-sheet forming peptides can be divided into 3 groups; *β*-hairpin peptides, short peptide derivatives and ionic-complementary peptides [109]. In general, the structure of *β*-sheet forming peptides consists of repeated sequences, alternating between hydrophobic and hydrophilic amino acids, which form two distinct hydrophobic and hydrophilic surfaces in aqueous solutions [125]. *β*-hairpin peptides are typically long in length and have amino acids that introduce a turn in the chain leading structure folding. An example is the 20 amino acid sequence MAX1 which underwent triggered self-assembly to form a highly cross-linked rigid hydrogel that allowed attachment and proliferation of fibroblasts [127]. As the name suggests, short peptide derivatives consist of only 2 to 3 amino acids linked to an aromatic group (e.g. Fluorenylmethyloxycarbonyl (Fmoc)). This allows a shorter amino acid sequence to be used due to the π-π stacking interactions which are hypothesised to play a key role in self-assembly [118, 122]. The systems have been shown to form fibrous hydrogels which can be utilised in cell culture. For example, the 3D culture of chondrocytes in short-peptide derivatives showed evidence of proliferation and produced the appropriate ECM components [118].

2.6.3. β-sheet forming self-assembled peptide

The first *de novo* self-assembling peptide hydrogel (SAPH) was discovered by Zhang *et al.* in 1992. The 16 amino acid sequence (EAK16) was identified in the Z-DNA binding protein zuotin, a protein found in yeast. The peptide consisted of a repeating motif alternating between cationic, hydrophobic and anionic amino acids which formed stable *β*-sheets under physiological conditions [128]. Results suggested that the driving force for self-assembly of ionic complementary peptides was either alignment of monomers due to electrostatic interactions between the charged side chains or the intermolecular hydrophobic interactions between the peptide side chains and the peptide backbone [117].

β-sheet forming peptides have the general (XY)n sequence, where X is a hydrophobic residue and Y is a hydrophilic residue, and typically incorporate amino acids that carry positive or negative charge at specific pHs [109]. Zhang *et al.* classified ionic-complementary peptides based on the charge of the amino acids present on the hydrophilic surfaces of the molecules. For example, modulus I is - + - + - + - +, modulus II is - - + + - - + +, modulus III is - - - + + + and modulus IV is - - - - + + + + [117]. The charge distribution of the peptide affects the self-assembly process; fibrillar assemblies or globular assemblies can be produced by varying the modulus.

Self-assembly is dependent on pH, concentration of peptide, peptide sequence and ionic strength. Peptide self-assembly occurs when intermolecular attraction dominates electrostatic repulsion between charged side chains [129]. The amino acid sequence determines peptide structure and properties as the charge and hydrophobicity of each amino acid will dictate the secondary structure [109]. By changing the charge distribution or length of the peptide chain, control over self-assembly can be accomplished [130]. Peptide concentration is also important

because peptide chains would be dispersed under the critical aggregation concentration (CAC). However at, or above, the CAC, aggregation occurs. Another factor that affects self-assembly is pH due to its influence on peptide ionisation. *Via* hydrogen bonds and electrostatic interactions, stabilisation of the peptide structure is governed by the charge of each amino acid. For example, for the *β*-sheet peptide QQRFQWQFEQQ (Q is glutamine, R is arginine, F is phenylalanine, W is tryptophan) when pH was less than 5, arginine was positively charged therefore a hydrogel was formed due to the stabilisation of the fibrillar dispersion. Above pH 5, both arginine and glutamine residues were charged so flocculation took place because of the electrostatic interactions of neighbouring charged residues [131]. Finally, ionic strength plays an important role in self-assembly as exposure to electrolyte solutions initiates *β*-sheet assembly into nanofibres. The ions present in solution screen the charged side-chains which decreases the electrostatic repulsion between the amino acids and drives self-assembly [129].

Anti-parallel *β*-sheet structures with 2 distinct surfaces are formed by the peptides in aqueous solution with strong hydrogen-bonding between the peptide back-bone [130]. The presence of hydrogen bonding means that the β-sheet structures are extremely stable under various physiological conditions and are impermeable to denaturing agents [109]. Alternating hydrophobic and hydrophilic amino acids in the peptide structure form a hydrophobic face and hydrophilic face. The hydrophobic face shields from H_2O so orientates on the inside of the structure whilst the hydrophilic face is exposed to the solvent [129]. This leads to self-assembly in H_2O comparable to how proteins fold *in vivo*. Complementary ionic bonds with regular repeats are present on the hydrophilic surface due to the presence of positively and negatively charged residues [117]. The equal number of positively and negatively charged amino acids introduces electrostatic interactions [130]. The burying of hydrophobic faces and electrostatic interactions are responsible for *β*-sheet structures forming into higher order fibrils and fibres (*figure 2.9*) [132]. Above the critical gelation concentration (CGC) the *β*-sheet forming peptides self-assemble into nanofibres. The fibres entangle together or associate to form a 3D nanofibrous network (the hydrogel) [123]. The SAPH properties are determined by fibre morphology and the network topology [133].

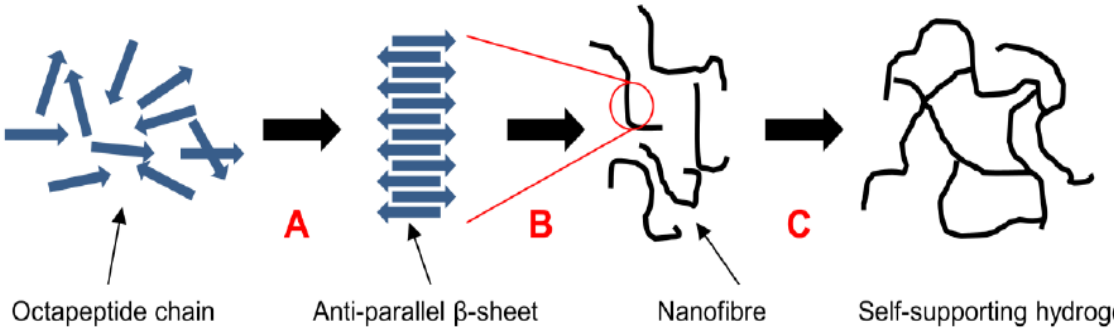

Figure 2.9. The self-assembly and gelation process of β-sheet forming peptides. [A] Peptide chains self-assemble into anti-parallel β-sheets due to chains having a hydrophobic and hydrophilic face. [B] β-sheet fibrils assemble into higher order fibrils and fibres due to burying of hydrophobic faces and electrostatic interactions. [C] Above the critical gelation concentration, nanofibres associate to form a self-supporting nanofibrous hydrogel.

SAPHs are easily modified and readily tuneable for specific applications. For example, by changing one amino acid in the peptide sequence, control over the type of nanofibrous network produced can be achieved. Entangled networks displayed superior mechanical properties to branched networks [109]. Altering peptide charge can also change mechanical properties, for example decreased charge modulus increases the tendency of nanofibres to associate due to increased hydrophobicity [133]. It is also possible to introduce responsiveness to a peptide system by reaction with enzymes during the sol-gel process *via* a reverse hydrolysis mechanism [18, 109]. Various functional motifs and cell-binding sequences can be easily incorporated with the SAPH [9, 134].

2.6.4. FEFEFKFK self-assembling peptide

Taking inspiration from Zhang's research, Saiani *et al.* designed the ionic-complementary sequence **FEFEFKFK** where F is phenylalanine, E is glutamic acid and K is lysine (*figure 2.10*) [123, 130]. The chemical formula is $C_{58}H_{76}N_{10}O_{13}$. Phenylalanine is a hydrophobic amino acid with no charge, glutamic acid is a hydrophilic amino acid with negative charge and lysine is a hydrophilic amino acid with positive charge [109]. FEFEFKFK SAPH melting temperature has been reported at between 45-85^{o}C depending on concentration [123].

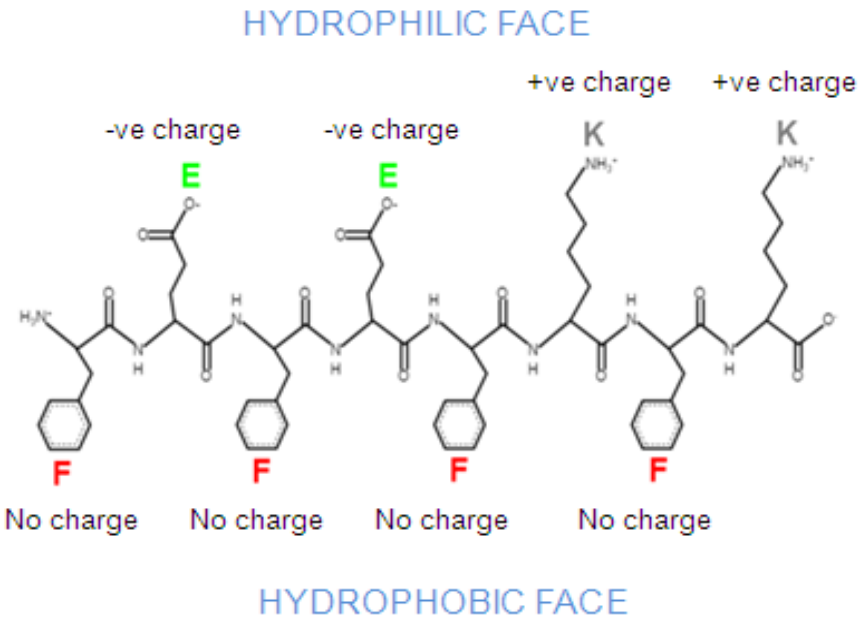

Figure 2.10. Schematic showing the chemical structure of FEFEFKFK octapeptide which was investigated for cell culture for NP tissue engineering in this study. *Peptide structure drawn using PepDraw (http://www.tulane.edu/~biochem/WW/PepDraw/index.html).*

FEFEFKFK SAPH has been investigated as mucoadhesives for topical delivery of drugs and was demonstrated to stiffen when lidocaine was added to the system with no affect on overall peptide release [17]. The study was designed to take advantage of the ease of modification of the peptide system; the release rate of drug could be controlled by manipulating the nature and strength of electrostatic interactions between guest and SAPH [135]. However, drug retention was not favoured due to the drug and peptide carrying the same charges [17]. A number of cell lines have been researched for cell culture applications in SAPHs. When human osteoblasts (HOBs) were encapsulated in the FEFEFKFK SAPH there was evidence of significant proliferation over the 14 day time period with HOBs also producing key osteogenic proteins with mineralisation increasing with time point [136]. Dermal fibroblasts have been demonstrated to proliferate and adopt characteristic stretched morphology when encapsulated in FEFEFKFK SAPHs [18]. Both cell culture studies demonstrated that production protocol modification could tailor the system for a specific application. It was concluded that the FEFEFKFK SAPH was suitable for the culture of HOBs [136] and dermal fibroblasts [18].

The similarity of chondrocytes and NPCs has been highlighted by numerous papers [27, 29]. When the 3D culture of chondrocytes in FEFEFKFK SAPHs was investigated, results demonstrated that cell viability was high over the 21 day period with evidence of cell proliferation. Rounded cell morphology was maintained throughout culture and the cartilage associated ECM component, type II collagen was deposited by encapsulated cells. System strength (10 kPa–35 kPa) was in the desired range for chondrocyte attachment and proliferation [118]. The author concluded that the scaffolds could act as a template for

cartilage tissue engineering [137] therefore it is conceivable that NPC population could also be supported.

2.6.5. Self-assembling peptide gels for nucleus pulposus tissue engineering

A number of recent studies investigated the potential of SAPHs as scaffolds and cell carriers for NP tissue engineering (*table 2.2*). Ma *et al.* and Wang *et al.* functionalised the C-terminus of the RADA-16-I self assembling peptide with the bioactive motif Link N. RADA16-I and RADA-16-Link N were mixed in a 1:1 ratio to produce the 'designer peptide' LN-NS [138, 139]. Link N is the N-terminal segment of the link protein found in both healthy and degenerated native NPs and it plays an important role in regulating IVD cellular functions [141]. When rabbit NCs were cultured in the LN-NS, the scaffolds accumulated more type II collagen and aggrecan in comparison to the positive control of RADA16. It was hypothesised that the bioactive motif might limit the diffusion of large ECM molecules which were then retained to the cytoplasm of cells and pericellular regions in the SAPH. The LN-NS scaffold also significantly promoted NC attachment [138]. Similar results were obtained for the culture of rabbit NPCs in LN-NS SAPH, with increased NPC adhesion, 3D migration and production of ECM components in comparison to RADA16 scaffolds [139].

Neither study investigated the mechanical properties of the LN-NS SAPHs however Wang *et al.* determined that the storage modulus of LN-NS scaffolds was around 5 to 6 kPa [141] within the 5.39 kPa – 20 kPa range quoted modulus of the native NP [39, 111] The ratio of *ACAN* to *COL2A1* produced by encapsulated cells was 1:1 for the LN-NS SAPH whilst the ratio is around 27:1 in the native NP tissue [28]. There was significantly higher gene expression for *COL2A1* compared to *ACAN* by 14 days [138, 139] which suggested that a more fibrous cartilage ECM was being produced than a gelatinous NP ECM.

PKP consisted of the functional group bone morphogenic protein-7 (BMP-7) linked to the C-terminal of RADA16-I. BMP-7 was chosen to functionalise the peptide as it has been shown to stimulate synthesis of PGs and type II collagen. NPCs cultured in the PKP SAPH displayed increased proliferation and migration compared to RADA16-I. There was also higher upregulation of *COL2A1*, *ACAN* and *SOX9* compared to RADA16. Despite promising biocompatibility and bioactivity results, the study did not investigate mechanical properties of the gel [143]. None of the studies found that functionalisation of the peptides inhibited the self-assembly process [138, 139, 143].

NP scaffold peptide sequence	Reference	Mechanical properties	Cell type	Animal study	ECM components	Gene expression
KLD-12	Sun *et al.* 2010 [142]	N/A	Rabbit NPCs	No	Sulphated GAGs & type II collagen	COL2A1 & β-actin upregulation
RAD-RKP	Tao *et al.* 2014 [143]	N/A	Human NPCs	No	N/A	ACAN, COL2A1, SOX9 upregulation
RADA16-I & RADA16-LinkN	Wang *et al.* 2012 [139]	N/A	Rabbit NPCs	No	N/A	ACAN & COL2A1 upregulation
RADA16-I & RADA16-LinkN	Ma *et al.* 2012 [138]	N/A	Rabbit notochordal cells	No	Aggrecan & type II collagen	ACAN & COL2A1 upregulation
RADA16-I & RADA16-LinkN	Wang *et al.* 2014 [141]	5 to 6 kPa	Rabbit BMMSCs	No	Type II collagen	ACAN & COL2A1 upregulation

Table 2.2. Summary of various NP tissue engineering strategies using various SAPHs. The cell line, mechanical properties of the system, gene expression of encapsulated cells and ECM production are listed.

FEFEFKFK SAPH is cheaper to produce than other SAPHs used for NP tissue engineering as it has a shorter amino acid sequence [138, 139, 143]. KLD-12 and LN-NS required the peptide

powder to be dissolved in 10% sucrose solution before cell encapsulation which is not required for FEFEFKFK SAPHs. The sucrose step protects cells from the toxic peptide environment. As a result of the potential that SAPHs have shown for NP tissue engineering in terms of biocompatibility and due to lack of mechanical investigation and absence of research into human cell culture, FEFEFKFK SAPH was considered to be worthwhile for investigation for NP tissue engineering.

2.7. SUMMARY

In conclusion, regenerative medicine is an emerging field that holds great potential for the future of medicine. One area that has received attention is the use of cell-based therapies for the treatment of DDD, a condition which is strongly associated with the globally ubiquitous LBP. DDD occurs when the catabolic and anabolic events in the IVD ECM are disrupted, due to a number of factors, causing dehydration and weakening of the structure leading to a loss of function. Current DDD and LBP treatments are ineffective whilst LBP prevalence is increasing due to an aging population therefore tissue engineering strategies to restore the degenerated IVD tissue are of great interest. SAPHs are regarded to combine the advantages of natural and synthetic biomaterials by having precise control over the manufacture process, being easily modified and having inherent biocompatibility. A *de novo* SAPH, developed by Saiani *et al*. has demonstrated promise as a cell culture system for a number of cell lines and was chosen to investigate as a cell carrier and scaffold for NP tissue engineering.

2.8. REFERENCES

1. **Mason C, Dunnill P** '*A brief definition of regenerative medicine*' Future Medicine (2008); Vol.3 pp.1-5
2. **Atala A** '*Tissue engineering and regenerative medicine: concepts for clinical application*' Rejuvenation Research (2004); Vol.7 pp.15-31
3. **Lanza R** *'Editorial: Tissue engineering; perspectives, challenges and future directions'* Tissue Engineering (2007); Vol.13 No.1 pp.1-2
4. **Nune M, Kumaraswamy P, Krishnan U, Sethuraman S** '*Self-assembling peptide nanofibrous scaffolds for tissue engineering: Novel approaches and strategies for effective functional regeneration*' Current Protein and Peptide Science (2013); Vol.14 pp.70-84
5. **Braun F, Becker T, Renders L, Ringe B** *'Immunosupressive drugs'* eLS John Wiley & Sons (2012); pp1-23
6. **Koh C, Atala A** *'Tissue engineering, stem cells and cloning; opportunities for regenerative medicine'* J Am Soc Nephrol (2004); Vol.15 pp.1113-1125
7. **Burdick J, Mauck R** '*Biomaterials for tissue engineering applications; a review of the past and future trends'* (2011); DOI 10.1007/978-3-7091-0385-2
8. **Chan B, Leong K** '*Scaffolding in tissue engineering: general approaches and tissue-specific considerations*' Eur Spine J (2008); Vol.17 pp.467-479
9. **Zhang S, Yokoi H, Gelain F, Horii A** *'Designer self-assembling peptide nanofibre scaffolds'* Nanotechnology for Biology and Medicine: At the Building Block Level (2012); pp.123-147
10. **Chou A, Reza A, Nicoll S** *'Distinct intervertebral disc cell populations adopt similar phenotype in three-dimensional culture'* Tissue Engineering (2008); Vol.14 No.12 pp.2079-2086
11. **Williams D** *'The Williams Dictionary of Biomaterials'* (1999); ISBN 0-85323-921-5
12. **Engler A, Sen S, Sweeney H, Discher D** '*Matrix elasticity directs stem cell lineage specification'* Cell (2006); Vol.126 pp.677-689
13. **Matson J, Stupp S** *'Self-assembling peptide scaffolds for regenerative medicine'* Chem. Commun. (2012); Vol.48 pp.26-33
14. **Ma P** 'Scaffolds for tissue fabrication' Materials Today (2007); pp.30-40
15. **Collin E, Grad S, Zeugolis D, Vinatier C, Clouet J, Guicheux J, Weiss P, Alini M, Pandit A** *'An injectable vehicle for nucleus pulposus cell-based therapy'* Biomaterials (2011); Vol.32 pp.2862-2870
16. **Nguyen KT, West JL** '*Photopolymerizable hydrogels for tissue engineering applications*' Biomaterials (2002); Vol.23 No.22 pp.4307–4314
17. **Tang C, Miller A, Saiani A** 'Peptide *hydrogels as mucoadhesive for local drug delivery*' International Journal of Pharmaceutics (2014); Vol.465 pp.427-435
18. **Szkolar L, Guilbaud J, Miller A, Gough J, Saiani A** '*Enzymatically triggered peptide hydrogels for 3D cell encapsulation and culture*' J of Peptide Science (2014); Vol.20 pp.578-584
19. **Foss B, Maxwell T, Deng Y** '*Chondroprotective stimulation promotes the mechanical properties of injectable scaffold for human nucleus pulposus tissue engineering*' J of Biomech Materials (2014); Vol.24 pp.56-67
20. **Sakai D, Grad S** '*Advancing the cellular and molecular therapy for intervertebral disc disease*' Advanced Drug Delivery Reviews (2014); Vol.84 pp.159-171
21. **Vadala G, Sowa G, Hubert M, Gilbertson L, Denaro V, Kang J** *'Mesenchymal stem cells injection in degenerated intervertebral disc: cell leakage may induce osteophyte formation'* Journal of Tissue Engineering and Regenerative Medicine (2012); Vol.6 pp.348-355
22. **Humzah M, Soames R** '*Human intervertebral disc: Structure and function*' Antatomical Record (1988); Vol.220 pp.337-356
23. **Roberts S, Menage J, Urban J** '*Biochemical and structural properties of the cartilage end-plate and its relation to the intervertebral disc' Spine(* 1989); Vol.14 pp.166-174.
24. **Raj P** *'Intervertebral disc: Anatomy-Physiology-Pathophysiology-Treatment'* Pain Practise (2007); Vol.8 Iss.1 pp.18-44
25. **Urban J, Roberts S** '*Degeneration of the intervertebral disc*' Arthritis Research & Therapy (2003); Vol.3 pp.120-131
26. **Bayliss M, Johnstone B** *'The lumbar spine and back pain'* Biochemistry of the IVD (1992); Edi.4 pp.111-127
27. **Erwin M** *'The enigma that is the nucleus pulposus cell: The search goes on'* Arthritis Research & Therapy (2010); Vol.12 pp.118-120
28. **Mwale F, Roughley P, Antoniou J** '*Distinction between the extracellular matrix of the nucleus pulposus and hyaline cartilage: A requisite for tissue engineering of intervertebral disc*' European Cells and Materials (2004); Vol.8 pp.58-64

29. **Minogue B, Richardson S, Zeef L, Freemont A, Hoyland J** *'Transcriptional profiling of bovine intervertebral disc cells: implications for identification of normal and degenerate human intervertebral disc cell phenotypes*' Arthritis (2010); Vol.12 pp.1-20
30. **Eyre D, Muir H** *'Quantative analysis of types I and II collagens in the human intervertebral disc at various ages'* Biochimica et Biophysica Acta (1977); Vol.492 pp.29-42
31. **Pereira D, Silva-Correia J, Oliveira J, Reis R** *'Hydrogels in acellular and cellular strategies for intervertebral disc regeneration'* J of Tissue Engineering and Regen Med (2011); Vol.7 pp.85-98
32. **Walker M, Anderson G** *'Molecular basis of intervertebral disc degeneration'* Spine J (2004); Vol.4 pp.158-166
33. **Nerurkar N, Elliot D, Mauck R** *'Mechanics of oriented electrospun nanofibrous scaffolds for annulus fibrosus tissue engineering'* Journal of Orthopaedic Research (2007); pp.1018-1028
34. **Grunhagen T, Wilde G, Soukane D, Shirazi S, Urban J** '*Nutrient supply and intervertebral disc metabolism*' J of Bone and Joint Surgery (2006); Vol.88 pp.30-35
35. **Bogduk N, Tynan W, Wilson A** '*The nerve supply to the human lumbar intervertebral discs*' J Anat (1981); Vol.132 pp.39-56
36. **Freemont A, Peacock T, Goupille P, Hoyland J, O'Brien J, Jayson M** '*Nerve ingrowth into diseased intervertebral disc in chronic back pain*' The Lancet (1997); Vol.350 pp.178-182
37. **Aladin D, Cheung K, Ngan A, Chan D, Leung V, Lim C, Luk K, Lu W** *'Nanostructure of collagen fibrils in human nucleus pulposus and its correlation with macroscale tissue mechanics'* Journal of Orthapaedic Research (2010) – Vol. 28 Iss.4 pp.497-503
38. **Adams M, Roughley P** '*What is intervertebral disc degeneration and what causes it*?' Spine (2006); Vol.31 pp.2151-2161
39. **Cloyd J, Malhotra N, Weng L, Chen W, Mauck R, Elliot D** '*Material properties in unconfined compression of human nucleus pulposus, injectable hyaluronic acid-based hydrogels and tissue engineering scaffolds*' Eur Spine J (2007); Vol.16 pp.1892
40. **Le Maitre C, Freemont A, Hoyland J** '*The role of interleukin-1 in the pathogenesis of human intervertebral disc degeneration*' Arthritis Research & Therapy (2005); Vol.7 No.4 pp.732-744
41. **Horner H, Roberts S, Bielby R, Menage J, Evans H, Urban J** '*Cells from different regions of the intervertebral disc'* Spine (2002); Vol.27 No.10 pp.1018-1028
42. **Le Maitre C, Pockert A, Buttle D, Freemont A, Hoyland J** *'Matrix synthesis and degradation in human intervertebral disc degeneration'* Biochemical Society Transactions (2007); Vol.35 pp.652-656
43. **Le Maitre C, Freemont A, Hoyland J** '*Localization of degradative enzymes and their inhibitors in the degenerate human intervertebral disc'* Journal of Pathology (2004); Vol.204 pp.46-54
44. **Risbud M, Shapiro I** '*Role of cytokines in intervertebral disc degeneration: pain and disc content*' Nature Reviews Rheumatology (2014); Vol.10 pp.44-56
45. **Kobayashi S, Meir A, Urban J** '*Effect of cell density on the rate of glycosaminoglycan accumulation by disc and cartilage cells in vitro*' J of Orthopaedic Research (2008); pp.493-504
46. **Iatridis J, MacLean J, O'Brien M, Stokes I** '*Measurements of proteoglycan and water content distribution in human lumbar intervertebral discs'* Spine (2007); Vol.32 No.14 pp.1493-1497
47. **Hardingham T, Fosang A** *'Proteoglycans: Many forms and functions'* FASEB Journal (1992); Vol.861-870
48. **Lyons G, Eisenstein S, Sweet M** *'Biochemical changes in intervertebral disc degeneration' BBA (1981); Vol.673 pp.443-453*
49. **Melrose J, Smith S, Ghosh P** '*Assessment of the cellular heterogeneity of the ovine intervertebral disc: comparison with synovial fibroblasts and articular chondrocytes*' Eur Spine J (2003); Vol.12 pp.57-65
50. **Maniadakis N, Gray A** '*The economic burden of back pain in the UK*' Pain (2000); Vol.84 pp.95-103
51. **Stewart W, Ricci J, Chee E, Morganstein D, Lipton R** 'Lost productive time and cost due to common pain conditions in the US workforce' JAM (2003); Vol.290 No.18 pp.2443–54
52. **Cheung K, Karppinen J, Chan D, Ho D, Song Y-Q, Sham P, Cheah K, Leong J, Luk K** *'Prevalence and pattern of lumbar magnetic resonance imaging changes in a population study of one thousand forty-three individuals'* Spine (2009); Vol.34 No.9 pp.934-940
53. **Luoma K, Riihiamki H, Luukkonen R, Raininko R, Juntura E, Lamminen A** '*Low back pain in relation to lumbar disc degeneration*' Spine (2000); Vol.25 pp.487-492
54. **Freemont A, Watkins A, Le Maitre C, Jeziorska M, Hoyland J** '*Current understanding of cellular and molecular events in intervertebral disc degeneration: implications for therapy'* Journal of Pathology (2002); Vol.196 Iss.4 pp.374-379
55. **Freburger J, Holmes G, Agans R, Jackman A, Darter J, Wallace A, Castel L, Kalsbeek W, Carey T** '*The rising prevalence of chronic low back pain'* Arch Intern Med (2009); Vol.169 No.3 pp.251-258
56. **Buckwalter J** *'Aging and degeneration of the human intervertebral disc'* Spine (1995); Vol.20 pp.1307-1314

57. **Hudson K, Alimi M, Grunert P, Hartl R, Bonassar L** '*Recent advances in biological therapies for disc degeneration: tissue engineering of the annulus fibrosus, nucleus pulposus and whole intervertebral disc*' Biotechnology (2013); Vol.24 pp.1-8
58. **Ciapetti G, Granchi D, Devescovi V, Leonardi E, Greggi T, Silvestre M, Baldini N** *'Ex vivo observation of human intervertebral disc tissue and cells isolated from degenerated intervertebral discs'* Eur Spine J (2012); Vol.21 pp.10-19
59. **Park J, Chang H, Kim K** '*Expression of Fas Ligand and apoptosis of disc cells in herniated lumbar disc tissue*' Spine (2001); Vol.26 No.6 pp.618-621
60. **Johnson W, Stephan S, Roberts S** '*The influence of serum, glucose and oxygen on intervertebral disc cell growth in vitro: Implications for degenerative disc disease*' Arthritis Res Ther (2008); Vol.10 pp.1-8
61. **Ding F, Shao Z, Xiong L** '*Cell death in intervertebral disc degeneration*' Apoptosis (2013); Vol.18 pp.777-785
62. **Schoenfeld A, Weiner B** '*Treatment of lumbar disc herniation: Evidence-based practise*' International J of General Medicine (2010); Vol.3 pp.209-214
63. **Boos N, Rieder R, Schade V, Spratt K, Semmer N, Aebi** '*1995 Volvo Award clinical sciences. The diagnostic accuracy of magnetic resonance imaging, work perception and psychosocial factors in identifying symptomatic disc herniations*' Spine (1995); Vol.20 No.24 pp.2613-25
64. **Maeda S, Kokubun S** '*Changes with age in proteoglycan synthesis in cells cultured in vitro from the inner and outer rabbit annulus fibrosus'* Spine (2000); Vol.25 No.2 pp.166-169
65. **Goupille P, Jayson M, Valat J, Freemont A** '*Matrix Metalloproteinases; The clue to intervertebral disc degeneration?'* Spine (1998); Vol.23 pp.1612-1626
66. **Zhao C, Zhang Y, Jiang S, Li H, Jiang L, Dai L** '*ADAMTS-5 and intervertebral disc degeneration: the results of tissue immunohistochemistry and in vitro cell culture'* J of Orthopaedic Research (2010); Vol.29 pp.718-725
67. **Kang J, Stefanovic-Racic M, McIntyre L, Georgescu H, Evans C** '*Toward a biochemical understanding of human intervertebral disc degeneration and herniation. Contributions of nitric oxide, interleukins, prostaglandin E2, and matrix metalloproteinases*' Spine (1997); Vol.22 pp.1065–1073
68. **Zhao C, Zhang Y, Jiang S, Li H, Jiang L, Dai L** '*ADAMTS-5 and intervertebral disc degeneration: the results of tissue immunohistochemistry and in vitro cell culture'* J of Orthopaedic Research (2010); Vol.29 pp.718-725
69. **Antoniou J, Steffen T, Nelson F, Winterbottom N, Hollander A, Poole A, Aebi M, Alini M** '*The human lumbar intervertebral disc: evidence for changes in the biosynthesis and denaturation of the extracellular matrix with growth, maturation, ageing, and degeneration' J Clin Invest (*1996); Vol.98 pp.996-1003.
70. **Kandel R, Roberts S, Urban J** '*Tissue engineering and the intervertebral disc: the challenges*' Eur Spine J (2008); Vol.17 pp.480-491
71. **Sambrook P, MacGregor A, Spector T** '*Genetic influences on cervical and lumbar disc degeneration: a magnetic resonance imaging study in twins*' *Arthritis Rheum (*1999) Vol.42 pp.366-372.
72. **Matsui H, Kanamori M, Ishihara H, Yudoh K, Naruse Y, Tsuji H** '*Familial predisposition for lumbar degenerative disc disease. A case-control study*' *Spine (*1998). Vol.23 pp.1029-1034.
73. **Annunen S, Paassilta P, Lohiniva J, Perala M, Pihlajamaa T, Karppinen J , Tervonen O, Kroger H, Lahde S, Vanharanta H, Ryhanen L, Goring HH, Ott J, Prockop DJ, Ala-Kokko L** '*An allele of COL9A2 associated with intervertebral disc disease*' Science (1999); Vol.285 pp. 409-412
74. **Williams F, Bansal A, Meurs J, Bell J, Meulenbelt I, Suri P, Rivadeneira, Sambrook P, Hofman A, Bierma-Zeinstra S, Menni C, Kloppenburg M, Slagboom P, Hunter D, MacGregor, Uitterlinden A, Spector T** *'Novel genetic variants associated with lumbar disc degeneration in northern Europeans: a meta-analysis of 4600 subjects'* Clinical and epidemiological research (2012); doi:10.1136/annrheumdis-2012-201551
75. **Indahl A** *'Low back pain: diagnosis, treatment and prognosis'* Acta Orthop Scand Suppl (2004); Vol.73 pp.20-25
76. **Andersson G** '*Epidemiological features of chronic low-back pain*' Lancet (1999); Vol.354 pp.581-85
77. **Keller A, Hayden J, Bombardier C, van Tulder M** '*Effect sizes of non-surgical treatments of non-specific low-back pain'* Eur Spine J (2007); Vol.16 pp.1776-1788
78. **Malmivaara A, Hakkinen U, Aro T, Heinrichs M, Koskenniemi L, Kuosma E, Lappi S, Paloheimo R, Servo C, Vaaranen V, Hernberg S** *'The treatment of acute low back pain – bed rest, exercises or ordinary activity'* New England Journal of Medicine (1995); Vol.332 No.6 pp.351-355
79. **Park P, Garton H, Gala V, Hoff J, McGillicuddy J** *'Adjacent segment disease after lumbar or lumbosacral fusion: review of literature'* Spine (2004); Vol.29 p.1938

80. **Feng G, Zhang Z, Jin X, Hu J, Gupte M, Holzwarth J, Ma P** '*Regenerating nucleus pulposus of the intervertebral disc using biodegradable nanofibrous polymer scaffold*' Tissue Engineering (2012); Vol.18 No.21 pp.1-8
81. **Yajun W, Yue Z, Xiuxin H, Cui C** '*A meta-analysis of artificial total disc replacement versus fusion for lumbar degenerative disc disease*' Eur Spine J (2010); Vol.19 pp.1250-1261
82. **Clarke L, McConnell J, Sherratt M, Derby B, Richardson S, Hoyland J** *'Growth differentiation factor 6 and transforming growth factor-beta differentially mediate mesenchymal stem cell differentiation, composition, and micromechanical properties of nucleus pulposus constructs'* Arthritis & Research (2014); Vol.16 pp.1-13
83. **Gilbert H, Hoyland J, Richardson S** '*Stem cell regeneration of degenerated intervertebral discs: Current status*' Curr Pain Headache Rep (2013); Vol.17 pp.1-9
84. **Orozco L, Soler R, Morena C, Alberca M, Sanchez A, Sancho J** *'Intervertebral disc repair by autologous mesenchymal bone marrow cells: A pilot study'* Clinical and Translational Research (2011); Vol.92 pp.822-829
85. **Masuda K, Oegema T, An H** '*Growth factor and treatment of intervertebral disc degeneration*' Spine (2004); Vol.29 pp.2757-2769
86. **Meisel H, Siodla V, Ganey T, Minkus Y, Hutton W, Alasevic O** '*Clinical experience in cell-based therapeutics: disc chondrocyte transplantation a treatment for degenerated or damaged intervertebral disc*' Biomolecular Engineering (2007); Vol.24 pp.5-21
87. **Coric D, Pettine K, Sumich A, Boltes M** '*Prospective study of disc repair with allogenic chondrocytes*' J Neurosurg Spine (2013); Vol.18 pp.85-95
88. **Ludwinski F, Gnanalingham K, Richardson S, Hoyland J** '*Understanding the native nucleus pulposus cell phenotype has important implications for intervertebral disc regeneration strategies*' Regenerative Medicine (2013); Vol.8 pp.75-87
89. **Wuertz K, Godburn K, Neidlinger-Wilke C, Urban J, Iatridis J** '*Behavoir of mesenchymal stem cells in the chemical microenvironment of the intervertebral disc'* Spine (2008); Vol.33 No.17 pp.1843-1849
90. **Minguell J, Erices A, Conget P** *'Mesenchymal stem cells'* Experimental Biology and Medicine (2001); Vol.226 pp.507-520
91. **Yamamoto Y, Mochida J, Sakai D, Nakai T, Nishimura K, Kawada H, Hotta *T*** *'Upregulation of the viability of nucleus pulposus cells by bone marrow-derived stromal cells'* Spine (2004); Vol.29 No.14 pp.1508-1515
92. **Richardson S, Walker R, Parker S, Rhodes N, Hunt J, Freemont A, Hoyland J** *'Intervertebral disc cell-mediated mesenchymal stem cell differentiation'* Stem Cells (2006); Vol.24 pp.707-716
93. **Tao F, Li F, Li G, Pan F** *'Differentiation of mesenchymal stem cells into nucleus pulposus cells in vitro'* J of Huazhong University of Science and Technology (2008); Vol.28 Iss.2 pp.156-158
94. **Lewis G** '*Nucleus pulposus replacement and regeneration / repair technologies: Present status and future prospects*' J Biomed Mater Re (2012); Vol.100 pp.1702-1720
95. **Walsh A, Bradford D, Lotz J** '*In vivo growth factor treatment of degenerated intervertebral discs*' Spine (2004); Vol.29 No.2 pp.156-163
96. **Johnson W, Wooton A, Haj A, Eisenstein S, Curtis A, Roberts S** '*Topographical guidance of intervertebral disc cell growth in vitro: towards the development of tissue repair strategies for the annulus fibrosus'* Eur Spine J (2006); Vol.15 Sup.3 pp.389-396
97. **Francisco A, Mancino R, Bowles R, Brunger J, Tainter D, Chen Y, Richardson W, Guilak F, Setton L** *'Injectable laminin-functionalised hydrogel for nucleus pulposus regeneration'* Biomaterials (2013); Vol.34 pp.7381-7388
98. **Sakai D, Mochida J, Iwashina T, Watanabe T, Nakai T, Ando K, Hotta T** '*Differentiation of mesenchymal stem cells transplanted into a rabbit degenerative disc model*' Spine (2005); Vol.30 No.21 pp.2379-2387
99. **Hiyama A, Mochida J, Iwashina T, Omi H, Watanabe T, Serigano K, Tamura F, Sakai D** '*Transplantation of mesenchymal stem cells in a canine disc degeneration model*' Journal of Orthopaedic Research (2008); Vol.26 no.5 pp.589–600
100. **Yoshikawa T, Ueda Y, Miyazaki K, Koizumi M, Takakura Y** *'Disc regenertation therapy using marrow mesenchymal stem cell transplantation'* Spine (2010); Vol.35 pp.475-480
101. **Fairbank J, Pynsent P** *'The Oswestry Disability Index'* Spine (2000); Vol.25 No.22 pp.2940-2952
102. **Nesti L, Li W, Shanti R, Jiang Y, Jackson W, Freedman B, Kuklo T, Giuliana J, Tuan R** '*Intervertebral disc tissue engineering using a novel hyaluronic acid-nanofibrous scaffold amalgam*' Tissue Engineering (2008); Vol.14 No.9 pp.1527-1537
103. **Mizuno H, Roy A, Zaporojan V, Vacanti C, Ueda M, Bonassar L** *'Biomechanical and biochemical characterization of composite tissue engineered intervertebral discs'* Biomaterials (2006); Vol.27 pp.362-370

104. **Gebhard H, Bowles R, Dyke J, Saleh T, Doty S, Bonassar L, Hart R** '*Total disc replacement using a tissue-engineered intervertebral disc in vivo: new animal model and initial results*' Spine Care (2010); Vol.1 pp.62-66
105. **Chou A, Nicoll S** *'Characterisation of photocrosslinked alginate hydrogels for nucleus pulposus cell encapsulation'* Wiley InterScience (2009) – pp.187-195
106. **Frith J, Cameron A, Menzies D, Ghosh P, Whitehead D, Gronthos S, Zannettino A, White J** '*An injectable hydrogel incorporating mesenchymal precursor cells and pentosan polysulphate for intervertebral disc regeneration'* Biomaterials (2013); Vol.34 pp.9430-9440
107. **Yang S, Wu C, Shih T, Chen P, Lin F** '*Three dimensional culture of human nucleus pulposus cells in fibrin clot: Comparisons on cellular proliferation and matrix synthesis with cells in alginate*' Artif Organs (2007); Vol.32 pp.70-73
108. **Calderon L, Collin E, Velasco-Bayon D, Murphy M, O'Halloran D, Pandit A** *'Type II collagen-hyaluronan hydrogel- a step towards a scaffold for intervertebral disc tissue engineering'* European Cells and Materials (2010); Vol.20 pp.134-1487
109. **Li Z, Kaplan K, Wertzel A, Peroglio M, Amit M, Grad S, Yayon A** '*Biomimetic fibrin-hyaluronan hydrogels for nucleus pulposus regeneration'* Regenerative Medicine (2014); Vol.9 pp.309-326
110. **Miller A, Saiani A** '*Engineering peptide based biomaterials: Structure, properties and application'* Chemistry Today (2010); Vol.28 No.1 pp.34-38
111. **Milani A, Freemont A, Hoyland J, Adlam D, Saunders B** '*Injectable doubly cross linked microgel for improving the mechanical properties of degenerated intervertebral discs*' Biomacromolecules (2012); Vol.13 pp.2793-2801
112. **Iatridis J, Setton L, Weidenbaum M, Mow V** '*The viscoelastic behaviour of the non-degenerate human lumbar nucleus pulposus in shear'* J Biomechanics (1997); Vol.30 No.10 pp.1005-1013
113. **Cheng Y, Yang S, Su W, Chen Y, Yang K, Cheng W, Wu S, Lin F** *'Thermosensitive chitosan-gelatin-glycerol phosphate hydrogels as a cell carrier for nucleus pulposus regeneration'* Tissue Engineering (2009); pp.1-10
114. **Kim D, Martin J, Elliott D, Smith L, Mauck R** 'Phenotypic stability, matrix elaboration and functional maturation of nucleus pulposus cells encapsulated in photocrosslinkable hyaluronic acid hydrogels' Acta Biomaterialia (2015); Vol.12 pp.21-29
115. **Fraylich M, Liu R, Richardson S, Baird P, Hoyland J, Freemont A, Alexander C, Shaesheff K, Cellesi F, Saunders B** *'Thermally-triggered gelation of PLGA dispersions: Towards an injectable colloidal cell delivery system'* Journal of Colloid and Interface Science (2010) – Iss.344 pp.61-69
116. **Whitesides G, Grzybowski B** '*Self-assembly at all scales*' Science (2002); Vol.295 pp.2418-2421
117. **Maude S, Tai L, R Davies, Liu B, Harris S, Kocienski P, Aggeli A** *'Peptide synthesis and self-assembly'* Top. Curr. Chem. (2011); Vol.310 pp.27-69
118. **Zhang S** *'Fabrication of novel biomaterials through molecular self-assembly'* Nature Biotechnology (2003); Vol.21 No.10 pp.1171-1178
119. **Jayawarna V, Ali M, Jowitt T, Miller A, Saiani A, Gough J, Ulijn R** '*Nanostructured hydrogels for 3D cell culture though self-assembly of fluorenylmethoxycarbonyl-dipeptides'* Advanced Materials (2006); Vol.18 pp.611-614
120. **Nelson D, Cox M** '*Lehninger Principles Of Biochemistry'* Fourth Edition (2005); Chapter 3-4.
121. **Lou Z, Zhao X, Zhang S** *'Self-organisation of a chiral D-EAK16 designer peptide into a 3D nanofiber scaffold'* Macromol. Biosci (2008); Vol.8 pp.785-791
122. **Eisenhaber F, Persson B, Argos P** '*Protein structure prediction: Recognition of primary, secondary and tertiary structural features from amino acid sequence*' Biochemistry and Molecular Biology (1995); Vol.30 pp.1-94
123. **Smith A, Williams R, Tang C, Coppo P, Collins R, Turner M, Saiani A, Uljin R** '*Fmoc-Diphenylalanine self assembles to a hydrogel via a novel architecture based on π-π interlocked β-Sheets*' Advanced Materials (2007); Vol.20 pp.37-41
124. **Saiani A, Mohammed A, Frielinghaus N, Collins R, Hodson N, Kielty C, Sherratt M, Miller A** *'Self-assembly and gelation properties of α-helix versus β-sheet forming peptides'* Soft Matter (2009); Vol.4 pp.193-202
125. **Hartgerink J, Beniash E, Stupp S** *'Self-assembly and mineralisation of peptide-amphiphile nanofibers'* Science (2001); Vol.294 pp.1684-1688
126. **Tsutsumi H, Mihara H** '*Soft materials based on designed self-assembling peptides: from design to application*' Molecular Biosystems (2013); Vol.9 pp.609-617
127. **Banwell E, Abelardo E, Adams D, Birchall M, Corrigan A, Donald A, Kirkland M, Serpell L, Butler M, Woolfson D** '*Rational design and application of responsive α-helical peptide hydrogels*' Nature Materials (2009); Vol.8 pp.596-600
128. **Kretsinger J, Haines L, Ozbas B, Pochan D, Schneider J** *'Cytocompatability of self-assembled β-hairpin peptide hydrogel surfaces'* Biomaterials (2005) – Vol.26 pp.5177-5186

129. **Zhang S, Holmes T, Lockshin C, Rich A** *'Spontaneous assembly of a self-complementary oligopeptide to form a stable macroscopic membrane'* Embo Journal (1993); Vol.11 pp.3787-3796
130. **Caplan M, Schwartzfarb E, Zhang S, Kamm R, Lauffenburger D** *'Control of self-assembling oligopeptide matrix formation through systemic varation of amino acid sequence'* Biomaterials (2002); Vol.23 pp.219-227
131. **Boothroyd S, Saiani A, Miller A** *'Formation of mixed ionic complementary peptide fibrils'* Macromol Symp (2008); Vol.273 pp.139-145
132. **Aggeli A, Bell M, Carrick L, Fishwick C, Harding R, Mawer P, Radford S, Strong A, Boden N** '*pH as a trigger of peptide β-sheet self assembly and reversible switching between nematic and isotrophic phases*' J Am Chem Soc (2003); Vol.125 pp.9619-9628
133. **Aggeli A, Nyrkova I, Bell M, Harding R, Carrick L, McLeish T, Semenov A, Boden N** '*Hierarchical self-assembly of chiral rod-like molecules as a model for peptide β-sheet tapes, ribbons, fibrils and fibres*' PNAS (2001); Vol.98 pp.11857-11862
134. **Boothroyd S, Miller A, Saiani A** '*From fibres to networks using self-assembling peptides*' Royal Society of Chemistry (2013); Vol.166 pp.195-207
135. **Horii A, Wang X, Gelain F, Zhang S** '*Biological designer self-assembling peptide nanofibre scaffolds significantly enhance osteoblast proliferation, differentiation and 3D cell migration'* PLoS ONE (2007); Iss.2 pp.1-9
136. **Roberts D, Rochas C, Saiani A, Miller A** '*Effect of peptide and guest charge on the structural, mechanical and release properties of β-sheet forming peptides*' American Chemical Society (2012); Vol.28 pp.16196-16206
137. **Diaz L, Saiani A, Gough J, Miller A** '*Human osteoblasts within soft peptide hydrogels promote mineralisation in vitro*' J of Tissue Engineering (2014); Vol.5 pp.1-12
138. **Mujeeb A, Miller A, Saiani A, Gough J** *'Self-assembled octapeptide scaffolds for in vitro chondrocyte culture'* Acta Biomaterialia (2012); Vol.9 Iss.1 pp.4609-4619
139. **Ma K, Wu Y, Wang B, Yang S, Wei Y, Shao Z** *'Effect of a synthetic link N peptide nanofiber scaffold on the matrix deposition of aggrecan and type II collagen in rabbit notochordal cells'* J Mater Sci (2012); pp.1-11
140. **Wang B, Wu Y, Shao Z, Yang S, Che B, Sun C, Ma Z, Zhang Y** *'Functionalized self-assembling peptide nanofiber hydrogel as a scaffold for rabbit nucleus pulposus cells'* Journal of Biomedical Materials Research (2012); Vol.100 Iss.3 pp.643-653
141. **Mwale F, Masuda K, Pichika R, Epure LM Yoshikawa T, Hemmad A, Roughley P** ' *The efficacy of Link N as a mediator of repair in a rabbit model of intervertebral disc degeneration*' J Arthritis Res Ther (2011); Vol.13 pp.2120
142. **Wang B, Sun C, Shao Z, Yang S, Che B, Wu Q, Liu J** 'Designer self-assembling peptide nanofibre scaffolds containg link protein N-terminal peptide to induce chondrogenesis of rabbit bone marrow stem cells' Biomed Research (2014); pp.1-10
143. **Sun J, Zheng Q, Wu Y, Liu Y, Guo X, Wu W** *'Culture of nucleus pulposus cells from intervertebral disc on self-assembling KLD 12 peptide hydrogel scaffold'* Materials Science and Engineering (2010); Vol.30 pp975-980
144. **Tao H, Zhang Y, Wang C, Zhang C, Wang X, Wang D, Bai X, Wen T, Xin H, Wu J, Liu Y, He Q, Ruan D** 'Biological evaluation of human degenerated nucleus pulposus cells in functionalised self-assembling peptide nanofibre hydrogel scaffold' Tissue Engineering (2014); Vol.20 pp.1621-1722

Chapter 3. *Materials & methods.*

3.1. MATERIALS

3.1. Raw materials

All experiments were carried out with FEFEFKFK peptide powder batch number LR294429 (*Biomatik, USA*). There was slight difference in powder appearance between lot numbers however this did not affect gelation or final SAPH significantly. The purity of the compounds (>95%) was checked at the site using mass spectrometry and results were sent alongside the order.

3.2. Sample preparation

Pre-determined amount of FEFEFKFK peptide powder was suspended in dH_2O (*table 3.1*). The suspension was incubated at 80ºC for 3 hours to aid complete dissolution. The desired amount of 1M sodium hydroxide (NaOH) was added to induce gelation and increase pH of the solution. To further assist gelation, due to presence of salt ions, and increase mechanical properties of the SAPH, 100 µl of 10x Dulbecco's phosphate buffered solution (DPBS) (*HyClone, USA*) was added. Heating at 80ºC for 12 hours, a vortexing step then cooling to room temperature (RT) ensured a homogenous and clear hydrogel was produced. SAPHs were tested with a S20 SevenEasy™ pH meter (*Mettler Toledo, UK*); the optimal pH range was 9.3 to 9.6. SAPHs were UV sterilised for 30 minutes in a MSC-Advantage™ Class II Biological Safety Cabinet (*Thermo Scientific, USA*) before cell seeding.

Final SAPH concentration / mg ml^{-1}	*Peptide powder / mg*	*dH_2O / µl*	*1M NaOH / µl*	*10x DPBS / µl*
25	31.25	811	89	100
30	37.5	802	98	100
35	43.75	786	114	100

Table 3.1. The various volumes and constituent amounts required to produce 25, 30 and 35 mg ml^{-1} SAPH.

Note. 250 µl of cell suspension with the appropriate cell density was added to the SAPHs at the seeding stage therefore the final total volume was 1.25 ml which explains the higher amount of peptide powder initially weighed (x1.25 final gel concentration).

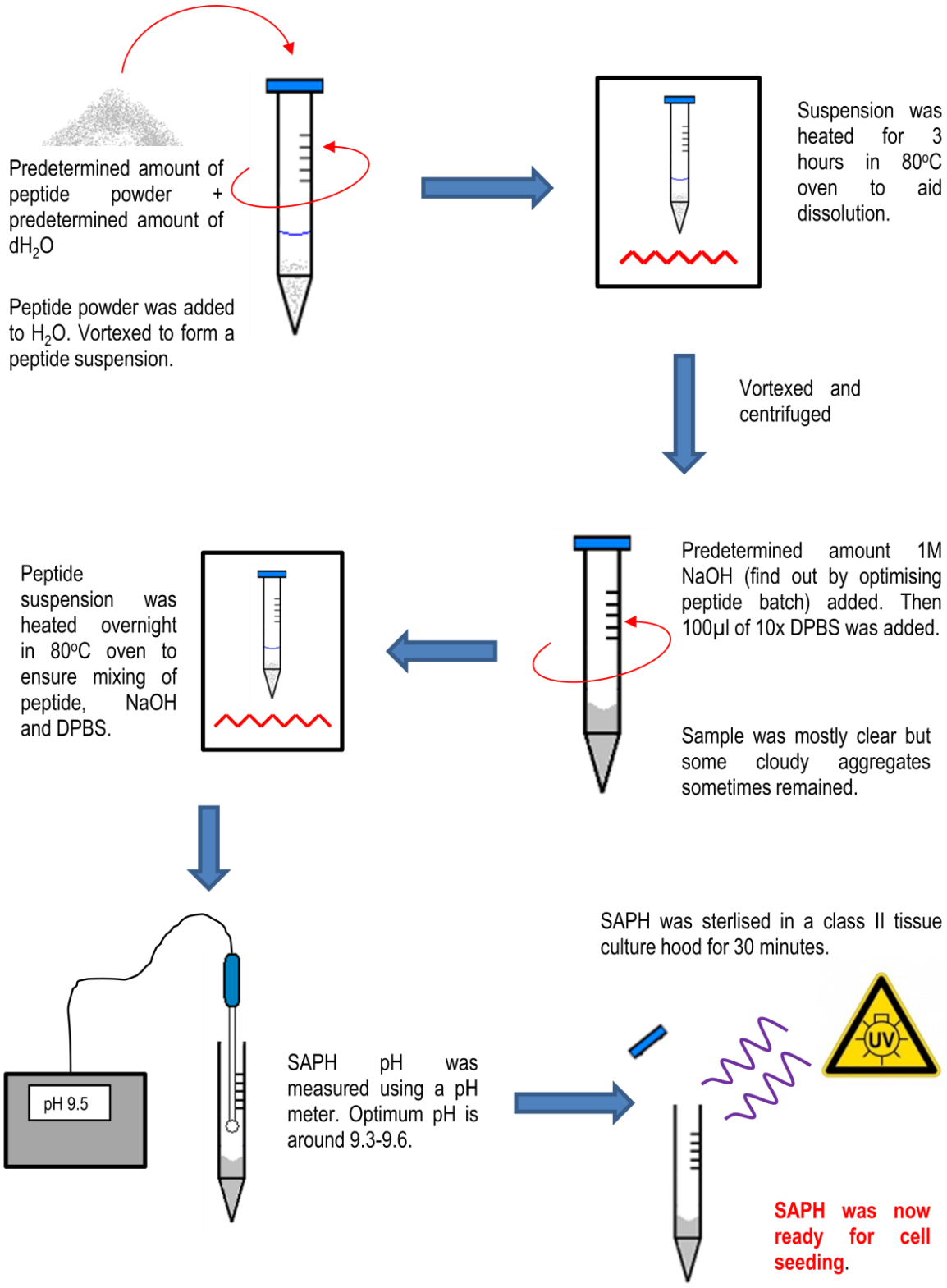

Figure 3.1. A step-by-step schematic for the FEFEFKFK SAPH production protocol. *Table 3.1* denotes the various amounts of peptide powder, dH_2O and 1M NaOH required to produce 25, 30 and 35 mg ml^{-1} FEFEFKFK SAPHs.

3.2. METHODS – CHARACTERISATION

3.2.1. Fourier transform infrared spectroscopy (FT-IR)

3.2.1.1. Theory

Atoms in a molecule oscillate around an equilibrium position causing variation in bond length and angle. Oscillation frequencies are within the infrared (IR) spectrum (700 nm to 1 mm) therefore radiation in the energy region can excite vibrational motions [1]. The radiation must cause a change in dipole moments of the bonds for IR absorption. When the applied IR frequency is equal to the chemical bonds' natural frequency of vibration then absorption and transfer of energy occurs, producing a peak.

Functional groups produce vibrational bands at characteristic frequency ranges. Therefore, FT-IR can be used to analyse peptide structures due to amide bonds absorbing IR radiation at particular frequencies. Various peptide secondary structure peak ranges when in heavy water (D_2O) include α-helix (1647-1654 cm^{-1}), parallel β-sheet (1615-1660 cm^{-1}) and anti-parallel β-sheet (1628-1635 cm^{-1}) [2].

3.2.1.2. Experimental procedure

SAPH samples were prepared in D_2O as H_2O has a large absorption peak. FT-IR spectra were collected on a Thermo Nicolet 5700 spectrometer (*Thermo Scientific, USA*) equipped with a ZnSe crystal trough plate. The SAPH was spread evenly on the plate and scanned between 1000 and 2000 cm^{-1} over 512 scans with a resolution of 4 cm^{-1}. An air and D_2O sample were used as background and subtracted from all spectra. The software used was Omnic version 7.2 (*Thermo Electron Corporation, USA*).

3.2.2. Atomic force microscopy (AFM)

3.2.2.1. Theory

AFM is a high resolution and magnification scanning probe technique used to produce 3D images of a sample. It measures the attractive and repulsive forces between a sharp tip attached to a flexible cantilever and the sample surface (*figure 3.2*) [3]. A feedback system reflects a laser off the cantilever and the reflected laser is then collected by a photodiode to detect the amount of deflection. Piezoelectric transducers control the probe motion as it scans a surface [4].

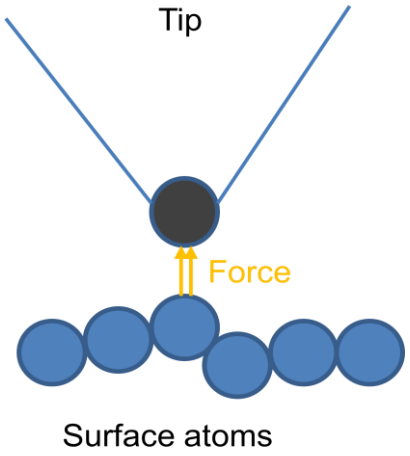

Figure 3.2. Schematic representation of the AFM principle. The tip scans the surface and maintains constant force between itself and the sample. *Adapted from [3].*

When the tip approaches the surface, it enters the attractive regime and is pulled towards the surface due to Van der Waals forces. When the tip comes into very close proximity to the surface, the tip is repulsed by short range Coulomb interactions (*figure 3.3*) [5].

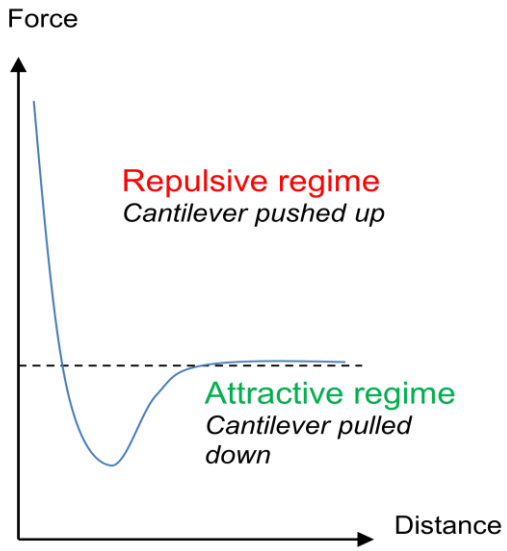

Figure 3.3. Graph plotting the interatomic force against the distance between tip and sample during AFM procedure. *Adapted from [4].*

Contact mode can damage the sample surface and image data may be distorted. For non-contact mode, the tip to sample interaction is minimal. The tip is oscillated at the resonance frequency whilst the amplitude of the oscillation is kept consistent [4] which produces low resolution images and the oscillating tip can be hindered by any surface contaminants. In tapping mode, the fast oscillating probe only contacts the sample for minimal amounts of time, reducing damage [6]. It overcomes the disadvantages of contact and non-contact mode by eliminating frictional forces via only intermittently contacting the surface and oscillating with

sufficient amplitude to avoid the tip being trapped by meniscus forces that could occur from the contaminant layer.

3.2.2.2. Experimental procedure

A 120 µl aliquot of SAPH (0.25 mg ml^{-1} and 30 mg ml^{-1}) was deposited onto a freshly cleaved mica surface (*AgarScientific, UK*). Samples were allowed to evaporate then the surfaces were washed twice with 1 ml of *d*H_2O. OTESPA visible apex tips (tip height 7-15 µm) with a nominal spring constant of 42N m^{-1} (*Bruker, USA*) were used for imaging with a Multimode Nanoscope IIIa Controller (*Bruker, USA*). The silicon cantilever had a rectangular cantilever with a reflective aluminium back side coating. Samples were imaged using tapping mode. Cantilever oscillation ranged from 300 to 350 kHz and the amplitude was determined using Nanoscope v5.3 software. Height, amplitude and phase micrographs were taken at a scan rate of 1.97 Hz with micrograph sizes of 5 μm^2 and 2 μm^2. Height data was first flattened and structural dimensions were measured using WSxM 4.0 (*www.nanotech.es*) software.

3.2.3. Oscillatory Rheology

3.2.3.1. Theory

Rheology is the study of deformation and flow of matter [7, 8]. Elastic properties are a characteristic of solid materials whilst viscosity is characteristic of liquid materials. Elastic solids obey Hooke's law ($\sigma = G \gamma$) (σ is stress, G is the shear modulus, γ is strain) whilst viscous (η) fluids obey Newton's law ($\sigma = \eta \gamma$). Most soft materials, like hydrogels, are viscoelastic as they have both elastic and viscous properties [9].

The basic principle of oscillatory rheology is to induce sinusoidal shear deformation in the sample with the resulting stress response analysed typically as a function of time. During an experiment, the top plate rotates whilst the stage is fixed (*figure 3.4*). A time-dependant γ ($\gamma(t) = \gamma.\sin(\omega t)$) is imposed on a sample and the time-dependent σ is quantified by measuring the torque that the sample produces on the stationary stage [9]. The storage modulus (G') measures the deformation energy stored during the shear process of the sample. The loss modulus (G'') is the amount of energy dissipated during shear. The linear viscoelastic region (LVR) of a material is where the measured properties are independent of the γ [7].

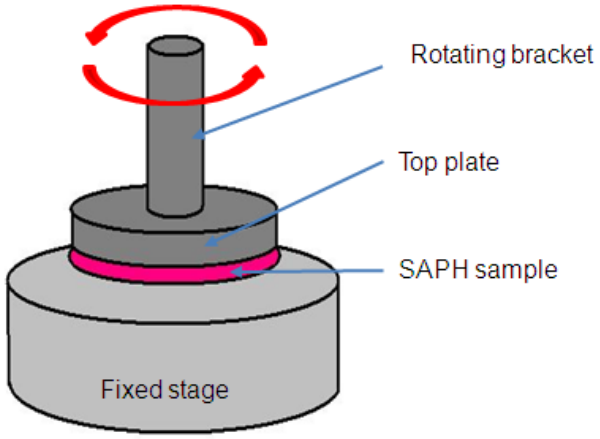

Figure 3.4. Schematic representation of oscillatory rheology set-up. The SAPH sample is placed between the top plate and stage where a sinusoidal shear deformation is induced.

3.2.3.2. Experimental procedure

The viscoelastic behaviour and mechanical properties of SAPH were determined using strain, shear rate and frequency sweeps. The AR-G2 rheometer (*TA Instruments, USA*) was set to oscillatory mode then 150 µl of SAPH was loaded onto the stage and the upper plate was lowered to a 0.25 mm gap. A strain amplitude sweep was performed at constant frequency (1 Hz) between 0.01 to 100% strain to determine the LVR. G' and G'' modulus was recorded at 1% strain between 0.1 and 100 Hz for a frequency sweep. For viscosity measurements, the rheometer was set to flow mode. Viscosity of the samples was measured as a function of shear rate between 10 to 1000 rad s^{-1}. A recovery cycle experiment, designed to mimic the injection process, involved breaking the SAPH by applying 160% strain, to simulate the system being forced through a small bore needle, after which the strain was reduced to 1%. A solvent trap was used to prevent sample dehydration during all experiments. All experiments, with and without cells, were performed at 37ºC.

3.3. METHODS – CELL CULTURE

3.3.1. Culture of primary bovine nucleus pulposus cells

Primary bovine nucleus pulposus cells (bNPCs) were isolated from the tail of a young adult bovine (18 to 36 months) purchased from a local abattoir. Isolation of bNPCs was carried out by the Richardson laboratory and provided to this study. All the appropriate COSHH Assessment Forms were completed, signed and approved by all applicable staff members.

3.3.1.1. Cell culture medium

Dulbecco's modified Eagle's medium (DMEM) containing 4500 mg L^{-1} D-glucose, 110 mg sodium pyruvate and L-glutamine (*Sigma-Aldrich, USA*) stimulated with 10% foetal bovine serum (FBS) (*Gibco Invitrogen, UK*) and 1% penicillin-streptomycin (*Gibco Invitrogen, UK*) was used for cell culture.

3.3.1.2. Cell culture

For cryopreservation, bNPCs were suspended in 1 part DMSO to 9 parts FBS. Freezing vials were stored in isoproponal chambers at -80^{o}C for 12 hours then transferred to cryostorage. For cell revival, freezing vials containing P3 $5x10^5$ bNPCs ml^{-1} were removed from the cryostore and defrosted. Cell suspension was spun at 1500 rpm for 5 minutes using a Rotofix 32A centrifuge (*Hettich, Germany*). The supernatant was removed and the cell pellet was re-suspended in 3 mls of fresh media. The cell suspension was then transferred to a tissue culture flask (75cm^2) and 15 mls of fresh media was added. Cells were incubated at 37^{o}C in humidified atmosphere (20% O_2, 5% CO_2). Passage 4 to 6 bNPCs were used for experiments.

3.3.1.3. Cell count

At 70-80% confluence, bNPCs were rinsed with 1xDPBS (*Sigma-Aldrich, USA*) then incubated at 37^{o}C with 1 ml of 0.05% trypsin-EDTA.4Na (0.53 mM) (*PAA, Austria*) until cells had fully detached. Fresh media was added to inhibit the action of the trypsin then the cell suspension was centrifuged at 1500 rpm for 5 minutes. The supernatant was removed and the cell pellet was re-suspended in 3 mls of fresh media. Total cell number was estimated using C-Chip haemocytometers (*HYPO$_2$XYGEN, USA*) and a Leica DMIL light microscope (*Leica Microsystems, Germany*). Cell seeding density was $2x10^5$ bNPCs ml^{-1} of SAPH. 100 µl of cell suspension was added to 100 µl of 0.4% trypan blue. 10 µl of stained cell suspension was added to a C-Chip haemocytometer. Stained bNPCs in 3 grids, each representing a volume of $1x10^{-7}$ m^3, were counted. Total cell number in original cell suspension was calculated using below equation:

Total cells = average cell number from cell count x dilution factor x ($1x10^4$) x original cell suspension volume

3.3.1.4. Seeding of SAPHs for 2D culture

450 µl of SAPH was pipetted into a 24 cell culture well plate (*Greiner Bio-One, UK*) (*figure 3.5*). For migration tests, 200 µl of SAPH was pipetted into 24 well Millicell® Cell Culture Inserts with 3 µm pore size (*Millipore, USA*). Media was added to the sample wells for 20 minutes then removed (media wash step). Media acted as a buffer and returned SAPHs to a pH of 7.4. Samples were incubated overnight at 37ºC. The required cell number in 100 µl of medium was added to the top of each SAPH. Cell suspension was gently pipetted to ensure homogenous bNPC dispersion on the surface. Samples were incubated at 37ºC in humidified atmosphere (20% O_2, 5% CO_2). Fresh media was exchanged for old every 2 days.

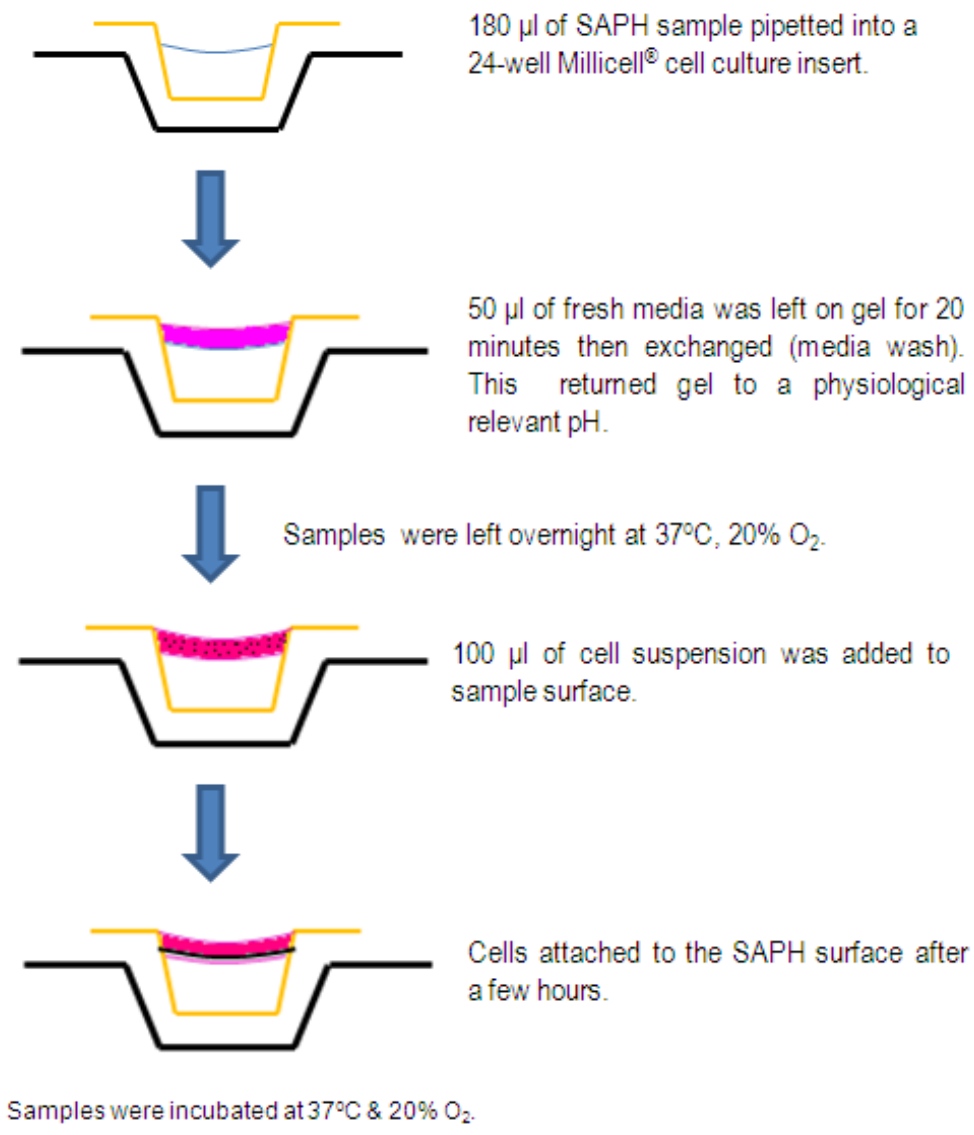

Figure 3.5. A step-by-step schematic for 2D cell seeding and cell culture on SAPH samples.

3.3.1.5. Seeding of SAPHs for 3D culture

A cell suspension of 2.5x10^5 bNPCs in 250 µl of media was added to 1 ml of SAPH to give a final cell density of 2x10^5 bNPCs per ml of SAPH (*figure 3.6*). The cell suspension was carefully mixed with the SAPH to establish homogenous cell dispersion. Millicell® 12-well Cell Culture Inserts with 3 µm pore size *(Millipore, USA)* were used for cell culture. 450 µl of SAPH was pipetted into each cell culture insert ensuring no air bubble formation. 900 µl of fresh media was added around the insert and 150 µl of media was added on top of the sample. Samples were incubated at 37ºC for 20 minutes. After 20 minutes, the old media was exchanged for fresh media to return the SAPH to a more physiological relevant pH (7.4). The media exchange was carried out for a total of 5 times. Then samples were incubated at 37ºC in humidified atmosphere (20% O_2, 5% CO_2). Fresh media was exchanged for old every 2 days. 0

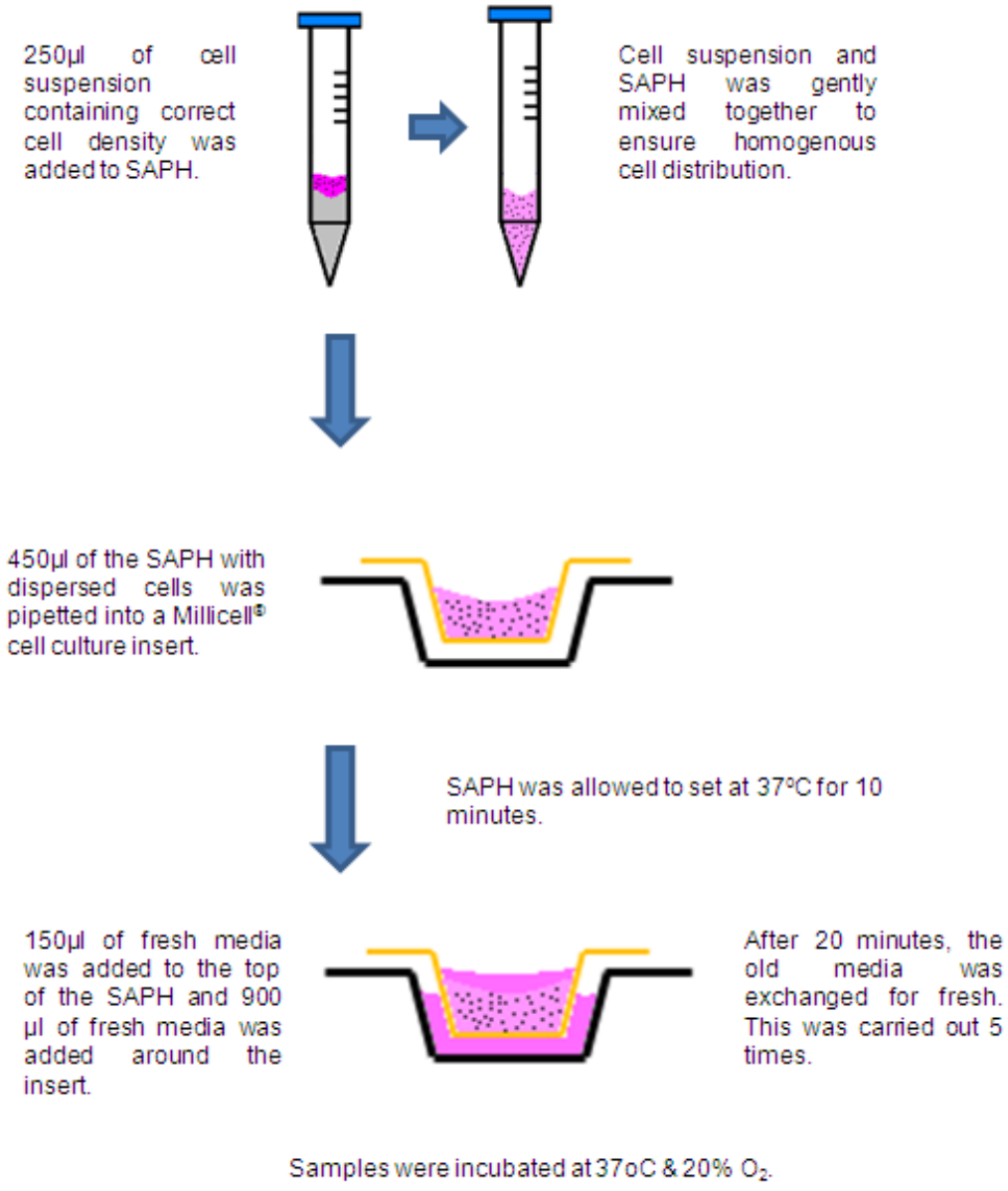

Figure 3.6. A step-by-step schematic for the 3D cell seeding and culture of bNPCs in SAPHs.

3.3.2. Culture of primary human bone marrow derived mesenchymal stem cells

Human BMMSCs were isolated from the femur of a 27-year old female after hip replacement surgery at Wrightington Hospital, Lancashire. A letter of consent was signed by the donor and NHS ethical approval was in place (18/05/2010) REC reference number: 10/H1013/27 (NW8 Research Ethics Committee – GM East). Ethics forms were considered and approved in March 2013 after being deliberated by Committee on the Ethics of Research on Human Beings. All the appropriate COSHH Assessment Forms were completed, signed and approved by all applicable staff members. Samples were received within 24 hours. Isolation of MSCs was carried out by the Richardson laboratory and provided to this study.

3.3.2.1. Growth medium

Human-BMMSCs were cultured and expanded in Mesenchymal Stem Cell Growth Medium (*Promocell, UK)* stimulated with 1% penicillin-streptomycin (*Gibco Invitrogen, UK*).

3.3.2.2. Cell culture

For h-BMMSCs revival, protocol followed *section 3.3.1.2* however 2 freezing vials containing P3 $5x10^5$ h-BMMSCs ml^{-1} each were seeded for each tissue culture flask ($175cm^2$) and 20 mls of MSC growth media was added. Cells were incubated at 37^{o}C in humidified atmosphere (20 % O_2, 5% CO_2). Passage 4 and 5 h-BMMSCs were used for experiments

3.3.2.3. Seeding of SAPHs for 3D culture

3D culture and seeding of h-BMMSCs followed *section 3.3.1.5* however cells were trypsinised at 50-60% confluence and final density was $1x10^6$ h-BMMSCs ml^{-1} of SAPH. h-BMMSCs were cultured in differentiation medium without GDF-6 (control samples) or differentiation medium with 100 ng ml^{-1} GDF-6 (*section 3.3.2.4*). Media was exchanged every 2 days and cells were incubated at 37^{o}C in humidified atmosphere (20% O_2, 5% CO_2).

3.3.2.4. Discogenic differentiation medium

The Richardson group formulated a recipe for discogenic induction media (*table 3.2*) adapted from the widely used chondrogenic medium [10]. Instead of using transforming growth factor beta-1 (TGF-β1) as the growth factor, growth differentiation factor-6 (GDF-6) was used to induce a NP-like phenotype from MSCs. Recent literature has demonstrated that GDF-6 significantly increased expression of ‘traditional’ and ‘novel’ NP markers by h-BMMSCs compared to current growth factors used for discogenic differentiation (TGF-β1, TGF-β3 and GDF-5) [11].

To AQ medium™ (*Sigma-Aldrich, USA*) containing 4500 mg L^{-1}, L-alanyl-glutamine and sodium bicarbonate was added:

Reagent	Company	Final concentration
Antibiotics	*Gibco Invitrogen, UK*	1%
Ascorbic acid 2-phosphate	*Sigma-Aldrich, USA*	100 µm
Bovine Serum Albumin	*Sigma-Aldrich, USA*	1.25 mg ml^{-1}
Dexamethasone	*Sigma-Aldrich, USA*	10^{-7} M
FBS	*Gibco Invitrogen, UK*	1%
Insulin-Transferrin-Selenium-Ethanolamine	*Gibco Invitrogen, UK*	Insulin 10 µg ml^{-1} Transferrin 5.5 µg ml^{-1} Selenium 670 ng ml^{-1}
L-proline	*Sigma-Aldrich, USA*	40 µg ml^{-1}
Linoleic acid	*Sigma-Aldrich, USA*	5.4 µg ml^{-1}
Sodium pyruvate	*Sigma-Aldrich, USA*	1m M
Growth Differentiation Factor 6 (GDF-6, BMP-13)	*PeproTech, USA*	100 ng ml^{-1}

Table 3.2. Final concentration of constituents in each bottle (1 litre) of AQ medium™ for NP induction medium.

3.4. METHODS – CELL CULTURE ANALYSIS TECHNIQUES

3.4.1. LIVE/DEAD® cell viability assay

3.4.1.1. Theory

LIVE/DEAD® cell viability assay (*Invitrogen, UK*) consists of two dyes; calcein AM and ethidium homodimer-1. Viable cells convert the non-fluorescent calcein AM to intensely fluorescent calcein due to intracellular esterase activity. The viable cells retain dye and produce a green fluorescence (excitation/emission 494 nm/515 nm). In contrast, ethidium homodimer-1 (EthD-1) enters the dead cells due to their damaged membranes and fluoresces upon binding to the nucleic acid producing red fluorescence (excitation/emission 495 nm/635 nm). Viable cells have intact plasma membranes therefore ethidium homodimer-1 dye cannot enter the cell.

3.4.1.2. Experimental procedure

Samples were incubated in PBS stimulated with 10 mM calcein AM and 1 mM ethidium homodimer-1 for 15 min at 37^{o}C. The solution was removed and samples were imaged using Nikon Eclipse E600 (*Nikon, Japan*) fluorescence microscope, with excitation filters of 494 nm (green, Calcein) and 528 nm (red, EthD-1) for 2D culture and Leica TCS SP5 confocal microscope (*Leica Microsystems, Germany*) for 3D culture (200 µm stacks were imaged at 5 µm intervals along the axial plane and 500 µm stacks were imaged at 5 µm intervals along the sagittal plane). Alginate gels were used as positive controls.

3.4.2. CytoTox 96® Cytotoxicity assay (cell population)

3.4.2.1. Theory

CytoTox 96® Non-radioactive Cytotoxicity (*Promega, UK)* is a colourmetric assay which quantitatively measures lactate dehydrogenase (LDH), a stable cytosolic enzyme that is released upon cell lysis. The released LDH converts the tetrazolium salt into a red formazan product. The higher the optical density then the more viable cells present in the sample.

3.4.2.2. Experimental procedure

SAPHs were transferred into microcentrifuge tubes then 500 µl of fresh medium was added. The samples underwent a freeze-thaw cycle 3 times by freezing at -80^{o}C freezer then thawing samples in a 37^{o}C incubator for 30 minutes to lyse the cells. Samples were centrifuged at 250g for 5 minutes then 50 µl of the supernatant was transferred to a clear 96-well plate. 50 µl of substrate mix was added to each sample well. The well plates were covered and incubated

at room temperature for 25 minutes then 50 µl stop solution was added to prevent anymore cellular reactions taking place. A Multiskan Ascent 96/386 96-well plate reader (*Labsystems, UK)* was used to measure absorbance at 492 nm wavelength and samples without cells used as negative controls and *d*H_2O was used as blanks.

A standard curve plotting known cell numbers against absorbance was produced so the unknown sample cell numbers could be estimated (*figure 8.1& 8.2*). Alginate gels were used as positive controls.

3.4.3. Quant-iT™ PicoGreen® dsDNA assay (cell population)

3.4.3.1. Theory

Quant-iT™ PicoGreen® dsDNA assay (*Life Technologies, USA*) is a sensitive fluorescent nucleic acid stain for quantifying double stranded DNA (dsDNA). Free dye has little background and does not fluoresce in solution but upon selective binding to dsDNA, it exhibits a >1000-fold fluorescence enhancement. The exhibited fluorescence can then be recorded and standard curves used to determine cell number [12]. As the amount of dsDNA should be consistent in viable cells, this method of population quantification is not affected by cell metabolism.

PicoGreen® assay was carried out in conjunction with Blyscan™ GAG assay on the same SAPH samples so the amount of s-GAG produced per cell could be calculated.

3.4.3.2. Protocol

PicoGreen® reagent was prepared using a 1:200 dilution with TE buffer (10mM Tris-HCl, 1mM EDTA, pH 7.5) then it was protected from light. A DNA standard curve (0.1 to 1000 ng ml^{-1}) was prepared.

Encapsulated cells had been papain digested in preparation for Blyscan™ GAG assay (*section 3.4.6*) so a lysis buffer step was not required. In triplicate, 100 µl of sample, blank and DNA standard dilutions were pipetted into a black 96 well plate. Then 100 µl of PicoGreen® working solution was added into each well and mixed. Samples were incubated at RT for 4 minutes, protected from light. The plate was analysed on an FLx800 microplate reader (*BioTEK, USA)* with the fluorescence being measured using filters with a 485 nm excitation and a 538 nm emission wavelength. A standard curve plotted known cell number against fluorescence and was used to calculate the unknown sample cell number (*figures 8.3 & 8.4*).

3.4.4. Quantitative Real-time polymerase chain reaction (gene expression)

3.4.4.1. Theory

Polymerase chain reaction (PCR) is a method for detecting deoxyribonucleic acid (DNA), responsible for encoding genetic information, and amplifying the molecule over several orders of magnitude [13]. Quantitative real-time PCR (qRT-PCR) allows the specific amount of DNA or gene to be quantified in the sample [14] and relies on the fluorescent probe detection of amplification products [15].

PCR involves a cyclic process where the amount of DNA targets is doubled with every cycle (*figure 3.7*). After heating to 90ºC+ in an initialising step, the denaturing step causes the two intertwined strands of DNA to separate from each other. Samples are cooled to between 40 to 60ºC to allow annealing of the primers to the single stranded DNA. Primers in the reaction specify the explicit DNA product that needs to be amplified [16]. DNA polymerases extend the primers by nucleotide addition (adenine, thymine, cytosine and guanine) producing copies of the original DNA strand targets [13].

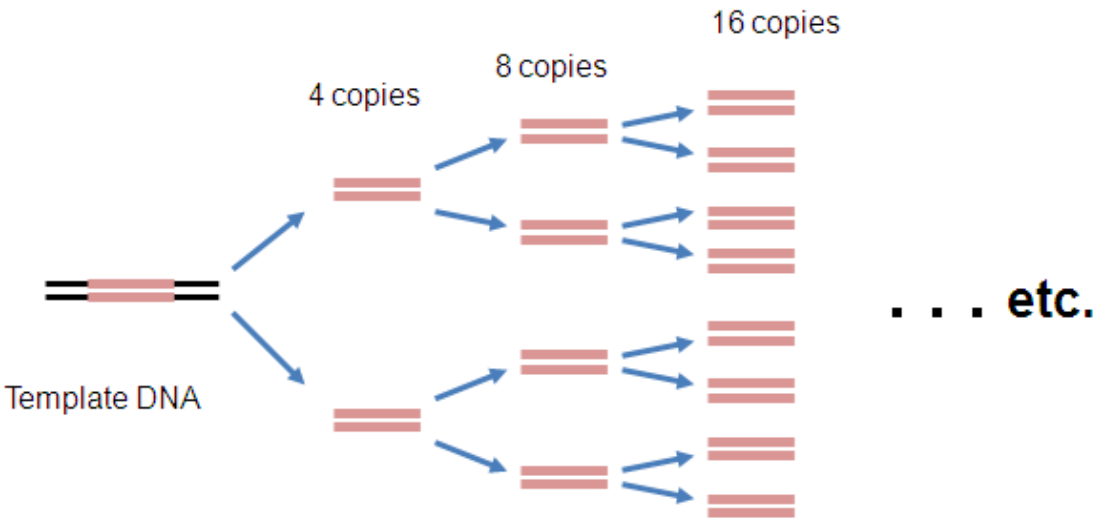

Figure 3.7. Schematic showing the repeated cyclic steps to amplify the target DNA. Each cycle produces double the copies of target DNA so by the final cycle, millions of copies of targeted DNA are present. *Diagram adapted from https://isbibbio.wikispaces.com/PCR*

The basic principle of qRT-PCR is the more abundant the specific complementary DNA (cDNA) in a sample then the earlier it is detected during the amplification sequence. Real-time detection and quantification of the PCR product can be carried out as it is being synthesised [14]. Fluorescent dyes are incorporated into newly synthesised DNA molecules during the amplification step. A fluorescent based method of signal generation relies upon the detection and quantification of a fluorescent reporter as the signal increases in direct proportion to the

amount of PCR product in a reaction [15]. There were two different methods used in this study for performing qRT-PCR:

SYBR® Green (*figure 3.8*) binds non-specifically to dsDNA leading to a thousand fold increase in fluorescent signal. Due to the PCR cyclic process doubling the amount of DNA per cycle, the fluorescence increases proportionally and the signal is used to measure the amplification of the target DNA [17]. To overcome the disadvantage of unspecific dsDNA binding, well-designed primers can ensure that non-specific background only appears at very late cycles.

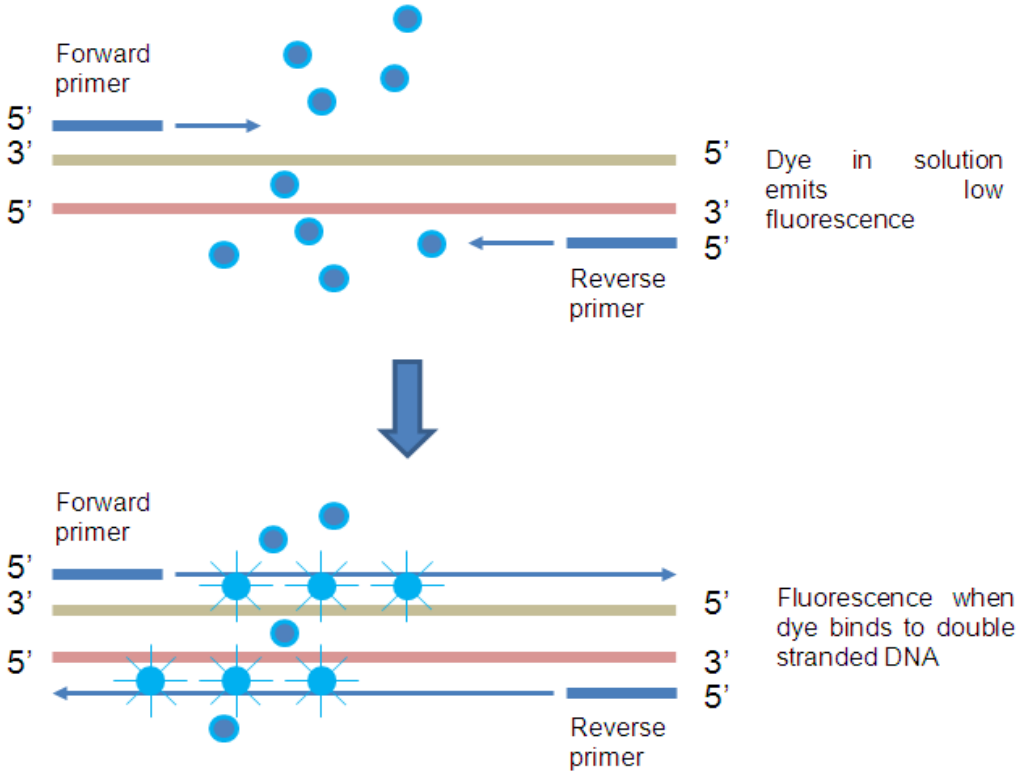

Figure 3.8. Schematic of the SYBR® Green method for qRT-PCR. The dye binds to double stranded DNA which causes a 1000 fold increase in fluorescent signal. The increase in fluorescence intensity is detected and monitored to determine the amount of PCR product produced. *Adapted from http://www.sigmaaldrich.com/technical-documents/protocols/biology/sybr-green-qpcr.html.*

TaqMan® is an alternative to SYBR® Green which relies on fluorescence resonance energy transfer (FRET) for quantification. TaqMan® probes are linear sequence-specific oligonucleotide probes that typically contain a fluorescent reporter dye at the 5'-end and a quencher molecule at the 3'-end [17] (*figure 3.9*). As the reporter dye and quencher molecule are in close proximity, little or no fluorescence is detectable. When the TaqMan DNA polymerase cleaves the probe, due to its inherent 5' nuclease activity, the released fluorescent and quenching dyes are separated [18]. The resultant increase in fluorescent signals can be measured to monitor the amplification of target DNA [17]. The advantage of using this probe is

that specific detection will only bind target sequences with no contaminating signals that might arise from primer dimer and other non-specific PCR events.

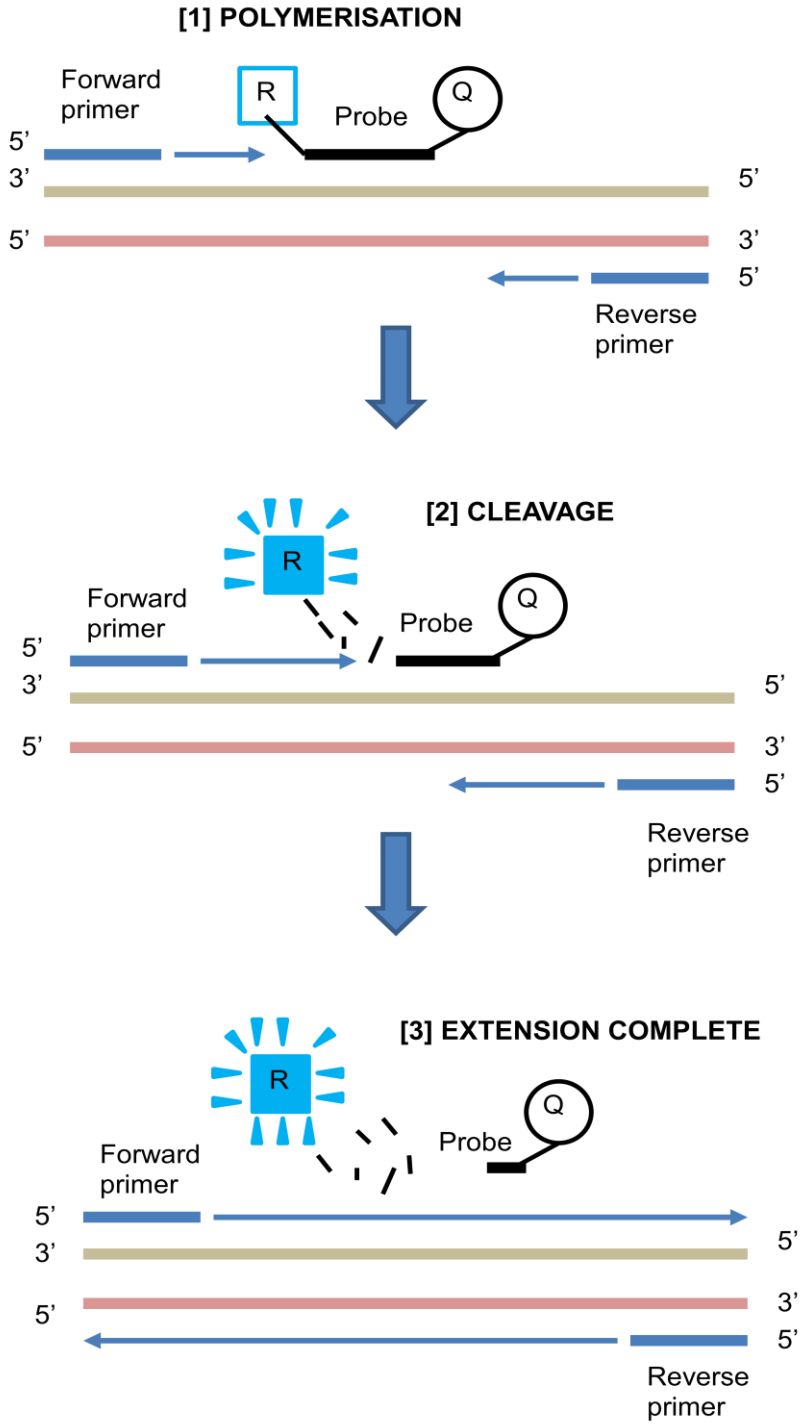

Figure 3.9. Schematic showing the TaqMan® method for q-RT-PCR. [1] A fluorescent reporter dye and quencher are attached to the 5' and 3' ends of the TaqMan® probe. Due to the close proximity between the dye and quencher, the dye emission is quenched. [2] During each extension cycle, the DNA polymerase cleaves the probe and the dye is separated from the quencher. [3] After separation of the quencher and dye, fluorescence is emitted and can be monitored to determine amplification of target DNA. *Adapted from [19].*

Glyceraldehyde 3-phosphate dehydrogenase (*GAPDH*) was chosen as the housekeeping gene so the relative expression of NP marker genes could be analysed. Expression levels of *GAPDH* should have remained approximately constant in cells throughout cell culture

3.4.4.2. Experimental procedure

Samples were lysed using TRIzol® (*Life Technologies, UK*) according to the manufacturer's instructions. RNA was quantified using a NanoDrop ND-1000 spectrophotometer (*NanoDrop Technologies, USA).* 1.2 µl of *d*H_2O and TE buffer were used as blanks. Then 1.2 µl of sample was loaded onto the stage. Optical density readings were used for the 260/280 and 260/230 ratio as an indicator of the purity of the samples (ratio of nucleic acid to contaminating proteins and PGs). cDNA was prepared from RNA using ABI high capacity kit (*Applied Biosystems, USA*) summarised in *table 3.3.* Reaction tubes were incubated at 25^oC for 10 minutes, 37^oC for 120 minutes, 85^oC for 5 seconds and then stored at 4^oC using a PTC-200 Peltier Cycler (*Bio-Rad, USA*). cDNA was diluted down to 5 ng / µl based on RNA readings. Sample were then stored at -20^oC in preparation for qRT-PCR.

Reagents for each sample	Volume of reagents used
10X RT Buffer	2 µl
25 dNTP mix (100 nM)	0.8 µl
10X RT Random Primers	2 µl
MultiScribe™ Reverse Transcriptase	1 µl
RNAse inhibitor	1 µl
molecular grade dH_2O	3.2 µl
RNA sample	10 µl

Table 3.3. Reagents for reaction mix used for reverse transcription of RNA using ABI kit.

FOR BOVINE NUCLEUS PULPOSUS CELLS (SYBR® Green):

Gene expression was analysed using real-time PCR Applied Biosystems StepOne™ Plus Real Time PCR system. Reactions were prepared in triplicate to a total volume of 20 µl.

Each reaction well contained 18 µl of mastermix consisting of 2x SYBR® Green mastermix, molecular grade H_2O, 600 nm of forward and reverse primer [20] (*table 3.4*) in ABI 96 well PCR plate. Then 2 µl of cDNA at 5 ng $µl^{-1}$ was added to each reaction well. The plate was sealed with optical adhesive film and centrifuged then samples were run.

Gene	Forward primers (5'-3')	Reverse primers (5'-3')
GAPDH	TGCCGCCTGGAGAGAAACC	CGCCTGCTTCACCACCTT
Aggrecan (*ACAN*)	GGGAGGAGACGACTGCAATC	CCCATTCCGTCTTGTTTTCTG
Type I collagen (*COL1A2*)	CTGTTCTGTTCCTTGTGTAACTGTGTT	GCCCCGGTGACACATCAA
Type II collagen (*COL2A1*)	CGGGCTGAGGGCAACA	CGTGCAGCCATCCTTAGA
Transcription factor SOX9 (*SOX9*)	GGGAAGCCTCACATCGACTTC	GGACATTACCTCATGGCTGATCT
Keratin 8 (*KRT8*)	ACCAGGAGCTCATGAATGTCAA	TCGCCCTCCAGCAGCTT
Keratin 18 (*KRT18*)	AAGGCCAGCTTGGAGAACAG	TTGAGCTGCTCCATCTGCAT
Forkhead Box F1 (*FOXF1*)	TCCCTCCCCACCTCAGAAGT	TGGCTTCAGAAATGCAAGTTACTC
Carbonic anhydrase 12 (*CA12*)	CCAACAACGGCCACTCAGT	CCCCGGACCTGCATGTC

Table 3.4. Primer and probe sequences used for qRT-PCR on bNPCs cultured in SAPHs designed by Minogue *et al* [20].

Note – *GAPDH*, *ACAN*, *COL2A1*, *SOX9*, *KRT8*, *KRT18*, *FOXF1* and *CA12* primers were purchased from *Invitrogen, USA*. *COL2A1* and *CA12* primers were purchased from *Eurofins, UK*.

Step	AmliTaq Gold® Enzyme activation	PCR	
		Cycles (40 cycles)	
	HOLD	Denature	Anneal / Extend
Time	10 min	15 sec	60 sec
Temp / ^{o}C	95	95	60

Table 3.5. Thermal cycling conditions for primer optimisation.
http://www3.appliedbiosystems.com/cms/groups/mcb_support/documents/generaldocuments/cms_042996.pdf

FOR HUMAN BONE MARROW MESENCHYMAL STEM CELLS (TaqMan®):

Gene expression was analysed using real-time PCR Applied Biosystems StepOne™ Plus Real Time PCR system. Reactions were prepared in triplicate to a total volume of 10 µl. Master mix for each reaction well contained 5 µl TaqMan® master mix (*Applied Biosystems, USA)* 1 µl of both the forward and reverse primer [20] (*Invitrogen, USA*), 0.5 µl of probe (*Applied Biosystems, USA)* (*table 3.6*), 0.5 µl of ROX™ reference dye. Then 2 µl of cDNA at 5 ng μl^{-1} was added to each reaction well. The plate was sealed with optical adhesive film and centrifuged then samples were run.

Gene	Forward primers (5'-3')	Reverse primers (5'-3')	Probe [6FAM]
GAPDH	CTCCTCTGACTTCAACAG	CGTTGTCATACCAGGAAA	CACCCACTCCTCCACCT
ACAN	GGCTTCCACCAGTGTGAC	GTGTCTCGGATGCCATACG	TGACCAGACTGTCAGAT
COL1A2	TCAGCTTTGTGGAACGC	CTGGGCCTTTCTTACAG	CAGTAACCTATGCCTA
COL2A1	GGCTTCCATTTCAGCTATG	CAGTGGTAGGTGATGTTC	CCAACACTGCCAACGTC
SOX9	CCTGTGGAGACTTCTGAA	GGTACTTGTAATCCGGGTG	TCCTTCTTGTGCTGCAC
KRT8	CCTCATCAAGAAGGATGTG	CCTGAAGAAGTTGATCTC	CTTCCAGGCGAGACTCC
KRT18	CTGCTGAACATCAAGGTC	AGGCATCACCAAGATTAAAG	CTGAGATCGCCACCTAC
Keratin 19 (*KRT19*)	CCATGAGGAGGAAATCAGTA	GTCACTCAGGATCTTGGC	AATCCACCTCCACAGTG
FOXF1	CCGTATCTGCACCAGAAC	TGGCGTTGAAAGAGAAGA	CCGAGCTGCAAGGCATC
CA12	TCCTGGCCTTTGTACTTTA	CCAGCAACAAGTCAGAAG	TCGCTGTCCGGCTGTT

Table 3.6. Primer and probe sequences used for qRT-PCR on h-BMMSCs cultured in SAPHs designed by Minogue *et al* [20].

Note – Primers and probes for all genes purchased from *Sigma-Aldrich, USA.*

For positive controls, 2 µl of human reference cDNA was added to each reaction well and 2 µl of molecular grade H_2O was added to each reaction well for negative controls.

Step	UNG incubation	Polymerase activation	PCR	
	HOLD	HOLD	Cycles (40 cycles)	
			Denature	Anneal / Extend
Time	2 min	20 sec	1 sec	20sec
Temp / ^{o}C	50	95	95	60

Table 3.7. Thermal cycling conditions for primer optimisation. *https://tools.lifetechnologies.com/content/sfs/manuals/cms_084554.pdf*

3.4.4.3. Analysis of RT-PCR results

Following the PCR process, the Applied Biosystems StepOne™ Plus Real Time PCR system expressed data as an amplification plot. The relative levels of gene expression were compared to the housekeeping gene.

Step	Calculations
1 ΔCt	ΔCt calculated: = Ct of target gene – Ct of GAPDH
2 average ΔCt	Average of sample ΔCt values
3 2 - ΔΔCt	= 2 - POWER(2, - ΔCt)
4 Standard Error	STDEV(average ΔCt) / SQRT(n)
5 Error bars	Error Bars + Error = (2-ΔΔCt-SE) – (2-ΔΔCt) - Error = (2-ΔΔCt) – (2-ΔΔCt + SE)

Table 3.8. Step-by-step calculation process for RealTime analysis.

Graphs were plotted to show the relative gene expression to GAPDH on days 1, 7 and 14 for h-BMMSCs stimulated with and without GDF-6.

3.4.5. Immunocytochemistry (ECM component production)

3.4.5.1. Theory

Immunocytochemistry (ICC) utilises antibodies (ABs), typically the immunoglobulin G (IgG) class, that recognise and bind to specific protein antigens. ICC allows cellular contents to be determined by the primary AB (pAB) specifically binding to an antigen on the molecule of interest. Then a secondary AB (sAB) with a fluorescent tag binds to the primary which allows the molecule to be visualised and imaged using fluorescence microscopy (*figure 3.10*).

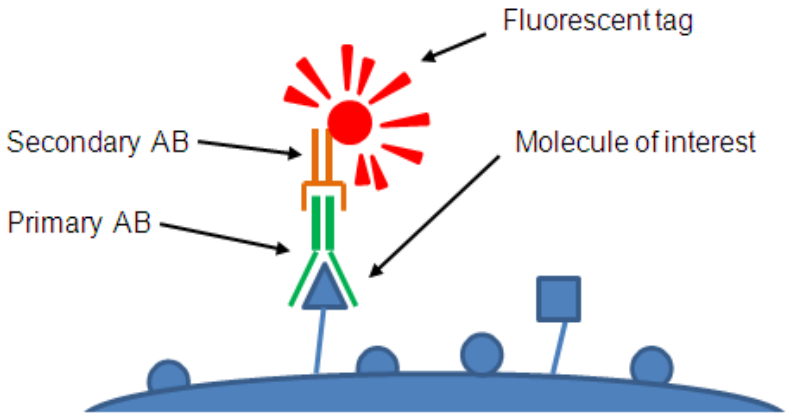

Figure 3.10. Schematic showing the principle of immunocytochemistry. The pAB specifically binds to the molecule of interest. The sAB with a fluorescent tag attached binds to the pAB which allows the molecule to be imaged.

3.4.5.2. Experimental procedure

SAPHs were washed with DPBS then fixed with 4% paraformaldehyde (PFA) (*Sigma-Aldrich, USA*) for 15 minutes at RT which stopped anymore chemical reactions occurring and maintained the cell shape. Cells were permeablised with 0.5% Triton X-100 (*Sigma-Aldrich,*

USA) in PBS at RT for 15 minutes to allow ABs to enter the cells. Samples were washed with DPBS then blocked using 1% bovine serum albumin (BSA) (*Sigma-Aldrich, USA*) for one hour at RT to reduce non-specific AB binding. The primary AB (pAB) was added to the samples and left overnight at 4^{o}C. Primary ABs included rabbit polyclonal to anti-collagen type I (ab34710) (*Abcam, UK*), rabbit polyclonal to anti-collagen type II (ab34712) (*Abcam, UK*) and mouse monoclonal to anti-aggrecan (7D4) (*AbD Serotec, USA*) at a ratio of 1:100, 1:200 and 1:500 respectively.

The next day, samples were incubated at RT for 90 minutes in the dark with a secondary goat anti-rabbit IgG-AlexaFluor 594 (1:500 dilution in BSA), secondary goat anti-mouse IgG AlexaFluor 568 (1:500 dilution) and AlexaFluor 488 phalloidin (1:150 dilution) to stain for F-actin (all from *Life Technologies, UK*).

To remove any unbound sAB, samples were soaked in DPBS and washed 5 times. Samples were mounted with DAPI-Prolong (*Invitrogen, UK*) on glass slides and left to cure for 2 days at 4^{o}C to increase brightness of staining. Samples were cured using DAPI-ProLong anti-fade and imaged using Leica TCS SP5 confocal microscope and LASAF software. Human BMMSCs seeded onto glass cover slips were used as controls whilst a SAPH incubated with only sAB was also imaged to ensure no unspecific sAB binding.

3.4.6. Blyscan™ sulphated glycosaminoglycan assay (ECM component production)

3.4.6.1. Theory

Blyscan™ assay (*Biocolor, USA*) is a quantitative dye-binding technique for the measurement of sulphated PGs and sulphated GAGs (s-GAGs). The cationic dye label used is 1, 9-dimethylmethylene blue (DMMB) which binds to s-GAGs. The higher the amount of s-GAG present then the more dye will bind and the higher the optical density measurements [21].

3.4.6.2. Experimental procedure

Papain extraction reagent, 200mM sodium phosphate buffer solution (pH 6.4) was made from sodium dihydrogen orthophosphate and disodium hydrogen orthophosphate. To 25 ml of the buffer solution, 200 mg sodium acetate, 100 mg ethylenediaminetetraacetic acid, 20 mg of L-cysteine hydrochloride and 3.125 mg of papain were added. 0.5 ml of papain extraction reagent were added to each sample and left on a 65^{o}C heating block overnight to allow removal of interfering proteins and to dissociate cells.

50 µl of test material (after papain digestion), 50 µl of *d*H_2O and 1 ml of Blyscan dye reagent were mixed together for 30 minutes on a mechanical shaker. To determine whether s-GAG was being released out of the SAPH, 50 µl of pooled media samples were also analysed. Samples were centrifuged at 12000 rpm for 10 minutes to produce a dye and s-GAG pellet.

The supernatant was carefully removed then 0.5 ml of dissociation reagent was added to the samples. To release the unbound dye into the solution, samples were placed in a mechanical shaker for 10 minutes. Then in duplicate, 200 µl of each sample was added to a 96 well plate. The samples were analysed at 650nM on a microplate reader. A standard curve plotting known s-GAG concentrations (1 to 5 µg) against absorbance was used to determine total amount of s-GAG in the samples (*figure 8.5 & 8.6*).

3.4.7. Specific glycosaminoglycan analysis (ECM component production)

3.4.7.1. Theory

Radiolabelling utilises radioactive isotopes to label chemical compounds [22]. Adding a radioactive species into cell culture medium allows metabolic incorporation into *de novo* synthesised GAGs and produces labelled species. The GAGs can be fractioned and purified using size and charge separation techniques; anion-exchange chromatography can be used to isolate GAGs. After purification and separation, various methods can be used to determine the structure and configuration of the isolated GAGs.

Ion exchange chromatography involves the reversible adsorption of charged molecules to immobilised ion groups on a matrix of the opposite charge [23]. Diethylaminoethyl (DEAE) is a positively charged resin. The DEAE columns allow chemically attached hydrophilic weak anion exchange type surface which causes separation of molecules including GAGs. The unbound GAGs will pass through the column faster. The bound GAGs can be eluted at a later time point by using sequentially increasing ionic strength buffer.

3.4.7.2. Experimental procedure

SAPH samples were analysed on day 7 therefore on day 5, the standard cell culture media (*section 3.3.1.1*) was exchanged with media containing 50 *µ*Ci/ml of [3H]-glucosamine (*PerkinElmer, USA*) for radio-labelling GAGs. Adding the [3H]-glucosamine 48 hours before the required time point gave sufficient time for it to be incorporated by cells.

On day 7, SAPH and media volume was made up to 20 mls in total using PBS then 40 ul of pronase was added to degrade the sample at 37ºC, vortexing periodically. 1 ml of DEAE was pipetted into the anion exchange column (*Sigma-Aldrich, USA)* then 10 mls of PBS was used to wash the column 10 times to equilibrate it. After the wash step, 5 mls of 1.5 M NaCl was added to remove any contaminants from the beads. The sample was then added to the column after another wash step. To get rid of all the weakly bound proteins, the column was

washed with 0.25M NaCl three times. The bound GAGs were eluted and collected by adding 1 ml aliquots of 1.5M NaCl four times. 50 µl of each fraction was processed for radioactivity with a Wallac 1409 liquid scintillation counter (*PerkinElmer, USA*). The presence of radioactive isotopes (^{3}H, counts per minute) was recorded.

Samples were de-salted using PD-10 disposable Sephadex G-25M size exclusion columns (*GE Healthcare, UK*). 6 falcon tubes were labelled 1 to 6. After washing, 1 ml of sample was added to the column and the wash was collected in falcon tube 1. 1 ml of Milli-Q® *dd*H_2O (*Millipore, USA*) was aliquoted into the tubes and the washes were collected in tubes 2 to 5. The GAG sample was collected in tubes 4 and 5. The washing steps were repeated until the entire sample has been washed through the column. The contents of falcon tubes 4 and 5 were collected. The GAG sample was then stored at -80^{o}C in preparation for the freeze-drying process. The samples were placed in the freeze-dryer overnight at -50^{o}C to increase sample concentration.

Chondroitinase ABC (*Iduron, UK*) was added to the sample to enzymatically digest the samples so major GAG species could be identified. Samples were placed on a heat block at 30^{o}C for 4 hours. Samples were vortexed and centrifuged then placed on a heat block overnight. The following day samples were stored at -20^{o}C. For CS, DS and HS analysis, GAGs were applied to a superdex-30 column and fractions of 0.5 ml at 4 ml per min was used to separate disaccharides from undigested material. Disaccharide fractions and undigested material were pooled separately and buffered exchanged via freeze drying, ready for re-suspension in HPLC grade H_2O (*Sigma-Aldrich, USA*) at pH 3.5. CS/DS disaccharides were run on Hewlett Packard 1100 series HPLC and separated using a Hypersil 5 µm SAX-HPLC column (*Thermo Scientific, USA*) with increasing concentration of 0.1 M NaCl (0.15 M to 0.7 M) at a flow rate of 1 ml per minute to elute species.

3.5. STATISTICAL ANALYSIS

All data was expressed as mean±standard deviation (SD) apart from gene expression results where data was expressed as mean±standard error (SE). Data was analysed using Student's t-test or One-way analysis of variance (ANOVA) test. Differences were considered as significant when probability was less than *P<0.05, **P<0.01 and ***P<0.001. No significant difference (NS) was taken when P>0.05. n number denotes the number of SAPH samples used to produce data whilst at least 2 experimental repeats were used to produce each figure.

3.6. REFERENCES

1. **Jiskoot W, Crommelin D** '*Methods for structural analysis of protein pharmaceuticals*' AAPS Press (2005); ISBN 0-97117767-2-8
2. **Pelton J, McLean L** '*Spectroscopic methods for analysis of protein secondary structure*' Analytical Biochemistry (2000); Vol.277 pp.167-176
3. **Binning G, Quate C, Gerber C** '*Atomic force microscopy*' Physical Review Letters (1986); Vol.56 No.9 pp.930-935
4. **West P** '*Introduction to Atomic Force Microscopy: Theory, Practise, Applications*' (2006)
5. **Meyer E** '*Atomic force microscopy*' Progress in Surface Science (1992); Vol.41 pp.3-49
6. **Magonov S, Elings V, Whangbo M** '*Phase imaging and stiffness in tapping-mode atomic force microscopy'* Surface Science (1997); Vol.375 pp.385-391
7. **Yan C, Pochan D** '*Rheological properties of peptide-based hydrogels for biomedical and other applications*' Chemical Society Reviews (2010); Vol.39 pp.3528-3540
8. **Barnes H, Fletcher J** '*An introduction to rheology'* 1989 ISBN 0-444087140-3
9. **Wyss H** '*Oscillatory rheology*' GIT Laboratory Journal (2007); Vol.4 pp.68-70
10. **Johnstone B, Hering T, Caplan A, Goldberg V, Yoo J** *'In vitro chondrogenesis of bone marrow – derived mesenchymal progenitor cells*' Exp Cell Res (1998); Vol.10 pp.265-272
11. **Clarke L, McConnell J, Sherratt M, Derby B, Richardson S, Hoyland J** *'Growth differentiation factor 6 and transforming growth factor-beta differentially mediate mesenchymal stem cell differentiation, composition, and micromechanical properties of nucleus pulposus constructs'* Arthritis & Research (2014); Vol.16 pp.1-13
12. **Ahn S, Costa J, Emanuel J** '*PicoGreen quantitation of DNA: effective evaluation of samples pre or post-PCR*' Nucleic Acids Research (1996); Vol.24 No.13 pp.2623-2625
13. **Mullis K** '*The unusual origin of the polymerase chain reaction*' Sci Am (1990); Vol.262 pp.56–61 pp. 64–5
14. **VanGuilder H, Vrana K, Freeman W** '*Twenty-five years of quantitative PCR for gene expression analysis*' BioTechniques (2008); Vol.44 No.5 pp.619-627
15. **Heid C, Stevens J, Livak K, Williams P** '*Real time quantitative PCR*' Genome Research (1996); Vol.6 pp.986-994
16. **Garibyan L, Avashia N** '*Polymerase chain reaction*' J of Investigative Dermatology (2013); Vol.133 pp.1-4
17. **Zahringer H** '*TaqMan or SYBR Green*' Lab Times (2009); Vol.1 pp.47-53
18. **Liu H, Wang H, Shi Z, Wang H, Yang C, Silke S, Tan W, Lu Z** '*TaqMan probe array for quantitative detection of DNA targets*' Nucleic Acid Research (2006); Vol.34 No.1 pp.1-8
19. **Provenzano M, Rossi C, Mocellin S** '*The usefulness of quantitative real time PCR in immunogenetics*' American Soc for Histocompatability and Immunogenetics Quarterly (2001); Vol.25 No.3 pp.89-91
20. **Minogue B, Richardson S, Zeef L, Freemont A, Hoyland J** '*Transcriptional profiling of bovine intervertebral disc cells: Implications for identification of normal and degenerate human intervertebral disc cell phenotypes*' Arthritis & Research (2010); Vol.12 pp.1-20
21. **Barbosa I, Garcia S, Chassefiere V, Caruelle J, Martelly I, Garcia D** '*Improved and simple micro assay for sulphated glycosaminoglycans quantification in biological extracts and it use in skin and muscle tissue studies*' Glycobiology (2003); Vol.13 No.9 pp.647-653
22. **Roman E, Roberts I, Lidholt K, Kusche-Gullberg M** '*Overexpression of UDP-glucose dehydrogenase in Escherichia coli results in decreased biosynthesis of K5 polysaccharide*' Biochem J (2003); Vol.374 pp.767-72
23. Harvard Apparatus http://www.harvardapparatus.co.uk/downloads/Ion%20Exchange%20Chroma%20SpinColumn%20Guide.pdf

Chapter 4. *Characterisation & optimisation of self-assembling peptide hydrogels.*

4.1. INTRODUCTION

4.1.1. Overview

Ionic-complementary SAPHs were discovered in 1992 [1]. Since then, a class of ionic-complementary SAPHs called β-sheet forming SAPHs have been demonstrated to hold potential for use in biomedical applications ranging from tissue engineering [2, 3] to drug delivery [4, 5]. The Saiani group took inspiration from the pilot study by Zhang *et al* [1] and designed the *de novo* β-sheet forming self-assembling octapeptide FEFEFKFK where F was phenylalanine, E was glutamic acid and K was lysine [6].

Numerous studies have extensively investigated the self-assembly, nanostructure and gelation of FEFEFKFK into self-supporting hydrogels [7, 8, 9]. Therefore in this study, characterisation of the SAPH was investigated with focus on optimising the production protocol and final mechanical properties in regards to the culture of bNPC and h-BMMSCs. Research into the FEFEFKFK SAPH as a potential scaffold / culture system for bovine chondrocytes [10], human dermal fibroblasts [11] and human osteoblasts [12] has been investigated by members of the group with results suggesting suitability of the SAPH for each cell line. However, the culture and behaviour of bNPCs and h-BMMSCs in the FEFEFKFK SAPHs in view of applications as a scaffold and / or cell delivery system for NP tissue engineering is novel.

4.1.2. Hypothesis

The gelatinous nature of the NP could make the SAPH more suitable for NP tissue engineering in terms of mechanical properties and microenvironment in comparison to bone [12] or cartilage [10] tissue engineering. The mechanical properties of FEFEFKFK SAPHs have been demonstrated to be tailorable [12] with the modulus ranging from 10 Pa [5] to 35 kPa [10] depending on production protocol, SAPH concentration and ionic strength. Therefore the SAPH strength should be able to mimic the biomechanical properties of the soft native NP where the modulus has been recorded as between 5.29 kPa [13] to 19.8 kPa [14].

Due to the high H_2O content of the system that allows easy diffusion of nutrients into and waste products out of the SAPH [9] and the inherent biocompatibility that SAPHs have demonstrated for a number of cell lines [10, 11, 12], the hypothesis was that SAPHs should be

able to support the culture of bNPCs (*chapter 5*) and h-BMMSCs (*chapter 6*). The nanofibrous SAPH architecture has been speculated to mimic the native ECM of some tissues [15, 16] allowing encapsulated cells to preserve phenotype and produce appropriate ECM components.

4.1.3. Aims

The key challenges faced when characterising and optimising the FEFEFKFK SAPH were to produce a consistent and homogenous sample that displayed comparable mechanical properties to the native NP and remained stable over *in vitro* cell culture. A number of techniques were used to characterise and optimise the SAPH:

- Scaffold molecular arrangement (FT-IR).
- Scaffold architecture and nanofibre characterisation (AFM).
- Viscoelastic behaviour and mechanical properties (Oscillatory rheology).
- Injectability (Recovery cycles).

4.2. CHECKING FOR β-SHEET STRUCTURE USING FOURIER TRANSFORM INFARED SPECTROSCOPY

FT-IR spectroscopy was used to check presence of anti-parallel β-sheets. Samples produced a distinct peak at 1625 cm^{-1} wavelength in the amide I region which determined that the SAPHs consisted of a β-sheet structure [17]. A secondary weaker peak was produced at 1675 cm^{-1} wavelength which indicated that the peptide was predominantly in an anti-parallel β-sheet formation (*figure 4.1*). FT-IR spectra results confirmed that the SAPHs were highly likely to be β-sheet forming peptides. Findings were in agreement with the literature where FT-IR spectra produced a strong absorption band at 1625 cm^{-1} and a weaker band at 1695 cm^{-1} for 40 mg ml^{-1} FEFEFKFK SAPHs [6]. It has been extensively reported that changing the SAPH concentration, over a range of 10 to 40 mg ml^{-1}, had no effect on presence of β-sheets. However intensity of peaks did increase with increased peptide concentration [10, 18]. No peak was observed at 1673 cm^{-1} (*figure 4.1*) which can be produced when there is TFA remaining in the sample [19].

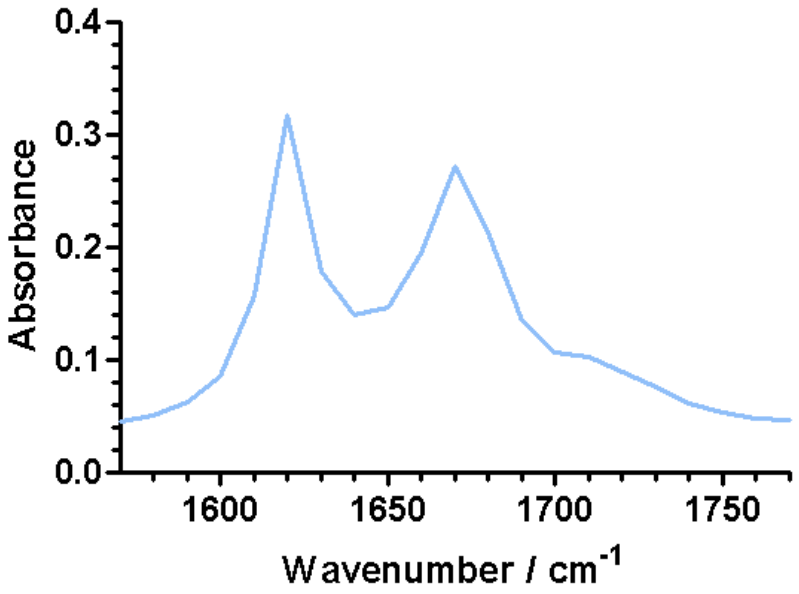

Figure 4.1. Average FT-IR spectra of 30 mg ml^{-1} FEFEFKFK SAPH in D_2O. Samples were tested at a pH of 3. n=2.

Mass spectrometry data was provided for each peptide batch by Biomatik which explained why extensive investigation into molecular arrangement of the SAPH was not carried out.

4.3. IMAGING THE NANOFIBROUS ARCHITECTURE USING ATOMIC FORCE MICROSCOPY

OTESPA visible apex tips (tip height 7-15 μm) with a nominal spring constant of 42N m^{-1} were used for imaging with a Multimode Nanoscope IIIa Controller. The silicon cantilever had a rectangular cantilever with a reflective aluminium back side coating. SAPHs were imaged on day 0 at 0.25 and 30 mg ml^{-1} concentrations.

4.3.1. Imaging 30 mg ml^{-1} SAPHs

A number of studies have imaged FEFEFKFK SAPHs using AFM at concentrations ranging from 0.25 mg ml^{-1} to 5 mg ml^{-1} [9, 20]. However, for cell culture applications, higher SAPH concentrations were required to ensure that sufficient mechanical properties were achieved in view of implantation into a degenerate NP [13] (*section 4.4*).

A very dense fibrillar network was observed (*figure 4.2*) in AFM phase, height and amplitude micrographs of 30 mg ml^{-1} SAPHs. Samples were dehydrated during the preparation process (*section 3.2.2.2*) which caused an increase in nanofibre density and collapsed the SAPH pores. Therefore the micrographs were not a true representation of fully hydrated SAPHs used for cell culture (*chapters 5 & 6*). AFM micrographs were a 2D depiction of a 3D network so the density of the nanofibres was even more exaggerated. To overcome this limitation, the samples needed to be imaged whilst still hydrated; AFM can be carried out in solution using specialist scanning microscopes [21] or cryo-SEM can be used [10]. The mesh size of FEFEFKFK SAPHs has been reported at around 15 to 30 nm, comparable to other SAPHs used for NP tissue engineering [22, 23], which decreased with increasing peptide concentration [6].

The diameter of fibre assemblies were estimated from measuring variations in height from the mica substrate. For 30 mg ml^{-1} SAPHs (*figure 4.2*), the average assembly diameter was 51±23.9 nm (*table 4.1*). It was highly likely that larger assemblies containing multiple nanofibres were measured due to the discrepancy with the published literature [7, 9]. The hypothesis was confirmed by profile measurement tool in WSxM software showing the presence of 3 or more nanofibres. Another explanation was that the samples were imaged at a pH of 9.5 whilst previous studies had imaged the SAPHs at a pH of 3 or less [6, 7]. The pH of SAPH has been shown to affect the final architecture of the system and determine how fibres assemble (*section 4.4.1*).

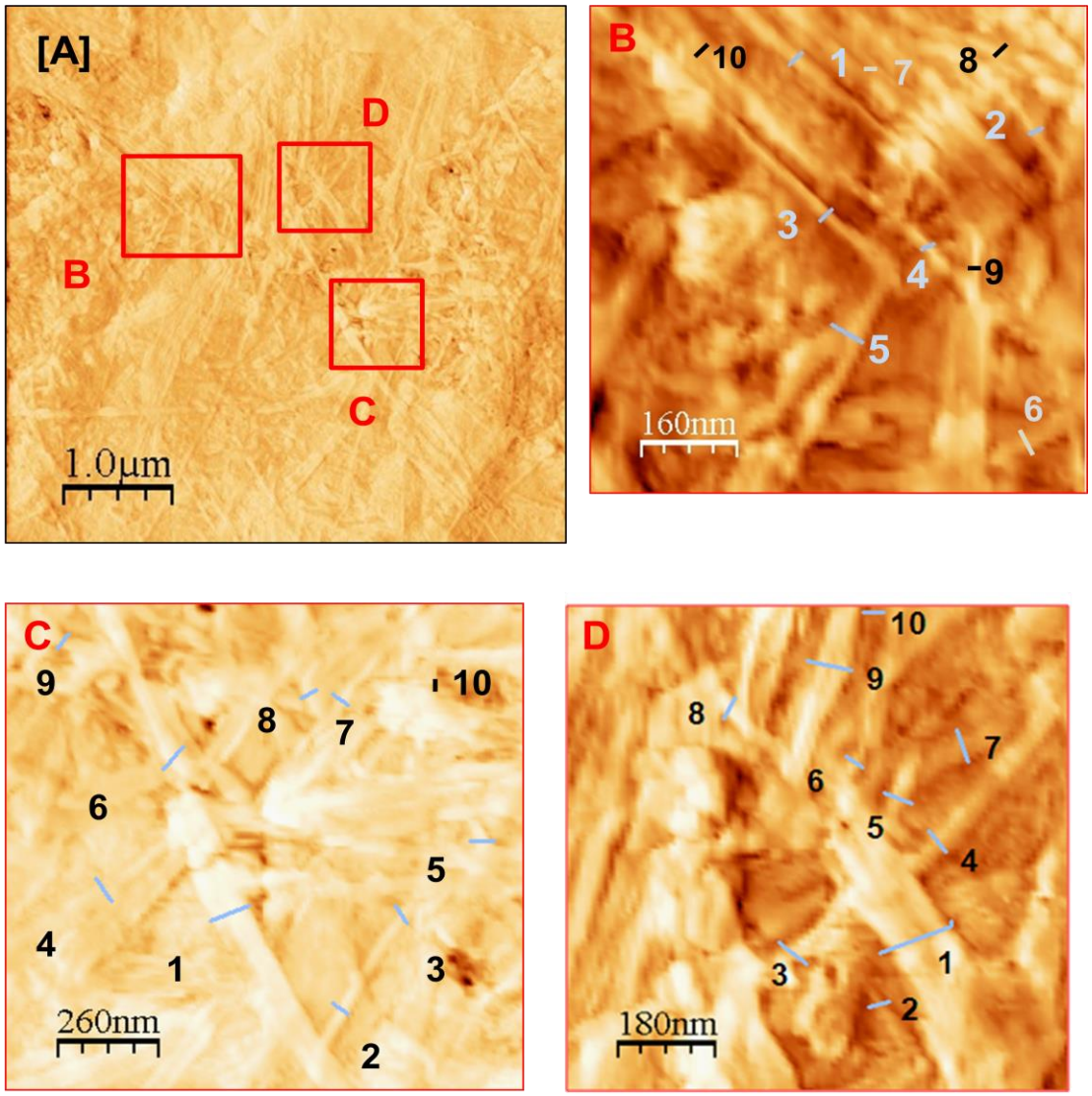

Figure 4.2. Phase mode micrographs of 30 mg ml^{-1} FEFEFKFK SAPH imaged using AFM. [A] 5 µm x 5 µm phase mode micrograph showing a very dense fibrillar network [B], [C] and [D] are magnified sections where the profile mode of WSxM 4.0 software was used to measure the size of features. *Table 4.1* shows the measured feature sizes. Samples were imaged at pH 9.5.

B	Profile		Profile
1	47 nm	6	48 nm
2	35 nm	7	31 nm
3	39 nm	8	42 nm
4	36 nm	9	27 nm
5	80 nm	10	42 nm

C	Profile		Profile
1	105 nm	6	68 nm
2	38 nm	7	37 nm
3	46 nm	8	43 nm
4	61 nm	9	52 nm
5	47 nm	10	28 nm

D	Profile		Profile
1	31 nm	6	34 nm
2	132 nm	7	74 nm
3	58 nm	8	52 nm
4	48 nm	9	81 nm
5	44 nm	10	24 nm

Table 4.1. Results of measured fibre diameter from *figure 4.2* using the profile mode of WSxM 4.0 software. Average feature diameter was 51±23.9 nm. The letters correspond to the image and the numbers correspond to the fibre which was measured.

4.3.2. Imaging 0.25 mg ml^{-1} SAPHs

30 mg ml^{-1} SAPHs produced a very dense fibrillar network (*figure 4.2*) and it proved difficult to measure nanofibre size. Previous studies had demonstrated that individual nanofibres could be analysed at 0.25 mg ml^{-1} [6, 20]. Although 0.25 mg ml^{-1} concentration was lower than the reported critical gelation concentration (CGC) of between 8 mg ml^{-1} and 17 mg ml^{-1} for FEFEFKFK SAPHs [6, 7], nanofibre formation could be observed in micrographs (*figure 4.3*). CGC describes the concentration at which nanofibres density is sufficient for gelation, not the concentration that self-assembly of peptides into nanofibres occurs. The 0.25 mg ml^{-1} height mode micrographs showed a dense fibrillar network comparable to the literature [6, 20]. The network structure was entangled which was expected due to the peptide having no overall charge. Presence of larger assemblies consisting of individual nanofibres associating together might be explained by presence of salts from either cell culture media or PBS (*section 3.2*) which cause aggregation of fibrils into larger assemblies [1]. Presence of larger fibre assemblies could be due to the instability of individual nanofibres causing them to aggregate into more stable larger assemblies. It was difficult to determine where fibres started and ended due to the high density and aggregation of fibres however fibre length has been reported as several microns [7]. The presence of shorter individual nanofibres was likely due to them being more easily absorbed onto the mica surface.

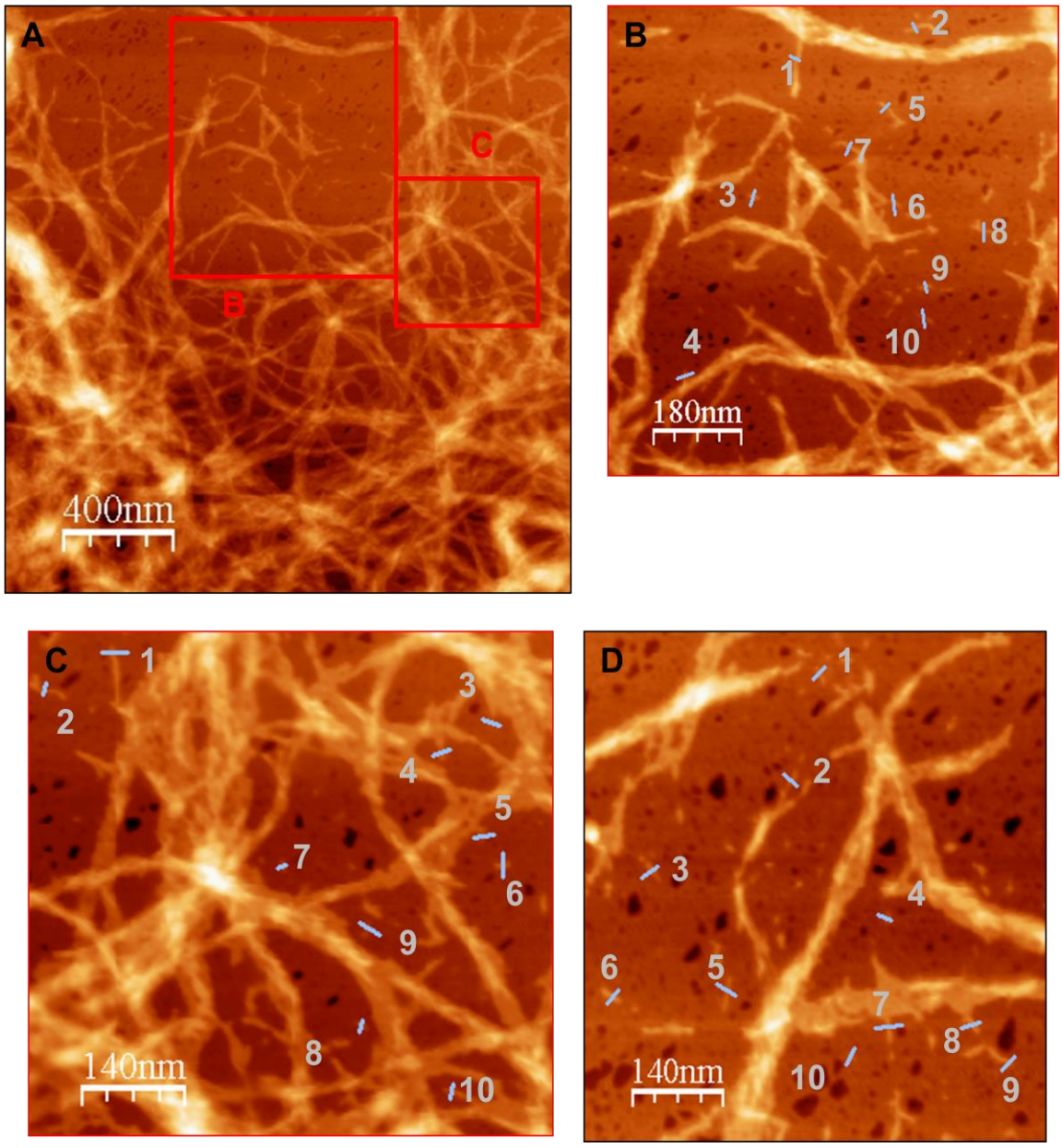

Figure 4.3. Height mode micrographs of 0.25 mg ml^{-1} FEFEFKFK SAPH imaged using AFM. [A] 2 µm x 2 µm height mode micrograph showing a dense fibrillar network with large nanofibre assemblies clearly visible. [B] and [C] are magnified sections where the profile mode of WSxM 4.0 software was used to measure the size of features. Image D is a magnified section of another micrograph. *Table 4.2* shows the measured feature sizes. Samples were imaged at pH 9.5.

Height micrographs demonstrated that nanofibres were clearly present (*figure 4.3*) with the average individual nanofibre diameter was 12.3±2.1 nm (*table 4.2*)**.** The smallest nanofibre diameter was measured at 10 nm, larger than the theoretical width of a single β-sheet fibre (2.9±0.2 nm) reported by Boothroyd *et al.* [7]. Other studies measured the nanofibre diameter as 8 nm [9] and around 4 nm [6]. The discrepancy in FEFEFKFK SAPH nanofibre diameter could be due to this study not taking into account the tip to sample correction distance. The tip was not in constant contact with the surface as tapping mode was used to scan the sample.

Other likely contributors include the amount of fibre aggregation that occurred, the sample preparation method and the conditions that AFM was carried out under. The measured nanofibre diameter of 12.3±2.1 nm (*table 4.2)* was comparable to 13.7±4.7 nm measured for KLD-12 SAPH nanofibre diameter [24] and 35 nm for LN-NS SAPH nanofibre diameter [23]. Crucially, the FEFEFKFK SAPH nanofibres were significantly smaller, by orders of magnitude, to the microfibers present in some scaffolds manufactured from synthetic or natural biomaterials [16, 25, 26].

B	Profile		Profile
1	13 nm	6	14 nm
2	15 nm	7	10 nm
3	13 nm	8	13 nm
4	10 nm	9	11 nm
5	12 nm	10	10 nm

C	Profile		Profile
1	13 nm	6	10 nm
2	19 nm	7	14 nm
3	10 nm	8	12 nm
4	14 nm	9	16 nm
5	11 nm	10	10 nm

D	Profile		Profile
1	15 nm	6	12 nm
2	12 nm	7	12 nm
3	10 nm	8	10 nm
4	14 nm	9	13 nm
5	11 nm	10	11 nm

Table 4.2. Results of measured single nanofibre diameter from *figure 4.3* calculated using the profile mode of WSxM 4.0 software. The letters correspond to the image and the numbers correspond to the fibre which was measured.

Larger nanofibre assemblies (*figure 4.4*) ranged from 28 nm to 115 nm in diameter and had an average estimated diameter of 77.1±44.6 nm (*table 4.3*). In cartilage, type II collagen forms fibrils which range from 10 to 140 nm in diameter [27]. The similarity between chondrocytes and NPCs in terms of cell morphology and production of ECM components has been highlighted by a number of studies [28, 29] so it is feasible that type II collagen produced by NPCs would be comparable. The native human NP consists of a randomly organised type II collagen network with radially organised elastin fibres which provides strength to the tissue. The mean diameter of type II collagen fibrils from the human NP has been measured at 92.1±26.54 nm using AFM [30]. Therefore the larger nanofibre assemblies present in the SAPHs were of similar diameter to type II collagen fibrils found in the NP (*table 4.3*) (*figure*

4.5). It has been speculated that nanofibrous matrices could mimic the native ECM architecture [15, 31]. This study hypothesised that the similarity in size of the larger nanofibre assemblies with the type II collagen fibrils present in the native human NP could mean that the SAPH architecture had the potential to mimic the native NP ECM. If this hypothesis was correct then SAPHs would be able to support and maintain the culture and phenotype of NPCs whilst stimulating production of appropriate ECM components (*chapter 5*). The nanofibrous SAPH architecture might also play a role in differentiation of MSCs towards a discogenic / chondrogenic phenotype with subsequent production of NP associated ECM components (*chapter 6)*.

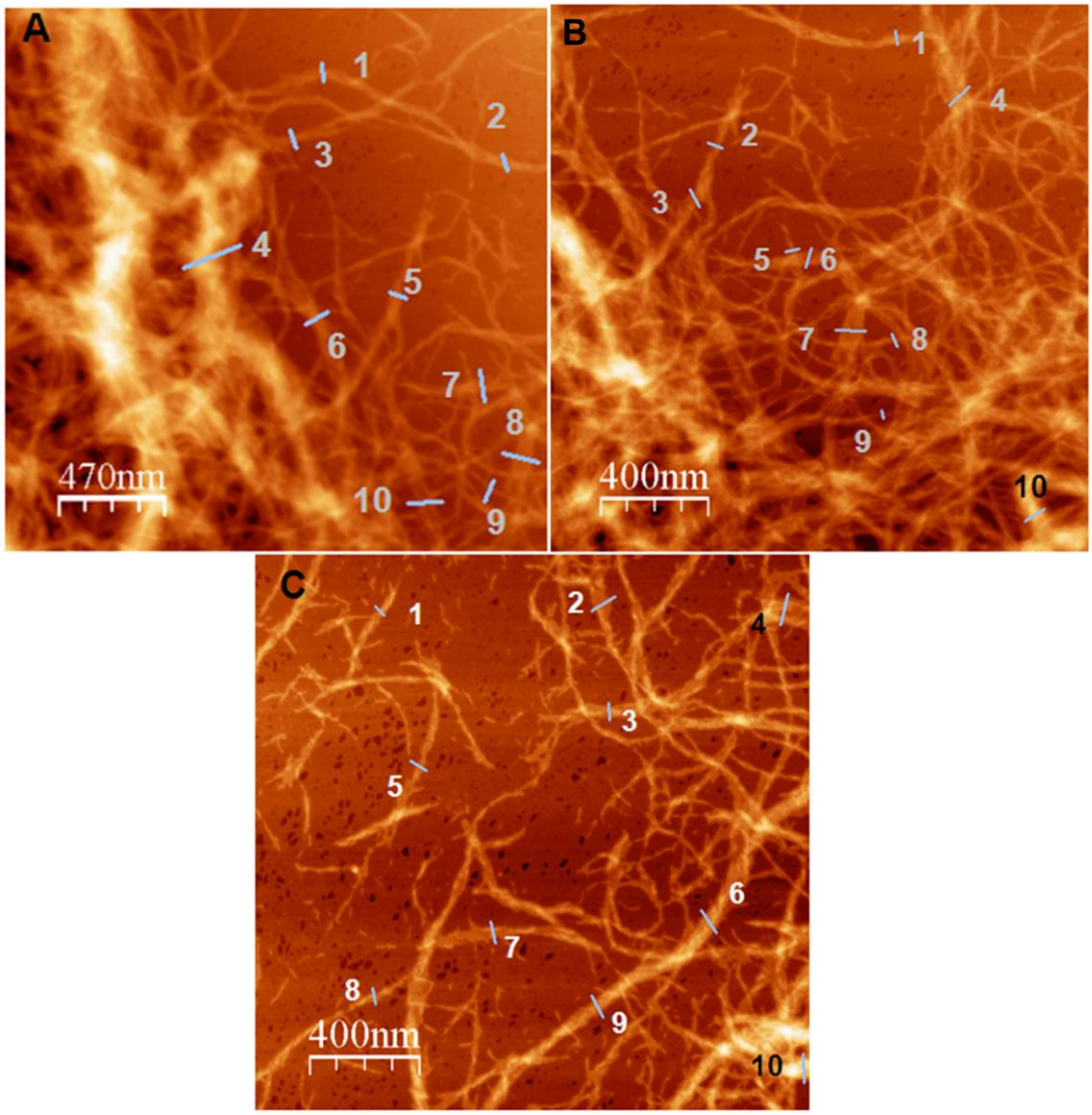

Figure 4.4. Height mode micrographs of 0.25 mg ml^{-1} FEFEFKFK SAPH imaged using AFM. The profile mode of WSxM 4.0 software was used to measure the size of features in [A], [B] and [C]. *Table 4.3* shows the measured feature sizes. Samples were at pH 9.5.

A	Profile		Profile
1	41 nm	6	74 nm
2	44 nm	7	112 nm
3	65 nm	8	42 nm
4	102 nm	9	38 nm
5	40 nm	10	86 nm

B	Profile		Profile
1	38 nm	6	92 nm
2	84 nm	7	62 nm
3	54 nm	8	41 nm
4	115 nm	9	72 nm
5	45 nm	10	107 nm

C	Profile		Profile
1	69 nm	6	92 nm
2	75 nm	7	75 nm
3	54 nm	8	127 nm
4	264 nm	9	35 nm
5	52 nm	10	114 nm

Table 4.3. Results of measured larger assembly diameter from *figure 4.4* calculated using the profile mode of WSxM 4.0 software. The letters correspond to the image and the numbers correspond to the fibre which was measured.

In summary, the dehydration step in the sample preparation process (*section 3.2.2.2*) caused the pores of the scaffold to collapse and the density of fibres to increase. Therefore AFM was not a suitable method for imaging the SAPH architecture as it appeared during cell culture conditions. However AFM did allow very high magnification and resolution micrographs of the nanofibrous network to be produced. Importantly it allowed the size of nanofibres and larger nanofibre assemblies to be measured which provided evidence to why SAPHs might be suited for NP tissue engineering.

4.4. DETERMINING VISCOELASTIC PROPERTIES USING RHEOLOGY

Oscillatory rheology was used to determine the viscoelastic behaviour and mechanical properties of the SAPHs [32]. Strain sweeps were first carried out to determine the LVR for the SAPH which ensured that the measured SAPH properties were independent of the magnitude or imposed stress or strain [33]. Strain sweeps determined that 1% strain was within the SAPH LVR therefore all frequency sweeps were carried out at this strain.

4.4.1. SAPHs at various pHs

Frequency sweeps showed that strength was below 1 kPa at acidic pH. At pH 2, G' was 59.45±17.2 Pa and at pH 3, G' was 482.9±385 Pa. At a physiologically relevant pH of 7.4, the pH that cell culture experiments were carried out at, the G' was 14.7±2.5 kPa. At a pH of 9.2 the G' value was 2.4±0.4 kPa, at pH 10.3 G' was 0.33±0.01 kPa and at the highest pH tested (pH 10.8) the G' value was 20±10.8 Pa.

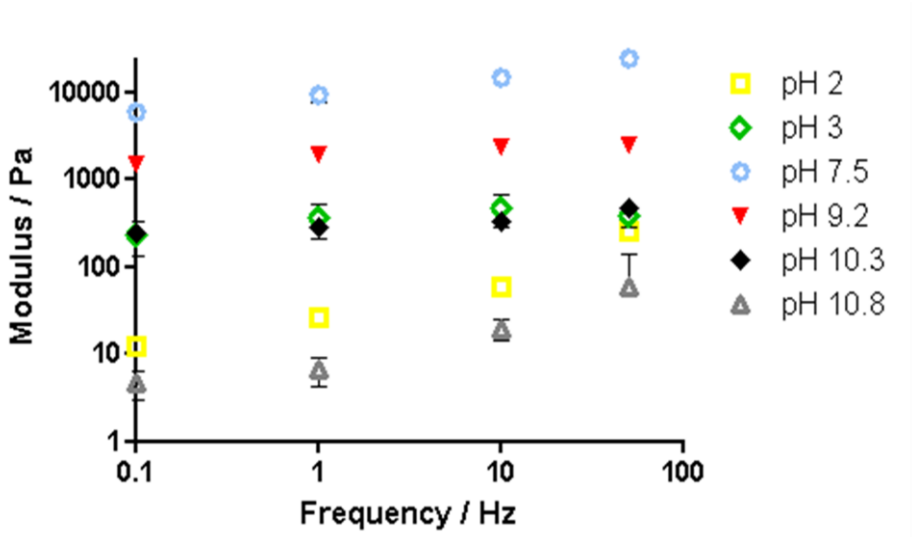

Figure 4.5. Frequency sweep G' values for 30 mg ml^{-1} SAPHs at various pHs at 1% strain. The pH of SAPHs was adjusted by titrating 1M NaOH. Values expressed as mean±SD where n=3.

Oscillatory rheology determined that the G' value was related to the pH (*figure 4.5*). The G' value measured the deformation energy stored during the shear process of the sample and is equivalent to the stiffness of the system [32]. Frequency sweep data showed that at pH 7, the SAPH was stiffest whilst at highly acidic or basic pHs, the mechanical properties were weakest as pH determines overall ionisation state. Due to β-sheet SAPHs containing both positively and negatively charged residues, variations in pH affected the self-assembly process. SAPHs have been shown to undergo conformational changes as a function of pH [34]. The acidic dissociation constant (pK_a) describes the pH value where each group is half-protonated (pK_a =

$-\log_{10}K_a$). The charge state of each amino or carboxyl group was dependent on pH therefore the overall net peptide charge also differed with changing pH.

Boothroyd *et al.* determined that at lower pHs (<6) or higher pHs (>8) different fibre morphologies and network topologies were present. A change in fibre morphology from rigid to twisted (coiled and helicoidal) depending on the pH of the SAPH was observed. It was hypothesised that the alteration in fibre architecture occurred due to a change in the intrinsic twist of the β-sheet ladder [8]. The changes in fibre morphology due to variations in pH likely explained the variations in mechanical properties with changing pH observed in this study (*figure 4.5*).

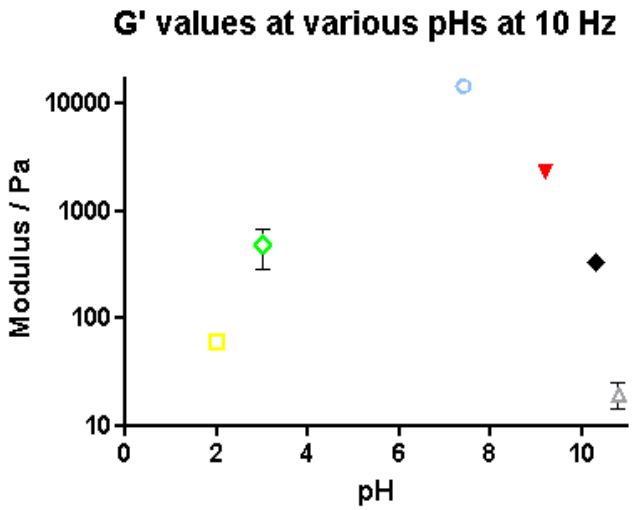

Figure 4.6. Frequency sweep G' values for 30 mg ml^{-1} SAPHs at various pHs when frequency was 10 Hz and strain was 1%. Values expressed as mean±SD where n=3.

When the peptide powder was suspended in dH$_2$O, the pH was around 2 - 2.8 due to TFA, used in the solid phase peptide synthesis, remaining in samples [6, 9]. The charge of the peptide was +2 at the acidic pH which caused repulsion forces between fibres causing the SAPH to be mechanically weak (*figure 4.6*). The net charge of the peptide was lowered with increasing pH which caused repulsion forces between fibres to also be reduced. Gao *et al.* observed a dense nanofibrous network consisting of long thin rigid fibres at pH 4 whilst at pH 7, bundles of nanofibres were observed as the reduction in repulsion forces and increase in attractive hydrophobic forces allowed fibres to associate together. At pH 7, the lysine and glutamic acid residues were neutral and more hydrophobic causing an increase in attractive forces between nanofibres producing thicker fibres with more entanglements present. Above pH 7, peptides carried negative charge. An increase in pH and hence overall peptide charge caused increased repulsion forces between fibres. At a pH of 10, the dense nanofibrous network consisted of long thin flexible fibres [18]. For this study, SAPHs had a pH of 9.3 to 9.6

before addition of cell suspension and media washes were used to return the SAPH to a physiologically relevant pH to increase chances of cell survival (*chapter 5 & 6*).

The final G' values could be readily changed (*figure 4.7*) by altering the amount of NaOH added during the production protocol (*section 3.2*). All samples were plated then subjected to media washes so at the time of analysis, the pH of all samples was 7.4. Addition of a high NaOH volume significantly reduced G' values due to the increase in sample pH (*table 4.4*). During the production process the pH of the sample was increased from ~2 to between 9.3-9.6 by addition of 1M NaOH so a clear homogenous product was produced. It has been documented that G' values of SAPHs started to gradually decrease above ~9.4 (1 kPa) and rapidly decrease above pH 10 (500 Pa). This study observed similar trends; SAPH pH was 9.5 when 98 µl of 1M NaOH was added with G' values of 14.95±1.11 kPa and SAPH pH was 10.5 when 120 µl of 1M NaOH was added with G' values of 0.95±0.26 kPa (*table 4.4*). Above pH 10, the fibre morphology changed from rigid to twisted which is thought to make lateral fibre association more difficult and hence reduce mechanical properties [8].

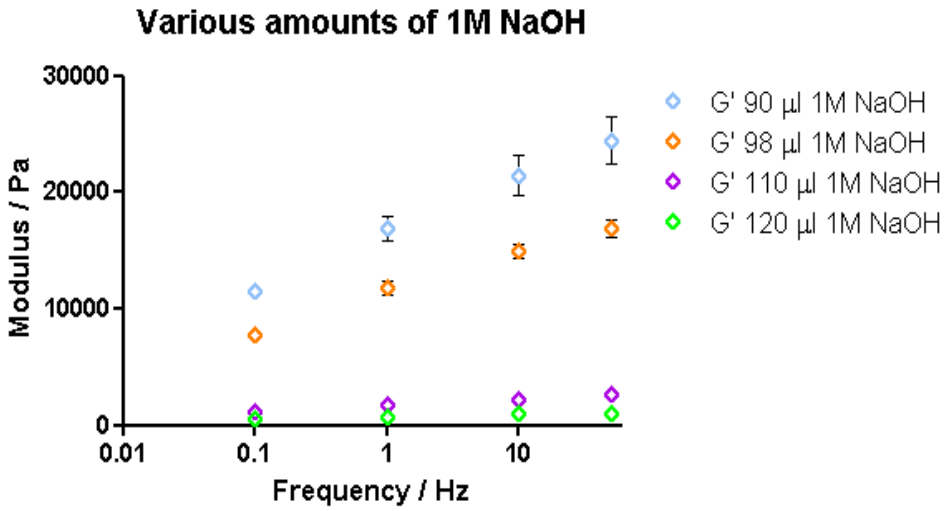

Figure 4.7. Frequency sweep G' value for 30 mg ml^{-1} FEFEFKFK SAPHs with varying amounts of 1M NaOH titrated during the SAPH production protocol. The samples were subjected to media washes so the final sample pH was 7.4 when rheology was carried out. Values expressed as mean±SD where n=3.

Amount of 1M NaOH / µl	*SAPH / pH*	*G' at 10 Hz / kPa*
90	~ 9.1	21.41±2.99
98	~ 9.5	14.95±1.11
110	~ 10	2.30±0.13
120	~10.5	0.95±0.26

Table 4.4. G' values presented in *figure 4.7* with corresponding SAPH pHs after addition of 1M NaOH. Values expressed as mean±SD where n=3.

The effect of salt concentration on the self-assembly process has been well documented [1, 35, 36]. In peptide solutions, salt ions will screen the charge of the peptide which will reduce the electrostatic repulsive effects between side-chains [37]. The negatively charged ions in PBS shielded the positive ions on the lysine chains which increased mechanical properties due to an enhancement of hydrophobic forces and hydrogen bonding [12, 36]. Cell culture medium, used to mimic the body fluid environment as well as provide nutrients for cells *in vitro*, contained a high concentration of NaCl which meant that addition of culture medium could be used to induce gelation. In this study, cell culture medium was used to return SAPH to a physiologically relevant pH to increase chances of cell survival.

4.4.2. Different concentrations of SAPH

Mechanical properties of acellular SAPHs (*figure 4.9 & 4.10*) and cell laden SAPHs (*figure 4.8*) were dependent on concentration. 25 mg ml^{-1} concentration displayed the lowest G' values and 35 mg ml^{-1} concentration demonstrated the highest stiffness. Above the CGC, an increase in SAPH concentration caused an increase in mechanical properties [38] due to higher fibre density in the samples [6, 9]. A higher density of fibres caused a greater amount of fibre aggregations and associations in the same volume [10]. Saiani *et al.* determined that mesh size was 30±3 nm at 10 mg ml^{-1} concentration in comparison to a mesh size of 15±3 at 40 mg ml^{-1} SAPHs [6].

G' values for all tested concentrations at any time point were 4 to 8 times higher than G'' (*figure 4.8*). G'' is representative of the energy dissipated during the shear process and describes the flow or liquid-like response of the material [32]. G'> G'' indicates that the SAPH behaved like an elastic solid [39]. It was important to note that even at low frequencies and long time scales the SAPH still demonstrated predominantly solid behaviour; some systems can be solid at high frequencies and fast time scales (G'>G'') but behave more liquid-like (G''>G') at low frequencies [32].

All concentrations experienced reductions in G' and G'' values with increasing time point however SAPHs still exhibited predominantly elastic behaviour. Despite SAPH mechanical properties closely matching the native NP (*section 4.4.4)* [13, 14], long term *in vitro* culture caused the systems to become mechanically unstable (*figures 8.6 & 8.7*). An explanation could be the mechanical effect of medium washes eroding SAPHs. Another contributor could be encapsulated cells remodelling the SAPH microenvironment and depositing ECM components (*chapter 5 & 6*). Cells are likely to have produced various factors and enzymes that reduced the stability of the scaffold [41].

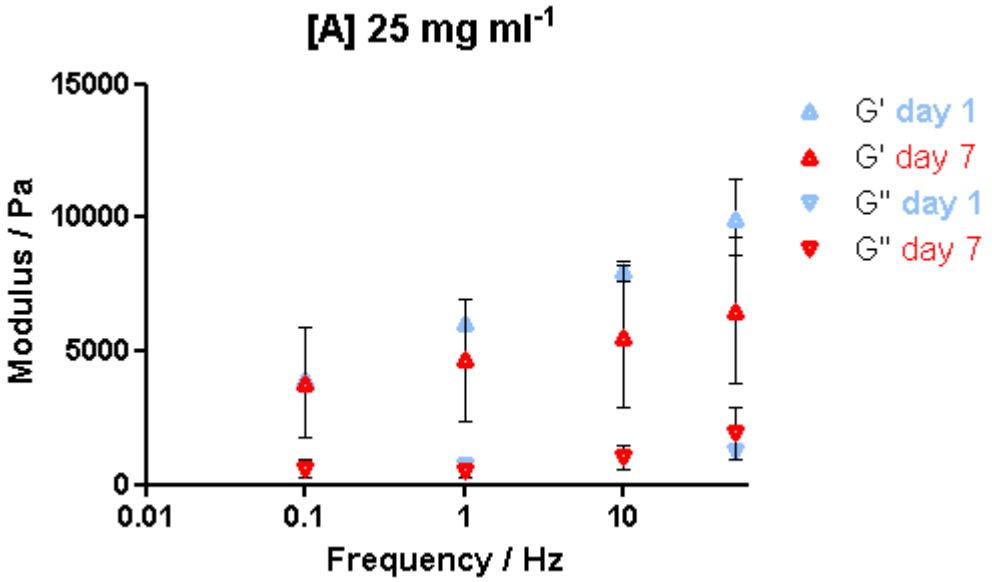
[A] 25 mg ml-1
15000
10000
5000
0
Modulus / Pa
0.01
0.1
1
10
Frequency / Hz
G' day 1
G' day 7
G'' day 1
G'' day 7

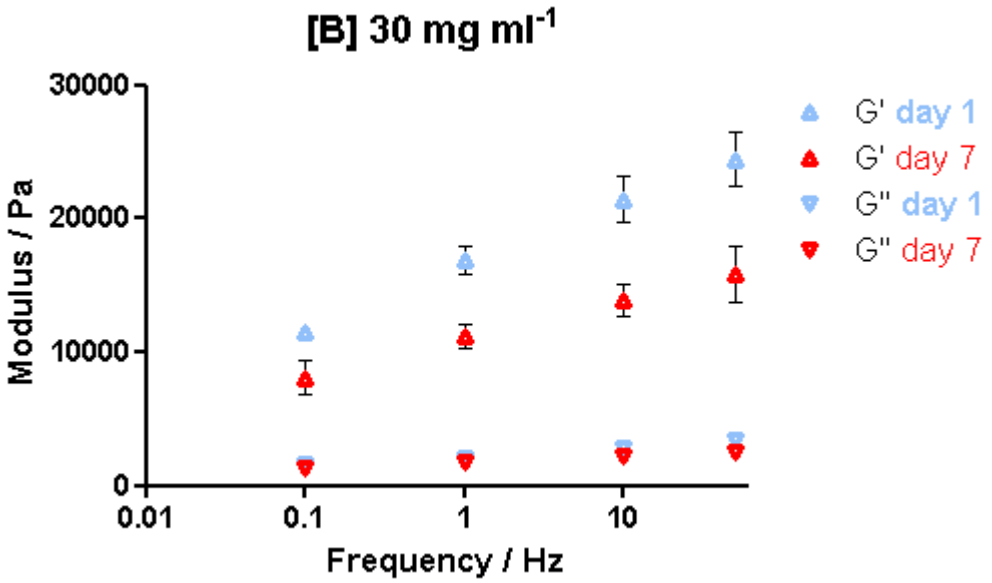
[B] 30 mg ml-1
30000
20000
10000
0
Modulus / Pa
0.01
0.1
1
10
Frequency / Hz
G' day 1
G' day 7
G'' day 1
G'' day 7

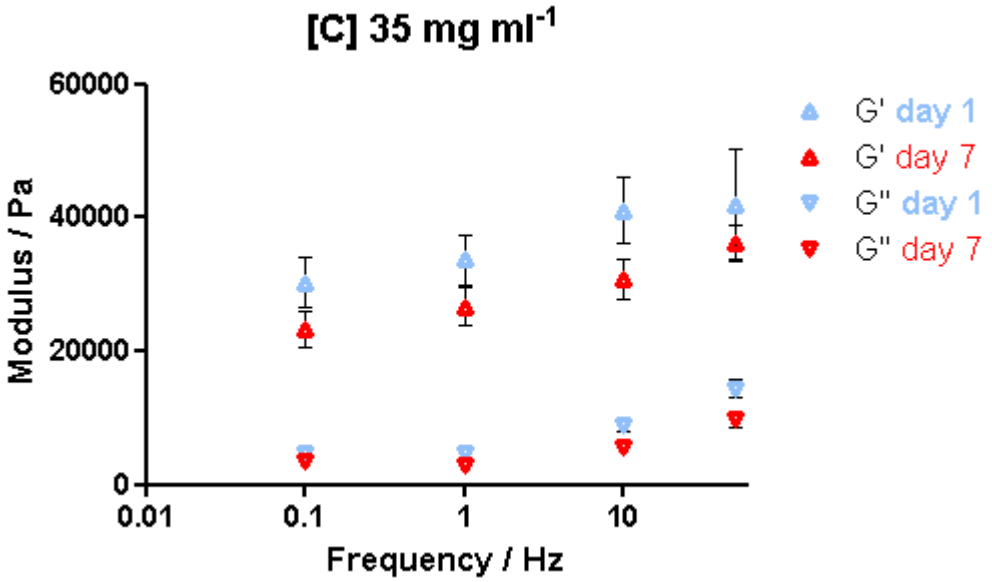

Figure 4.8. Frequency sweep G' and G'' values for various FEFEFKFK SAPH concentrations with 2x10^5 bNPCs ml^{-1}. [A] 25 mg ml^{-1} oscillatory rheology results. [B] 30 mg ml^{-1} oscillatory rheology results. [C] 35 mg ml^{-1} oscillatory rheology results. SAPHs were at a pH of 9.4 but following addition of cell suspension and media washes, the pH of the sample was reduced to the physiologically relevant pH 7.4. Values expressed as mean±SD where n=3.

An increase in mechanical properties should make the SAPHs more stable during *in vitro* culture [10, 41] however all concentrations demonstrated around a 20-30% loss of original strength from days 1 to 7 (*figure 4.8*). Results suggested that the decrease in SAPH stiffness with time point was similar in all tested concentrations despite the original SAPH strength. This could mean that for this particular system, an increase in mechanical properties may not significantly improve long term stability. Nevertheless, methods to improve mechanical properties include using sonication to produce SAPHs [11]. Increasing SAPH salt concentration produces stiffer scaffolds due to the effect of peptide group charge screening [36]. However addition of excessive salt will alter the physiological culture conditions and could lead to cell death. A compromise might have to be made between stability of the system *in vivo* and its stiffness as scaffold mechanical properties should be specific for the intended role [13] (*section 4.4.4*). It is also crucial to consider the effect that mechanical stiffness has on cell behaviour [42] and determining stem cell fate [40, 43]. For example, sonicated SAPHs can display G' values of 2.8 MPa for 150 mg ml^{-1} hydrogels [11] which would likely encourage encapsulated NPCs to attach to the scaffold and lead to loss of phenotype and production of inappropriate ECM components.

4.4.3. SAPHs with and without cells

There were no significant differences in G' values between acellular and cell-laden SAPHs for 25 and 30 mg ml^{-1} concentrations (*figures 4.9 & 4.10*) which suggested that cell encapsulation did not have a significant effect on SAPH mechanical properties. Contrastingly, at 35 mg ml^{-1} concentration day 1 results determined that acellular scaffolds displayed superior mechanical properties to the cell-laden SAPHs (*figure 4.9*). On day 7 (*figure 4.10*), when the frequency was below 1 Hz, the acellular scaffold had significantly higher G' values than the seeded scaffold however by 10 Hz, the seeded scaffold displayed similar mechanical properties. An explanation could be that cells had started producing and depositing ECM components which have important mechanical roles in the native tissue [44]. After the 3D culture of bovine chondrocytes in FEFEFKFK SAPHs, a significant increase in mechanical properties over culture period was reported. Scaffold behaviour was attributed to bovine chondrocytes depositing ECM components [10]. Evidence of ECM production by encapsulated bNPCs and h-BMMSCs were presented in *chapters 5 & 6* respectively.

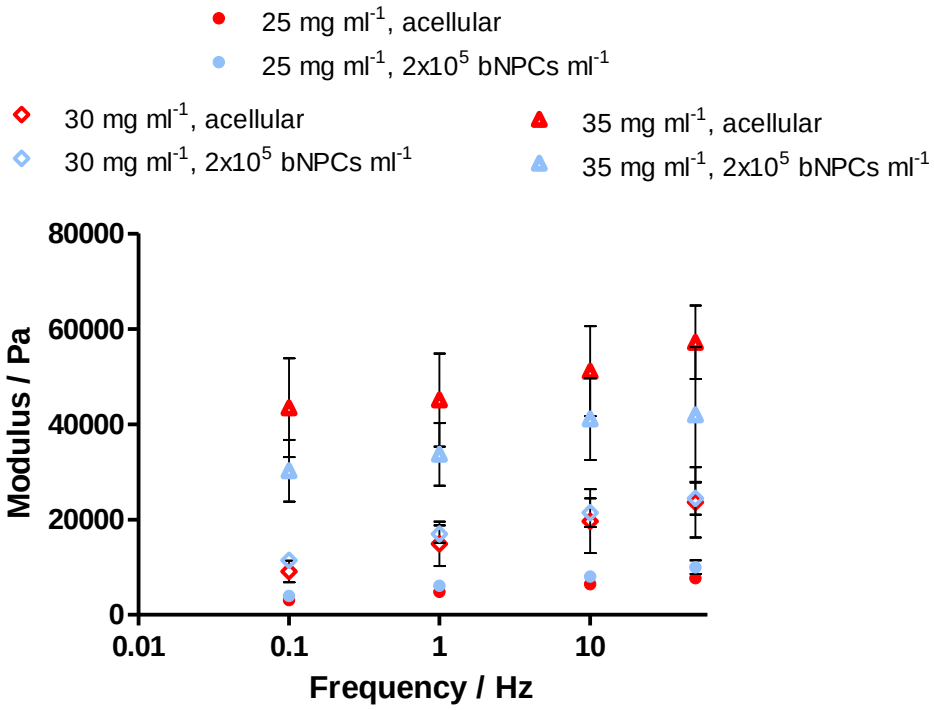

Figure 4.9. Frequency sweep G' values comparing acellular SAPHs and SAPHs with 2x10^5 bNPCs ml^{-1} on day 1. SAPHs were at a pH of 9.4 but following addition of cell suspension and media washes, the pH of the sample was reduced to the physiologically relevant pH 7.4. Values expressed as mean±SD where n=3.

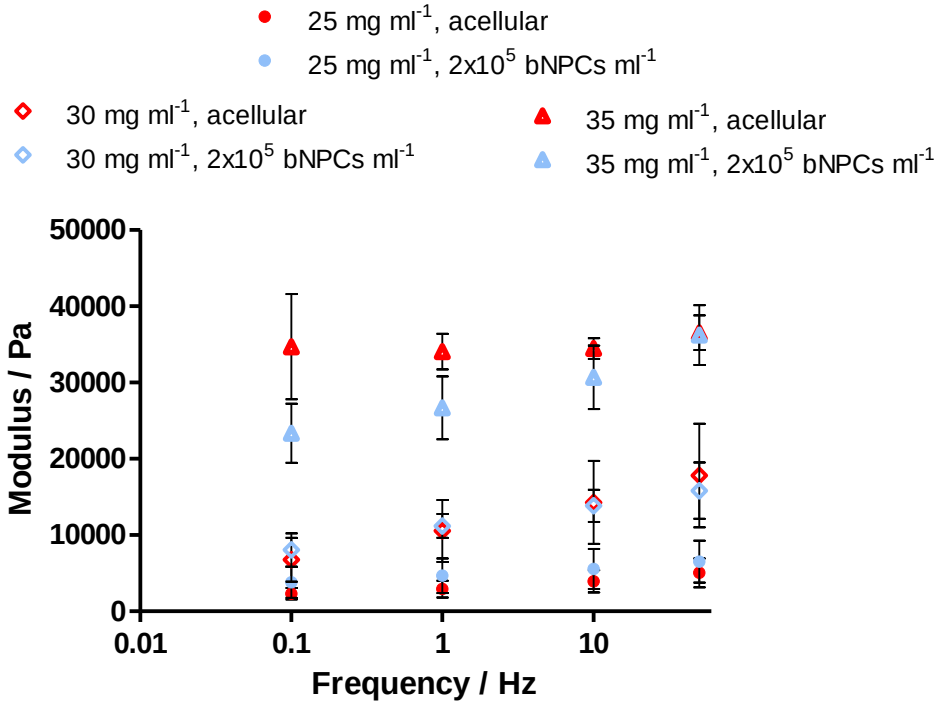

Figure 4.10. Frequency sweep G' values comparing acellular SAPHs and SAPHs with 2x10^5 bNPCs ml^{-1} on day 7. SAPHs were at a pH of 9.4 but following addition of cell suspension and media washes, the pH of the sample was reduced to the physiologically relevant pH 7.4. Values expressed as mean±SD where n=3.

Reza *et al*. determined that cell-laden and acellular carboxymethylcellulose scaffolds experienced significant decreases in strength from days 1 to 14 with no significant differences in mechanical properties caused by cell encapsulation. It was speculated that a non-cellular mediator was responsible for hydrogel weakening [45]. In contrast, some comparable potential tissue engineering scaffolds demonstrated no significant decrease in mechanical properties over *in vitro* culture. Foss *et al*. determined that alginate scaffolds seeded with human NPCs did not decrease in stiffness from days 1 to 28 [46]. Similarly Kim *et al*. established that alginate gels with NPCs encapsulated had Young's Modulus ranging from 30.52±1.78 to 43.50±1.345 kPa and 0.59±0.17 to 8.82±0.6 kPa dependent on the crosslinking density of the polymer with no significant difference in strength from days 3 to 14 [41]. There was an increase in HA hydrogel dynamic modulus (|G*|) with *in vitro* culture after bNPC encapsulation which was attributed to deposition of ECM components [47]. The |G*| or complex shear modulus describes the stiffness of a material. It represents the total resistance of a material to deformation when repeatedly sheared [14].

4.4.4. Comparison of SAPH mechanical properties to native NP

Iatridis *et al*. investigated the mechanical properties of non-degenerate NPs from 13 human subjects and determined that the average |G*| value was 11 kPa. NP stiffness varied from 7.4±11.6 to 19.8±31.4 kPa over a range of angular frequencies (1 to 100 rad s^{-1}) [14]. Frequency sweeps showed that SAPHs had comparable |G*| values to the native NP (*figure 4.11*). The SAPH displayed greater |G*| values but not significantly (P>0.05). When the frequency increased, the |G*| of the native NP also increased and similar behaviour was demonstrated by SAPHs. At higher frequencies, the |G*| values of the SAPHs closely matched the native tissue (*table 4.5*).

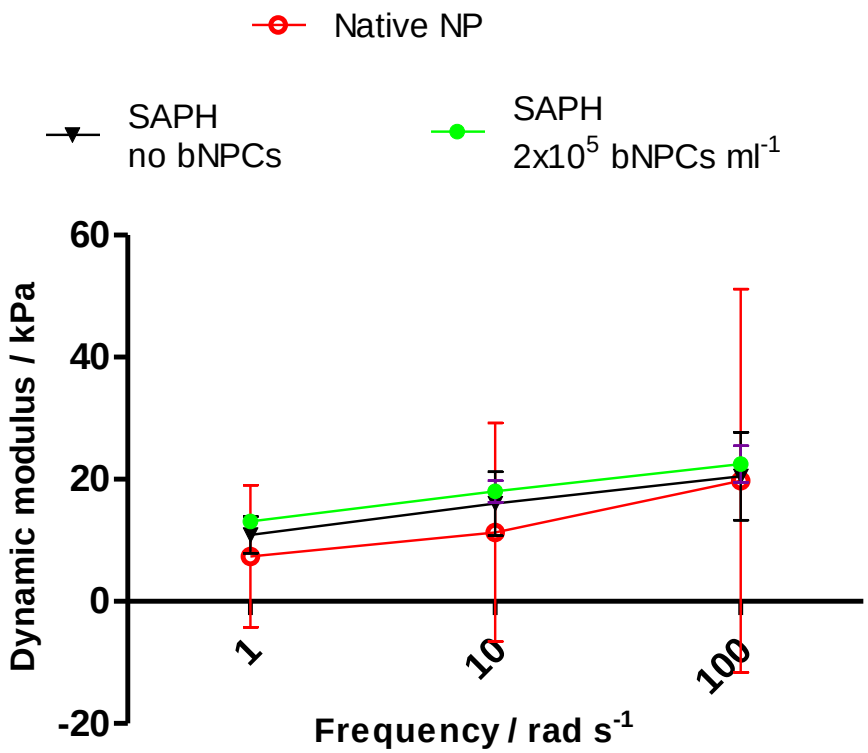

Figure 4.11. Comparison of the dynamic modulus of the native NP (red) [14], acellular 30 mg ml^{-1} FEFEFKFK SAPH (black) and 30 mg ml^{-1} FEFEFKFK SAPH with $2x10^5$ bNPCs ml^{-1} (green). SAPHs were at a pH of 9.4 but following addition of cell suspension and media washes, the pH of the sample was reduced to the physiologically relevant pH 7.4. SAPH values expressed as mean±SD where n=3, native NP values expressed as mean±SD where n=13.

Scaffold mechanical properties should be similar to the tissue that it is replacing or mimicking [31, 48]. The NP has an important role in motion segment mechanics therefore an implanted NP replacement system should be effective in transferring loads experienced by the IVD to the AF [13]. The ability of an injectable system to remain localised in the area of application as a well-defined material is directly related to system stiffness and network architecture [32]. Due to the high compressive loads that the IVD is subjected to [49], a scaffold with insufficient

mechanical properties is likely to fail after implantation. Inappropriate NP mechanical properties make it likely that transfer of hydraulic pressure to the AF will not occur efficiently. A scaffold that displays very high mechanical properties might damage the already mechanically weak NP tissue. It has been hypothesised that too stiff hydrogels could possibly have a negative effect on the culture of NPCs as the rigid microenvironment places them in a stressed environment rather than an appropriate gel-like environment [50]. Another hypothesis is that too high hydrogel rigidity could prevent remodelling of the pericellular matrix which is essential for maintaining cell activity [41]. Due to scaffold mechanical properties affecting cell behaviour and MSC differentiation [43, 51], a scaffold with significantly higher or lower mechanical properties than the native NP is likely to cause cellular de-differentiation leading to changes in cell physiology, ECM component production or morphology [53]. *In vivo* data for NP tissue engineering scaffolds that displayed high mechanical properties (>1 MPa) is limited. Other hydrogels investigated for applications in NP tissue engineering displayed comparable stiffness to the SAPHs optimised in the study (*tables 2.1 & 2.2*).

Frequency	**1 rad s^{-1}**		
	Native NP	SAPH (no bNPCs)	SAPH ($2x10^5$ bNPC ml^{-1})
|*G**| / *kPa*	7.4±11.6	10.9±3	13.1±0.8
δ / *deg*	23±5	7.4±1	6.6±0.3

Frequency	**10 rad s^{-1}**		
	Native NP	SAPH no bNPCs)	SAPH ($2x10^5$ bNPC ml^{-1})
|*G**| / *kPa*	11.3±17.9	16±5.1	18±1.8
δ / *deg*	24±5	7.1±0.9	7.2±0.9

Frequency	**100 rad s^{-1}**		
	Native NP	SAPH (no bNPCs)	SAPH ($2x10^5$ bNPC ml^{-1})
|*G**| / *kPa*	19.8±31.4	20.5±7.1	22.5±3
δ / *deg*	30±6	6.8±0.7	7.7±1

Table 4.5. Comparison of the native NP [14], acellular 30 mg ml^{-1} FEFEFKFK SAPH and 30 mg ml^{-1} FEFEFKFK SAPH with $2x10^5$ bNPCs ml^{-1}. |G*| is the dynamic modulus which describes the stiffness of the material and δ is the phase shift angle which describes energy dissipation during shearing and can be used to determine how elastic and viscous a

material is. SAPHs were at a pH of 9.4 but following addition of cell suspension and media washes, the pH of the sample was reduced to the physiologically relevant pH 7.4. SAPH values expressed as mean±SD where n=3.

The standard error for average |G*| values varied greatly (*figure 4.11*) when Iatridis *et al.* tested non-degenerated human IVDs indicating that NP strength between subjects was not consistent. The extensive variation of NP |G*| values was likely due to a range of subject ages, 16 to 68 years old, being tested [14]. Age is directly related to NP hydration and strength [53] which plays a key role in the ability of the NP to withstand loads and stresses as well as its ability to equalise loading on the vertebrae [54]. Genetics and lifestyle also impact NP health and degeneration. Therefore caution needs to be taken using the |G*| value as a definite indicator of NP strength however it does give an useful estimation of the required value that NP tissue engineering scaffolds need to achieve.

The NP has been described as being neither entirely confined or completely unconfined. Cloyd *et al.* used unconfined compression testing to measure the native tissue and determined that native human NP G' value was 5.39±2.56 kPa [13] which was used by the majority of NP tissue engineering scaffolds (*tables 2.1 & 2.2*) as the benchmark for scaffold stiffness [40, 41, 45]. Decreasing the SAPH concentration lowered mechanical properties (*figure 4.9*) so the G' value of 5.39±2.56 kPa [13] could be achieved. Alternatively, decreasing the hydrophobicity of the peptide side chains will increase critical coagulation concentration [9, 36] and hence lower mechanical properties.

The quoted NP strength is considerably lower than the IVD confined compressive aggregate modulus of 1.01±0.43 MPa which is the sum of confined compressive modulus and the osmotic pressure of the IVD [56]. However this value comprises the NP and AF working in conjunction, with the much tougher AF responsible for managing the high loads. The main role of the NP is to transfer stresses and loads to the AF [13, 54]. Therefore it is more important for a NP tissue engineering scaffold to behave in a gel-like manner and be able to transfer loads to the AF, to replicate the biomechanical role of the native tissue, than to display high stiffness.

The phase shift angle (δ) value indicates energy dissipation during shearing and can be used to determine how elastic and viscous the behaviour of a material is [56]. The δ of the human NP increased from 23^{o} to 31^{o} when the frequency increased from 1-100 rad s^{-1} [14]. At 10 rad s^{-1}, the δ value of native NP was 24^{o} which indicated that the tissue was a visco-elastic gel where the elastic component was dominant although the tissue still had a high viscous component. At the same frequency on day 1, the δ value for cell laden 30 mg ml^{-1} SAPH was 7.2±0.9^{o} (*table 4.5*) meaning that it was less viscous and more elastic than the native NP. The δ value could be increased to more closely match the native tissue by reducing the stiffness of the SAPH. For example at 10 rad s^{-1}, the |G*| value was 5.6±2.2 kPa whilst the δ value was

9.2±0.8^{o} for cell laden 25 mg ml^{-1} SAPH [14]. However there needs to be a compromise between scaffold stiffness and elastic to viscous ratio due to the native NP demonstrating a high δ value whilst also having a comparatively high stiffness. Chen *et al*. determined that a HA-gelatin hydrogel had |G*| values of 11-14 kPa with δ values of between 0 to 3^{o} [56]. The discrepancy in δ values meant that the scaffold would likely behave differently to the native tissue if implanted *in vivo* and might not be able to transfer the loads of the spine to the AF as effectively as the native NP.

The main limitation when comparing mechanical properties of the native NP to tissue engineering scaffolds was that construct behaviour could not be accurately assessed until *in vivo* implantation. In degenerated NPs, the microenvironment conditions are harsh with low O_2 levels, an acidic pH of 5.5 to 6.5 [57] and poor vascularisation [58]. From a biomechanical standpoint, the NP is subject to constant high loading and pressure due to body weight and muscle activity [59]. Therefore *in vitro* culture conditions are markedly different to the *in vivo* NP environment. Studies have investigated the use of bioreactors where the culture systems have been subjected to loading cycles similar to those experienced *in vivo* [60, 61]. However there has not been extensive research into the behaviour of seeded NP tissue engineering scaffolds in bioreactors.

It was interesting to note that biomaterials which displayed inferior mechanical properties to SAPH have observed positive biological effect after *in vivo* implantation. For example, Francisco *et al.* determined that a PEG hydrogel functionalised with laminin displayed a |G*| value of between 0.9-1.4 kPa and was retained initially at the site of injection after implantation into a rat model [62]. Orozco *et al.* discovered that pain relief occurred with significant increases in NP H_2O content when MSCs were injected directly into degenerated NPs of human LBP sufferers without a scaffold [63]. When PBS was injected into a degenerated IVD and subjected to a range of mechanical tests although the toughness and compressive resilience was significantly different to the native NP, the ability to withstand pressure and measurement of elasticity was not significantly different to the native tissue [64]. PBS is a liquid (G''>G') so its contribution to mechanical properties would have been negligible. This is encouraging as the SAPH is more gel-like and similar in mechanical properties to the NP so should be superior in mimicking the native tissue. It has been speculated that using a hydrogel to transfer MSCs into the NP might improve the survival of cells compared with injecting MSCs directly. A hydrogel is also likely to protect MSCs from leaking into the disc from the site of implantation [65].

4.5. INJECTABILITY OF SAPH

A potential NP tissue engineering cell carrier or scaffold is required to be deliverable via minimally invasive procedure [13, 59]. The spinal cord is located in close proximity to the IVDs and can be affected by cervical disc prolapse [66]. Therefore major surgery, for example spinal fusion, scoliosis surgery or potentially implantation of a non-injectable NP construct, always carries a risk [67]. DDD is strongly believed to originate in the NP so at the early stages of the disease, the AF might still be intact and show little signs of degeneration [13, 68]. In theory, an injectable scaffold could be delivered to the degenerate NP whilst minimising the damage to a conceivably healthy AF [59]. Crucially, it has been demonstrated that major surgery on the IVD can accelerate DDD [63, 69]. Therefore application of a scaffold via minimally invasive procedure would reduce the damage to the IVD. SAPHs were plated using micropipette tips with diameter of around 1 mm and the SAPHs set fully after a few minutes. SAPHs were also plated by injecting through a 21G needle with a diameter 0.5 mm suggesting that the SAPH displayed shear thinning properties (*section 4.5.1*) as well as having the ability to self-heal (*section 4.5.2*).

4.5.1. Shear thinning SAPH properties

Viscous properties were investigated by applying continuous shear then recording the viscosity as a function of shear rate. Results demonstrated that the viscosity of SAPHs decreased significantly for all concentrations with increasing shear rate (*figure 4.12*). The viscosity profiles highlighted SAPH shear thinning behaviour which allowed it to flow under shear stress. Results supported the hypothesis that the SAPH could be delivered to the degenerated NP via minimally invasive procedure. The recovery of original SAPH strength after shear-thinning is also crucial as NPs have an important biomechanical role in the body and the scaffold will be constantly subjected to loads and stresses [54]. A recovery cycle experiment was designed to replicate the injection process and determine the self-healing properties of the SAPH (*section 4.5.2*).

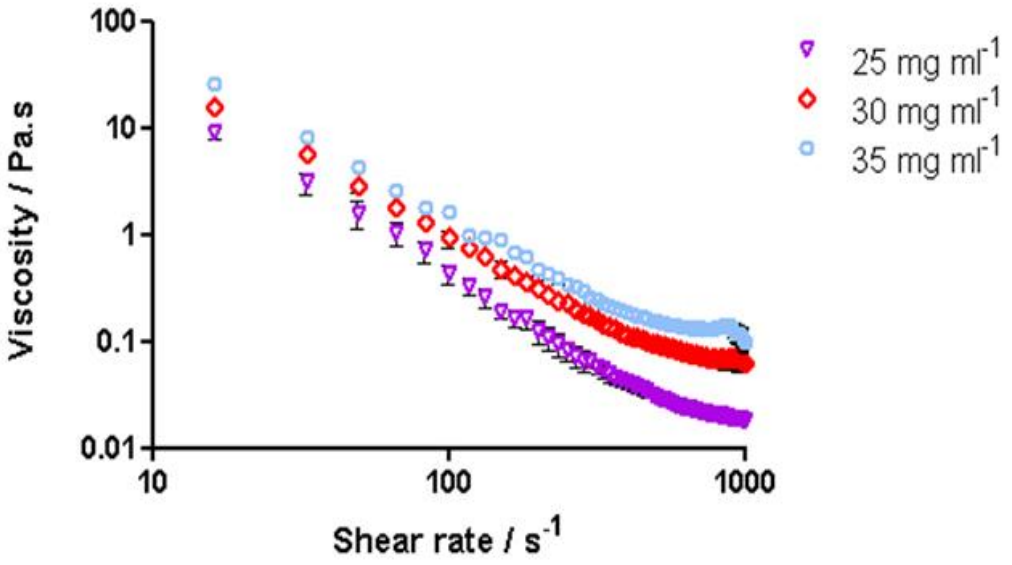

Figure 4.12. Viscosity profile of FEFEFKFK SAPHs at 25, 30 and 35 mg ml^{-1} concentrations. With increasing shear rate, the viscosity of all samples decreased. SAPHs were at a pH of 9.4 but following addition of cell suspension and media washes, the pH of the sample was reduced to the physiologically relevant pH 7.4. Values expressed as mean±SD where n=3.

The viscosity profile determined that the higher the SAPH concentration then the higher the viscosity of the sample was at defined shear rates (*figure 4.12*). A factor that affected final SAPH mechanical properties was the concentration of the system as discussed in *section 4.4.2.* [38]. Viscosity profiles of the various concentrations closely matched the reported literature for the same peptide sequence hydrogel [5].

4.5.2. Recovery cycles

A recovery cycle experiment was designed to mimic the injection process. The recovery cycle demonstrated that the SAPH sheared by applying 160% strain (G'' > G') when tested at pH 10.1 (*figure 4.13*) meaning more dominant liquid behaviour. When the strain was reduced to 1%, G' > G'' within 6 seconds of the high strain being alleviated (*table 4.6*) which meant that solid state behaviour was occurring. Within a few minutes at 1% strain, the original SAPH strength was recovered (~100 Pa). A number of recovery cycles could be conducted on the same sample demonstrating that the sample shearing and recovery process was reproducible.

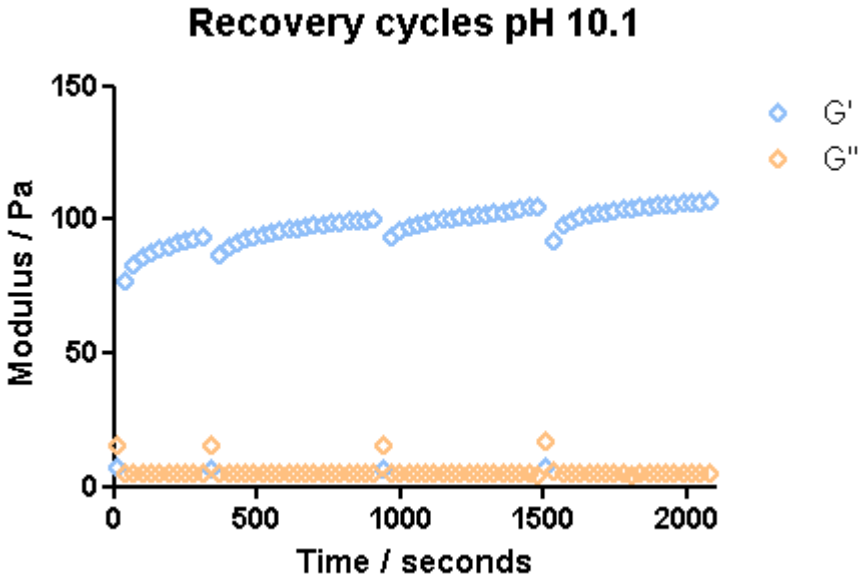

Figure 4.13. Recovery cycles for 30 mg ml^{-1} FEFEFKFK SAPHs at pH 10.1. Values expressed as mean±SD where n=3.

Time / s	Average G' / Pa	Average G'' / Pa
6	7.1	15.2
12	6.2	14.8
18	6.1	14.7
24	6.1	14.7
30	6.0	14.6
36	76.9	5.1
42	78.1	5.8
48	80.4	5.9
54	81.4	5.1
60	82.4	5.5

Table 4.6. Data for *figure 4.13* showing the average G' and G'' values at 6 second increments. A large percentage of the original SAPH strength was recovered within 6 second.

After samples had undergone 1 day of *in vitro* culture and were pH 7.4 (*figure 4.14*) similar biomechanical behaviour to samples at pH 10.1 occurred (*figure 4.13*). The recovery cycle demonstrated that the SAPH was sheared when 160% strain was applied (G'' > G'). When the strain was reduced to 1% G' > G'' within 6 seconds of the high strain being alleviated (*table 4.7*) which meant that solid state behaviour was occurring. Within a few minutes the original SAPH strength was recovered (~15.7 kPa) which is in agreement with *figure 4.8* for the stiffness of 30 mg ml^{-1} concentration.

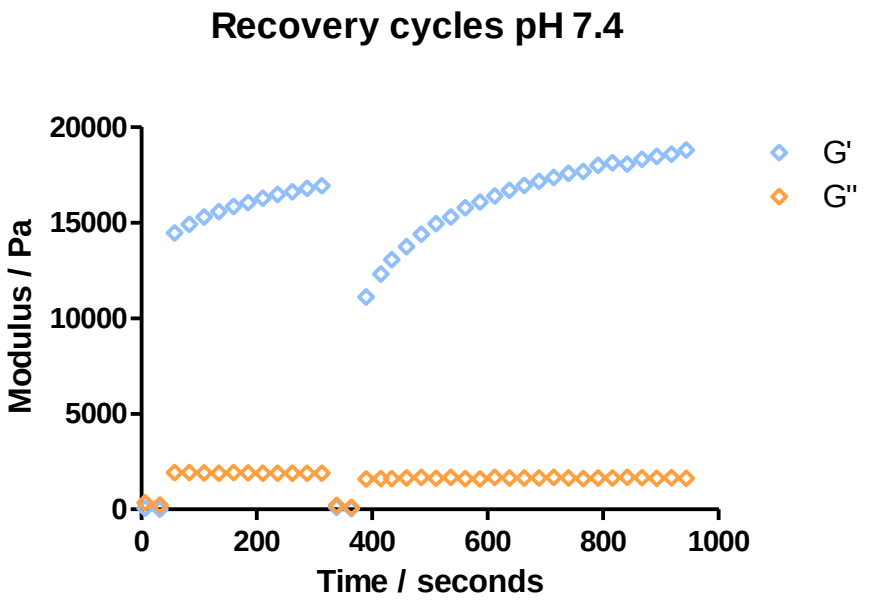

Figure 4.14. Recovery cycles for 30 mg ml^{-1} FEFEFKFK SAPHs at pH 7.4 after 1 day of *in vitro* culture. SAPHs were at a pH of 9.4 but following addition of cell suspension and media washes, the pH of the sample was reduced to the physiologically relevant pH 7.4.

Time / s	Average G' / Pa	Average G'' / Pa
6	51.9	345.6
12	35.4	281.7
18	25.1	242
24	17.3	217.7
30	14.6	220.2
36	14260	1945
42	14130	1956
48	14300	1935
54	14460	1929
60	14570	1936

Table 4.7. Data for *figure 4.14* showing the average G' and G'' values at 6 second increments. A large percentage of the original SAPH strength was recovered within 6 seconds.

The recovery cycle was designed to mimic the injection process and demonstrated that after cessation of high shear stress, gel-like behaviour recovered almost immediately (G'>G'') and the original strength of the SAPH was restored within seconds (*tables 4.6 & 4.7*). It has been demonstrated that SAPHs will recover approximately the same percentage of stiffness relative to the original system strength despite the sample rigidity at day 1 [70]. SAPHs at a pH of 10.1 had a lower strength than SAPHs that were originally at pH 9.4 (*figures 4.13 & 4.14*). The effect that pH had on SAPH stiffness was discussed in *section 4.4.1*.

The mechanism behind shear-thinning and self-healing is complex. When Yan *et al.* investigated β-hairpin SAPHs no anisotropy was displayed in structure at any studied shear rate so results excluded the possibility of fibril alignment along flow direction. Therefore a model was proposed where the non-covalently stabilised hydrogel network fractured during application of shear stress allowing flow of the material and hence the rise of shear-thinning properties [35, 70]. On removal of stress, the SAPH domains were immediately percolated and formed a macroscopic network throughout the entire sample which gave rise to the instantaneous return to solid-like behaviour. The original SAPH strength was further recovered via healing of the network structure through relaxations and interpenetration amongst fibrils [70]. The mechanism for shear thinning and self-healing of β-sheet forming SAPHs has not been fully investigated. An educated guess would assume that the self-healing mechanism of β-sheet forming SAPHs is akin to β-hairpin SAPHs due to the similarity in system structure and properties (*section 2.6.2*) [2, 35].

To determine whether the injection process significantly affected the cell population, a comparison was made between cell numbers after 1 day *in vitro* culture and cell numbers after 1 day *in vitro* culture which were then subjected to 3 recovery cycles. The hypothesis was that recovery cycles and the shear thinning process would not have a significant adverse effect on cell population as NPCs are exposed to high hydrostatic and osmotic pressures in the native tissue [14, 54]. There was no significant differences in bNPC numbers for those that had been subjected to recovery cycles compared with cell populations *in vitro* (*figure 4.15*) (P>0.05). This is in agreement with previous studies where the injection process had little impact on cell viability or distribution [70].

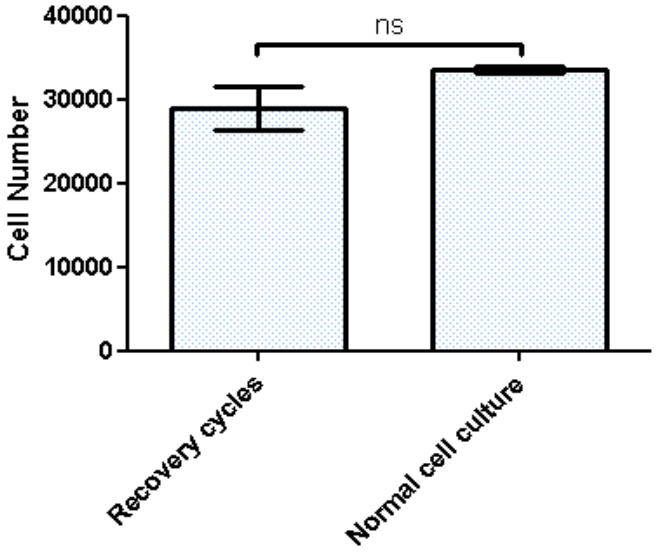

Figure 4.15. Cell numbers calculated using CytoTox 96® non-radioactive cytotoxicity assay for 30 mg ml^{-1} FEFEFKFK SAPHs with 2x10^{5} bNPCs ml^{-1}. There was no significant difference between cell population after 1 day of *in vitro* cell culture and after cells had been subjected to recovery cycles (P>0.05). Values expressed as mean±SD where n=3.

An alternative approach to injectable scaffold design involve systems with low viscosity *ex vivo* that can then be easily injected then undergo gelation *in vivo* [22]. This class of hydrogel relies on the sol-gel transition to be triggered by external stimuli for example physical (temperature), chemical (pH) or biochemical (enzyme action) [5, 11, 31]. Shear thinning hydrogels do not depend on external stimuli to trigger gelation [5, 10]. For example, it might prove difficult to expose an implanted scaffold to external stimuli after delivery into a degenerated NP [64]. Low viscosity scaffolds can experience leakage from the site of implantation before the sol-gel transition has occurred [70]. SAPHs recover original strength almost immediately which reduces the likelihood of leakage from implantation site (*tables 4.6 & 4.7*).

4.6. LIMITATIONS & FUTURE WORK

Limitations of this study include the fact that a number of scaffold mechanical properties that were likely to play a key role for successful reproduction of the biomechanical NP role were not investigated. For example, swelling ratio describes the increase in the weight of a system due to absorption of H_2O [41]. A key function of the NP is the ability to transfer loads to the AF therefore the compressive strength, the compressive resilience and the rate of change in osmotic pressure with material dilation are all scaffold mechanical properties that should be explored [64]. As discussed in *section 4.4.4* the *in vitro* environment is dramatically different to the *in vivo* environment therefore it is difficult to predict how the SAPH would behave exactly after implantation. The culture length for this study was 14 days which was shorter than the majority of NP tissue engineering investigations (*table 2.1 & 2.2*). Methods to improve SAPH degradation rate were discussed in *section 4.4.2*. Other SAPH studies concluded experiments on day 14 likely due to the culture systems weakening with *in vitro* culture length [22, 23, 24].

An interesting study would involve fluorescently tagging the SAPH then injecting it into an artificially degenerated bovine disc. This would allow visualisation of how the SAPH filled the defect, allow analysis of the localisation of the system and whether hydrogel leakage from site of implantation occurred. Testing how cell laden and cell-free SAPHs responded after culture in a hypoxic environment or after culture in a bioreactor that mimicked the constant loading that the native IVD is subjected to would be worthwhile investigations.

4.7. CONCLUSION

There are numerous challenges that a potential NP tissue engineering scaffold has to overcome in regards to replicating the biomechanical role of the native NP [13, 31, 59]. The prime focus of a number of NP tissue engineering studies was attempting to replicate the mechanical role of the NP. These systems typically displayed significantly higher stiffness than the native NP so the scaffolds could theoretically withstand the high loads and stresses experienced *in vivo* [56, 64]. However in this study, along with the majority of other published journals (*table 2.1 & 2.2*), the focus was on mimicking the native NP microenvironment so either encapsulated NPCs retained their phenotype (*chapter 5*) or implanted MSCs were differentiated towards an NP-like phenotype (*chapter 6*). If scaffold mechanical properties were comparable to the native tissue and the scaffold architecture mimicked the NP matrix then hopefully preservation of NPC phenotype and stimulation of the appropriate NP associated ECM components could occur. Type II collagen and aggrecan have key structural roles in the NP [44] therefore deposition of significant amounts of ECM components would lead to the formation of neo-tissue. Repair of the degenerated NP would contribute to restoration of NP biomechanical function instead of solely relying on the mechanical properties of a construct to replicate the NP function. Encapsulated cells would also be able to remodel the microenvironment and respond accordingly to changing factors in the IVD therefore would be curative rather than symptomatic. A number of synthetic and natural biomaterials have been investigated with varying degrees of success; the majority used the 5.39 kPa as the native human NP strength [13] however a smaller percentage used 11 kPa as the native NP strength [14] (*table 2.1 & 2.2*). Few studies investigated the injectability of their systems.

AFM determined that the SAPH architecture consisted of a dense nanofibrous network. The nanofibrous nature of the scaffold was hypothesised to mimic the native NP matrix due to large fibre assemblies being of the same scale to type II collagen fibrils found in the NP. Oscillatory rheology determined that the native NP strength could be replicated by the SAPHs with both human NP strength values determined by Iatridis *et al.* (11.3 kPa) and Cloyd *et al.* (5.39 kPa) being readily achieved with slight modifications to production protocol. Recovery cycles showed that the SAPHs could be applied via minimally invasive procedure due to the self-healing and shear thinning properties of the scaffold.

In conclusion, the characterisation of FEFEFKFK SAPH determined that the system displayed potential in terms of mimicking the mechanical properties of the native NP and deserved further investigation into the behaviour of NPCs and h-BMMSCs cultured in the system.

4.8. REFERENCES

1. **Zhang S, Holmes T, Lockshin C, Rich A** *'Spontaneous assembly of a self-complementary oligopeptide to form a stable macroscopic membrane'* Embo Journal (1993); Vol.11 pp.3787-3796
2. **Matson J, Stupp S** *'Self-assembling peptide scaffolds for regenerative medicine'* Chem. Commun. (2012); Vol.48 pp.26-33
3. **Horii A, Wang X, Gelain F, Zhang S** '*Biological designer self-assembling peptide nanofibre scaffolds significantly enhance osteoblast proliferation, differentiation and 3D cell migration'* PLoS ONE (2007); Iss.2 pp.1-9
4. **Roberts D, Rochas C, Saiani A, Miller A** '*Effect of peptide and guest charge on the structural, mechanical and release properties of β-sheet forming peptides*' Langmuir (2012); Vol.28 pp.16196-16206
5. **Tang C, Miller A, Saiani A** 'Peptide *hydrogels as mucoadhesive for local drug delivery*' International Journal of Pharmaceutics (2014); Vol.465 pp.427-435
6. **Saiani A, Mohammed A, Frielinghaus N, Collins R, Hodson N, Kielty C, Sherratt M, Miller A** *'Self-assembly and gelation properties of α-helix versus β-sheet forming peptides'* Soft Matter (2009); Vol.4 pp.193-202
7. **Boothroyd S, Saiani A, Miller A** *'Formation of mixed ionic complementary peptide fibrils'* Macromol Symp (2008); Vol.273 pp.139-145
8. **Boothroyd S, Miller A, Saiani A** '*From fibres to networks using self-assembling peptides*' Royal Society of Chemistry (2013); Vol.166 pp.195-207
9. **Miller A, Saiani A** '*Engineering peptide based biomaterials: Structure, properties and application'* Chemistry Today (2010); Vol.28 No.1 pp.34-38
10. **Mujeeb A, Miller A, Saiani A, Gough J** *'Self-assembled octapeptide scaffolds for in vitro chondrocyte culture'* Acta Biomaterialia (2012); Vol.9 Iss.1 pp.4609-4619
11. **Szkolar L, Guilbaud J, Miller A, Gough J, Saiani A** '*Enzymatically triggered peptide hydrogels for 3d cell encapsulation and culture'* J of Peptide Science (2014); Vol.20 pp.578-584
12. **Diaz L, Saiani A, Gough J, Miller A** '*Human osteoblasts within soft peptide hydrogels promote mineralisation in vitro*' J of Tissue Engineering (2014); Vol.5 pp.1-12
13. **Cloyd J, Malhotra N, Weng L, Chen W, Mauck R, Elliot D** '*Material properties in unconfined compression of human nucleus pulposus, injectable hyaluronic acid-based hydrogels and tissue engineering scaffolds*' Eur Spine J (2007); Vol.16 pp.1892
14. **Iatridis J, Setton L, Weidenbaum M, Mow V** '*The viscoelastic behaviour of the non-degenerate human lumbar nucleus pulposus in shear'* J Biomechanics (1997); Vol.30 No.10 pp.1005-1013
15. **Tibbitt M, Anseth K** 'Hydrogels as extracellular matrix mimics for 3D cell *culture'* Biotech Bioeng (2009); Vol.103 pp.655-663
16. **Zhang S, Yokoi H, Gelain F, Horii A** *'Designer self-assembling peptide nanofibre scaffolds'* Nanotechnology for Biology and Medicine: At the Building Block Level (2012); pp.123-147
17. **Aggeli A, Bell M, Carrick L, Fishwick C, Harding R, Mawer P, Radford S, Strong A, Boden N** '*pH as a trigger of peptide β-sheet self-assembly and reversible switching between nematic and isotropic phases*' JACS (2003); Vol.125 pp.9619-9628
18. **Gao J** '*Self-assembly and gelation properties of novel peptides for biomedical applications'* UoM PhD thesis – passed in 2013.
19. **Giacomelli C, Valenti L, Paci M, De Pauli C** '*Infrared study of trifluoroacetic acid unpurified synthetic peptides in aqueous solution: Trifluoroacetic acid removal and band assignment*.' Analytical Biochemistry (2011); Vol.410 pp.118-123
20. **Maslovskis A, Tirelli N, Saiani N, Miller A** *'Peptide-PNIPAAm conjugate based hydrogels: synthesis and characterisation'* Soft Matter (2011); Vol.7 pp.6025-6033
21. **Johnson W** '*Imaging DNA in solution with the AFM*' Agilent Technologies (2008); https://www.toyo.co.jp/file/pdf/spm/files/agi/5989-9932EN.pdf
22. **Ma K, Wu Y, Wang B, Yang S, Wei Y, Shao Z** *'Effect of a synthetic link N peptide nanofiber scaffold on the matrix deposition of aggrecan and type II collagen in rabbit notochordal cells'* J Mater Sci (2012); pp.1-11
23. **Wang B, Wu Y, Shao Z, Yang S, Che B, Sun C, Ma Z, Zhang Y** *'Functionalized self-assembling peptide nanofiber hydrogel as a scaffold for rabbit nucleus pulposus cells'* Journal of Biomedical Materials Research (2012); Vol.100 Iss.3 pp.643-653
24. **Sun J, Zheng Q, Wu Y, Liu Y, Guo X, Wu W** *'Culture of nucleus pulposus cells from intervertebral disc on self-assembling KLD 12 peptide hydrogel scaffold'* Materials Science and Engineering (2010); Vol.30 pp.975-980

25. **Feng G, Zhang Z, Jin X, Hu J, Gupte M, Holzwarth J, Ma P** '*Regenerating nucleus pulposus of the intervertebral disc using biodegradable nanofibrous polymer scaffold*' Tissue Engineering (2012); Vol.18 No.21 pp.1-8
26. **Yuan M, Yeung C, Li Y, Diao H, Cheung K, Chan D, Cheah K, Chan P** *'Effects of nucleus pulposus cell-derived acellular matrix on the differentiation of mesenchymal stem cells*' Biomaterials (2013); Vol.34 pp.3948-3961
27. **Shield K, Beckman M, Bowlin G, Wayne J** *'Mechanical properties and cellular proliferation of electrospun collagen type II'* Tissue Engineering (2004); Vol.10 1510-1518
28. **Mwale F, Roughley P, Antoniou J** '*Distinction between the extracellular matrix of the nucleus pulposus and hyaline cartilage: A requisite for tissue engineering of intervertebral disc*' European Cells and Materials (2004); Vol.8 pp.58-64
29. **Sive J, Baird P, Jeziorsk M, Watkins A, Hoyland J, Freemont A** '*Expression of chondrocyte markers by cells of normal and degenerate intervertebral discs*' J Clin Pathol: Mol Pathol (2002); Vol.55 pp.91-97
30. **Aladin D, Cheung K, Ngan A, Chan D, Leung V, Lim C, Luk K, Lu W** *'Nanostructure of collagen fibrils in human nucleus pulposus and its correlation with macroscale tissue mechanics'* Journal of Orthapaedic Research (2010) – Vol. 28 Iss.4 pp.497-503
31. **Nune M, Kumaraswamy P, Krishnan U, Sethuraman S** *'Self-assembling peptide nanofibrous scaffolds for tissue engineering: Novel approaches and strategies for effective functional regeneration'* Current Protein and Peptide Science (2013); Vol.14 pp.70-84
32. **Yan C, Pochan D** '*Rheological properties of peptide-based hydrogels for biomedical and other applications*' Chemical Society Reviews (2010); Vol.39 pp.3528-3540
33. **Mezger T** '*The rheology handbook: for users of rotational andoscillatory rheometers*' Vincentz Network GmbH and Co KG, Hannover, 2nd edn, 2006
34. **Altman M, Lee P, Rich A, Zhang S** '*Conformational behaviour of ionic self-complementary peptides*' Protein Science (2000); Vol.9 pp.1095-1105
35. **Haines-Butterick L, Rajagopal K, Branco M, Salick D, Rughani R, Pilarz M, Lamm M, Pochan D, Schneider J** '*Controlling hydrogelation kinetics by peptide design for three-dimensional encapsulation and injectable delivery of cells*' PNAS (2007); Vol.104 No.19 pp.7791-7796
36. **Caplan M, Schwartzfarb E, Zhang S, Kamm R, Lauffenburger D** *'Control of self-assembling oligopeptide matrix formation through systemic varation of amino acid sequence'* Biomaterials (2002); Vol.23 pp.219-227
37. **Kretsinger J, Haines L, Ozbas B, Pochan D, Schneider J** *'Cytocompatability of self-assembled β-hairpin peptide hydrogel surfaces'* Biomaterials (2005) – Vol.26 pp.5177-5186
38. **Leon E, Verma N, Zhang S, Lauffenburger D, Kamm R** '*Mechanical properties of a self-assembling oligopeptide matrix*' J Biomater Sci Polymer Edn (1998); Vol.9 No.3 pp.297-312
39. **Zhou M, Smith A, Das A, Hodson N, Collins R, Ulijin R, Gough J** '*Self-assembled peptide-based hydrogels as scaffolds for anchorage dependent cells*' Biomaterials (2009); Vol.30 pp.2523-2530
40. **Frith J, Cameron A, Menzies D, Ghosh P, Whitehead D, Gronthos S, Zannettino A, White J** '*An injectable hydrogel incorporating mesenchymal precursor cells and pentosan polysulphate for intervertebral disc regeneration'* Biomaterials (2013); Vol.34 pp.9430-9440
41. **Chou A, Nicoll S** *'Characterisation of photocrosslinked alginate hydrogels for nucleus pulposus cell encapsulation'* Wiley InterScience (2009) – pp.187-195
42. **Guilak F, Cohen D, Estes B, Gimble J, Liedtke, Chen C** '*Control of stem cell fate by physical interactions with the extracellular matrix*' Cell Stem Cell (2009); Vol.5 pp.17-27
43. **Engler A, Sen S, Sweeney H, Discher D** '*Matrix elasticity directs stem cell lineage specification'* Cell (2006); Vol.126 pp.677-689
44. **Shoukry M, Li J, Pei M** '*Reconstruction of an in vitro niche for the transition from intervertebral disc development to nucleus pulposus regeneration'* Stem Cells and Development (2013); Vol.22 No.8 pp.1-15
45. **Reza A, Nicoll S** *'Characterization of novel photocrosslinked carboxymethylcellulose hydrogels for encapsulation of nucleus pulposus cells'* Acta Biomaterlia (2010); Vol.6 pp.179-86
46. **Foss B, Maxwell T, Deng Y** '*Chondroprotective stimulation promotes mechanical properties of injectable scaffold for human nucleus pulposus tissue engineering'* J of Mech Beh of Biomed Mat (20014); Vol.29 pp.56-67
47. **Kim D, Martin J, Elliott D, Smith L, Mauck R** 'Phenotypic stability, matrix elaboration and functional maturation of nucleus pulposus cells encapsulated in photocrosslinkable hyaluronic acid hydrogels' Acta Biomaterialia (2015); Vol.12 pp.21-29
48. **Kemppainen J, Hollister S** '*Tailoring the mechanical properties of 3D-designed poly(glycerol sebacate) scaffolds for cartilage applications*' J of Biomedical Materials Research (2010); Vol.94 pp.9-19

49. **Cortes D, Jacobs N, DeLucca J, Elliot D** '*Elastic, permeability and swelling properties of human intervertebral disc tissue: A benchmark for tissue engineering*' J of Biomechanics (2014); Vol.47 pp.2088-2094
50. **Halloran D, Grad S, Stoddart M, Dockery P, Alini M, Pandit A** '*An injectable cross-linked scaffold for nucleus pulposus regeneration*' Biomaterials (2008); Vol.29 pp.438-447
51. **Dado D, Levenberg S** '*Cell-scaffold mechanical interplay with engineered tissue*' Seminars in Cell & Developmental Biology (2009); Vol.20 pp.656-664
52. **Horner H, Roberts S, Bielby R, Menage J, Evans H, Urban J** '*Cells from different regions of the intervertebral disc'* Spine (2002); Vol.27 No.10 pp.1018-1028
53. **Cheung K, Karppinen J, Chan D, Ho D, Song Y-Q, Sham P, Cheah K, Leong J, Luk K** *'Prevalence and pattern of lumbar magnetic resonance imaging changes in a population study of one thousand forty-three individuals'* Spine (2009); Vol.34 No.9 pp.934-940
54. **Adams M, McMillan D, Green T, Dolan P** '*Sustained loading generates stress concentrations in lumbar intervertebral discs*' Spine (1996); Vol.21 No.4 pp.434-438
55. **Johannessen W, Elliot D** '*Effects of degeneration of the biphasic material properties of human nucleus pulposus in confined compression*' Spine (2005); Vol.30 pp.724-729
56. **Chen Y, Su W, Yang S, Gefen A, Lin F** '*In situ forming hydrogels composed oxidised high molecular weight hyaluronic acid and gelatine for nucleus pulposus regeneration'* Acta Biomaterial (2012); pp.1-13
57. **Li H, Liang C, Tao Y, Zhou X, Li F, Chen G, Chen Q** '*Acidic pH conditions mimicking degenerative intervertebral discs impair the survival and biological behaviour of human adipose-derived mesenchymal stem cells*' Experimental Biology and Medicine (2012); Vol.237 pp.845-852
58. **Diamant B, Karlsson J, Nachemson A** '*Correlation between lactate levels and pH in discs of patients with lumbar rhizopathies*' Specialia (1968); Vol.24 pp.1195-1196
59. **Kandel R, Roberts S, Urban J** '*Tissue engineering and the intervertebral disc: the challenges*' Eur Spine J (2008); Vol.17 pp.480-491
60. **Haglund L, Moir J, Beckman L, Mulligan K, Jim B, Ouellet J, Roughley P, Steffen T** '*Development of a bioreactor for axially loaded intervertebral disc organ culture*' Tissue Engineering (2011); Vol.17 No.10 pp.1011-1019
61. **Tsai T, Nelson B, Anderson P, Zbeblick T, Li W** '*Intervertebral disc and stem cells cocultured in biomimetic extracellular matrix stimulated by cyclic compression in perfusion bioreactor*' The Spine Journal (2014); Vol.14 pp.2127-2140
62. **Francisco A, Mancino R, Bowles R, Brunger J, Tainter D, Chen Y, Richardson W, Guilak F, Setton L** *'Injectable laminin-functionalised hydrogel for nucleus pulposus regeneration'* Biomaterials (2013); Vol.34 pp.7381-7388
63. **Orozco L, Soler R, Morena C, Alberca M, Sanchez A, Sancho J** *'Intervertebral disc repair by autologous mesenchymal bone marrow cells: A pilot study'* Clinical and Translational Research (2011); Vol.92 pp.822-829
64. **Milani A, Freemont A, Hoyland J, Adlam D, Saunders B** '*Injectable doubly crosslinked microgels for improving the mechanical properties of degenerated intervertebral discs*' Biomacromolecules (2012); Vol.13 pp.2793-2801
65. **Vadala G, Sowa G, Hubert M, Gilbertson L, Denaro V, Kang J** *'Mesenchymal stem cells injection in degenerated intervertebral disc: cell leakage may induce osteophyte formation'* Journal of Tissue Engineering and Regenerative Medicine (2012); Vol.6 pp.348-355
66. **O'Laoire S, Thomas G** '*Spinal cord compression due to prolapse of cervical intervertebral disc (herniation of nucleus pulposus)*' J of Neurosurgery (1983); Vol.59 No.5 pp.847-853
67. **Nuwer M, Dawson E, Carlson L, Kanim L, Sherman J** '*Somatosensory evoked potential spinal cord monitoring reduces neurologic deficits after scoliosis surgery: results of a large multicenter survey*' Neurophysiology (1995); Vol.96 pp.6-11
68. **Pearce R, Grimmer B, Adams M** '*Degeneration and the chemical composition of the human lumbar intervertebral disc*' J Orthopaedics Research (1987); Vol.5 No.2 pp.198-205
69. **Park P, Garton H, Gala V, Hoff J, McGillicuddy J** *'Adjacent segment disease after lumbar or lumbosacral fusion: review of literature'* Spine (2004); Vol.29 p.1938
70. **Yan C, Altunbas A, Yucel T, Nagarkar R, Schneider J, Pochan D** '*Injectable solid hydrogel: mechanism of shear-thinning and immediate recovery of injectable β-hairpin peptide hydrogels*' Soft Matter (2010); Vol.6 pp.5143-5156

Chapter 5. *The culture of bovine nucleus pulposus cells in self-assembling peptide hydrogels.*

5.1. INTRODUCTION

5.1.1. Overview

Chapter 4 described SAPH characterisation and the attempt and subsequent success in tailoring the stiffness to closely match the native NP.

Chapter 5 summarises the analysis of bNPC culture in FEFEFKFK SAPH. The ultimate aim of this study is to deliver cells via minimally invasive procedure into a degenerated NP where the SAPH would act first as a delivery system. After implantation the SAPH would act as a scaffold to protect cells from the harsh degenerate NP environment, mimic the native tissue so encapsulated cells produced the appropriate ECM components for tissue regeneration and contribute a biomechanical role.

5.1.2. Hypothesis

It has been demonstrated that FEFEFKFK SAPHs maintained the 3D culture of bovine chondrocytes with high viability throughout culture, stimulated cellular proliferation and production of the cartilage related ECM component type II collagen [1]. It was concluded that successful exploitation of the system meant that SAPHs could serve as a template for cartilage tissue engineering.

The similarity in morphology and ECM components produced between chondrocytes and NPCs has been highlighted [2, 3]. Therefore due to FEFEFKFK SAPH acting as successful culture environment for chondrocytes [1], in theory the system should be able to support the culture of NPCs. A nanofibrous environment has been hypothesised to mimic the native ECM. Larger nanofibre assemblies were measured in *section 4.3.2* to be of similar size to type II collagen fibrils found in the human NP [4]. The stiffness was optimised to match the native tissue (*section 4.4.4*). Therefore the architecture and mechanical properties of the SAPH would hopefully mimic the native NP tissue and maintain the culture of NPCs, preserve their phenotype and stimulate appropriate ECM production.

5.1.3. Aims

Bovine NPCs were chosen for *in vitro* culture as the bovine disc has comparable size and *in vivo* pressure in the prone position [5] to the human IVD. Therefore bNPCs would hopefully behave in a similar manner to native NPCs following culture in the SAPH. A number of assays were conducted to determine cell behaviour after encapsulation in the SAPH to establish whether the system could effectively function for the culture of bNPCs.

- Cell viability and morphology (LIVE/DEAD® cell viability assay)
- Cell population (CytoTox 96® Non-Radioactive Cytotoxicity Assay, Quant-iT™ Picogreen® dsDNA assay)
- Cell phenotype (SYBR® Green qRT-PCR)
- ECM production (Blyscan™ sulphated GAG assay, ICC staining, specific GAG assay)

5.2. 2D CELL CULTURE

5.2.1. Phase contrast micrographs (cell viability, morphology and migration)

NPCs were polygonal in morphology when highly confluent or fibroblastic in morphology when cells were individual (*figure 5.1*) when cultured on glass or tissue culture plastic (TCP) which was in agreement with the literature [6]. Cell viability was high (*figure 5.1B*). Spread NPC morphology is not typically found in healthy native tissue [7]. Horner *et al.* determined that monolayer NPC culture significantly decreased type II collagen and significantly increased type I collagen deposition whilst production of aggrecan was absent [8]. Deposition of inappropriate ECM components strongly suggested de-differentiation of NPCs when cultured in monolayer [8, 9]. It has been well documented that substrate stiffness plays an important role in determining cell morphology, cytoskeletal structure and adhesion [10]. Cells tend to spread and attach to stiffer substrates as observed in *figure 5.1*. It was highly likely that 2D culture of NPCs provided an inappropriate culture environment when the preservation of the NP phenotype was required. Various 3D culture systems have been shown to restore NPC morphology after monolayer culture (*tables 2.1 & 2.2*).

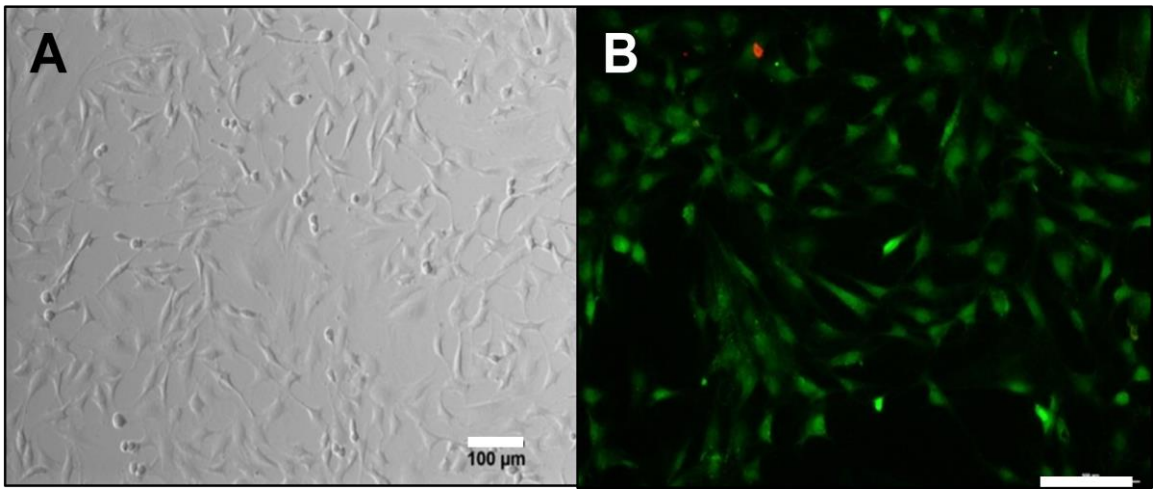

Figure 5.1. Phase contrast micrographs of 1x10^5 bNPCs ml^{-1} 2D culture on glass on day 7. [A] Light micrograph where cells displayed a fibroblast-like morphology [B] Fluorescence micrograph where LIVE/DEAD assay showed high cell viability. Viable cells were stained green and dead cells were stained red. Scale bar represents 100 µm.

As discussed in *section 2.1.2*, monolayer cell culture is in sharp contrast to the body's 3D environment including differences in how cells interact with substrates and the contrast in chemical and biological gradient diffusion systems which play a key role in signal transduction, cell–cell communications and cell behaviour [11]. In 2D culture, cells are exposed to homogenous concentrations of growth factors, nutrients and growth factors from the cell culture medium [12]. Examples that highlighted the difference between 2D and 3D cell culture include the distinction in NPC morphology when cultured in either system or the distinction in type of ECM component production [8, 13].

The majority of individual bNPCs remained rounded (*figure 5.2A&B*) or formed cell clusters (*figure 5.2C&D*) when seeded on the surface of SAPHs. A minority of cells spread and attached to the substrate *(denoted with red arrows*) with comparable morphology to bNPCs cultured on TCP or glass (*figure 5.1*). Bovine chondrocytes displayed a similar combination of rounded and spread morphology when cultured on the surface of FEFEFKFK SAPHs [1]. Cell viability remained high (*figure 5.2B*). Cell clusters were more numerous at later time points (*figure 5.2C&D*) and likely formed due to the high glucose and high oxygen environment of *in vitro* cell culture. NPC cluster formation is not typical of healthy IVDs and is associated with NPC proliferation, a process NPCs typically undergo only when under stress [14] or when expanded in monolayer [15].

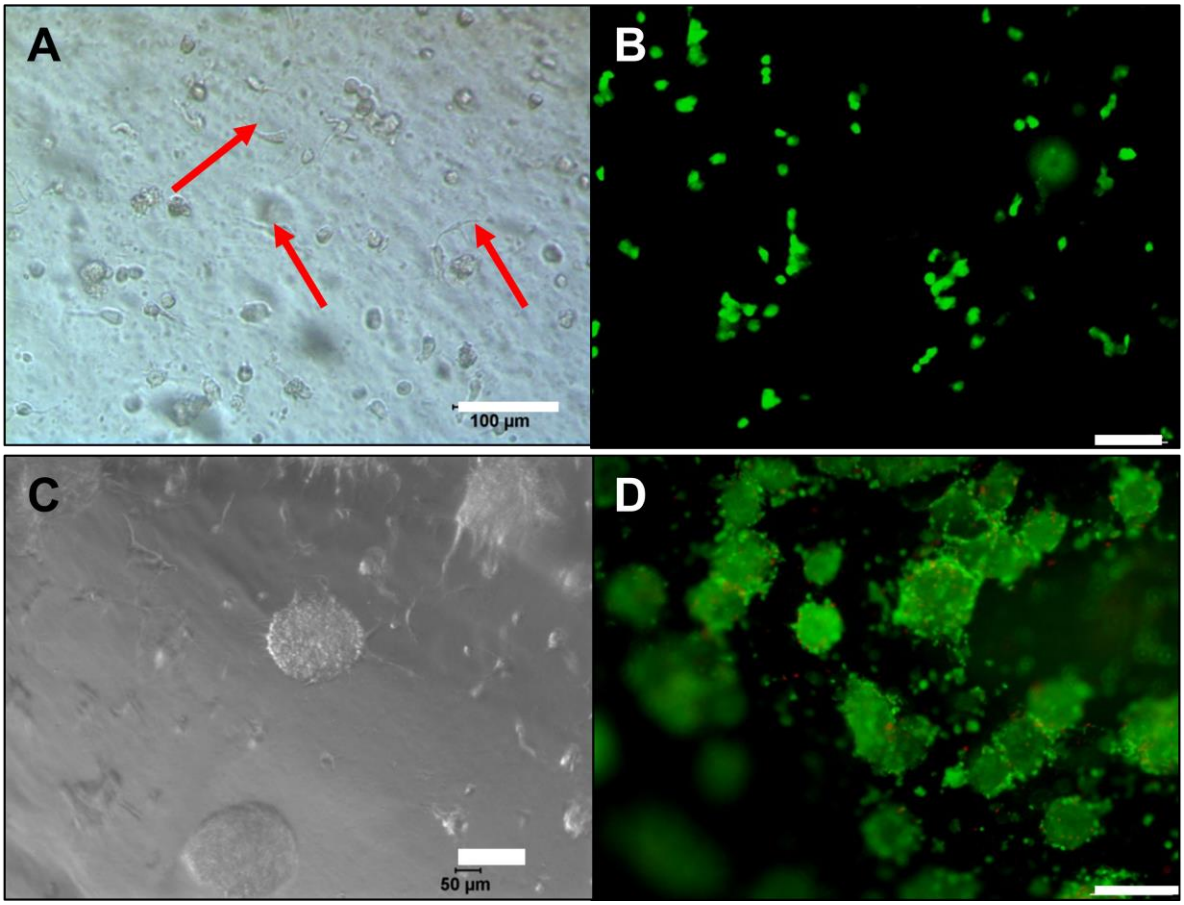

Figure 5.2. Phase contrast micrographs of 1x10^5 bNPCs ml^{-1} 2D culture on 30 mg ml^{-1} FEFEFKFK SAPH. [A] Light micrograph on day 3 demonstrated that the majority of cells displayed a rounded morphology with some adopting a fibroblast-like morphology (denoted with red arrows) [B] LIVE/DEAD assay on day 3 showed high cell viability and the majority of cells displayed a rounded morphology. [C] Light micrograph on day 7 demonstrating cell clusters. [D] LIVE/DEAD assay on day 7 showed high cell viability even within the centre of cell clusters. Viable cells were stained green and dead cells were stained red. Scale bar represents 100 µm.

JuLI™ Br Live cell movie analyser (*NanoEnTek, Korea*) was used to live-cell image the 2D culture of bNPCs on SAPHs over a 24 hour time period. At 0 hours (*figure 5.3A*), bNPCs were

individual after seeding. The footage showed cells migrating across the SAPH surface and aggregating together into small cell clusters by 8 hours (*figure 5.3B*). Cell motility was high as individual bNPCs migrated hundreds of micrometres to aggregate. Cell clusters also displayed high motility as bNPCs in clusters collectively migrated over the SAPH surface to combine into larger clusters (*figure 5.3C&D*). The apparatus could not be used to image migration of bNPCs in 3D culture.

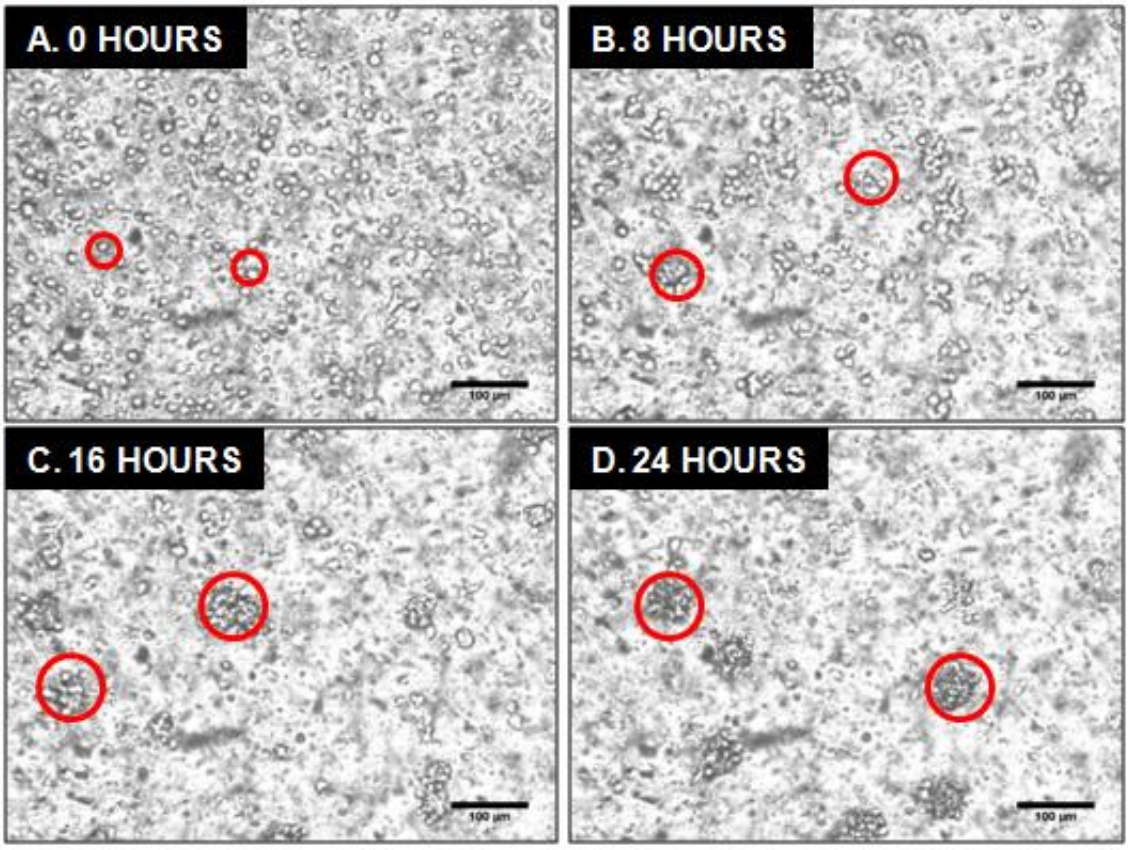

Figure 5.3. Light micrographs of 1x10^5 bNPCs ml^{-1} 2D culture on 30 mg ml^{-1} FEFEFKFK SAPH over 24 hours. [A] At 0 hours cells were individual. [B] At 8 hours, bNPCs had begun to migrate over the surface and started to aggregate. [C] At 16 hours, larger cell clusters were present. [D] By 24 hours the majority of cells were in cell clusters. The red rings highlight a proportion of cells that aggregated into larger cell clusters. Scale bar 100 µm.

To summarise, monolayer culture of bNPCs caused cells to adopt fibroblastic morphology which is associated with de-differentiation of the NP phenotype [8, 13]. For 2D culture on SAPHs, some bNPCs adopted a fibroblastic morphology whilst the majority were either rounded or migrated and aggregated into clusters. Cell cluster formation is associated with NPC proliferation. Therefore 2D cell culture was of little relevance when researching tissue engineering scaffolds which explained the focus of this study (and comparable NP tissue engineering studies) on investigation into biomaterial scaffolds that allowed truly 3D cell culture.

5.3. ASSESSING CELL VIABILITY AND MORPHOLOGY USING LIVE/DEAD® ASSAY

5.3.1. Cell viability for different SAPH concentrations

LIVE/DEAD® assay was used to determine the viability of encapsulated bNPCs over the 14 day culture period. SAPHs were imaged on days 1, 3, 7 and 14 at concentrations of 25 mg ml^{-1}, 30 mg ml^{-1} and 35 mg ml^{-1} to determine the optimal SAPH concentration for highest NPC viability.

All fluorescence micrographs showed that bNPCs embedded in FEFEFKFK SAPHs displayed high cell viability and adopted the characteristic rounded morphology that NPCs exhibit in the native tissue (*figure 5.4*) [7, 16]. Cells maintained rounded morphology throughout *in vitro* culture which is one-, of a number-, of indicators that the phenotype of cells was discogenic [17], chondrogenic [1] or adipogenic [18]. Further assays were required to assess gene expression to confirm the phenotype of cells (*section 5.5*). At a seeding density of $2x10^5$ bNPCs ml^{-1}, cells remained individual although there was evidence of doublet cells at later time points which suggested proliferation.

Objectively, when comparing the cell viability over the range of SAPH concentrations (*figure 5.4*), it appeared that the 25 mg ml^{-1} concentration had the highest percentage of dead cells whilst 30 mg ml^{-1} concentration displayed highest percentage of live cells.

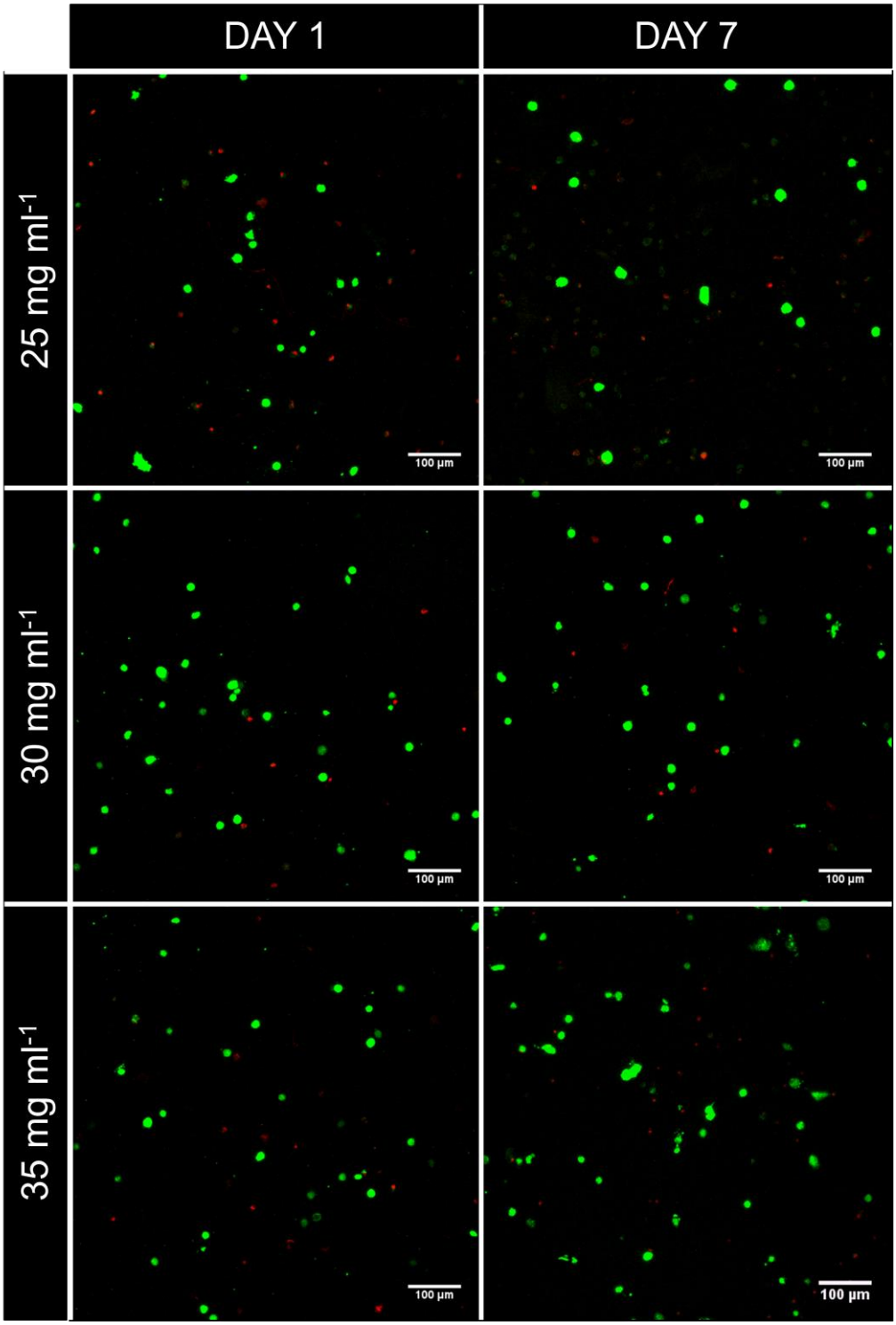

Figure 5.4. Fluorescence micrographs along the axial plane demonstrating cell viability of $2x10^5$ bNPCs ml^{-1} in FEFEFKFK SAPHs at 25 mg ml^{-1}, 30 mg ml^{-1} and 35 mg ml^{-1} concentrations. There was high cell viability throughout culture with cells displaying rounded morphology. Viable cells were stained green and dead cells were stained red. 200 µm slice. Scale bar represents 100 µm.

The percentage of viable bNPCs was calculated by counting total number of live and dead cells in 5 randomly selected fluorescence micrographs for each SAPH concentration. On day 7

30 mg ml^{-1} SAPHs (80.2%) had significantly higher percentage viable cells than 25 mg ml^{-1} SAPHs (68.2%) and 35 mg ml^{-1} SAPHs (73.7%) (*P<0.05) (*figure 5.5*).

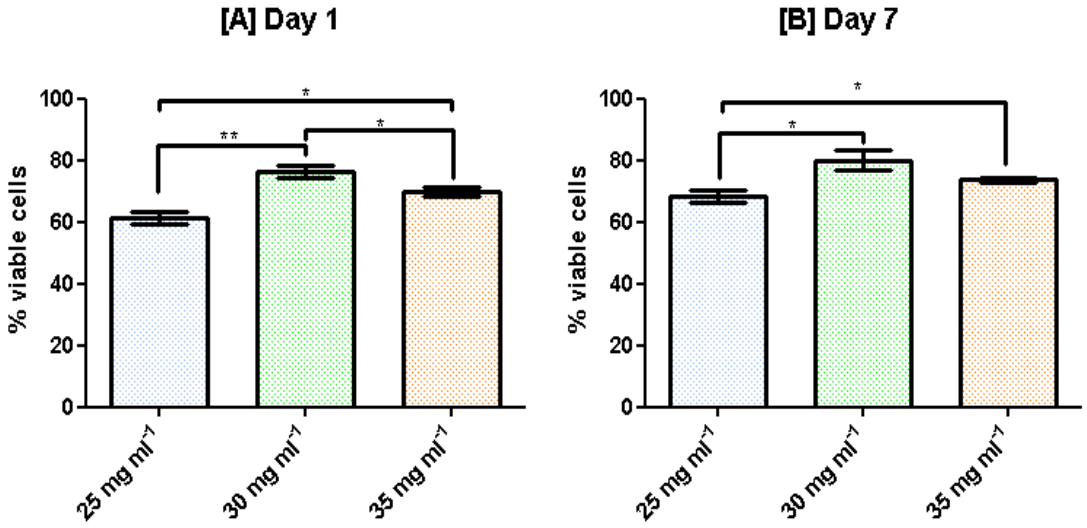

Figure 5.5. Percentage viable bNPCs present in LIVE/DEAD assay fluorescence micrographs for 25 mg ml^{-1}, 30 mg ml^{-1} and 35 mg ml^{-1} SAPH concentrations. [A] Cell viability on day 1 at 2x10^5 bNPCs ml^{-1} [B] Cell viability displayed on day 7 at 2x10^5 bNPCs ml^{-1}. (P>0.05, P*<0.05, P<0.01) Values expressed as mean±SD where n=3 from 3 experimental repeats.**

30 mg ml^{-1} concentration stiffness most closely matched the native NP [19] (*section 4.4.4*) therefore could have been most suitable for NPC culture at a cell to substrate interaction level. Cells sense matrix mechanical properties through binding events between integrins on the cell surface and motifs presented by the ECM components [12]. Mechanotransduction is an important role for NPCs [7] so the similar mechanical properties of 30 mg ml^{-1} SAPHs may have placed NPCs in a mechanically appropriate microenvironment. 25 mg ml^{-1} SAPHs had started to become unstable and displayed around 25% volume loss (*figure 4.8A*) by day 7 which likely impacted cell viability due to scaffold mechanical properties influencing cellular function [20]. Literature suggests that typically higher scaffold mechanical properties displayed the lowest cell viability. Chou *et al.* determined that the lowest bNPC viability after culture in alginate hydrogels was observed with highest cross linking density and mechanical properties [21]. It was hypothesised that a too dense nanofibre network might have restricted diffusion of nutrients into and waste products out of the system [22]. A too rigid scaffold might prevent elaboration and remodelling of the pericellular matrix which could adversely affect maintenance of cellular activity [21]. In contrast, Halloran *et al.* determined that there were no significant differences in cell viability over a range of scaffold stiffness when bNPCs were cultured in atelocollagen type II scaffolds. However, storage modulus only varied by a maximum of 1 kPa between each scaffold [23] whilst in this study the difference in concentration stiffness could exceed 8 kPa (*figure 4.8A*).

All concentrations displayed a non-significant (P>0.05) higher percentage of dead cells on day 1 in comparison to day 7 micrographs. Cell death was induced by pH shock due to the basic nature of the system at the time of seeding. SAPH pH was neutralised to a more physiological relevant level after media washes which likely explained the lower dead cell percentage on day 7. The effect of media washes demonstrated that addition of cell suspension reduced the pH from 9.4 to 8.7 and after 5 media washes the pH was 7.5 (*table 5.1*). There was a large majority of dead cells when samples did not undergo cell wash steps which highlighted the importance of returning the pH to physiologically relevant levels to maximise cell survival (*figure 8.8*).

SAPH after preparation process	SAPH after addition of 250 µl of cell suspension
pH 9.4	pH 8.7

After 1x media wash	After 2x media wash	After 3x media wash	After 4x media wash	After 5x media wash
pH 8.2	pH 8	pH 7.7	pH 7.6	pH 7.5

Table 5.1. The recorded pH of SAPHs for a set of experiments after addition of cell suspension then subsequent media washes.

5.3.2. Choosing SAPH concentration for cell culture experiments

30 mg ml^{-1} concentration was chosen to continue cell culture experiments as mechanical properties were most comparable to the native NP (*section 4.4.4*) and cell viability was highest (*figure 5.5*) compared to 25 mg ml^{-1} and 35 mg ml^{-1} SAPHs.

All cells displayed a rounded morphology which is characteristic of NPCs [16]. When SAPHs were imaged along the sagittal plane, the majority of bNPCs were viable (*figure 5.6*). On days 1, 3 and 7, there was homogenous dispersion of cells throughout the SAPH. By day 14, the majority of cells had migrated to the bottom of the SAPH and settled at the interface between the scaffold and cell culture insert membrane. On day 14, there was a lower total amount of cells present in micrographs. As the SAPH became weaker and less structurally stable with *in vitro* culture length (*figure 4.8B*), the act of media changes could have washed cells out of the system. The loss of scaffold volume also reduced the suitable available culture environment for cells.

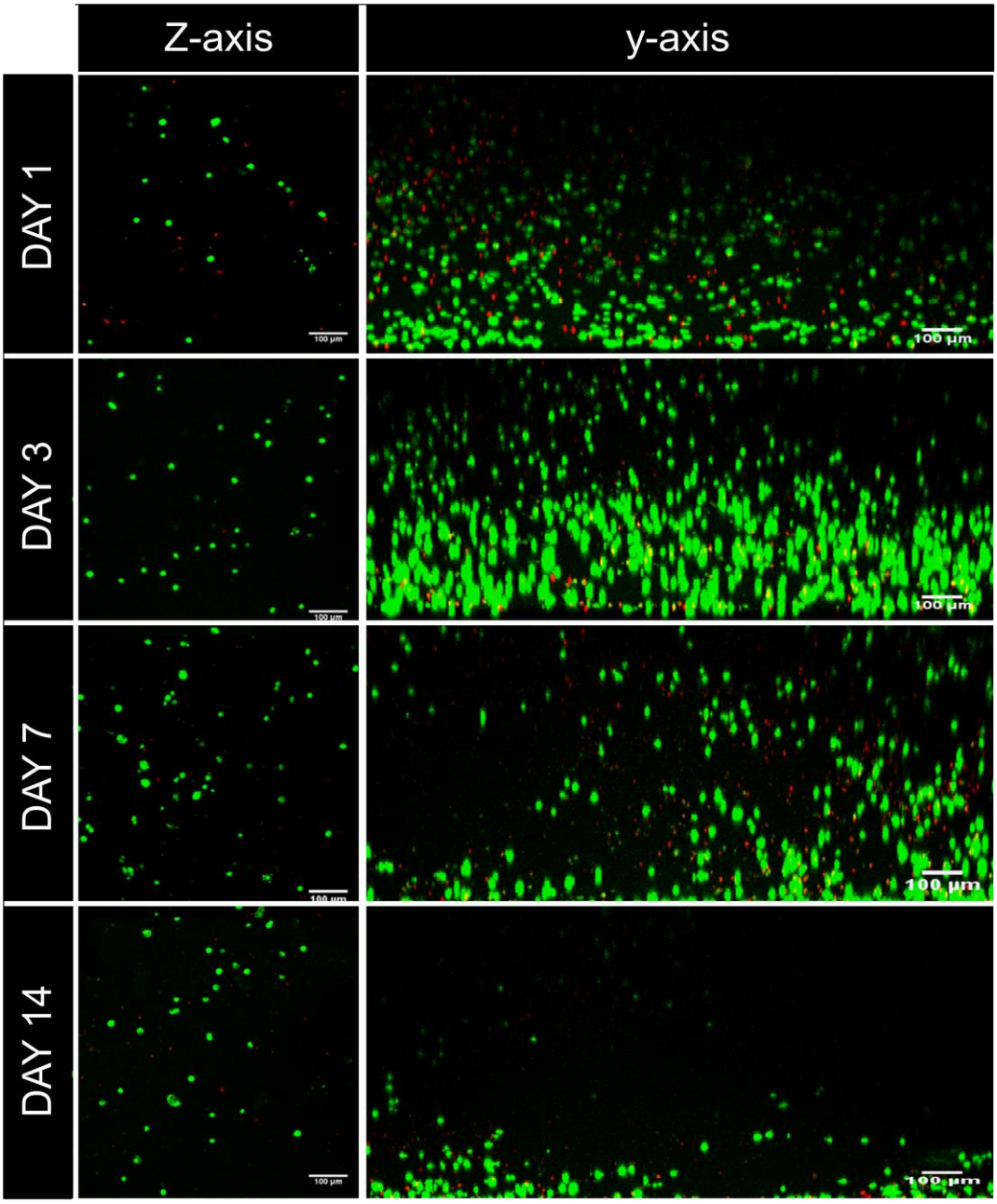

Figure 5.6. Fluorescence micrographs demonstrating cell viability of $2x10^5$ bNPCs ml^{-1} in 30 mg ml^{-1} FEFEFKFK SAPHs on days 1, 3, 7 and 14. Micrographs were taken along the z-axis (axial plane) and y-axis (sagittal plane). Viable cells were stained green, dead cells were stained red. Axial plane slice 200 µm, sagittal plane slice 500 µm. Scale bar represents 100 µm.

Total viable and dead cells were counted in 5 fluorescence micrographs and results demonstrated that a significant majority of viable cells were present throughout cell culture (*figure 5.7*). The percentage of viable cells remained consistent with no significant difference between consecutive time points. There was a trend of percentage viable cells decreasing from day 3 (82.5%) to day 7 (75.8%) to day 14 (70.8%) with a significant decrease from days 3 to 14 (*P<0.05). There was no significant difference in percentage viable cells for days 1 (77.6%) and 14 (P>0.05). In comparison, Ma *et al.* determined that cell viability remained

around 95% over *in vitro* cell culture with no evidence of cell proliferation when rabbit NCCs were cultured in the nanofibrous LN-NS SAPH [24].

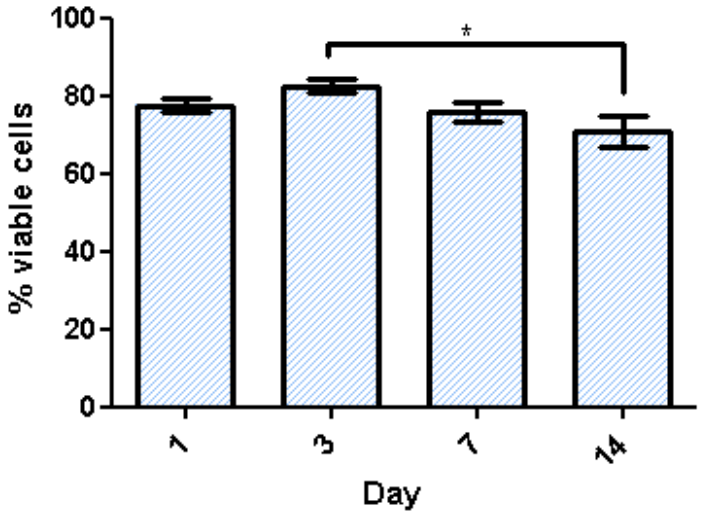

Figure 5.7. Percentage viable bNPCs present in LIVE/DEAD assay fluorescence micrographs for 30 mg ml^{-1} FEFEFKFK SAPHs. There was no significant difference in percentage viable cells when comparing days 1 and 14. (P>0.05, *P<0.05). Values expressed as mean±SD where n=3 from 3 experimental repeats.

The major limitation of using LIVE/DEAD assay was that it only allowed the ratio of viable to dead cells in a small area of the sample to be visualised. It was not a reliable method for determining the overall amount of viable cells in samples as this would need to assume an entirely homogenous distribution of cells throughout the scaffold with the same percentage of viable bNPCs. However, the cell count method did allow the ratio of viable to dead cells in the particular fluorescence micrographs to be quantified to get an overview of cell viability. Total cell number assays were carried out to obtain a more accurate representation of overall cell population numbers in the SAPH.

The overwhelming majority of studies investigating natural or synthetic biomaterials as NPC scaffolds or cell carriers demonstrated that the studied system supported high cell viability and rounded morphology of NPCs (*tables 2.1 & 2.2*). If rounded morphology was not adopted by cells after 3D culture then it was highly likely that the scaffold would not be suitable for NP tissue engineering [25]. When cultured in inappropriate culture environments that did not support the phenotype, NPCs tend to adopt a spread and fibroblastic morphology which is associated with production of type I collagen and low production of NP associated ECM components such as type II collagen and aggrecan [26].

5.3.3. Cell migration experiment through the SAPH

A homogenous cell dispersion was observed on days 1 to 7 (*figure 5.6*) when samples were imaged along the sagittal plane. An even distribution of cells throughout the SAPH was desirable to increase likelihood of consistent matrix formation. However on day 14 (*figure 5.6*), micrographs showed that bNPCs had migrated to the bottom of the sample.

A migration experiment involved seeding bNPCs on SAPH surface after the samples had completely set (*section 3.3.1.4)* then imaging samples along the sagittal plane to determine whether any cells were present inside. Micrographs supported the hypothesis that cells could migrate through the SAPH as bNPCs were imaged in the bulk and the bottom of the sample (*figure 5.8*). A system that allowed or stimulated cell migration could prove advantageous for NP tissue engineering as NPCs can be recruited from the native tissue to accelerate tissue regeneration [27].

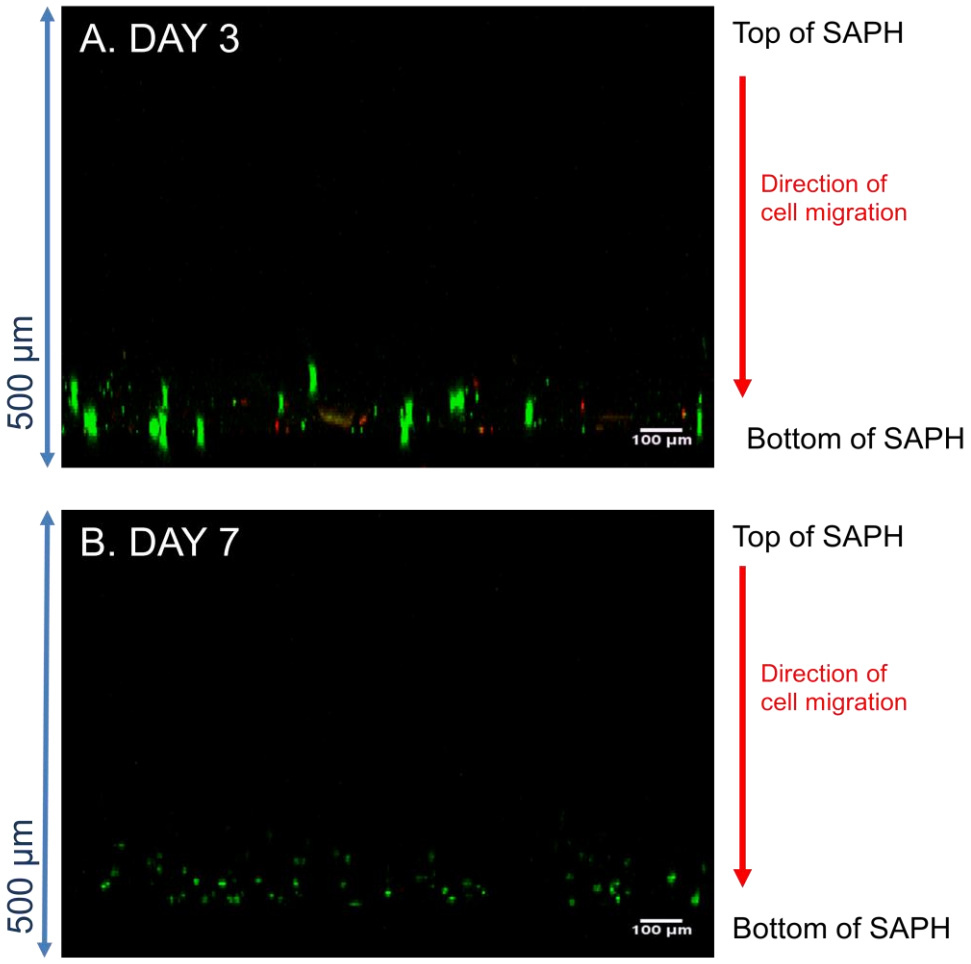

Figure 5.8. Migration experiment micrographs where bNPCs were seeded on the surface of 30 mg ml^{-1} FEFEFKFK SAPH and samples were imaged along the y-axis (sagittal plane) on day 3 [A] and day 7 [B]. Cells were present in the bulk of the scaffold and at the SAPH to cell membrane interface which demonstrated that cells could migrate through the system. Scale bar is 100 µm.

FEFEFKFK SAPH pore size has been quoted as between 15 to 30 nm [28], too small for bNPCs to pass through. Therefore it has been speculated that cells can 'migrate freely without hindrance' through the scaffold due to 97% H_2O content [11]. Also the peptide nanofibres have been described as semi-flexible so might be able to deform to allow cells to pass [28]. Cell migration has been reported in SAPHs with pore sizes ranging from 5 to 200 nanometres. Tao *et al.* demonstrated cell migration into the scaffold caused by functionalising the peptide with bioactive motif Link N. The non-functionalised RADA-16 controls also showed significant migration but not to the extent of the RADA-16 SAPHs functionalised with Link N [29, 30]. A limitation of the experimental design was that gravity may have been responsible for the movement of cells instead of stimulation of migration by the SAPH.

5.3.4. Overview and further discussion

Bovine NPCs cultured in alginate gel positive controls adopted rounded morphology and displayed similar cell viability throughout *in vitro* culture (*figure 5.9*) to bNPCs cultured in SAPHs (*figures 5.4 & 5.6*).

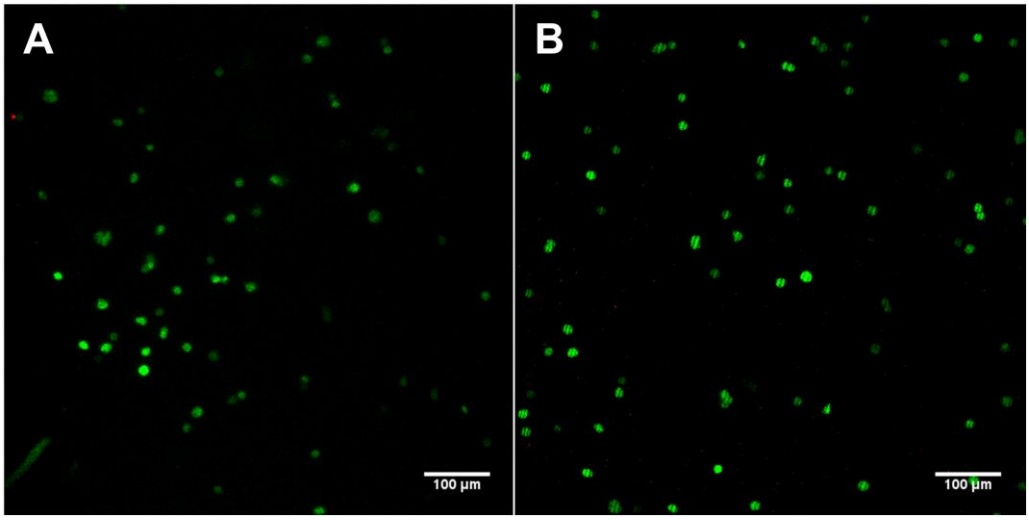

Figure 5.9. Fluorescence micrographs demonstrating cell viability of $2x10^5$ bNPCs ml^{-1} in [A] 30 mg ml^{-1} FEFEFKFK SAPHs or [B] 30 mg ml^{-1} alginate gels on day 3. Axial plane, 200 µm slice. Scale bar represents 100 µm.

In summary, bNPC viability remained high throughout 3D cell culture and cells adopted a rounded morphology which is the native NPC morphology [16]. The SAPH could restore the morphology of NPCs after 2D cell culture where cells adopted fibroblastic morphology.

5.4. DETERMINING CELL NUMBERS USING CYTOTOX 96® CYTOTOXICITY ASSAY

5.4.1. Overview and further discussion

Total cell number was estimated from a standard graph which plotted known cell numbers against absorbance (*figure 8.1*). Results determined that the viable cell population remained stable as there were no significant increases or decreases in cell number from day 1 to 14 (*figure 5.10*) (P>0.05). On day 1, viable cell numbers were estimated at $5.8x10^5$ which dropped to $4.8x10^5$ on day 3. From day 3 to day 7 ($5.1x10^5$) then day 7 to day 14 ($6.2x10^5$) there was a slight increase in viable cell number.

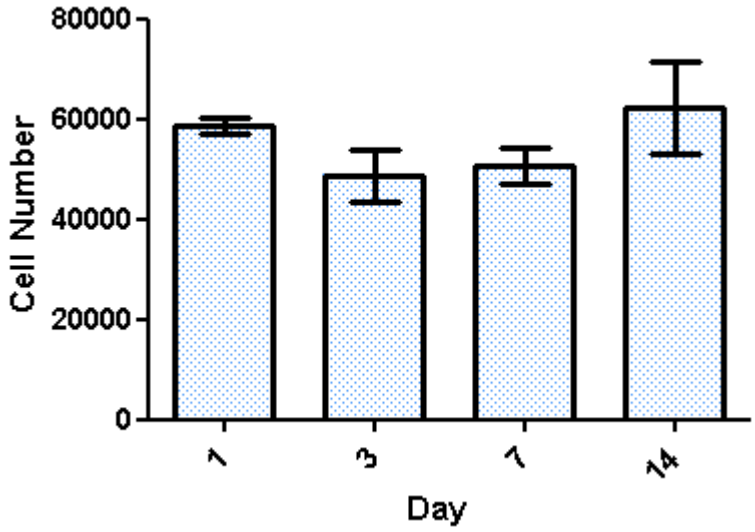

Figure 5.10. Cell numbers over 14 days *in vitro* culture for $2x10^5$ bNPC ml^{-1} in 30 mg ml^{-1} FEFEFKFK SAPH. There were no significant increases or decreases in cell number over culture period (P>0.05). Values expressed as mean±SD where n=4 from 3 experimental repeats.

There was an initial drop in viable cell numbers during seeding and plating due to the basic nature of the culture environment inducing pH shock in some bNPCs (*table 5.1*). SAPH ppH was returned to a more physiologically relevant level following media washes which was crucial for the health of cells [31] and explained the lack of significant cell death after day 1. This study hypothesised that absence of significant bNPC proliferation was not of particular concern. NPCs will only significantly proliferate when under stress [14], when cultured in monolayer [15] or during DDD [32]. Under these conditions, NPCs express inappropriate ECM components not associated with healthy NPCs; typically high amounts of type I collagen and significantly decreased amounts of type II collagen and aggrecan [8] are deposited [33]. When NPCs are in a proliferative state, they are not able to produce significant amounts of ECM components. Evidence for the link between non-proliferative cells and high ECM component deposition was provided by a number of NP tissue engineering studies. Other studies that

reported high cell proliferation rates in a variety of biomaterials (alginate and atelocollagen scaffolds) detected low amounts of s-GAG production [34, 35]. Conversely, when there were no significant changes in NPC population, encapsulated cells produced high amounts of relevant ECM components [17, 36].

The main objective of the system was to mimic the native NP so that encapsulated cells would be stimulated into producing high amounts of NP associated ECM components [37] (*section 5.1.3*). ECM has an important role in tissue regeneration and is crucial in regulating the behaviour of cells that come into contact with it [38]. The stable bNPC population suggested that the scaffold could have been successfully mimicking the native tissue as bNPCs were behaving, in terms of proliferation, as they would in the native NP.

Alginate gels are considered the 'gold-standard' control for NP tissue engineering scaffolds [21, 35, 39] as NPCs maintain rounded morphology and produce NP associated ECM components after encapsulation. There were no significant differences in bNPC numbers at either time point when comparing the FEFEFKFK SAPHs to alginate gels (P>0.05) (*figure 5.11*).

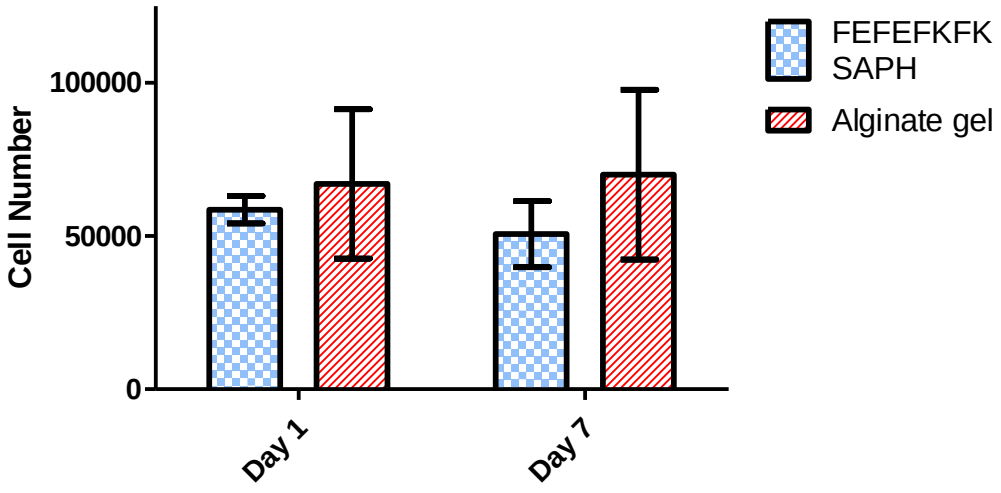

Figure 5.11. Cell numbers on days 1 and 7 for 2x10^5 bNPC ml^{-1} in 30 mg ml^{-1} FEFEFKFK SAPH and 30 mg ml^{-1} alginate gels. There were no significant increases or decreases in cell number over culture period (P>0.05). Values expressed as mean±SD where n=4 from 3 experimental repeats for SAPH and n=2 from 2 experimental repeats for alginate gel.

Mujeeb *et al.* determined that significant bovine chondrocyte proliferation occurred from days 1 to 21 after culture in FEFEFKFK SAPHs [1]. Chondrocytes, like NPCs, have a low turnover rate whilst mature chondrocytes do not proliferate in the native tissue [40, 41]. After injury to articular cartilage, chondrocytes have been demonstrated to proliferate [42]; possibly as an attempt to repair the tissue. It was hypothesised that the chondrocytes could have been attaching to the scaffold which induced cell proliferation as the SAPH system displayed higher

mechanical properties in comparison to this study (*figure 4.8*) [1]. Cheng *et al.* determined that no significant changes in NPC population occurred after culture in chitosan-glycerol hydrogels [43]. Collagen microspheres [17] and fibrin-HA [35] scaffolds also saw no evidence of NPC proliferation, in fact cell numbers decreased with time. Similar results to this study were produced by Ma *et al.* and Wang *et al.* where no significant changes in NPC numbers were detected after culture in LN-NS SAPHs [24, 30]. The absence of proliferation in conjunction with deposition of appropriate ECM components by NPCs cultured in SAPHs [30, 44] supported the hypothesis that the nanofibrous architecture of SAPHs (*section 4.3*) could be mimicking the native NP.

There was evidence of cell proliferation in one set of experiments (*figure 8.9*) where cell numbers dropped significantly from days 1 to 3 (***$P<0.001$) then a significant increase in cell numbers was observed from days 3 to 7 (**$P<0.01$). Cell population recovered so that there was no significant difference between days 1 and 14 ($P>0.05$). Results supported the hypothesis that NPCs might be able to 'sense' when cell density significantly decreased and respond by proliferating to restore population [45].

The LDH assay total cell population results contradicted the LIVE/DEAD assay micrographs particularly at later time points (*section 5.3.2*). On day 14, the fluorescence micrographs demonstrated that there was a higher percentage of dead bNPCs and lower amount of total bNPCs present (*figure 5.6*). However, micrographs only present a small area of the entire SAPH. LDH assay allowed the total cell number to be determined in the entire SAPH therefore was a much more accurate method for determining changes in cell population.

The overall trend was that bNPC numbers remained stable after encapsulation in the SAPH as there were no significant increases or decreases in cell population between time points from day 1 to 14.

5.5. DETERMINING CELL PHENOTYPE USING QUANTITATIVE POLYMERASE CHAIN REACTION

Quantitative RT-PCR was used to determine whether NP associated genes were being up- and downregulated by bNPCs after culture in SAPHs. Gene profiles would allow a better understanding of the phenotype of cells. Genes of interest were the 'traditional' discogenic and chondrogenic markers of *COL1A2*, *COL2A1*, *ACAN* and *SOX9* [46]. Recently identified 'novel' NP markers, specific to the bNPC phenotype [46], of *KRT8*, *KRT18*, *FOXF1* and *CA12* were also tested [47].

5.5.1. Gene expression for individual 'traditional' NPC markers

NPCs, like chondrocytes, have a rounded morphology and both cells are enclosed within a lacuna in their respective tissues. Therefore initial research into the NPC phenotype focused on upregulation of chondrogenic markers [2, 25]. Results demonstrated that NPCs and chondrocytes shared *COL2A1*, *ACAN* and *SOX9* as phenotypic markers [2]. This was logical as type II collagen [48] and aggrecan [49] are major ECM components of both tissues.

For the 'traditional' NP markers there were no significant changes for either *ACAN* or *COL1A2*. *COL1A2* relative gene expression normalised to *GAPDH* value was expressed at low levels (day 1; $1.19x10^{-3}\pm5.99x10^{-4}$, day 7; $8.56x10^{-3}\pm3.31x10^{-3}$ and day 14; $3.66x10^{-3}\pm2.19x10^{-3}$) ($P>0.05$) *(figure 5.12)*. *COL1A2* expression was consistently low which supported the hypothesis that the SAPH could support the 3D culture of NPCs. An increase in *COL1A2* expression would indicate de-differentiation of NP phenotype [50, 51]. Small amounts of *COL1A2* expression is typical for NPCs in the native tissue [52].

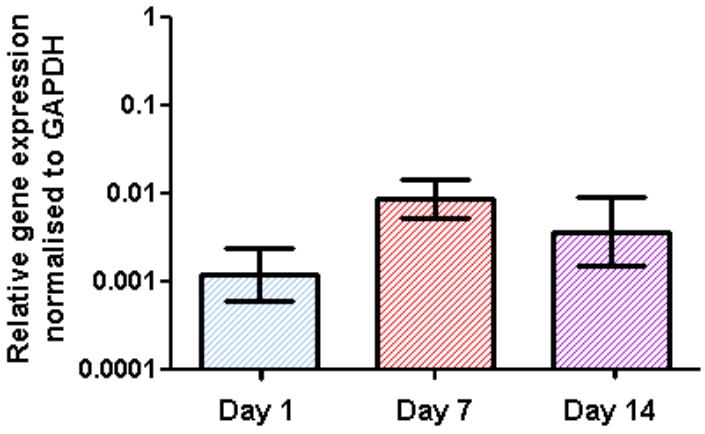

Figure 5.12. *COL1A2* relative expression for $1.5x10^6$ bNPC ml^{-1} in 30 mg ml^{-1} FEFEFKFK SAPHs. Gene expression was normalised to *GAPDH*. ($P>0.05$). Values expressed as mean±SE where n=4 from 2 experimental repeats.

There were no significant differences in *ACAN* relative gene expression normalised to *GAPDH* values between time points (day 1; 0.37±0.04, day 7; 0.8±0.09 and day 14; 0.48±0.07) (P>0.05). High levels or an increase of *ACAN* gene expression is one indicator of the presence of the NP phenotype [53, 54]. Several other NP tissue engineering studies detected a decrease in *ACAN* gene expression over culture period when bNPCs were cultured in collagen-HA scaffolds [55] or fibrin-HA scaffolds [36]. This suggested that the systems were not capable of stimulating significant amounts of *ACAN* gene expression which was confirmed by subsequent protein quantification assays [55]. A crucial requirement for any potential NP tissue engineering scaffold is the ability to stimulate aggrecan porduction due to its crucial role in maintaining tissue hydration [37].

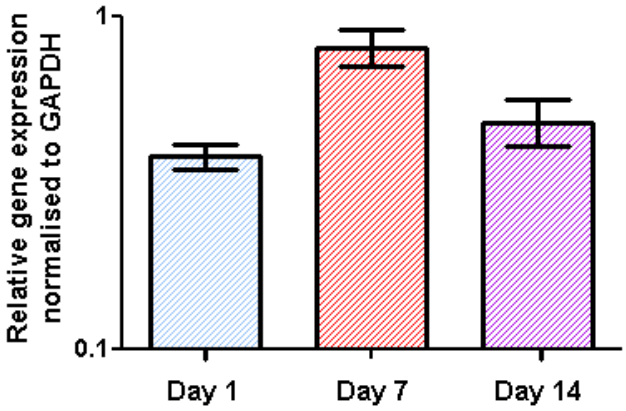

Figure 5.13. *ACAN* relative expression for 1.5x10^{6} bNPC ml^{-1} in 30 mg ml^{-1} FEFEFKFK SAPHs. Gene expression was normalised to *GAPDH*. (P>0.05). Values expressed as mean±SE where n=4 from 2 experimental repeats.

There were significant increases (***P<0.001) from days 1 to 7, days 7 to 14 (***P<0.001) and days 1 to 14 (***P<0.001) in *COL2A1* relative gene expression normalised to *GAPDH* values (day 1; 9.25x10^{-3}±3.27x10^{-4}, day 7; 0.054±5.28x10^{-3} and day 14; 0.17±0.023) (*figure 5.14*). High *COL2A1* expression was expected for NPCs cultured in appropriate environments [44, 53] as type II collagen is the main structural NP ECM component [30, 56]. The significant increases in *COL2A1* expression could be explained by the SAPH mimicking the native NP environment therefore stimulating NPCs to produce the protein. It was also possible that due to the SAPH becoming mechanically weaker with *in vitro* culture (*figure 4.8*), bNPCs increased type II collagen production in an attempt to remodel the SAPH and make it more structurally stable. Similar *COL2A1* gene expression profiles were detected by Kim *et al.* when bNPCs were cultured in HA gels and it was hypothesised that the scaffold was upregulating the NP phenotype after monolayer culture [53]. Contrastingly, when bNPCs were cultured in fibrin-HA hydrogel beads [36] or collagen-HA scaffolds [55], results demonstrated that *COL2A1* gene expression significantly decreased with culture period which suggested de-differentiation of the NP phenotype [9].

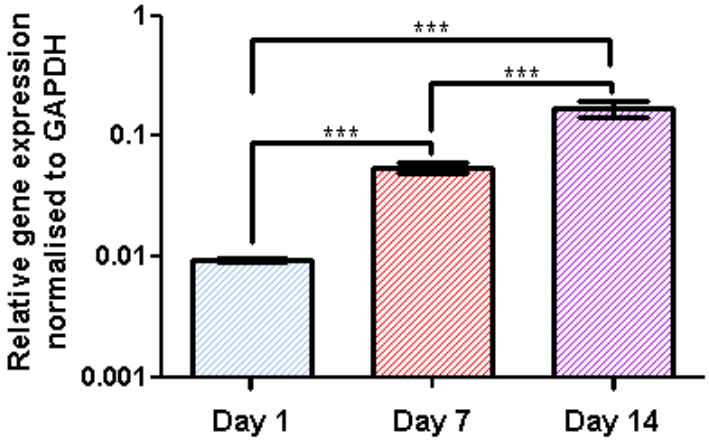

Figure 5.14. *COL2A1* relative expression for 1.5x10^{6} bNPC ml^{-1} in 30 mg ml^{-1} FEFEFKFK SAPHs. Gene expression was normalised to *GAPDH*. (*P<0.001). Values expressed as mean±SE where n=4 from 2 experimental repeats.**

There was a significant increase from days 1 to 7 (***P<0.001) and days 1 to 14 (***P<0.001) in *SOX9* relative gene expression normalised to *GAPDH* values (day 1; 4.31x10^{-4}±5.9x10^{-5}, day 7; 2.67x10^{-3}±1.62x10^{-4} and day 14; 1.96x10^{-3}±3.35x10^{-4}) (*figure 5.15*). *SOX9* is the main regulator of the chondrogenic phenotype, is a promoter of the *COL2A1* [57] and plays a role in type II collagen activation and synthesis [58]. Therefore it is logical that a significant increase in *COL2A1* expression (*figure 5.14*) was accompanied by a significant increase in *SOX9* expression.

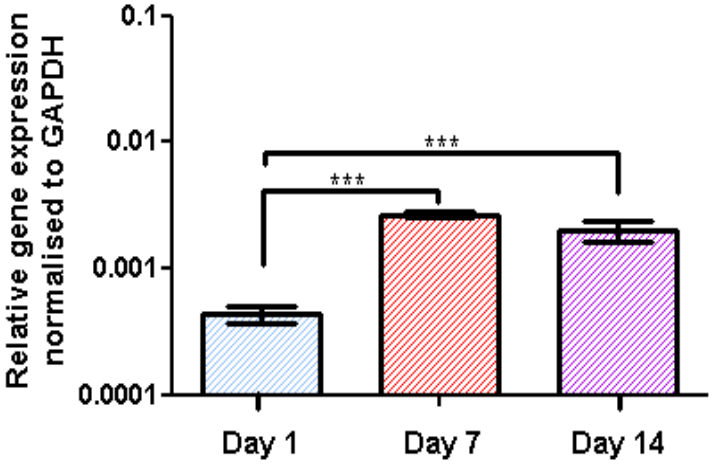

Figure 5.15. *SOX9* relative expression for 1.5x10^{6} bNPC ml^{-1} in 30 mg ml^{-1} FEFEFKFK SAPHs. Gene expression was normalised to *GAPDH*. (P>0.05, ***P<0.001). Values expressed as mean±SE where n=4 from 2 experimental repeats.

5.5.2. Gene expression for individual 'novel' NPC markers

The disadvantage of using only 'traditional' markers for NP phenotype is that chondrocytes share this small panel of markers [2] (*section 5.5.1*). Cartilage and the NP have distinct morphological and physiological differences especially in the composition of their respective ECMs [3]. For example, when chondrocytes were implanted into the NP of a rabbit model, the resultant ECM was more akin to hyaline cartilage than NP tissue and the neo-tissue could not effectively transfer loads to the AF [60]. Therefore identification of the exact NPC phenotype was crucial to ensure correct NP ECM was being deposited. Minogue *et al.* used microarray technology to identify several novel bNPC marker genes. Results concluded that *KRT8*, *KRT18* and *FOXF1* were expressed significantly higher in NPCs compared to chondrocytes or AFCs and were subsequently identified as novel bNPC markers [47].

There was a significant increase from days 1 to 7 (***P<0.001), days 7 to 14 (***P<0.001) and from days 1 to 14 (***P<0.001) in *KRT8* relative gene expression normalised to *GAPDH* values (day 1; $2.13x10^{-3}$±$2.9x10^{-5}$, day 7; 0.013±$3.62x10^{-4}$ and day 14; 0.085±$1.82x10^{-3}$) (*figure 5.16*). KRT8 is an intermediate filament protein that is strongly expressed by bNPCs [47]. Bovine NPCs typically express *KRT8* when clustered together and it has been hypothesised that *KRT8* positive cells could be the remnants of the original notochordal cell population of the bovine disc [62].

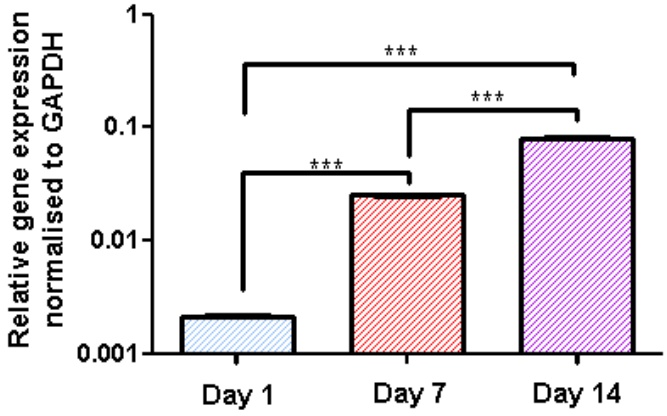

Figure 5.16. *KRT8* relative expression for $1.5x10^{6}$ bNPC ml^{-1} in 30 mg ml^{-1} FEFEFKFK SAPHs. Gene expression was normalised to *GAPDH*. (*P<0.001). Values expressed as mean±SE where n=4 from 2 experimental repeats.**

There was a significant increase from days 1 to 7 (***P<0.001) and from days 1 to 14 (***P<0.001) in *KRT18* relative gene expression normalised to *GAPDH* values (day 1; $4.78x10^{-4}$±$1.1x10^{-4}$, day 7; 0.02±$1.55x10^{-3}$ and day 14; 0.021±$3.33x10^{-3}$) (*figure 5.17*). KRT18 is an intermediate filament protein that is also strongly expressed by notochordal cells [63]. In degenerate IVDs, *KRT18* expression was significantly decreased compared to healthy NPCs [47]. Therefore the gene expression profile for *KRT18* (*figure 5.17*) suggested that encapsulated bNPCs were more akin to healthy NPCs than cells from degenerate IVDs. If

bNPCs were non-degenerate then the appropriate ECM components would have been deposited [8, 9].

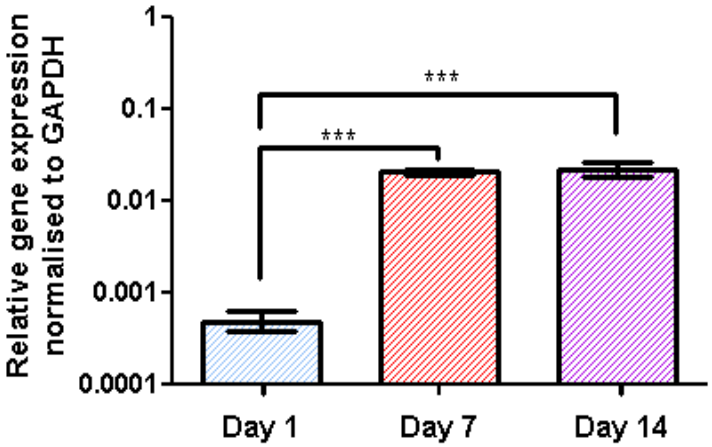

Figure 5.17. *KRT18* relative expression for 1.5x10^{6} bNPC ml^{-1} in 30 mg ml^{-1} FEFEFKFK SAPHs. Gene expression was normalised to *GAPDH*. (P>0.05, ***P<0.001). Values expressed as mean±SE where n=4 from 2 experimental repeats.

There was a significant increase from days 1 to 7 (***P<0.001) and from days 1 to 14 (***P<0.001) in *FOXF1* relative gene expression normalised to *GAPDH* values (day 1; 6.42x10^{-3}±3.67x10^{-4}, day 7; 0.016±8.92x10^{-4} and day 14; 0.015±1.66x10^{-3}) (*figure 5.18*). FOXF1 is a transcription factor that has essential functions in organ development and repair [64]. Upregulation of *FOXF1* expression is associated with cell growth, cell proliferation and increased life expectancy of cells [47, 65]. *FOXF1* expression profile suggested that bNPCs retained their phenotype and could also provide support for the SAPH maintaining high cell viability as demonstrated in *section 5.3* although cell proliferation was not recorded (*section 5.4*).

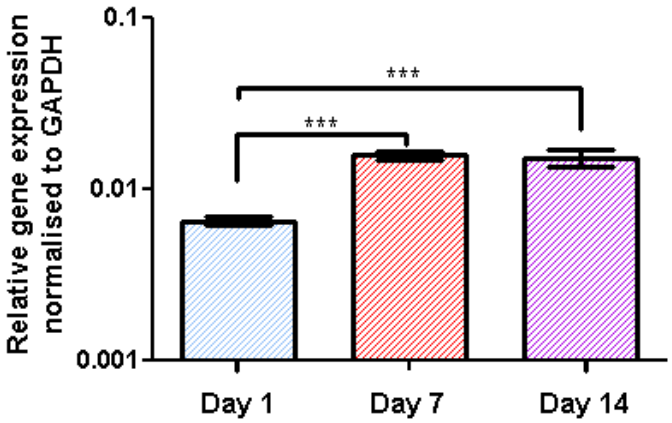

Figure 5.18. *FOXF1* relative expression for 1.5x10^{6} bNPC ml^{-1} in 30 mg ml^{-1} FEFEFKFK SAPHs. Gene expression was normalised to *GAPDH*. (P>0.05, ***P<0.001). Values expressed as mean±SE where n=4 from 2 experimental repeats.

There were no significant differences in *CA12* relative gene expression normalised to *GAPDH* values between time points (day 1; $1.41x10^{-3}\pm2.49x10^{-4}$, day 7; $5.49x10^{-4}\pm2.7x10^{-4}$ and day 14; $5.55x10^{-4}\pm1.94x10^{-4}$) (*figure 5.19*). *CA12* is a novel marker more associated with human NPCs than animal NPCs therefore low expression of the gene was not unexpected [46]. In the IVD, CA12 is thought to play a role in intracellular pH regulation [61]. Presence of the molecule in the NP is thought to counteract increased acidicity of the tissue as a result of lactic acid accumulation following glucose metabolism and ineffective waste product removal [46]. It has been hypothesised that as enhanced expression of CA12 has been detected in moderate to severly degenerated discs, the production of the molecule could be a response to increased metabolic activity after inflammatory or catabolic events [61]. Due to the SAPH environment being around 7.4 after media changes (*table 5.1*), increased or high expression of *CA12* was not expected.

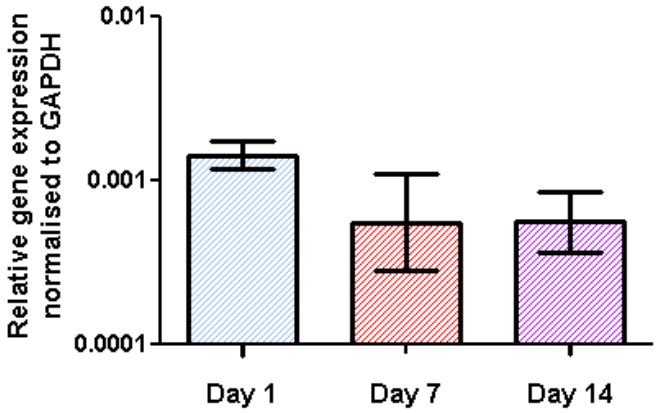

Figure 5.19. *CA12* relative expression for $1.5x10^6$ bNPC ml^{-1} in 30 mg ml^{-1} FEFEFKFK SAPHs. Gene expression was normalised to *GAPDH*. (P>0.05). Values expressed as mean±SE where n=4 from 2 experimental repeats.

To summarise, the significant increases in *COL2A1* and *SOX9* expression over the culture period coupled with the low *COL1A2* expression suggested that a more chondrogenic than discogenic phenotype was present. However when analysed in conjunction with the 'novel' NP markers (*section 5.5.2*), significant increases in *KRT8*, *KRT18* and *FOXF1* expression suggested that a more discogenic than chondrogenic phenotype was present. Gene expression results highlighted the importance of using an appropriately diverse panel of genes when determining cell phenotype.

5.5.3. Comparing overall gene expression

Analysing expression for the whole panel of genes allowed a better understanding of the phenotype of cells after culture in SAPHs. *COL1A2* expression was low compared to the traditional discogenic markers of *COL2A1* and *ACAN* and the novel discogenic phenotype

markers of *KRT8*, *KRT18* and *FOXF1*. By day 14, *COL1A2* expression was significantly lower than *ACAN*, *COL2A1* and *KRT8* (*figure 5.22 & table 5.4*). Type I collagen is produced in small amounts by NPCs in the native tissue [52] but at significantly lower levels than type II collagen or aggrecan [8]. Low *COL1A2* expression profile (*figures 5.20-5.22*) was in agreement with the literature where it was concluded that scaffolds supported a NPC phenotype [53, 66].

COL2A1 expression was high compared to the other NP phenotype marker genes apart from *ACAN*. On day 1, *COL2A1* expression was significantly higher than *COL1A2*, *SOX9*, *KRT18* and *CA12* (***P<0.01) (*figure 5.20 & table 5.2*). By day 14, *COL2A1* expression was significantly higher than *COL1A2*, *SOX9*, *FOXF1*, *CA12* and *KRT18* (*figure 5.22 & table 5.4*). High *COL2A1* expression was expected if NP phenotype was present as type II collagen is a major NP ECM component with an important structural role [4].

Consistently high levels of *ACAN* expression were detected throughout *in vitro* culture. On days 1 (*figure 5.20 & table 5.2*) and days 7 (*figure 5.21 & table 5.3*), *ACAN* expression was significantly higher than all the other tested genes (***P<0.01). On day 14 (*figure 5.22 & table 5.4*), *ACAN* expression was significantly higher than all the other genes (***P<0.01) apart from *COL2A1* and *KRT8* both genes associated with the NP phenotype. Aggrecan is highly important in the native NP due to its roles in keeping the tissue hydrated, inflating the collagen network and maintaining tissue turgor pressure [37]. Gene expression results suggested that the SAPH promoted high amounts of aggrecan production by bNPCs. In particular, the significantly higher ratio of *ACAN* to *COL1A2* expression ranging from 100:1 on day 7 to 320:1 on day 1 is used by some studies as an indicator of upregulation of NP phenotype and production of a gelatinous matrix [43, 53] although a wider panel of NPC markers also needs to be considered. Other NP tissue engineering studies observed high expression of *ACAN* to *COL1A2* for NPC culture in chitosan-gelatin-glycerol gels [43], HA gels [53] and atelocollagen type I scaffolds [34] where the studies concluded that a NP-like cells were present.

KRT8, *KRT18* and *FOXF1* expression significantly increased with culture period (*figures 5.16-18*). By day 14 (*figure 5.22 & table 5.4*), *KRT8*, *KRT18* and *FOXF1* were expressed higher than *CA12*, *SOX9* and *COL1A2*. *KRT8* gene expression on day 14 was not significantly different to *ACAN* (P>0.05). Kim *et al.* determined that *KRT8* and *KRT18* expression was significantly lower than *ACAN* and *COL2A1* after bNPCs were cultured in HA gels [53] which suggested that the SAPH were more effective at upregulating a ‘healthy’ NP phenotype than HA gels. The gene expression profiles for the novel NP markers strongly suggested that a NP-like phenotype was being upregulated by encapsulated cells. In this study, high expression of NP-specific *KRT8*, *KRT19* and *FOXF1* strongly suggested that the NP phenotype had been restored after monolayer culture and was preserved for the duration of *in vitro* culture [46, 47].

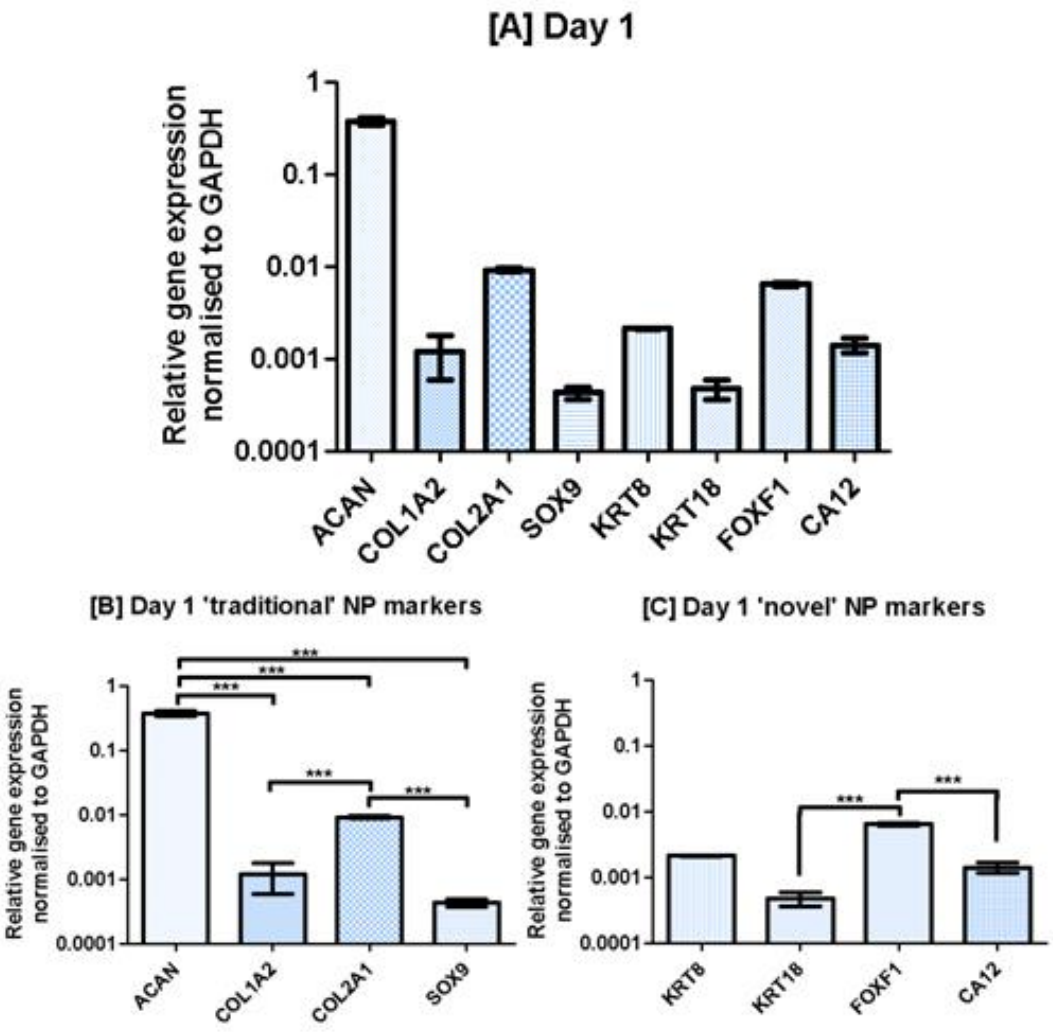

Figure 5.20. The gene expression of NPC markers for 1.5x10^{6} bNPC ml^{-1} in 30 mg ml^{-1} FEFEFKFK SAPHs on day 1. [A] The whole panel of genes. Statistics are quoted in *table 5.2.* [B] 'Traditional' NPC phenotype markers [C] 'Novel' NPC phenotype markers. Gene expression normalised to *GAPDH*. (P>0.05, **P<0.01, ***P<0.001). Values expressed as mean±SE where n=4 from 2 experimental repeats.

Gene	Significant differences
ACAN	*** > *COL1A2, COL2A1, SOX9, KRT8, KRT18, FOXF1, CA12*
COL1A2	
COL2A1	*** > *COL1A2, SOX9, KRT18, CA12*
SOX9	
KRT8	
KRT18	
FOXF1	*** > *SOX9, KRT18* ** > *COL1A2,CA12*
CA12	

Table 5.2. Table showing the panel of genes on day 1 with the statistical significant differences for each gene. For example *COL2A1* expression was significantly higher than *COL1A2*, *SOX9*, *KRT18* and *CA12* (*P<0.001). *COL2A1* expression was significantly lower than *ACAN* (***P<0.001). *COL2A1* expression was not significantly higher or lower than *KRT8* or *FOXF1* (P>0.05). n=4.**

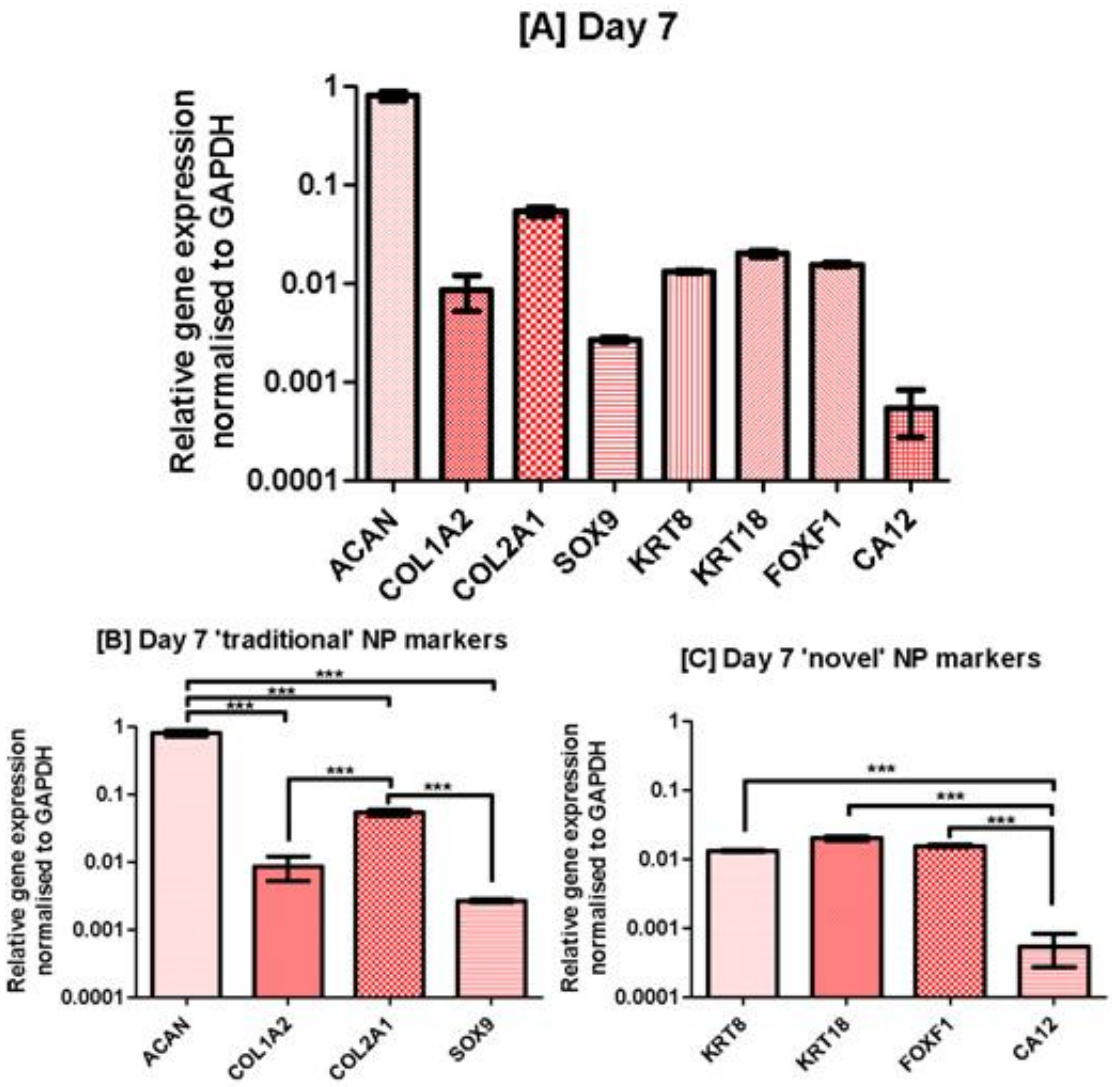

Figure 5.21. The gene expression of NPC markers for 1.5x10^{6} bNPC ml^{-1} in 30 mg ml^{-1} FEFEFKFK SAPHs on day 7. [A] The whole panel of genes. Statistics are quoted in *table 5.3*. [B] 'Traditional' NP phenotype markers [C] 'Novel' NP phenotype markers. Gene expression normalised to *GAPDH*. (P>0.05, **P<0.01, ***P<0.001). Values expressed as mean±SE where n=4 from 2 experimental repeats

Gene	Significant differences
ACAN	*** > *COL1A2, COL2A1, SOX9, KRT8, KRT18, FOXF1, CA12*
COL1A2	*** > *CA12*
COL2A1	*** > *COL1A2, SOX9, CA12* * > *FOXF1*
SOX9	** > *CA12*
KRT8	*** > *CA12*
KRT18	*** > *SOX9, CA12*
FOXF1	*** > *SOX9, CA12*
CA12	

Table 5.3. Table showing panel of genes on day 7 with the statistical significant differences for each gene. For example *SOX9* expression was significantly higher than *CA12* (P<0.01). *SOX9* gene expression was significantly lower than *ACAN*, *COL2A1*, *KRT18*, *FOXF1* (***P<0.001). *SOX9* expression was not significantly higher or lower than *COL1A2* or *KRT8* (P>0.05). n=4.**

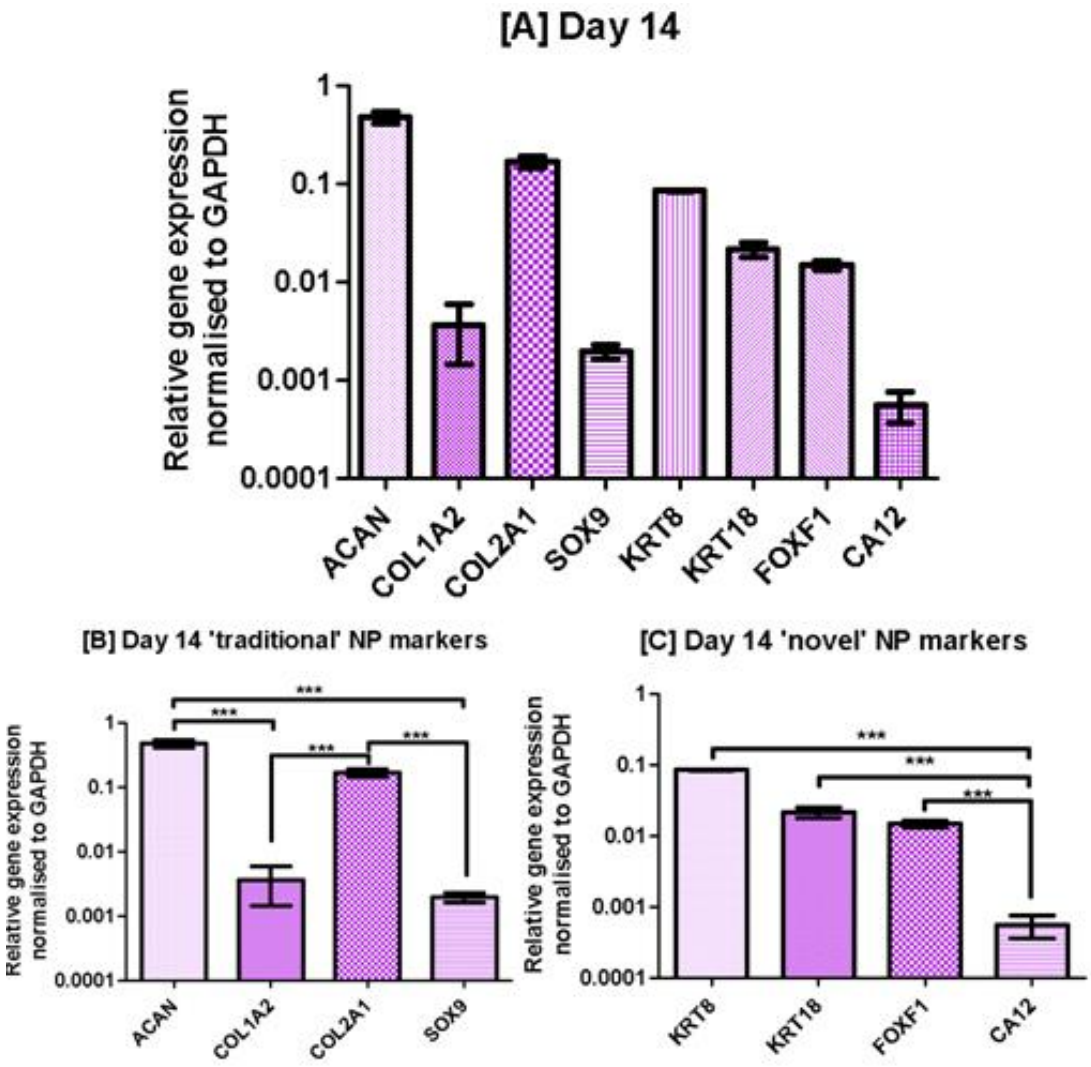

Figure 5.22. The gene expression of NPC marker genes for 1.5x10^{6} bNPC ml^{-1} in 30 mg ml^{-1} FEFEFKFK SAPHs on day 14. [A] The whole panel of genes. Statistics are quoted in *table 5.4.* [B] 'Traditional' NPC phenotype markers [C] 'Novel' NPC phenotype markers. Gene expression normalised to *GAPDH*. (P<0.01, ***P<0.001). Values expressed as mean±SE where n=4 from 2 experimental repeats**

Gene	Significant differences
ACAN	*** > *COL1A2, SOX9, KRT18, FOXF1, CA12*
COL1A2	* > *CA12*
COL2A1	*** > *COL1A2, SOX9, FOXF1, CA12* * > *KRT18*
SOX9	
KRT8	*** > *CA12* ** > *COL1A2, SOX9*
KRT18	*** > *CA12* ** > *SOX9*
FOXF1	*** > *CA12* ** > *SOX9*
CA12	

Table 5.4. Table showing panel of genes on day 14 with the statistical significant differences for each gene. For example *SOX9* gene expression was significantly lower than *ACAN*, *COL2A1* (*P<0.001) and *KRT8*, *KRT18* and *FOXF1* (**P<0.01). *SOX9* gene expression was not significantly higher or lower than *COL1A2* or *CA12* (P>0.05). n=4.**

5.5.4. Ratio of aggrecan to type II collagen gene expression

The ratio of aggrecan to type II collagen deposition in the healthy human NP ECM is 27 to 1 whilst in human articular cartilage the ratio is closer to 2 to 1, making the NP more gelatinous [3]. At a gene transcription level there is a higher *ACAN* to *COL2A1* expression ratio. Deposition of aggrecan and type II collagen in the ECM are closely related to their respective cellular gene expression levels [30, 67] with a number of NP tissue engineering studies demonstrating time-dependent increases in gene expression accompanied by increasing corresponding protein deposition [9, 53]. In this study, the ratio of *ACAN* to *COL2A1* expression decreased from around 41 to 1 on day 1 to 3 to 1 by day 14 (*figure 5.23*). The ratio change was due to a significant increase in *COL2A1* expression (*figure 5.14*) whilst *ACAN* expression remained consistently high (*figure 5.13*). Due to SAPH weakening at later time points (*figures 4.8, 8.6 & 8.7*) it was possible that *COL2A1* expression increased in an attempt by NPCs to establish a more structurally stable microenvironment. Interestingly, when gene expression ratios were analysed for bNPCs harvested from freshly obtained bovine tails, *COL2A1* expression was higher than *ACAN* expression [47]. This suggested that despite aggrecan being the prevalent NP ECM component [3, 48, 49] this did not necessarily mean that *ACAN* expression was significantly higher than *COL2A1*.

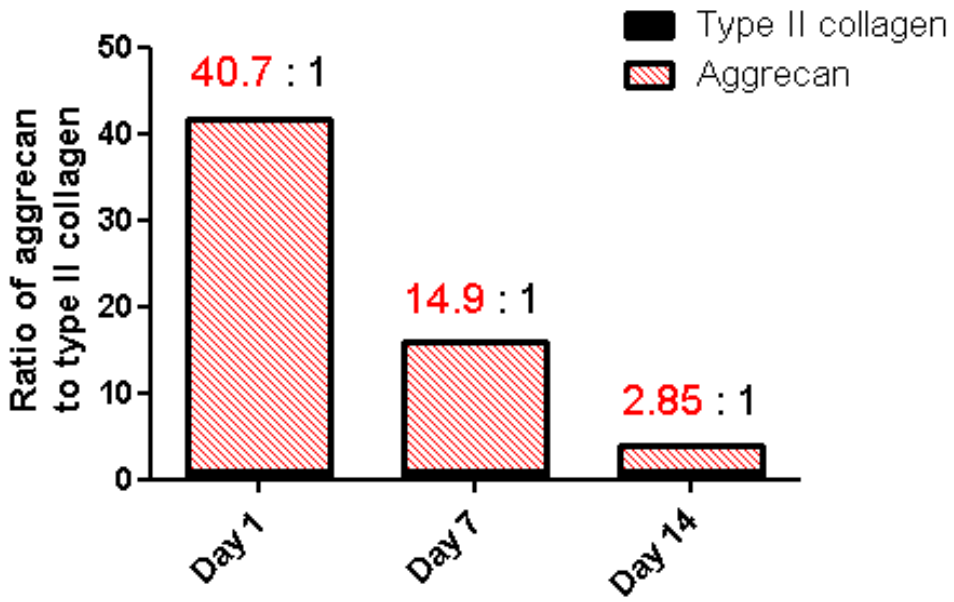

Figure 5.23. The ratio of *ACAN* to *COL2A1* for 1.5x10^{6} bNPC ml^{-1} in 30 mg ml^{-1} FEFEFKFK SAPHs calculated from relative gene expression to *GAPDH*. The ratio of *ACAN* to *COL2A1* decreased with increasing *in vitro* culture. n=4 from 2 experimental repeats.

Chen *et al.* determined that the *ACAN* to *COL2A1* ratio when rat NPCs were cultured in HA-gelatin hydrogels was around 10 to 1 on day 7 comparable to day 7 results for this study (*figure 5.23*) [66]. Other studies observed *ACAN* to *COL2A1* expression ratios of approximately 1 to 1 in HA gels after 28 days [53], RADA-16 SAPH after 7 days [24] and LN-NS SAPH after 14 days [30]. It was evident that stimulation of encapsulated NPCs to express

significantly higher amounts of *ACAN* to *COL2A1* throughout long term *in vitro* culture was an issue that needed addressing, a potential solution could be utilisation of appropriate NP phenotype induction growth factors throughout cell culture (e.g. GDF-5 [64] or GDF-6 [68]) to constantly provide stimulation and signals to maintain the NP phenotype.

5.5.5. Overview and further discussion

Wang *et al*. saw increases in *COL2A1* and *ACAN* expression results compared to RADA16 controls after culture of rat NPCs in LN-NS scaffolds [30]. LN-NS SAPHs had been functionalised with the link N bioactive motif which has been shown to increase accumulation of both aggrecan and type II collagen [69]. The panel of genes chosen was small, with only 2 genes tested for and no 'novel' makers used, which meant that either a discogenic or chondrogenic cell phenotype could have been present especially as the *ACAN* to *COL2A1* expression ratio was approximately 1:1. It was evident that due to 'novel' NP markers being only recently identified [47] few NP tissue engineering studies (*tables 2.1 & 2.2*) investigated an extensive panel of novel NP markers which made it difficult to confirm NP phenotype.

Quantitative RT-PCR is a powerful tool for tracking up- and downregulation of specific genes which can then be analysed to determine phenotype of cells or to predict protein deposition [30, 67]. However discrepancies in protein deposition and gene expression may be attributed to differences in detection limits between mRNA and protein expression, instability of mRNA, short protein half-life or inhibition at the transitional level [75].

To summarise, overall gene expression confirmed the hypothesis that SAPHs could restore the NP phenotype following de-differentiation during monolayer culture and preserve the phenotype of encapsulated bNPCs [46]. An extensive panel of appropriate NP marker genes was tested [47] to ensure that an accurate representation cell phenotype could be established as the type of ECM components produced by NPCs and chondrocytes are similar [2]. The 'traditional' NPC gene marker of *COL2A1* was upregulated whilst *ACAN* was the most highly expressed gene. *COL1A2* and *SOX9* expression was significantly lower than the NP associated ECM components of *COL2A1* and *ACAN*. For the 'novel' NP markers of *KRT8*, *KRT18* and *FOXF1*, expression significantly increased from days 1 to 14 which strongly suggested that bNPCs maintained their phenotype throughout *in vitro* culture in the FEFEFKFK SAPHs.

5.6. VISUALISING THE DEPOSITION OF EXTRACELLULAR MATRIX COMPONENTS USING IMMUNOCYTOCHEMISTRY

Since NPCs produce and remodel the native tissue, the interactions between NPCs and their ECM is an important factor to consider for tissue engineered constructs [38, 70]. If the SAPH successfully mimicked the native tissue then bNPCs should have produced the appropriate ECM components [25]. The normal biochemistry of NPCs is to highly express aggrecan [37] and type II collagen [4]. However in degenerated discs, NPCs switch from producing type II collagen to type I collagen and aggrecan production is diminished which accelerates DDD [71].

5.6.1. Type I collagen staining

No significant amounts of type I collagen positive staining was present extracellularly at any time points when bNPCs were cultured in SAPHs (*figures 5.24A & 5.25A*). Small amounts of intercellular staining was present on day 7 (*figure 5.25A*); type I collagen is expressed by NPCs in small quantities [52]. Gene expression results confirmed that significantly less *COL1A2* was expressed in comparison to *COL2A1* or *ACAN* (*figures 5.20-5.22*). Sun *et al.* also determined that type I collagen was being produced by rat NPCs after encapsulation in a KLD-12 SAPH with the fluorescence yield being lower than for type II collagen staining [44].

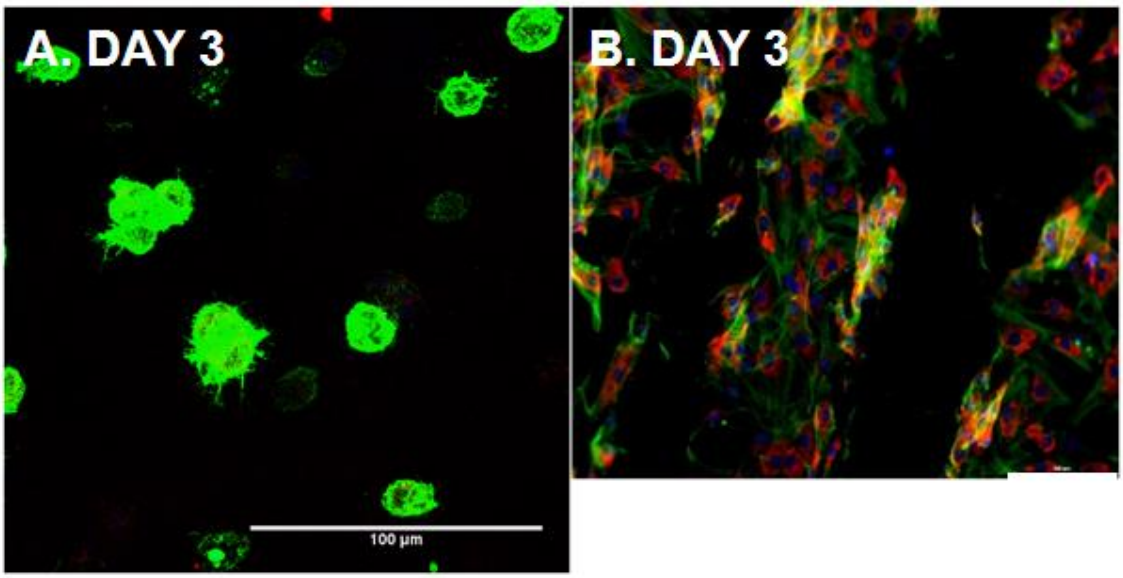

Figure 5.24. Fluorescence micrographs showing type I collagen ICC staining for $2x10^5$ bNPCs ml^{-1} on day 3. [A] There was little positive staining for type I collagen after 3D culture in 30 mg ml^{-1} SAPHs. [B] Positive staining was present in 2D culture on glass. Type I collagen was stained red, F-actin was stained green and nuclei were stained blue. Scale bar represents 100 µm.

Micrographs confirmed high amounts of bNPC intracellular type I collagen production in monolayer (*figures 5.24B & 5.25B*) which was in agreement with the literature [8, 9]. During DDD, due to the increased amount of cytokines in the NP, there is an alteration in the expression of anabolic genes and matrix proteins [33] causing production of type I collagen. The NP becomes more fibrous which negatively affects the biomechanics of the IVD [25, 33]. Therefore low production of type I collagen is desired when NPCs are cultured in biomaterial scaffolds [6, 43]. The contrast in distribution and amount of type I collagen staining between the SAPH and glass control highlighted the importance of 3D culture and suitable matrix environment for production of appropriate NP ECM components.

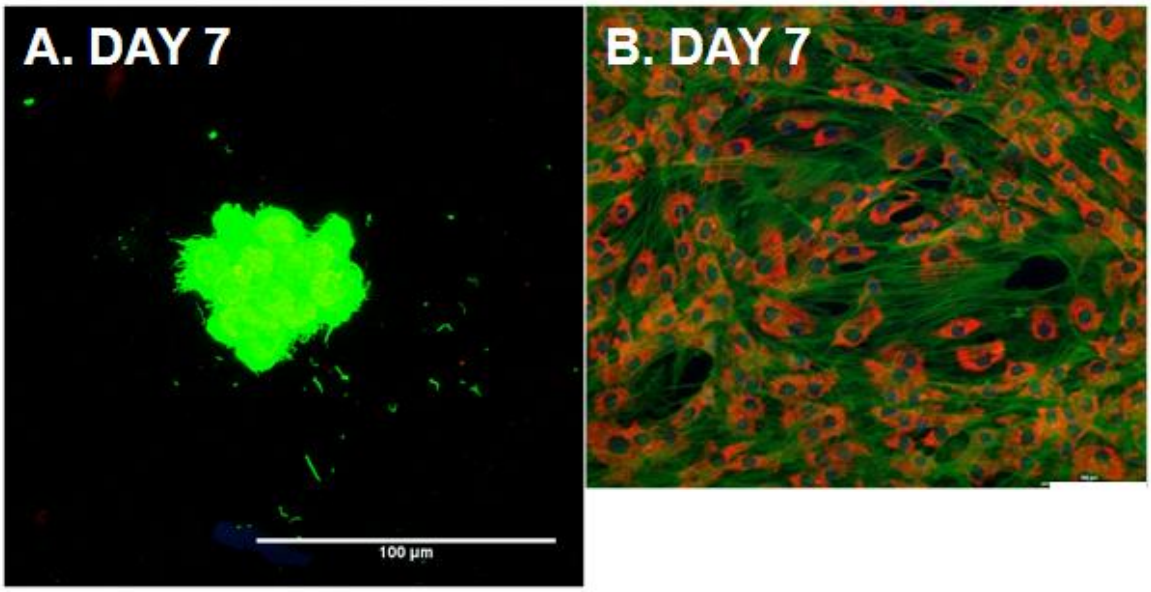

Figure 5.25. Fluorescence micrographs showing type I collagen ICC staining for $2x10^5$ bNPCs ml^{-1} on day 7. [A] There was some positive intracellular staining for type I collagen after 3D culture in 30 mg ml^{-1} SAPH. [B] Bright positive staining was present for 2D culture on glass. Type I collagen was stained red, F-actin was stained green and nuclei were stained blue. Scale bar represents 100 µm.

5.6.2. Type II collagen staining

For bNPC culture in SAPHs, intracellular staining for type II collagen was dim with no extracellular staining on day 3 (*figure 5.26A*). By day 7, micrographs showed bright type II collagen staining intracellularly and extracellularly (denoted by white arrows) (*figure 5.27A*). Staining extended into the SAPH and was most intense pericellularly with the cell membrane denoted by F-actin staining [72]. The increase in type II collagen staining at day 7 could be due to bNPCs remodelling the SAPH as it became less structurally stable (*figure 4.8*). *COL2A1* expression significantly increased with time point (*figure 5.14*) so there was an analogous increase in type II collagen staining and intensity in fluorescence micrographs (*figure 5.26A & 5.27A*).

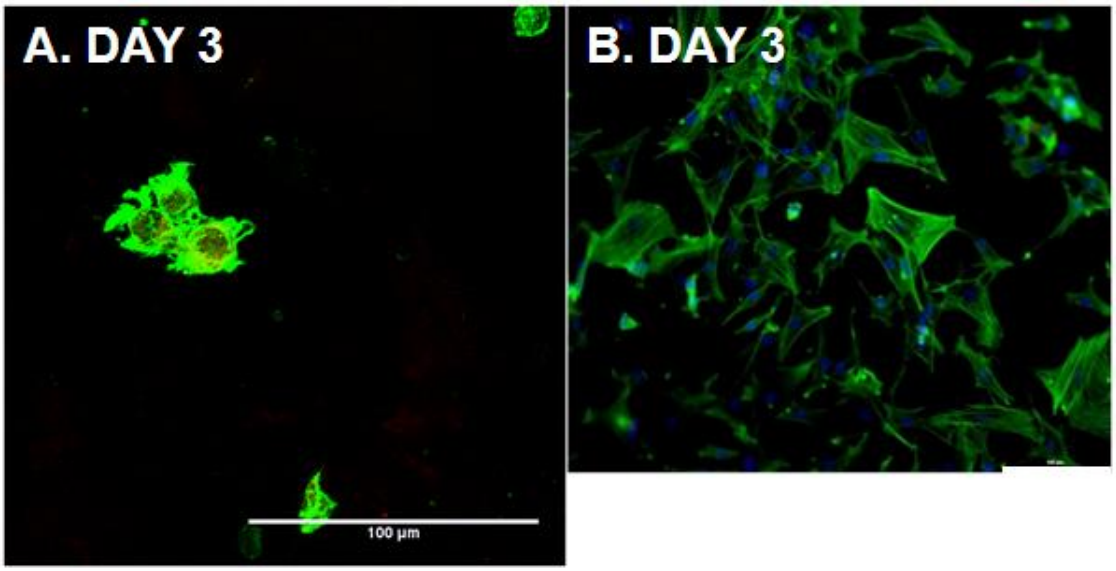

Figure 5.26. Fluorescence micrographs showing type II collagen ICC staining for $2x10^5$ bNPCs ml^{-1} on day 3. [A] There was little positive staining for type II collagen after 3D culture in 30 mg ml^{-1} SAPH. [B] There was no positive staining for 2D culture on glass. Type II collagen was stained red, F-actin was stained green and nuclei were stained blue. Scale bar represents 100 µm.

In comparison to 3D culture, there was no positive staining for type II collagen on day 3 in monolayer culture (*figure 5.26B*) and little positive staining on day 7 (*figure 5.27B*). The distribution of type II collagen was in agreement with literature where little type II collagen was produced when NPCs were cultured in 2D [8, 9].

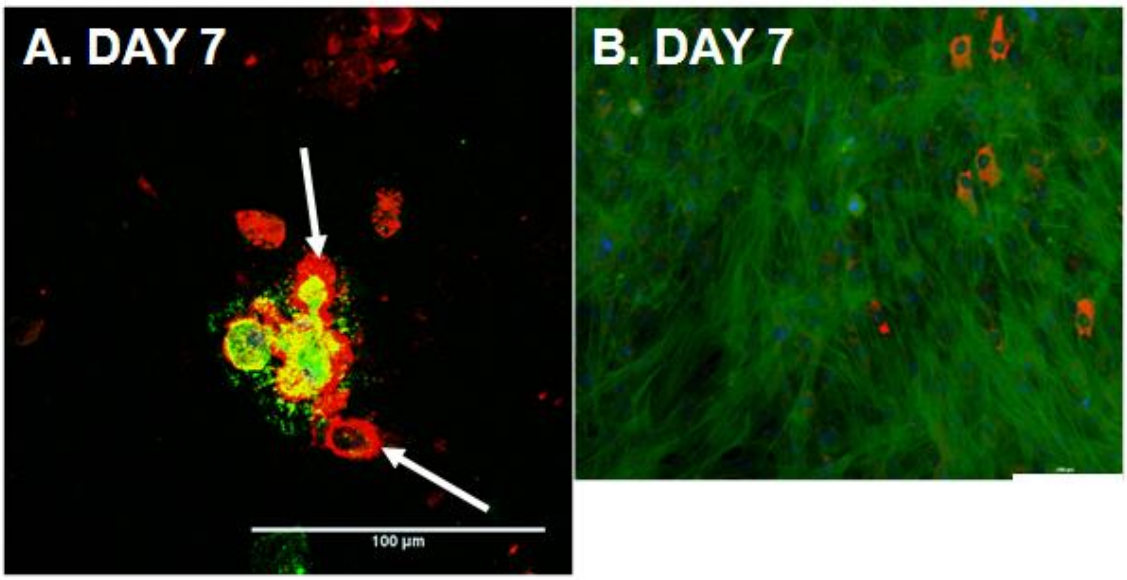

Figure 5.27. Fluorescence micrographs showing type II collagen ICC staining for $2x10^5$ bNPCs ml^{-1} on day 7. [A] There was intense intra- and extracellular staining (denoted by white arrows) for type II collagen after 3D culture in 30 mg ml^{-1} SAPH. [B] There was little positive staining for 2D culture on glass. Type II collagen is stained red, F-actin is stained green and nuclei are stained blue. Scale bar represents 100 µm.

5.6.3. Aggrecan staining

There was dim extracellular staining (*denoted by white arrows*) for aggrecan as early as day 3 (*figure 5.28A*) after bNPC culture in SAPH. Aggrecan deposition is linked to the corresponding gene expression levels [30, 67] therefore as *ACAN* expression was high on day 1 (*figure 5.20*), extracellular aggrecan deposition on day 3 was expected. By day 7 (*figure 5.29A*), there was intense intracellular and extracellular aggrecan staining (*denoted by white arrows*). Aggrecan was deposited extensively beyond the cell membrane and into the SAPH and appeared fibrillar.

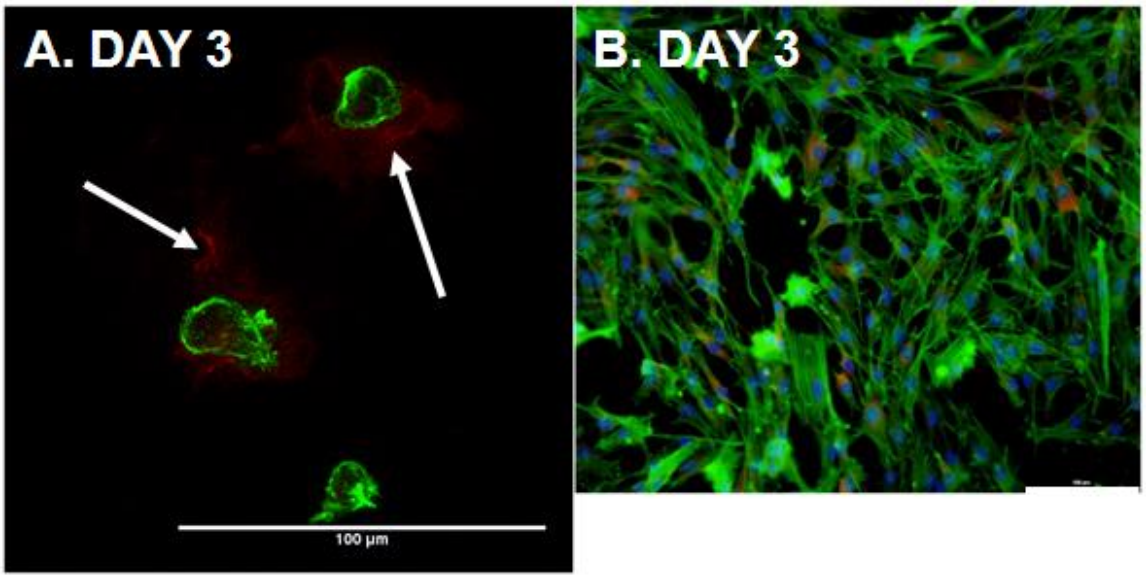

Figure 5.28. Fluorescence micrographs showing aggrecan ICC staining for 2x10^5 bNPCs ml^{-1} on day 3. [A] There was some positive intra- and extracellular staining (denoted by white arrows) for aggrecan after 3D culture in 30 mg ml^{-1} SAPHs [B] There was little positive staining for 2D culture on glass. Aggrecan was stained red, F-actin was stained green and nuclei were stained blue. Scale bar represents 100 µm.

Cells cultured on glass showed little positive aggrecan staining on day 3 (*figure 5.28B*) and no positive staining by day 7 (*figure 5.29B*). Micrographs for the 2D culture of bNPCs were in agreement with previous studies that determined that NPCs in monolayer produced insignificant amounts of aggrecan [8, 9].

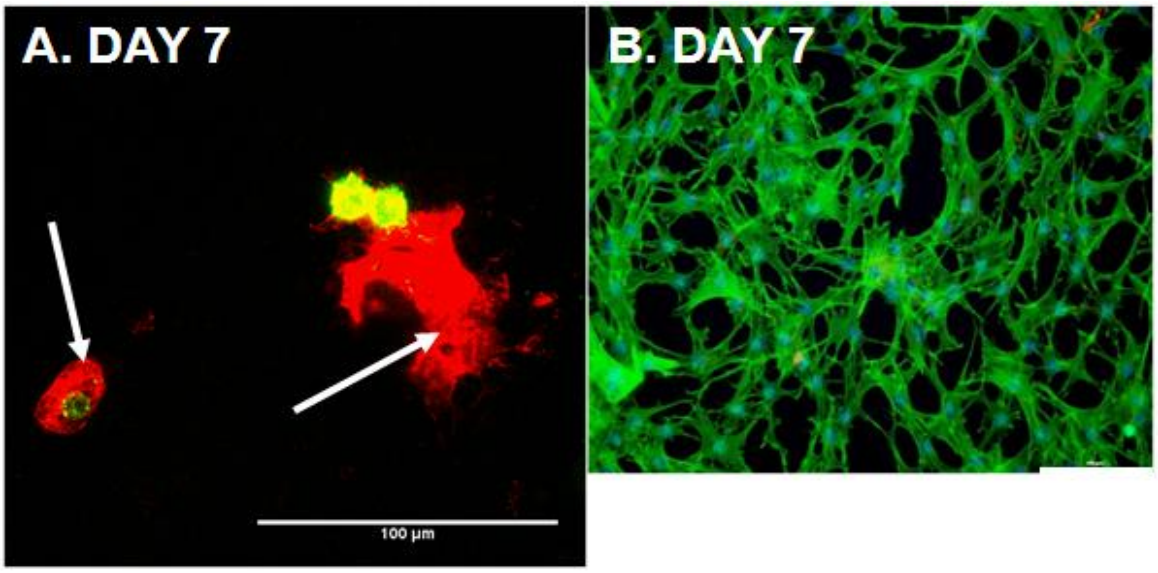

Figure 5.29. Fluorescence micrographs showing aggrecan ICC staining for $2x10^5$ bNPCs ml^{-1} on day 7. [A] There was intense positive intra- and extracellular staining (denoted by white arrows) for aggrecan after 3D culture in 30 mg ml^{-1} SAPHs. [B] There was no positive staining for 2D culture on glass. Aggrecan was stained red, F-actin was stained green and nuclei were stained blue. Scale bar represents 100 µm.

5.6.4. Overview and further discussion

The type of ECM components produced by bNPCs cultured in FEFEFKFK SAPHs was comparable to native NPCs (*figures 5.25A, 5.27A & 5.29A*). Type II collagen and aggrecan are the major NP ECM components [4, 37] therefore extensive intense staining for both components supported the hypothesis that the SAPH was an appropriate culture environment for bNPCs. It has been demonstrated that an unsuitable culture environment, for example monolayer culture [8, 9] or scaffolds with microscaled architecture [6, 11] induced high amounts of type I collagen production and low amounts of type II collagen or aggrecan by NPCs [6] (*figures 5.25B, 5.27B & 5.29B*).

Sufficient culture length was required for ECM components deposition which explained the more intense staining for type II collagen and aggrecan at day 7 (*figures 5.27A & 5.29A*) compared to day 3 (*figures 5.26A & 5.28A*). Yuan *et al.* observed similar trends in staining intensity between time points for the culture of rabbit NPCs in collagen microspheres [17]. Objectively in this study, there appeared to be more widespread and brighter staining for aggrecan in comparison to type II collagen which was supported by higher *ACAN* expression compared to *COL2A1* expression profiles (*figure 5.23*). Micrographs were in agreement with previous studies which determined that NPCs produced relatively little fibrillar collagen during *in vitro* culture in comparison to aggrecan [8, 73]. Distribution and accumulation of type II collagen and aggrecan staining was comparable to ICC micrographs presented by Ma *et al.* for rabbit NC cells cultured in a LN-NS SAPH [24].

The cell cytoskeleton consists of actin filaments therefore F-actin staining can be used to define cell architecture in fluorescence micrographs [22]. At high magnifications (x400 to x600), it was clear that despite bNPCs displaying an overall rounded chondrocyte-like morphology, most cells had numerous thin processes extending into the SAPH (*figure 5.30A, denoted with white arrows*). The displayed NPC morphology was in agreement with the study by Errington *et al.* where bNPCs were imaged displaying cellular projections extending into the matrix at high magnifications. It was hypothesised that the cytoplasm filled processes were acting as mechano-tranducers. Mechanotransduction describes the various mechanisms that cells use to convert mechanical stimulus into chemical activity. The process is particularly important for NPCs as cells need to be able to respond appropriately to the deformation, pressurisation and flow that the IVD is subject to [7, 74]. Another study that investigated the cytoskeleton of bovine IVD cells, stained bNPCs from NP cryosections and results showed comparable F-actin staining to this study [75]. Horner *et al.* determined that NPCs cultured in alginate gels displayed rounded morphology (*figure 5.9*) but lost the long processes seen *in vivo* and for this study [8], which suggested that morphology was not maintained [7]. F-actin staining of the control samples cultured on glass showed that bNPCs had spread and attached to the surface and had adopted a fibroblastic morphology (*figures 5.25B, 5.27B & 5.29B*). Cells in monolayer had highly organised cytoskeletons with abundant stress fibres. The observed change in bNPC morphology is associated with production of type I collagen (*figure 5.24B & 5.25B*) and de-differentiation of the phenotype [9, 13].

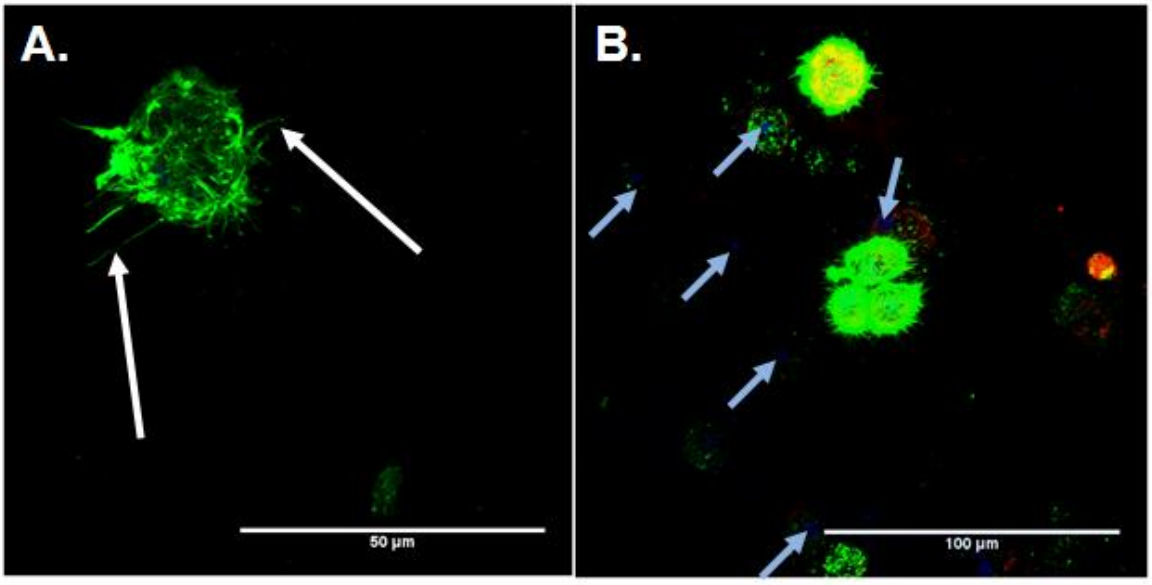

Figure 5.30. Fluorescence micrographs showing aggrecan ICC staining for $2x10^5$ bNPCs ml^{-1} on day 7. [A] Negative control using only secondary antibody 3D culture in 30 mg ml^{-1} SAPHs. The white arrows denote cellular processes extending from the main cell body into the matrix. [B] Type I collagen staining. The blue arrows denote cell nuclei which were not brightly stained in some micrographs. Aggrecan and type I collagen were stained red, F-actin was stained green and nuclei were stained blue. Scale bar represents 100 µm.

In some of the presented micrographs (*figure 5.29A*), the cell nuclei were not clearly visible. The SAPH did not autofluoresce but did absorb the DAPI stain which made it difficult to distinguish nuclei. *Figure 5.30B* demonstrated visible cell nuclei denoted with blue arrows. Hoescht 33342 stain is an alternative reagent that can be used to stain DNA that might produce brighter staining [24]. Negative controls using only the secondary antibody showed that there was no unspecific AB binding occurring as only F-actin staining was present denoting stress fibres around bNPCs (*figure 5.30A*).

To summarise, ICC fluorescence micrographs for the 3D culture of bNPCs in SAPHs demonstrated that the appropriate NP ECM components were being deposited by cells. ECM production in the SAPH was comparable to NPCs in the native tissue. Encapsulated bNPCs expressed high amounts of type II collagen and aggrecan intra- and extracellularly whilst there was little type I collagen staining. In contrast, bNPCs cultured in monolayer stained brightly for intra- and extracellular type I collagen and there was little type II collagen or aggrecan positive staining. It was evident that to ensure phenotypic stability of NPCs and production of NP associated ECM components, 3D culture in an appropriate scaffold was essential [6].

5.7. QUANTIFYING THE PRODUCTION OF SULPHATED GLYCOSAMINOGLYCANS USING BLYSCAN™ s-GAG ASSAY

Blyscan™ sulphated GAG assay was used to determine total accumulated s-GAG content in the SAPHs on days 1, 3, 7 and 14. The s-GAG content reflected all sulphated PGs; aggrecan is the main PG found in the native NP and consists of s-GAG chains attached to a HA core [17, 76].

5.7.1. Cell seeding density

At a cell seeding density of $2x10^5$ bNPCs ml^{-1}, used for all bNPC culture experiments (*sections 5.3, 5.4 & 5.6*) apart from gene expression samples (*section 5.5*), low levels of s-GAG accumulation were detected (*figure 5.31*). The assay was not sensitive as the limit for detection was 0.25 µg s-GAG in a 100 µl sample. The hypothesis was that seeding density had to be increased before detectable levels of s-GAG could be accumulated and quantified due to ICC micrographs confirmed aggrecan deposition at $2x10^5$ bNPCs ml^{-1} cell seeding density (figure 5.29A),. Studies have highlighted the effect of cell seeding density on total s-GAG accumulation [17, 37], with the higher cell seeding density producing increased s-GAG accumulation due to a higher total number of cells producing ECM components. Therefore seeding densities of $1x10^6$ bNPCs ml^{-1} (*figure 5.31*) and $1.5x10^6$ bNPCs ml^{-1} (*section 5.7.2*) were chosen to carry out experiments. *Figure 5.31* demonstrated that there was an increase in s-GAG accumulation after increasing the initial cell seeding density.

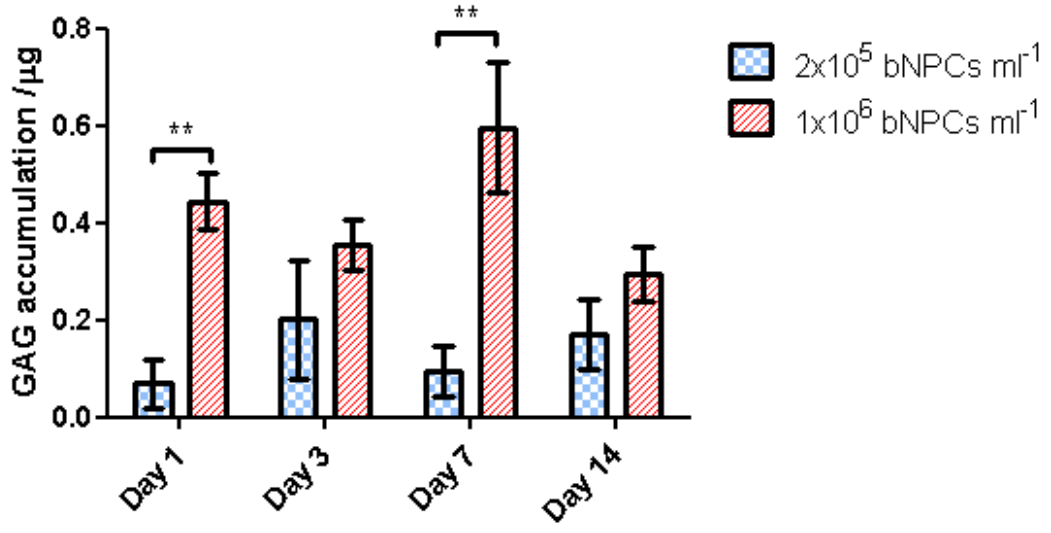

Figure 5.31. Total s-GAG accumulation for 3D culture of bNPCs in 30 mg ml^{-1} FEFEFKFK SAPHs comparing $2x10^5$ bNPCs ml^{-1} and $1x10^6$ bNPCs ml^{-1} seeding density. (P>0.05, *P<0.05, **P<0.01). Values expressed as mean±SD where n=4 from 2 experimental repeats.

Higher cell seeding densities were used in comparable studies; for example $2x10^6$ bNPCs per 150 µl [77], $3x10^6$ bNPCs ml^{-1} [78] and $20x10^6$ rNPCs ml^{-1} [44] - respectively. Kobayashi *et al.* demonstrated that by increasing the cell density to as high as $25x10^6$ ml^{-1} the amount of GAG accumulation also increased but the subsequent fall in oxygen, nutrients and culture space meant that cell metabolism was slowed and cell death occurred. The study hypothesised that despite an overall increase in GAG accumulation due to the very high cell density normalised GAG production per cell actually decreased [37].

5.7.2. Production of s-GAG at $1.5x10^6$ bNPCs ml^{-1}

It was determined that s-GAG accumulation could be increased by increasing the initial cell seeding density (*figure 5.31*). Results demonstrated that s-GAG accumulation was time dependent (*figure 5.32*) with a significant increase in total s-GAG accumulation from days 1 to 14, 0.71±0.03 µg to 2.08±0.21 µg respectively (***P<0.001).

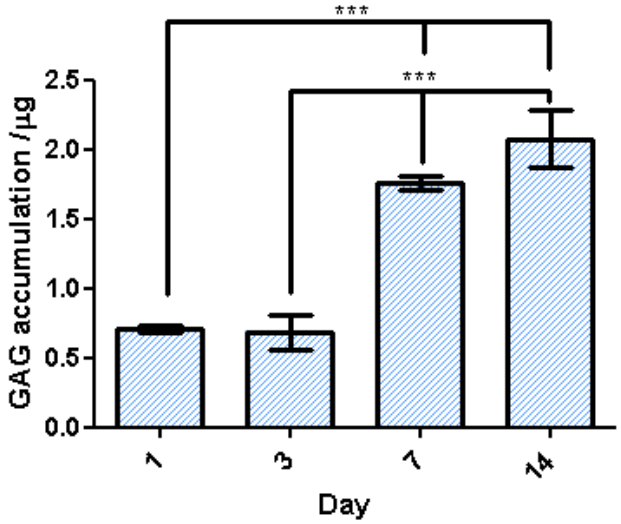

Figure 5.32. Graph showing total s-GAG accumulation in samples for $1.5x10^6$ bNPC ml^{-1} in 30 mg ml^{-1} FEFEFKFK SAPHs. s-GAG accumulation was calculated from a standard graph plotting absorbance against standard s-GAG concentrations. (P>0.05, ***P<0.001). Values expressed as mean±SD where n=4 from 2 experimental repeats.

A significant indicator of DDD is NP dehydration due to the degradation and leaching of aggrecan from the tissue [79] causing the IVD to become fibrous and resulting in a loss of IVD height. Disc height is used to determine efficacy of in *vivo* NP tissue engineering cell-based therapies [6, 11, 80] as it is directly linked to the NP hydration [81]. Therefore a crucial scaffold requirement is the production of s-GAGs which are responsible for attracting H_2O into the NP [6, 37].

Overall s-GAG accumulation per day (*figure 5.32*) was normalised with viable cell number using Quant-iT™ PicoGreen® assay (*section 3.4.3*) to allow the bioactivity of each bNPC to be

assessed. s-GAG production per bNPC significantly increased with time point from days 1 (0.0085 ng) to 14 (0.041 ng) (***P<0.001) (*figure 5.33*) which was in agreement with high *ACAN* expression throughout culture (*figure 5.13*) and ICC that demonstrated that aggrecan was deposited extracellularly as early as day 3 (*figure 5.28*) with increased widespread aggrecan deposition by day 7 (*figure 5.29*). The increasing production of s-GAG per cell with day could have occurred as a result of bNPCs attempting to establish a matrix similar to the native tissue.

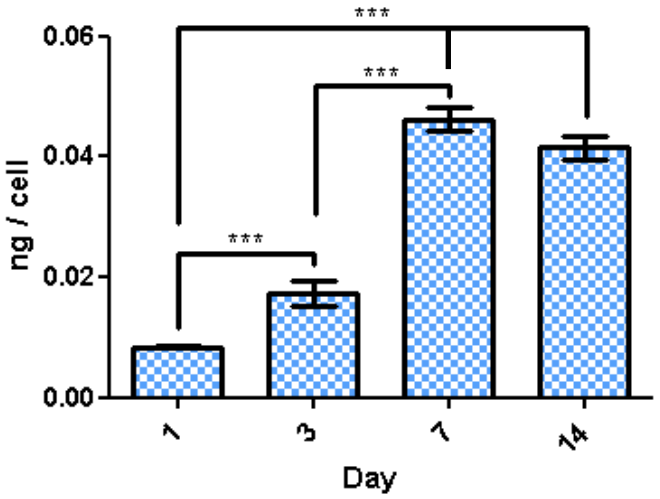

Figure 5.33. Normalised s-GAG production per bNPC at a seeding density of 1.5x10^{6} bNPC ml^{-1} in 30 mg ml^{-1} FEFEFKFK SAPHs. The total accumulated s-GAG in samples (*figure 5.32*) was divided by viable cell number on corresponding time point to estimate s-GAG production per cell. (P>0.05, ***P<0.001). Values expressed as mean±SD where n=4 from 2 experimental repeats.

5.7.3. Overview

No significant amounts of s-GAG were detected in the pooled media (*figure 8.10*) which suggested that the SAPH was effective in retaining the majority of the ECM component.

Sun *et al.* determined that s-GAG accumulation in KLD-12 SAPH significantly increased from day 1 to 14 however results were not normalised. s-GAG was present in the media samples which suggested that the KLD-12 SAPH was not completely effective in retaining the ECM component [44]. Other studies reported significant increases in normalised s-GAG to DNA ratios for NPCs cultured in thermoreversible HA based hydrogels (HA-pNIPAM) [78] and collagen I-HA hydrogels used in combination with TGF-β1 [77]. Foss *et al*. determined that no increases in s-GAG production over a 28 day culture period were observed when human NPCs were cultured in alginate gels with various ratios of chondroprotective stimulation (glucosamine and CS),. In fact, due to CS being present in the scaffold, significant decreases in s-GAG occurred from day 1 to 14 as chondroprotective stimulation leached from the scaffolds [35].

Despite time-dependent increases in s-GAG production by encapsulated NPCs a limitation of this study was that the s-GAG levels were not comparable to the native tissue [3]. This was expected as *in vitro* culture was conducted for only 14 days. It has been speculated that it might take months for seeded constructs to approach s-GAG concentrations found in the native tissue [37]. In native bovine discs, GAG comprises around 4.7% of the native tissue wet weight [82]. In this study, the SAPH started to become mechanically unstable after 14 days therefore *in vitro* culture over months was not possible with current production protocol or SAPH composition (*section 3.2*). FEFEFKFK SAPHs has been reported to be mechanically stable after 21 days [1] and SAPHs produced by sonication demonstrated significantly higher mechanical properties which in turn should increase mechanical stability during cell culture [83]. Another option would be to increase the initial cell seeding density to increase s-GAG accumulation (*section 5.7.1*). Therefore to better understand the potential of NPCs to produce s-GAGs after encapsulation in the SAPH, a longer term study was required with a higher cell seeding density.

The overall trend was that total amount of s-GAG accumulated in the system increased significantly from day 1 to 14. A significant increase of s-GAG production per cell with time point was detected when results were normalised,

5.8. SPECIFIC GLYCOSAMINOGLYCAN IDENTIFICATION

A crucial requirement for NP tissue engineering scaffolds and cell carriers is the ability to stimulate aggrecan production [37]. ICC confirmed that extracellular aggrecan was being produced by bNPCs (*section 5.6.3*) and Blyscan™ sulphated GAG assay (*section 5.7*) quantified that s-GAG production per cell significantly increased from days 1 to 14. To the knowledge of the author, the specific composition of GAG chains synthesised by bNPCs cultured in tissue engineering scaffolds has not been investigated. Horner *et al.* used incorporation of the radioactive species [^{35}S] to compare GAG synthesis rates by NPCs and AFCs in alginate gel, collagen gels and in monolayer but did not quantify amounts of specific GAG chains [8]. Chiba *et al.* also used radiolabelling to characterise PG production by rabbit NPCs and AFCs with the ratios of keratan sulphate and HA to PG presented [73]. Both studies observed no significant differences with time point for rate of PG synthesis [8, 73].

5.8.1. Ratio of s-GAGs between samples

There were no significant differences (P>0.05) in ratio of chondroitin-4-sulphate (C-4-S) to chondroitin-6-sulphate (C-6-S) detected when $1.5x10^6$ bNPCs ml^{-1} were cultured in 30 mg ml^{-1} FEFEFKFK SAPHs (*figure 5.34*). The ratio was approximately 1 to 1, each sample had the same variables and were analysed on day 7 so results demonstrated that the production of either C-4-S and C-6-S was consistent.

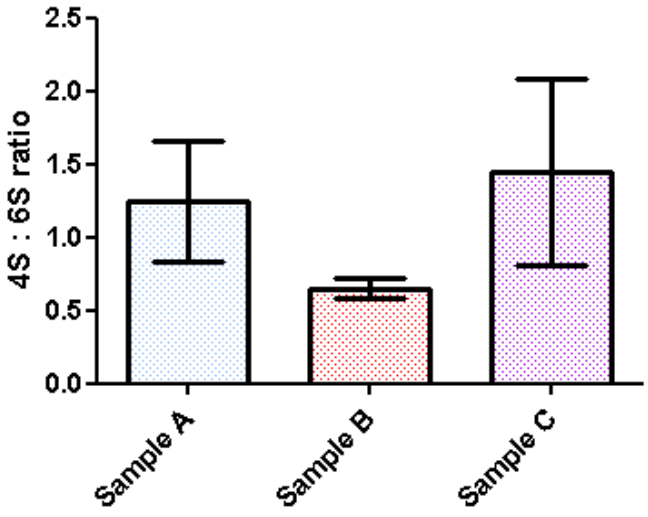

Figure 5.34. The ratio of chondroitin-4-sulphate to chondroitin-6-sulphate produced by $1.5x10^6$ bNPCs ml^{-1} in 30 mg ml^{-1} FEFEFKFK SAPHs on day 7. There was no significant difference in C-4-S to C-6-S ratios between samples (P>0.05). Values expressed as mean±SD where sample A n=4, sample B n=2 and sample C n=2 for HPLC runs. Ion exchange chromatography and radiolabelling was performed by S.Haq, HPLC fractioning was performed by S.Borland.

5.8.2. Specific s-GAG chain composition

There were no significant differences between samples (*figure 5.35*) (P>0.05) when comparing peaks for each detected GAG. The overall GAG composition was approximately 45.9±8.8% C-4-S, 42.7±9.6% C-6-S and 9.3±2.1% non-sulphated disaccharides. The remainder consisted of various disulphated disaccharides. In comparison, the GAG composition for canine NPCs in alginate beads was measured as 31% C-4-S, 61% C-6-S and 8% chondroitin 4,6- sulphate [84]. The lengthy and complex extraction protocol (*section 3.4.7*) was likely a key contributor to discrepancies in percentage GAG composition between samples. An attempt was made to reduce the steps and length of the protocol however it was inevitable that material would be lost during the column exchange and freeze dryer steps.

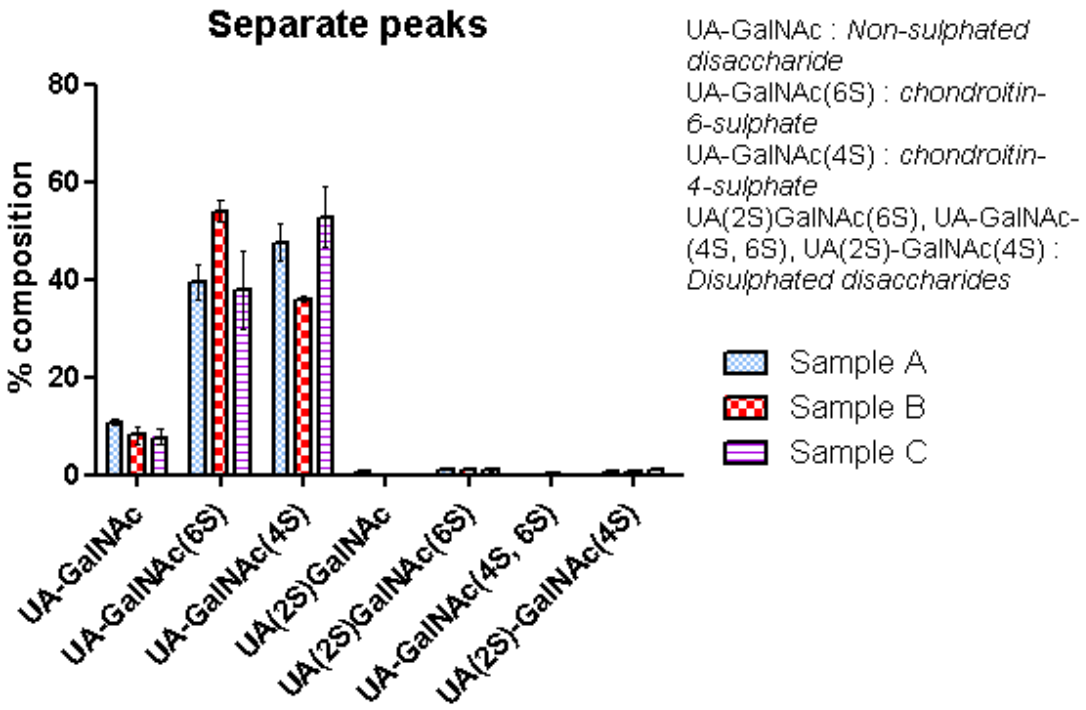

Figure 5.35. The separate percentage composition GAG peaks for each sample for $1.5x10^6$ bNPCs ml^{-1} in 30 mg ml^{-1} FEFEFKFK SAPHs on day 7. Values expressed as mean±SD where sample A n=4, sample B n=2 and sample C n=2 for HPLC runs. Ion exchange chromatography and radiolabelling was performed by S.Haq, HPLC fractioning was performed by S.Borland.

It was suggested that the C-4-S and C-6-S peak could be combined due to the variability in relative contributors for monosulphated disaccharides between experimental runs (*figure 5.35*). When the percentage of monosulphated disaccharide contributors was combined, this allowed simpler comparison between samples (*figure 5.36*). Both C-4-S and C-6-S are present in the native NP [85]. The combined results determined that mono-sulphated disaccharides made up approximately 90% of the detected s-GAGs with around 9% composed of non-sulphated disaccharides. There were no significant differences in detected amounts of non-

sulphated disaccharides between samples (P>0.05). A very low concentration of disulphated disaccharides was detected in samples with total contributions of less than 1%. Chelberg *et al.* determined that for human NPCs cultured in alginate gels, the percentages of cells that stained positive for various GAGs was 73.6±18.2% for KS and CS, 2.5±2.7% for only KS, 2.5±3.4% for only CS and 21.2±14.3% for neither KS nor CS [86]. The synthesis of GAGs by cells is tissue-specific and strongly influenced by the microenvironment [84]. There is little available information on types of s-GAG produced by NPCs possibly due to them being present at such low concentrations in the native tissue. Therefore it was difficult to compare the GAG compositions detected in this study to literature and it could be that the observed composition profile (*figure 5.*35) was representative for the culture of bNPCs in SAPHs.

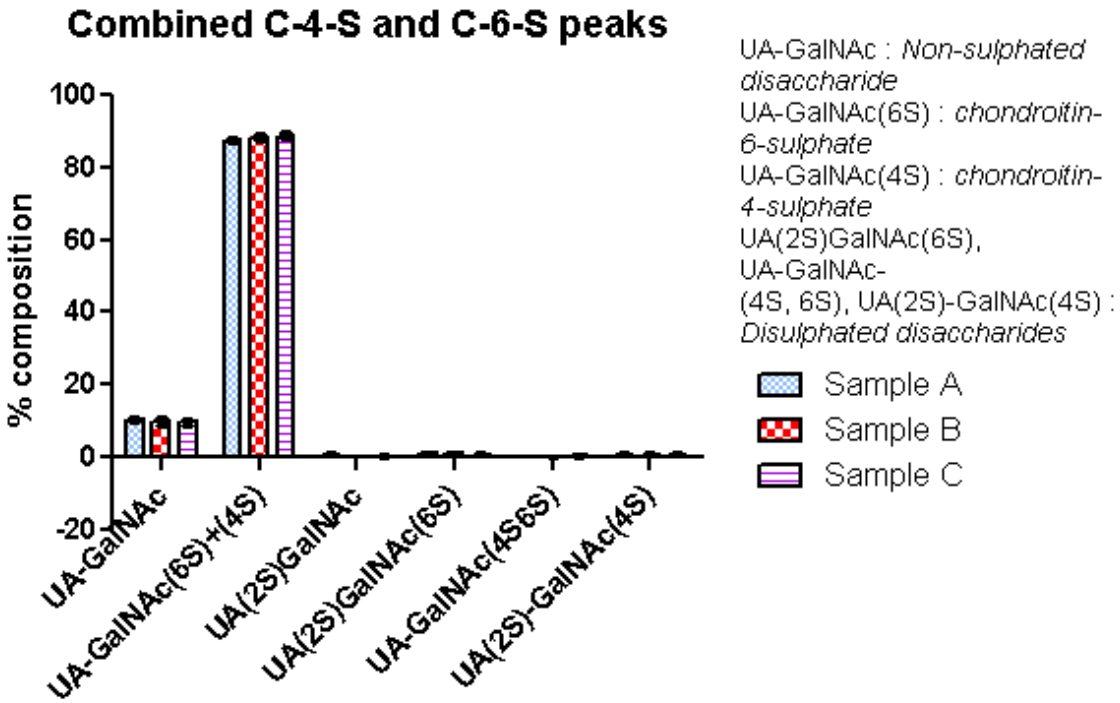

Figure 5.36. Graph showing combined percentage composition GAG peaks for three samples for 1.5x10^{6} bNPCs ml^{-1} in 30 mg ml^{-1} FEFEFKFK SAPHs on day 7. (P>0.05). Values expressed as mean±SD where sample A n=4, sample B n=5 and sample C n=6 for HPLC runs. Ion exchange chromatography and radiolabelling was performed by S.Haq, HPLC fractioning was performed by S.Borland.

The main PG of the native NP is aggrecan, which consists of KS and CS chains, with lower concentrations of the smaller CS PG veriscan [87]. Both C-4-S and C-6-S are present in human NP ECM in varying amounts dependent on age. At 1 to 4 years old, the ratio between C-4-S and C-6-S is around 2:1 with C-4-S becoming dominant at older ages [85]. With age, the overall NP CS content decreases with an increase in KS [88]. In comparison to human NPs, C-6-S is the prevalent s-GAG in bovine NPs [89] which is not in agreement with *figure*

5.35. The ratio of C-4-S to C-6-S production has not been extensively investigated but Horner *et al.* did determine that in monolayer culture, C-6-S was immunostained for bNPCs whilst inner annulus cells stained positive for C-4-S. However, not all NPCs stained for the various epitopes and staining intensity appeared low. Aggrecan is not typically produced by NPCs in 2D culture (*section 5.6.3*) which explained the faint staining. When cultured in the appropriate 3D systems of alginate gels Horner *et al.* determined that there was intense staining extracellularly for both C-4-S and C-6-S by bNPCs. GAG amounts were not quantified but the study concluded that there appeared to be more C-4-S present in alginate samples [8].

A drawback of this technique was that two samples did not produce consistent peaks for C-4-S to C-6-S on the HPLC and typically came out as a single peak. Therefore the variability within HPLC runs meant that the ratio between types of CS was difficult to determine. Analysis was only carried out on day 7 so changes in ratio of C-4-S or C-6-S production over culture period could not be determined. The expectation would be a time-dependent increase in PG biosynthesis by NPCs as seen in the literature [84] and s-GAG quantification assay (*figure 5.33*). This technique did not allow the type of PG to be identified as the radiolabel was taken up by all cells and GAG was extracted using charge based separation with no selection step for a specific PG core. Mass spectroscopy would allow the protein cores to be identified and the ratio of aggrecan to versican to be distinguished.

In conclusion the majority of CS/DS chains were composed of mono-sulphated disaccharides carrying either 4S or 6S. Only ~10% of disaccharides were found to be non-sulphated in all 3 samples. There is also a very low concentration of di-sulphated disaccharides. The study demonstrated that GAGs can be extracted from the SAPHs and by using a metabolic radiolabel, only GAGs generated over a specific time period could be analysed.

5.8. CONCLUSION

The main challenges facing potential NP tissue engineering scaffolds are ensuring that the NPC phenotype is preserved after encapsulation and stimulating significant production of appropriate NP ECM components. A number of synthetic and natural biomaterials have been investigated as potential scaffolds (*table 2.1 & 2.2*) with varying degrees of success. Most studies produced satisfactory results in terms of encapsulated animal NPC viability, population and ECM component production. However, no studies used an extensive panel of NP phenotype markers including NP specific genes for animal cells nor did any study determine what specific s-GAGs were produced by cells.

This study hypothesised that as the system exhibited nanofibrous architecture with features of similar scale to native NP type II collagen fibrils (*section 4.3*) and could be optimised to possess comparable stiffness to the native tissue (*section 4.4.4*), the SAPH was able to mimic the NP and therefore presented an effective culture environment for bNPCs with preservation of NP phenotype.

The aim of this chapter was to establish whether FEFEFKFK SAPHs could support the culture and phenotype of NPCs. By analysing the viability, population and phenotype of encapsulated cells as well as using three different methods to determine ECM component production, the aims set out for this chapter were completed and produced encouraging results.

To summarise, results presented in *chapter 5* strongly suggested that the FEFEFKFK SAPH was suitable for culture of bNPCs. The scaffold restored the NPC phenotype after monolayer culture and preserved the cell phenotype throughout *in vitro* cell culture (*section 5.5*). Encapsulated cell viability remained high (*sections 5.3 & 5.4*) whilst cells were stimulated into producing NP-associated ECM components (*sections 5.5-5.7*). Therefore data demonstrated that the system held great promise for applications as scaffolds and cell carriers in NP tissue engineering. It was concluded that the promising animal cell results provided sufficient evidence and data for further research into the culture of the more clinically relevant cell source of h-BMMSCs in FEFEFKFK SAPHs (*chapter 6*).

5.9. REFERENCES

1. **Mujeeb A, Miller A, Saiani A, Gough J** *'Self-assembled octapeptide scaffolds for in vitro chondrocyte culture'* Acta Biomaterialia (2012); Vol.9 Iss.1 pp.4609-4619
2. **Sive J, Baird P, Jeziorsk M, Watkins A, Hoyland J, Freemont A** '*Expression of chondrocyte markers by cells of normal and degenerate intervertebral discs*' J Clin Pathol: Mol Pathol (2002); Vol.55 pp.91-97
3. **Mwale F, Roughley P, Antoniou J** '*Distinction between the extracellular matrix of the nucleus pulposus and hyaline cartilage: A requisite for tissue engineering of intervertebral disc*' European Cells and Materials (2004); Vol.8 pp.58-64
4. **Aladin D, Cheung K, Ngan A, Chan D, Leung V, Lim C, Luk K, Lu W** *'Nanostructure of collagen fibrils in human nucleus pulposus and its correlation with macroscale tissue mechanics'* Journal of Orthapaedic Research (2010) – Vol. 28 Iss.4 pp.497-503
5. **Wilke H-J** *'Animal models for spinal research'* Eur. Spine Journal (2008); Vol.17 p.1
6. **Feng G, Zhang Z, Jin X, Hu J, Gupte M, Holzwarth J, Ma P** '*Regenerating nucleus pulposus of the intervertebral disc using biodegradable nanofibrous polymer scaffold*' Tissue Engineering (2012); Vol.18 No.21 pp.1-8
7. **Errington R, Puustjarvi K, White I, Roberts S, Urban J** '*Characterisation of cytoplasm-filled processes in cells of the intervertebral disc*' J Anat (1998); Vol.192 pp.369-378
8. **Horner H, Roberts S, Bielby R, Menage J, Evans H, Urban J** '*Cells from different regions of the intervertebral disc'* Spine (2002); Vol.27 No.10 pp.1018-1028
9. **Chou A, Reza A, Nicoll S** *'Distinct intervertebral disc cell populations adopt similar phenotype in three-dimensional culture'* Tissue Engineering (2008); Vol.14 No.12 pp.2079-2086
10. **Yeung T, Georges P, Flanagan L, Marg B, Ortiz M, Funaki M, Zahir N, Ming W, Weaver V, Janmey P** '*Effects of substrate stiffness on cell morphology, cytoskeletal structure and adhesion*' Cell Motility and the Cytoskeleton (2005); Vol.60 pp.24-34
11. **Zhang S, Yokoi H, Gelain F, Horii A** *'Designer self-assembling peptide nanofibre scaffolds'* Nanotechnology for Biology and Medicine: At the Building Block Level (2012); pp.123-147
12. **Tibbitt M, Anseth K** 'Hydrogels as extracellular matrix mimics for 3D cell *culture'* Biotech Bioeng (2009); Vol.103 pp.655-663
13. **Johnson W, Wooton A, Haj A, Eisenstein S, Curtis A, Roberts S** '*Topographical guidance of intervertebral disc cell growth in vitro: towards the development of tissue repair strategies for the annulus fibrosus'* Eur Spine J (2006); Vol.15 Sup.3 pp.389-396
14. **Sharp C, Roberts S, Evans H, Brown S** '*Disc cell clusters in pathological human intervertebral discs are associated with increased stress protein immunostaining*' Eur Spine J (2009); Vol.18 pp.1587-1594
15. **Kluba T, Niemeyer T, Gaissmaier C, Grunder T** '*Human annulus fibrosus and nucleus pulposus cells of the intervertebral disc'* Spine (2005); Vol.30 No.24 pp.2743-2748
16. **Trout J, Buckwalter J, Moore K** '*Ultrastructure of the human intervertebral disc: cells of the nucleus pulposus*' The Anatomical Record (1982); Vol.204 pp.307-314
17. **Yuan M, Leong K, Chan B** *'Three-dimensional culture of rabbit nucleus pulposus cells in collagen microspheres'* Spine Journal (2011); Vol.11 pp.947-960
18. **MacQueen L, Sun Y, Simmons C** '*Mesenchymal stem cell mechanobiology and emerging experimental platforms*' J R C Soc Interface (2013); Vol.10 pp.1-16
19. **Iatridis J, Setton L, Weidenbaum M, Mow V** '*The viscoelastic behaviour of the non-degenerate human lumbar nucleus pulposus in shear'* J Biomechanics (1997); Vol.30 No.10 pp.1005-1013
20. **Georges P, Janmey P** '*Cell type-specific response to growth on soft materials*' J Appl Physiol (2005); Vol.98 pp.1547-1553
21. **Chou A, Nicoll S** *'Characterisation of photocrosslinked alginate hydrogels for nucleus pulposus cell encapsulation'* Wiley InterScience (2009) – pp.187-195
22. **Diaz L, Saiani A, Gough J, Miller A** '*Human osteoblasts within soft peptide hydrogels promote mineralisation in vitro*' J of Tissue Engineering (2014); Vol.5 pp.1-12
23. **Halloran D, Grad S, Stoddart M, Dockery P, Alini M, Pandit A** '*An injectable cross-linked scaffold for nucleus pulposus regeneration*' Biomaterials (2008); Vol.29 pp.438-447
24. **Ma K, Wu Y, Wang B, Yang S, Wei Y, Shao Z** *'Effect of a synthetic link N peptide nanofiber scaffold on the matrix deposition of aggrecan and type II collagen in rabbit notochordal cells'* J Mater Sci (2012); pp.1-11
25. **Gilbert H, Hoyland J, Richardson S** '*Stem cell regeneration of degenerated intervertebral discs: Current status*' Curr Pain Headache Rep (2013); Vol.17 pp.1-9

26. **Le Maitre C, Freemont A, Hoyland J** '*The role of interleukin-1 in the pathogenesis of human intervertebral disc degeneration*' Arthritis Research & Therapy (2005); Vol.7 No.4 pp.732-744
27. **Horii A, Wang X, Gelain F, Zhang S** '*Biological designer self-assembling peptide nanofibre scaffolds significantly enhance osteoblast proliferation, differentiation and 3D cell migration'* PLoS ONE (2007); Iss.2 pp.1-9
28. **Saiani A, Mohammed A, Frielinghaus N, Collins R, Hodson N, Kielty C, Sherratt M, Miller A** *'Self-assembly and gelation properties of α-helix versus β-sheet forming peptides'* Soft Matter (2009); Vol.4 pp.193-202
29. **Tao H, Zhang Y, Wang C, Zhang C, Wang X, Wang D, Bai X, Wen T, Xin H, Wu J, Liu Y, He Q, Ruan D** 'Biological evaluation of human degenerated nucleus pulposus cells in functionalised self-assembling peptide nanofibre hydrogel scaffold' Tissue Engineering (2014); Vol.20 pp.1621-1722
30. **Wang B, Sun C, Shao Z, Yang S, Che B, Wu Q, Liu J** 'Designer self-assembling peptide nanofibre scaffolds containg link protein N-terminal peptide to induce chondrogenesis of rabbit bone marrow stem cells' Biomed Research (2014); pp.1-10
31. **Bibby S, Jones D, Ripley R, Urban J** '*Metabolism of the intervertebral disc: Effects of low levels of oxygen, glucose and pH on rates of energy metabolism of bovine nucleus pulposus cells*' Spine (2005); Vol.30 No.5 pp.487-496
32. **Johnson W, Eisenstein S, Roberts S** '*Cell cluster formation in degenerate lumbar intervertebral discs is associated with increased cell proliferation*' Connective Tissue Research (2001); Vol.42 pp.197-207
33. **Le Maitre C, Pockert A, Buttle D, Freemont A, Hoyland J** *'Matrix synthesis and degradation in human intervertebral disc degeneration'* Biochemical Society Transactions (2007); Vol.35 pp.652-656
34. **Lee K, Moon S, Kim H, Kwon U, Kim H, Park S, Sun H, Lee H, Kim H, Chun H, Kwon I, Jang J** '*Tissue engineering of the intervertebral disc with cultured nucleus pulposus cells using atelocollagen scaffold and growth factors*' Spine (2012); Vol.37 No.6 pp.452-458
35. **Foss B, Maxwell T, Deng Y** '*Chondroprotective stimulation promotes the mechanical properties of injectable scaffold for human nucleus pulposus tissue engineering*' J of Biomech Materials (2014); Vol.24 pp.56-67
36. **Li Z, Kaplan K, Wertzel A, Peroglio M, Amit M, Grad S, Yayon A** '*Biomimetic fibrin-hyaluronan hydrogels for nucleus pulposus regeneration'* Regenerative Medicine (2014); Vol.9 pp.309-326
37. **Kobayashi S, Meir A, Urban J** '*Effect of cell density on the rate of glycosaminoglycan accumulation by disc and cartilage cells in vitro*' J of Orthopaedic Research (2008); pp.493-504
38. **Frantz C, Stewart K, Weaver V** '*The extracellular matrix at a glance*' J Cell Sci (2010); Vol.123 pp.4195-4200
39. **Blanquer S, Grijpma D, Poot A** '*Delivery systems for the treatment of degenerated intervertebral discs*' Advanced Drug Delivery Reviews (2014); Vol.84 pp.172-187
40. **Buckwalter J, Mankin H** '*Articular cartilage: tissue design and chondrocyte matrix interactions*' AAOS Inst Course Lect (1998); Vol. 47 pp.477-486.
41. **Kisiday J, Jin M, Kurz B, Hung H, Semino C, Zhang S, Grodzinsky A** *'Self-assembling peptide hydrogel fosters chondrocyte extracellular matrix production and cell division: Implications for cartilage tissue repair'* PNAS (2002); Vol.99 No.15 pp.9996-10001
42. **Temenoff J, Mikos A** '*Review: Tissue engineering for regeneration of articular cartilage*' Biomaterials (2000); Vol.21 pp.431-440
43. **Cheng Y, Yang S, Su W, Chen Y, Yang K, Cheng W, Wu S, Lin F** '*Thermosensitive chitosan-gelatin-glycerol phosphate hydrogels as a cell carrier for nucleus pulposus regeneration: An in vitro study*' Tissue Engineering (2010); Vol.16 No.2 pp.695-703
44. **Sun J, Zheng Q, Wu Y, Liu Y, Guo X, Wu W** *'Culture of nucleus pulposus cells from intervertebral disc on self-assembling KLD 12 peptide hydrogel scaffold'* Materials Science and Engineering (2010); Vol.30 pp975-980
45. **Stephan S, Johnson W, Roberts S** '*The influence of nutrient supply and cell density on the growth and survival of intervertebral disc cells in 3D culture*' European Cells and Materials (2011); Vol.22 pp.97-108
46. **Rodrigues-Pinto R, Richardson S, Hoyland J** '*Identification of novel nucleus pulposus markers*' Bone Joint Res (2013); Vol.2 pp.169-178
47. **Minogue B, Richardson S, Zeef L, Freemont A, Hoyland J** '*Transcriptional profiling of bovine intervertebral disc cells: Implications for identification of normal and degenerate human intervertebral disc cell phenotypes*' Arthritis & Research (2010); Vol.12 pp.1-20
48. **Eyre D, Muir H** *'Quantative analysis of types I and II collagens in the human intervertebral disc at various ages'* Biochimica et Biophysica Acta (1977); Vol.492 pp.29-42
49. **Iatridis J, MacLean J, O'Brien M, Stokes I** '*Measurements of proteoglycan and water content distribution in human lumbar intervertebral discs'* Spine (2007); Vol.32 No.14 pp.1493-1497

50. **Hu M, Hung L, Yang S, Sun Y, Shih T, Lin F** '*Lovastatin promotes redifferentiation of human nucleus pulposus cells during expansion in monolayer*' Artificial Organs (2010); Vol.35 No.4 pp.411-425
51. **Wang J, Baer A, Kraus V, Setton L** '*Intervertebral disc cells exhibit differences in gene expression in alginate and monolayer culture*' Spine (2001); Vol.26 No.16 pp.1747-1752
52. **Melrose J, Smith S, Ghosh P** '*Assessment of the cellular heterogeneity of the ovine intervertebral disc: comparison with synovial fibroblasts and articular chondrocytes*' Eur Spine J (2003); Vol.12 pp.57-65
53. **Kim D, Martin J, Elliott D, Smith L, Mauck R** 'Phenotypic stability, matrix elaboration and functional maturation of nucleus pulposus cells encapsulated in photocrosslinkable hyaluronic acid hydrogels' Acta Biomaterialia (2015); Vol.12 pp.21-29
54. **Vadala G, Studer R, Sowa G, Spiezia F, Lucu C, Denaro V, Gilbertson L, Kang J** '*Coculture of bone marrow mesenchymal stem cells and nucleus pulposus cells modulate gene expression profile without cell fusion*' Spine (2008); Vol.33 pp.870-876
55. **Collin E, Grad S, Zeugolis D, Vinatier C, Clouet J, Guicheux J, Weiss P, Alini M, Pandit A** *'An injectable vehicle for nucleus pulposus cell-based therapy'* Biomaterials (2011); Vol.32 pp.2862-2870
56. **Park J, Kuh S, Park H, Kim K** '*Comparative expression of matrix-associated genes and inflammatory cytokines-associated genes according to disc degeneration*' J Spinal Disord Tech (2011); Vol.24 No.6 pp.352-357
57. **Zhao Q, Eberspaecher H, LeFebrve V, de Crombrugghe B** '*Parallel expression of SOX9 and COL2A1 in cells undergoing chondrogenesis*' Developmental Dynamics (1997); Vol.209 pp.377-386
58. **Lefebvre V, Huang W, Harley V, Goodfellow P, de Crombrugghe B** '*SOX9 is a potent activator of the chondrocyte-specific enhancer of the pro alpha1 collagen gene*' Mol Cell Biol (1997); Vol.17 pp.2336-2346
59. **Richardson S, Hoyland J** '*Stem cell regeneration of degenerated intervertebral discs: Current status'* Pain Management (2008); Vol.12 pp.83-88
60. **Gorensek M, Jaksimovic C, Kregar-Velikonja N, Knezevic M, Jeras M, Pavlovcic V, Cor A** '*Nucleus pulposus repair with cultured autologous elastic cartilage derived chondrocytes*' Cell Mol Biol Lett (2004); Vol.9 pp.363-373
61. **Power K, Grad S, Rutges J, Creemers L, van Rijen M, O'Gaora P, Wall J, Alini M, Pandit A, Gallagher W** '*Expression of Carbonic Anhydrase XII varies with age and degeneration*' Arthritis & Degeneration (2011); Vol.63 No.12 pp.3876-3886
62. **Gilson A, Dreger M, Urban J** '*Differential expression level of cytokeratin 8 in cells of the bovine nucleus pulposus complicates the search for specific intervertebral disc cell markers*' Arthritis Research & Therapy (2010); Vol.12 pp.1-12
63. **Gotz W, Kasper M, Fischer G, Herken R '***Intermediate filament typing of the human embryonic and fetal notochord*' Cell & Tissue Research (1995); Vol.280 pp.455-462
64. **Stoyanov J, Gantenbein-Ritter B, Bertolo A, Aebli N, Baur M, Alini M, Grad S** '*Role of hypoxia and growth and differentiation factor-5 on differentiation of human mesenchymal stem cells towards intervertebral nucleus pulposus-like cells'* European Cells and Materials (2011); Vol. 21 pp.533-547
65. **Kalinichenko V, Zhou Y, Bhattacharyya D, Kim W, Shin B, Bambal K, Costa R** '*Haploinsufficiency of the mouse Forkhead Box f1 gene causes defects in gall bladder development'* J Biol Chem (2002); Vol.277 pp.12369-12374
66. **Chen Y, Su W, Yang S, Gefen A, Lin F** '*In situ hydrogels composed of oxidised high molecular weight hyaluronic acid and gelatin for nucleus pulposus regeneration'* Acta Biomater (2013); Vol.9 pp.5181-5193
67. **Mwale F, Demers C, Petit A, Roughley P, Poole A, Steffen T, Aebi M, Antoniou J** '*A synthetic peptide of link protein stimulates the biosynthesis of collagens II, IX and proteoglycan by cells of the intervertebral disc*' J Chem Biochem (2003); Vol.88 pp.1202-1213
68. **Clarke L, McConnell J, Sherratt M, Derby B, Richardson S, Hoyland J** *'Growth differentiation factor 6 and transforming growth factor-beta differentially mediate mesenchymal stem cell differentiation, composition, and micromechanical properties of nucleus pulposus constructs'* Arthritis & Research (2014); Vol.16 pp.1-13
69. **Rodriguez E, Roughley P** '*Link protein can retard the degradation of hyaluronan in proteoglycan aggregates*' Osteoarthritis Cartilage (2006); Vol.14 No.8 pp.823-829
70. **Rosso F, Giordano A, Barbarisi M, Barbarisi A** '**From cell-ECM interactions to tissue engineering**' J of Cellular Physiology (2004); Vol.199 No.2 pp.174-180
71. **Antoniou J, Steffen T, Nelson F, Winterbottom N, Hollander A, Poole A, Aebi M, Alini M** '*The human lumbar intervertebral disc: evidence for changes in the biosynthesis and denaturation of the extracellular matrix with growth, maturation, ageing, and degeneration' J Clin Invest (*1996); Vol.98 pp.996-1003.

72. **Ballestrem C, Wehrle-Haller B, Imhof B** '*Actin dynamics in living mammalian cells*' J of Cell Science (1998); Vol.111 pp.1649-1658
73. **Chiba K, Andersson G, Masuda K, Thonar J** '*Metabolism of the extracellular matrix formed by intervertebral disc cells cultured in alginate*' Spine (1998); Vol.22 No.24 pp.2885-2893
74. **Adams M, Roughley P** '*What is intervertebral disc degeneration and what causes it*?' Spine (2006); Vol.31 pp.2151-2161
75. **Li S, Duance V, Blain E** '*F-actin cytoskeletal organisation in intervertebral disc health and disease*' Biochemical Society Transactions (2007); Vol.35 pp.683-686
76. **Sztrolovics R, Alini M, Roughley P, Mort J** '*Aggrecan degradation in human intervertebral disc and articular cartilage*' Biochem J (1997); Vol.326 pp.235-241
77. **Alini M, Li W, Markovic P, Aebi M, Spiro R, Roughley P** '*The potential and limitations of a cell-seeded collagen/hyaluronan scaffold to engineer and intervertebral disc-like matrix*' Spine (2003); Vol.28 No.5 pp.446-454
78. **Peroglio M, Grad S, Mortisen D, Sprecher C, Junger S, Alini M, Eglin D** '*Injectable thermoreversible hyaluronan-based hydrogels for nucleus pulposus cell encapsulation*' Eur Spine J (2011); Vol.21 pp.839-849
79. **Lyons G, Eisenstein S, Sweet M** *'Biochemical changes in intervertebral disc degeneration' BBA (1981); Vol.673 pp.443-453*
80. **Woiciechowsky C, Abbushi A, Zenclussen M, Casalis P, Kruger J, Freymann U, Endres M, Kaps C** '*Regeneration of nucleus pulposus tissue in an ovine intervertebral disc degeneration model by cell-free resorbable polymer scaffold*' J of Tissue Engineering and Regenerative Medicine (2012);
81. **Sakai D, Mochida J, Iwashina T, Watanabe T, Nakai T, Ando K, Hotta T** '*Differentiation of mesenchymal stem cells transplanted into a rabbit degenerative disc model*' Spine (2005); Vol.30 No.21 pp.2379-2387
82. **Smith L, Chiaro J, Nerurkar N, Cortes D, Horava S, Hebela N, Mauck R, Dodge, Elliot D** '*Nucleus pulposus cells synthesise a functional extracellular matrix and respond to inflammatory cytokine challenge following long-term agarose culture*' European Cells and Materials (2011); Vol.22 pp.291-301
83. **Szkolar L, Guilbaud J, Miller A, Gough J, Saiani A** '*Enzymatically triggered peptide hydrogels from 3D cell encapsulation and culture*' J of Peptide Science (2014); Vol.20 pp.578-584
84. **Maldonado B, Oegema T** '*Initial characterisation of the metabolism of intervertebral disc cells in microspheres*' J of Orthopaedic Research (1992); Vol.10 pp.677-690
85. **Postacchini F** '*Lumbar disc herniation*' SpringerWeinNewYork (1999); ISBN 3-211-83118-5
86. **Chelberg M, Banks G, Geiger D, Oegema T** '*Identification of heterogeneous cell populations in normal human intervertebral disc*' J Anat (2005); Vol.186 pp.43-53
87. **Melrose J, Ghosh P, Taylor T** '*A comparative analysis of the differential spatial and temporal distributions of the large (aggrecan, versican) and small (decorin, biglycan, fibromodulin) proteoglycans of the intervertebral disc*' J Anat (2001); Vol.198 pp.3-15
88. **Adams P, Eyre D, Muir H** '*Biochemical aspects of development and ageing of human lumbar intervertebral discs*' Rheumatology & Rehabilitation (1977); Vol.16 pp.22-30
89. **Rosenberg L, Schubert M** '*The protein polysaccharides of bovine nucleus pulposus*' J of Biological Chemistry (1967); Vol.242 No.20 pp.4691-4701

Chapter 6. *The culture of bone marrow mesenchymal stem cells in self-assembling peptide hydrogels.*

6.1. INTRODUCTION

6.1.1. Overview

Chapter 4 described optimising the SAPH so stiffness matched the native NP tissue and demonstrating that it was deliverable via minimally invasive procedure. *Chapter 5* described analysis of bNPC behaviour after 3D culture in the FEFEFKFK SAPH. Results demonstrated that NPCs maintained their phenotype, viability remained high throughout *in vitro* culture and cells were stimulated into depositing NP associated ECM components. It was hypothesised that the SAPH microenvironment mimicked the native NP matrix which allowed preservation of bNPC phenotype and stimulated production of appropriate ECM components. Therefore it was determined that FEFEFKFK SAPH warranted further investigation using a more clinically relevant cell source.

This chapter described the analysis of 3D h-BMMSC culture in FEFEFKFK SAPHs with and without a discogenic induction growth factor of GDF-6 (*section 6.1.3*). Human BMMSCs are regarded to hold potential in regards to NP tissue engineering [1] and would be a likely cell source if this system progressed to *in vivo* trials (*section 6.1.2.*).

6.1.2. Human bone marrow derived mesenchymal stem cells

MSCs are regarded to be a promising cell source for NP tissue engineering [1, 2, 3] due to the high *in vitro* expansion potential of MSCs [4], their relative availability [3] and the fact that a NP-like phenotype can be induced from MSCs using appropriate growth factors and culture environments [5, 6]. Crucially, injection of MSCs into degenerated human NPs has been demonstrated to increase H_2O content of IVDs and provide significant analgesic effects for LBP sufferers [7, 8].

In this study, h-BMMSCs from a 27 year old female were harvested after elective surgery then cultured, expanded and encapsulated in FEFEFKFK SAPH to assess cell behaviour and determine whether BMMSCs could be differentiated towards a NP-like phenotype.

For h-BMMSC culture, 30 mg ml^{-1} FEFEFKFK SAPHs were used due to the concentration most closely matching the native NP stiffness (*section 4.4.4*). The SAPH |G*| values were akin to the human NP whilst the SAPH δ value was a better match to the native tissue in comparison to contemporary studies. Scaffold stiffness has been identified as a crucial cue to guide MSC differentiation and to stimulate appropriate ECM production [9, 10]. Tissue-level elasticity has been shown to play a key role in the lineage and phenotype that undifferentiated MSCs commit to [11]. Therefore it was rational to attempt and match SAPH mechanical properties as closely as possible with the native NP to increase likelihood of h-BMMSC differentiation to NP-like cells and preservation of the phenotype after encapsulation.

6.1.3. Growth differentiation factor-6

A promising approach to the treatment of LBP is the use of growth factors to modulate matrix production and degradation of the IVD [12]. Growth factors provide molecular cues which commit MSCs to a specific lineage [13]. Methods involve delivering growth factors via direct injection of the molecules into a degenerated IVD *in vivo* [14] or use of growth factors in conjunction with scaffolds to differentiate MSCs towards a NP-like phenotype before implantation [5, 15].

TGF-β plays a critical role in activating intracellular signalling cascades for promotion of cartilage specific gene expression [16]. It was hypothesised that TGF-β might have been able to induce discogenic differentiation due to the comparable morphology of chondrocytes and NPCs and similarity in ECM component production [17]. *SOX9*, *ACAN* and *COL2A1* expression was increased after MSC stimulation with TGF-β [13]. Investigation occurred prior to identification of ‘novel’ NPC markers.

GDF-5 is currently regarded to be one of the most promising growth factors for the induction of NP-like phenotypes from MSCs [5, 18]. Stoyanov *et al.* demonstrated that MSCs treated with GDF-5 showed higher expression of NP-specific genes (*FOXF1*, *KRT19*) than TGF-β. TGF-β treated samples lead to a hypertrophic chondrogenic phenotype, as opposed to a stable NPC phenotype [5]. Four Phase I / II clinical trials investigating interdiscal injection of GDF-5 are currently in progress or recently completed (NCT01182337, NCT01158924, NCT00813813, and NCT01124006) with results yet to be published.

GDF-6 is a member of the transforming growth factor beta superfamily and has been demonstrated to play a key role in spinal column development. Mutations at the GDF-6 gene locus resulted in joint fusion and caused IVD developmental complications [20]. Healthy human NPCs and cells from degenerate NPs were shown to immuopositive stain for GDF-6 [21]. Therefore it was hypothesised that the growth factor might have an influence on IVD development and homeostasis [6, 21]. GDF-6 protected against DDD after injection into the degenerated discs of an ovine model as increased amounts of collagen and PGs were

detected whilst prevention of disc narrowing by increased IVD hydration was also observed [22]. Clarke *et al.* seeded patient matched h-AdMSCs and h-BMMSCs in type I collagen hydrogels and cultured the samples in media stimulated with TGF-β3, GDF-5 and GDF-6. GDF-6 stimulated samples for both cell types produced a higher *ACAN* to *COL2A1* expression ratio and upregulated NP-specific markers significantly higher than TGF-β3 and GDF-5. GDF-6 treated samples also accumulated more s-GAGs [6].

The signal transduction pathway for GDF-6 involves cell-signalling via trans-membrane kinase receptor complexes [23] which contain both Type I and Type II receptor molecules. When GDF ligand binds to the Type II receptor, recruitment and phosphorylation of Type I receptor leads to kinase domain activation and initiates the intracellular signalling cascade [24, 25]. Intracellular signalling downstream events involve the recruitment and activation of Receptor-associated-Smad signalling molecules to propagate the GDF receptor signals to the cell nucleus via binding to specific DNA sequences which promotes gene expression [26, 27]. GDF-6 signalling pathways are associated with embryonic development and the molecule has been detected in cartilage and tendons as well as playing a role in IVD development [28].

6.1.4. Hypothesis

In *chapter 5,* FEFEFKFK SAPHs were shown to restore and preserve the NPC phenotype with stimulation of NP associated ECM component production. Therefore if MSCs could be differentiated towards a NP-like phenotype after culture in the SAPH then the microenvironment should be appropriate for preserving the discogenic phenotype due to the system mimicking the native NP ECM. An appropriate niche could direct stem cell differentiation towards a specific lineage whether by replicating mechanical properties [10, 29] or presenting appropriate ECM components [30].

GDF-6 was chosen as the exogenous growth factor to induce a NP-like phenotype from h-BMMSCs due to the findings by Clarke *et al.* (*section 6.1.3*) [6]. The hypothesis was that GDF-6 would induce discogenic differentiation so behaviour associated with NPCs would be observed including upregulation of ‘traditional’ and ‘novel’ NPC gene markers, rounded cell morphology, a stable cell population and deposition of extracellular aggrecan and type II collagen.

Non-stimulated h-BMMSCs cultured with the same recipe for NP induction media but in absence of the discogenic differentiation factor of GDF-6 were used as controls (*section 3.3.2.4*). The hypothesis was that GDF-6 stimulated samples would express NP associated markers significantly higher, and deposit more NP ECM components, than non-stimulated cells as observed in the literature [6]. Samples without GDF-6 stimulation would not have the appropriate cues provided by the exogenous growth factor to induce differentiation towards a discogenic phenotype. However as the SAPH has been demonstrated to restore and maintain

the NP phenotype after NPC de-differentiation during monolayer culture (*chapter 5*), it is possible that the biomaterial microenvironment could play a role in determining stem cell fate [10, 30] as the SAPH could mimic the NP ECM.

6.1.5. Aims

The behaviour of h-BMMSCs after culture in SAPHs was assessed following GDF-6 stimulation to determine whether discogenic differentiation could be induced. Cell behaviour in without GDF-6 stimulation was investigated to assess whether the biomaterial had an effect on determining stem cell fate. The same analysis techniques were used so a comparison could be made between growth factor stimulated samples and non-stimulated samples.

A number of assays were conducted to determine cell behaviour after encapsulation in the FEFEFKFK SAPHs.

- Cell viability and morphology (LIVE/DEAD® cell viability assay)
- Cell population (CytoTox 96® Non-Radioactive Cytotoxicity Assay, Quant-iT™ Picogreen® dsDNA assay)
- Cell phenotype (TaqMan® probe qRT-PCR)
- ECM production (Blyscan™ sulphated GAG assay, ICC staining)

6.2. ANALYSING CELL MORPHOLOGY USING OPTICAL MICROSCOPY

In 2D culture, h-BMMSCs were spindle shaped and fibroblastic in appearance which is the morphology undifferentiated h-BMMSCs adopt during *in vitro* expansion [31, 32] *(figure 6.1)*. Undifferentiated h-BMMSCs tend to attach and spread to substrates [33]. In contrast, h-BMMSCs adopted a rounded morphology with and without GDF-6 stimulation during 3D cell culture in FEFEFKFK SAPHs. The alteration in morphology indicated that h-BMMSCs had undergone differentiation. Due to the documented effect that GDF-6 has on h-BMMSCs [6] it was likely that a discogenic phenotype was induced for stimulated samples however further assays were required to confirm phenotype as it is difficult to identify cell populations based on morphology alone [34] (*section 6.5*).

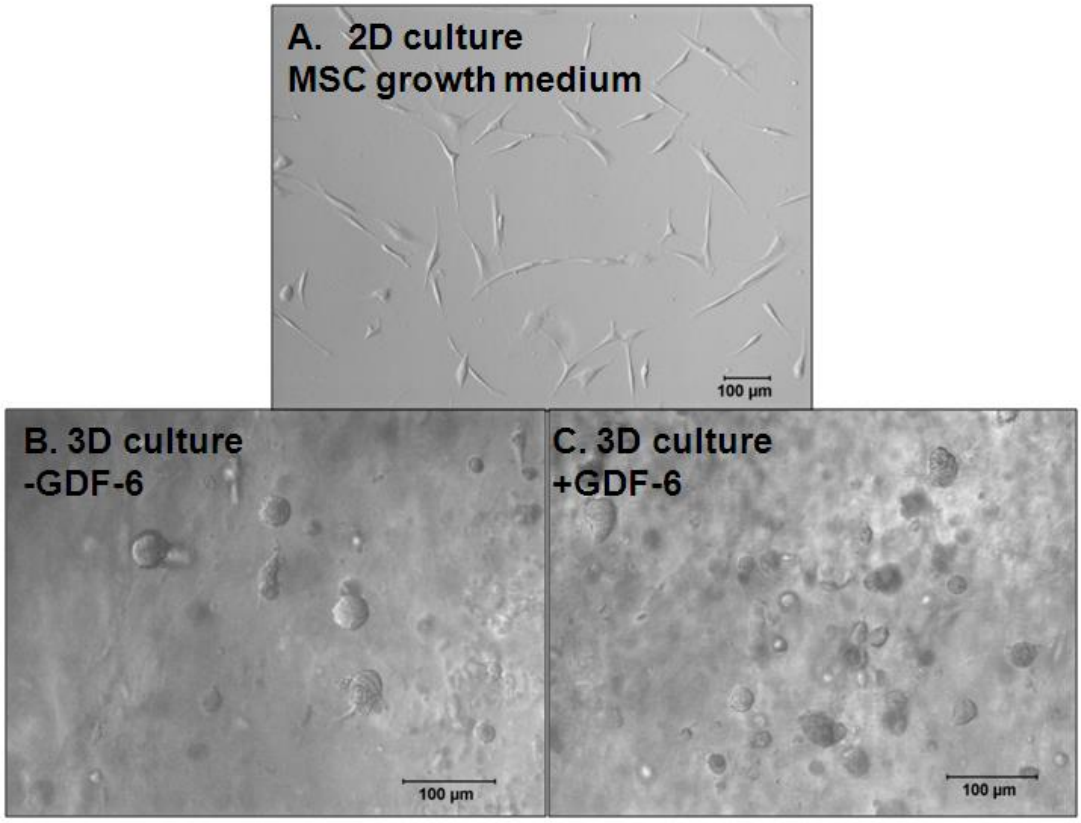

Figure 6.1. Light micrographs demonstrating cell culture of $1x10^6$ h-BMMSCs ml^{-1} on day 7. [A] 2D cell culture on TCP with MSC growth medium. Cells adopted spindle-like spread morphology. [B] 3D cell culture in 30 mg ml^{-1} FEFEFKFK SAPH cultured in absence of GDF-6. Cells adopted a rounded morphology. [C] 3D cell culture in 30 mg ml^{-1} FEFEFKFK SAPH cultured with 100 ng ml^{-1} GDF-6. Cells adopted a rounded morphology. Scale bar represents 100 µm.

6.3. ASSESSING CELL VIABILITY AND MORPHOLOGY USING LIVE/DEAD® ASSAY

LIVE/DEAD® assay was used to determine the viability of encapsulated h-BMMSCs with and without GDF-6 stimulation on days 1, 3, 7 and 14.

6.3.1. Cell viability and morphology

High viability was maintained by h-BMMSCs encapsulated in FEFEFKFK SAPHs cultured with and without GDF-6 stimulation throughout culture (*figure 6.2*). Objectively, there was little difference in live to dead cell ratio or total number of cells between time points for samples without GDF-6 stimulation. Day 7 fluorescence micrographs for samples with GDF-6 stimulation showed a decrease in total cell number which recovered slightly by day 14. An increase in dead cells was observed at later time points *(discussed in section 6.3.2)*. It was important to note that *figure 6.2* only showed a small percentage of the total number of cells in the SAPH therefore only provides an overview of cell viability.

All cells in GDF-6 stimulated and non-stimulated samples adopted rounded morphology which is characteristic of native NPCs [35, 36] (*figure 6.2*) and comparable to bNPC morphology after culture in SAPHs (*figures 5.4 & 5.6*). It was a distinct morphological alteration from undifferentiated h-BMMSCs in monolayer culture (*figure 6.1*). Absence of cell binding domains in the peptide sequence meant that no attachment sites were available which could explain rounded morphology [37]. Alternatively, h-BMMSCs adopt a rounded morphology after differentiation towards a chondrogenic [38], adipogenic [39] or discogenic phenotype [15]. Due to the evidence that h-BMMSCs cultured with GDF-6 induced a NP-like phenotype [6], it was likely that h-BMMSCs had differentiated towards a discogenic lineage however gene expression of encapsulated cells was required to confirm phenotype (*section 6.5*). With increasing time point it was evident that more rounded cells displayed long cellular processes extending into the scaffold (*figure 6.2B*) (denoted with white arrows) which is typical of NPCs in the native tissue [36]. For samples without GDF-6 stimulation (*figure 6.2A*) it was hypothesised that the nanofibrous SAPH architecture likely had a role in determining h-BMMSC morphology.

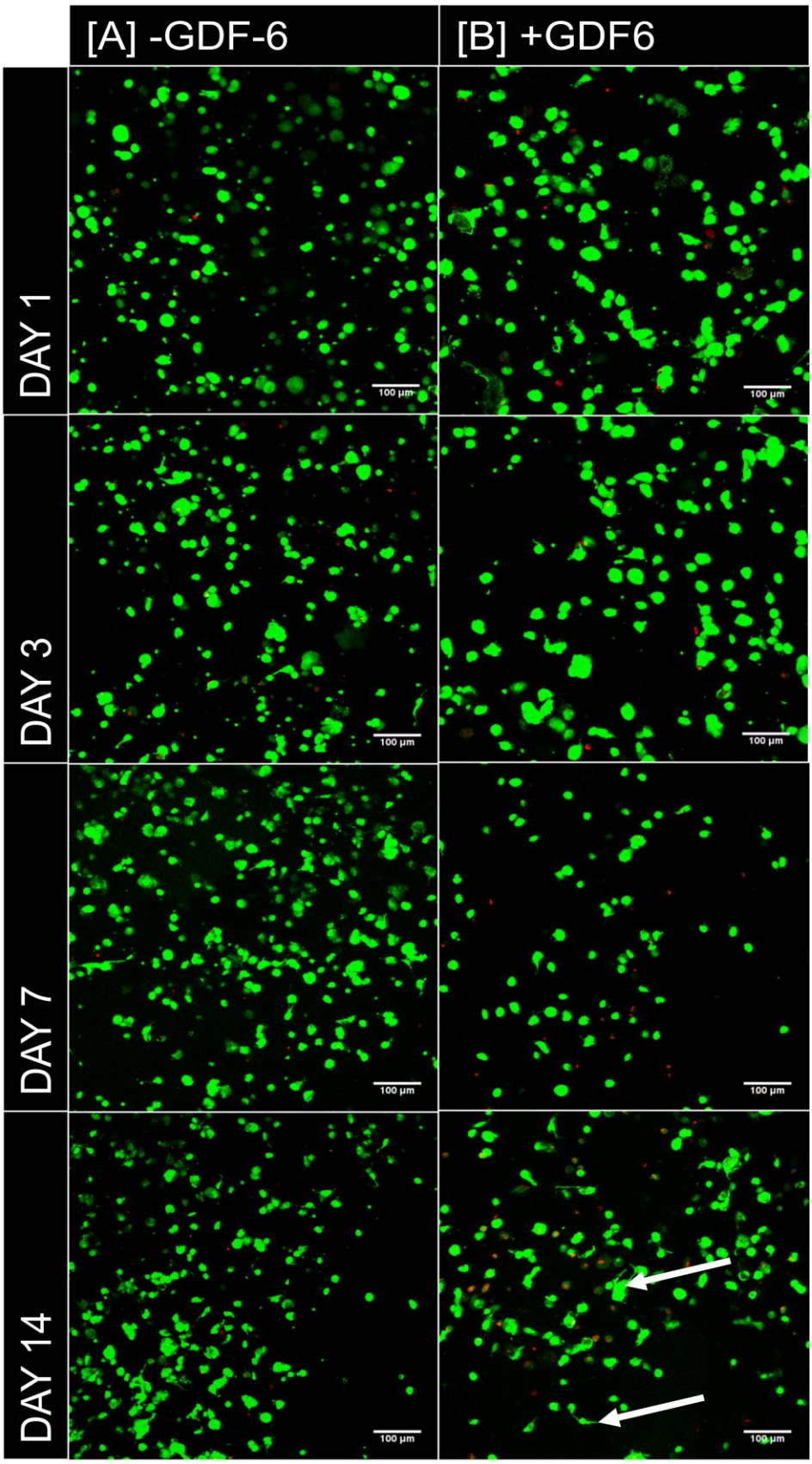

Figure 6.2. Fluorescence micrographs demonstrating cell viability of 1x10^{6} h-BMMSCs ml^{-1} in 30 mg ml^{-1} FEFEFKFK SAPHs without [A] and with [B] GDF-6 stimulation on days 1, 3, 7 and 14. Micrographs were taken along the z-axis (axial plane) and demonstrated high cell viability for all timepoints. Viable cells were stained green, dead cells were stained red. Scale bar represents 100 µm.

6.3.2. Cell counts for fluorescence micrographs

There was a significant majority of viable h-BMMSCs present throughout culture for both stimulated and non-stimulated samples (>80% viable cells for all time points) (*figure 6.3*). The general trend was a non-significant decrease in viable cells with *in vitro* culture length (P>0.05).

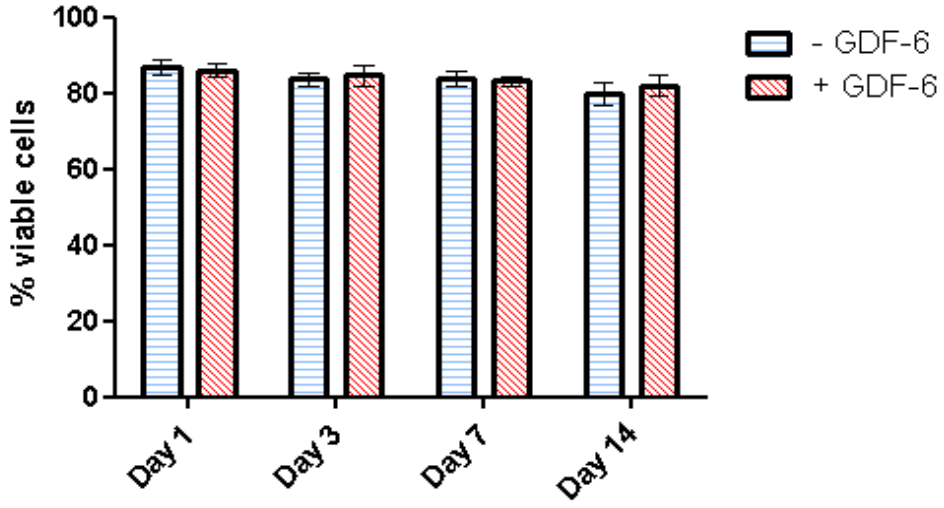

Figure 6.3. A comparison of percentage viable h-BMMSCs present in LIVE/DEAD assay fluorescence micrographs for $1x10^6$ h-BMMSCs ml^{-1} in 30 mg ml^{-1} FEFEFKFK SAPHs. The variable was cell culture medium with and without GDF-6 stimulation. There were no significant differences between culture conditions. (P>0.05). Values expressed as mean±SD where n=3 from 2 experimental repeats.

Oscillatory rheology determined that SAPHs weakened with culture period (*figures 4.8B & 8.6*) therefore this study hypothesised that the change in mechanical properties might have affected cell viability. On day 1, SAPH mechanically properties closely matched the native NP [40] (*section 4.4.4*) however by day 14 the SAPH stiffness was significantly lower (*figure 8.6*). Even with evidence of ECM deposition from day 3 onwards (*sections 5.6-5.8*) the system still became unstable with *in vitro* culture length. It is possible that an increase in seeding cell density would increase ECM component accumulation [41] therefore improving SAPH stability. It has been demonstrated that changes in scaffold mechanical properties can impact cellular function. Cell-interactive signals and cell-to-substrate interactions play a crucial role in determining cell viability and function [42]. Cell viability would likely be affected by *in vitro* culture time, additional environmental factors [43] and loss of SAPH structural stability.

Reza *et al.* determined that there was a significant decrease in viable bNPCs after culture in carboxymethylcellulose hydrogels. The equilibrium Young's modulus also decreased from days 1 to 14 therefore it was speculated that the lack of structural integrity resulted in a significant loss of material and may have contributed to the lower than expected activity/viability measurements [44]. Chou *et al.* observed no significant changes in

photocrosslinked alginate hydrogel Young's modulus over 14 day culture period however a decrease in bNPC viability was recorded [43].

The cell count method demonstrated that there were no significant differences in cell viability at any time point between the two culture conditions (*figure 6.3*). Results indicated that GDF-6 did not significantly affect the viability of cells. TGF-β1 and IGF-1 were effective in stimulating higher human NPC proliferation than non-stimulated cells [45] however experiments were carried out in monolayer which has been proven to increase cellular proliferation [46]. GDF-5 has been shown to promote proliferation *in vivo* [47]. However, similar to results for this study, the DNA content after the culture of h-BMMSCs with and without GDF-5 and TGF-β was not significantly different [5, 48].

6.3.3. Dispersion of h-BMMSCs throughout SAPHs

At later time points there was a reduction in total cell number most evident for day 7 samples stimulated with GDF-6 (*figure 6.4*). However there did not appear to be a substantial change in ratio of viable to dead cells which was confirmed by the non-significant difference in percentage viable cells from days 1 to 14 ($P>0.05$) (*figure 6.3*).

Micrographs demonstrated that a homogenous dispersion of h-BMMSCs were present in samples on days 1 and 3 when imaged along the sagittal plane (*figures 6.2 & 6.4*). Day 7 micrographs demonstrated that cells had begun to migrate to the bottom of the SAPH. In *section 5.3.3* a migration test determined that it was possible for cells to migrate through the system, likely due to SAPH high H_2O content (97%) coupled with the semi-flexibility of the nanofibres [37].

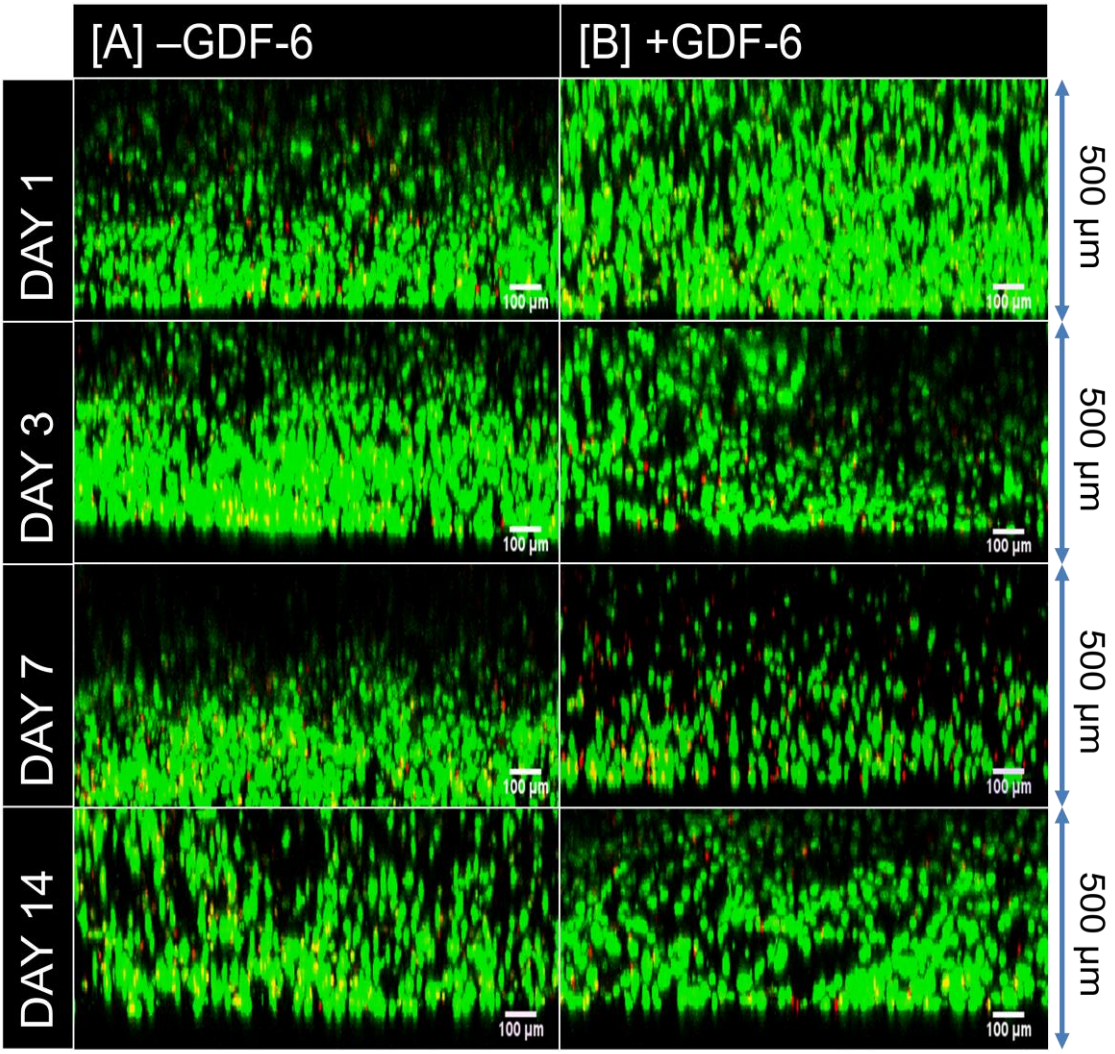

Figure 6.4. Fluorescence micrographs demonstrating cell viability of 1x10^{6} h-BMMSCs ml^{-1} in 30 mg ml^{-1} FEFEFKFK SAPHs [A] without and [B] with GDF-6 stimulation on days 1, 3, 7 and 14. Micrographs were taken along the y-axis (sagittal plane) to allow analysis of cell dispersion throughout the system and whether cell migration occurred. Viable cells were stained green, dead cells were stained red. Scale bar represents 100 µm.

There appeared to be lower migration of h-BMMSCs (*figure 6.4)* in comparison to bNPC samples (*figure 5.6*) which could be explained by cell seeding density differences (2x10^{5} bNPCs ml^{-1} and 1x10^{6} h-BMMSCs ml^{-1}). It was possible that there was increased accumulation of ECM components for h-BMMSCs in comparison to bNPCs [41]. Type II collagen is the main ECM component responsible for NP structural strength [49] whilst aggrecan plays a crucial role in NP hydration [50]. Despite the SAPH weakening with culture period, a higher density of cells would likely contribute more to scaffold rigidity in comparison to a lower density of cells (*figure 4.8*). In turn, this would slow degradation and volume loss of the SAPH at later time points and might hinder migration of cells. It might be possible to track migration of cells using apparatus that allow for real-time monitoring for example xCELLigence RTCA (*ACEA Biosciences, USA*).

6.3.4. Overview and further discussion

A potential NP tissue engineering system that does not support high cell viability is not suitable for the application. A number of studies that investigated various biomaterial scaffolds for NP tissue engineering determined that high MSC viability was present throughout *in vitro* culture [29, 51, 52]. Kumar *et al.* determined that h-BMMSCs cultured in a synthetic polymer hydrogel adopted a rounded morphology with chondrogenic media stimulation. In media without a differentiation factor, h-BMMSCs attached to the scaffold and adopted a fibroblastic morphology with a higher percentage of cell apoptosis [51]. Wang *et al.* observed 80 to 90% viability on days 3 and 7 when rabbit BMMSCs were cultured in LN-NS and RADA16 SAPHs, [53].

The limitation of using the cell count method was that only the percentage viable cells present in fluorescence micrographs could be calculated. It was not an effective technique for determining total cell numbers in the sample as this would need to assume that an entirely homogenous distribution of h-BMMSCs existed with the same ratio of viable to dead cells throughout. However the method allowed the ratio of viable to dead cells in particular fluorescence micrographs to be quantified and an estimate of percentage viable cells could be calculated. Total hydrogel cell number assays were carried out to produce an accurate representation of overall cell population numbers (*chapter 6.4*).

To summarise, h-BMMSC viability was consistently high throughout culture with and without GDF-6 stimulation (*figures 6.2 & 6.4*) which strongly suggested that the SAPH could support high viability. It was determined that there was no significant changes ($P>0.05$) in percentage viable cells over culture period and the addition of GDF-6 did not affect the viability of cells (*figure 6.3)*. A rounded morphology was adopted by cells in both culture conditions which is typical of NPCs in the native tissue and a distinct morphological alteration from the conventional undifferentiated spindle-like h-BMMSC morphology.

6.4. DETERMINING CELL NUMBERS USING CYTOTOX 96® CYTOTOXICITY ASSAY

The CytoTox 96® non-radioactive cytotoxicity assay was used to determine viable h-BMMSC numbers after culture with and without GDF-6 stimulation on days 1, 7 and 14. The cell number was calculated from a standard graph which plotted known cell numbers against absorbance (*figure 8.2*).

6.4.1. Human BMMSCs cultured without GDF-6 stimulation

There were no significant changes in viable cell population over *in vitro* culture (P>0.05) (*figure 6.5)* for samples without GDF-6 stimulation. On day 1, cell numbers were estimated at $8.42x10^5$ which dropped to $7.45x10^5$ on day 7. From day 7 to day 14 ($7.58x10^5$) there was a slight increase in cell number. Importantly there was no significant difference in cell number from days 1 to 14 (P>0.05).

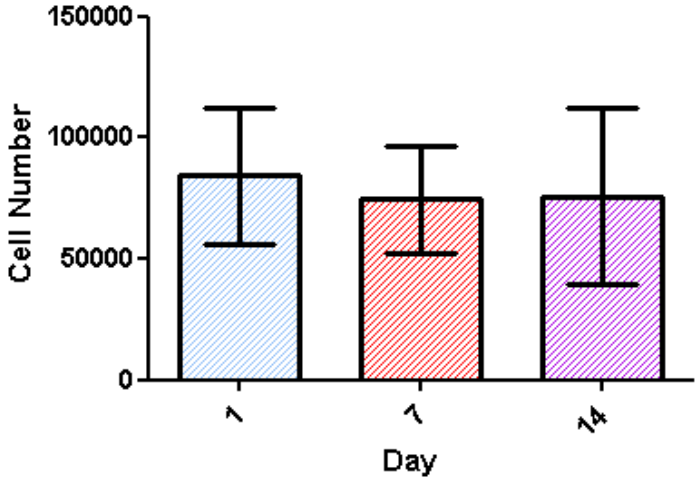

Figure 6.5. Cell numbers over 14 days *in vitro* culture for $1x10^6$ h-BMMSCs ml^{-1} in 30 mg ml^{-1} FEFEFKFK SAPH in absence of GDF-6 stimulation. Cell population remained stable over culture period. (P>0.05). Values expressed as mean±SD where n=5 from 2 experimental repeats. N.B. initial seeding amount $1.5x10^5$ h-BMMSCs.

The initial drop in cell numbers during SAPH seeding and plating was due to the basic nature of the culture environment which induced pH shock for some cells (*table 5.1*). SAPH pH was returned to more physiologically relevant levels following media washes. It was important to note that after cell washes on day 0, no significant amounts of cell death occurred which suggested that the SAPH was a suitable culture environment at pH 7.4 (*figure 6.5*). A similar percentage of cell death was observed after encapsulation of bNPCs in SAPHs (*figure 5.10*). Peptide powder could be dissolved in 10% sucrose solution during the production protocol

(*section 3.2*) prior to cell seeding to improve initial cell survival [53, 54, 55] as this reduces any adverse effects of acidic or basic aqueous SAPHs environments until cells were stabilised in neutral culture medium (PuraMatrix guidelines). Alternatively by reducing the amount of 1M NaOH addition in the production protocol (*table 3.1*), SAPH pH would be less basic and closer to physiologically relevant levels at the time of seeding.

6.4.2. Human BMMSCs cultured with GDF-6 stimulation

There was no significant change in viable cell number comparing days 1 to 14 for samples stimulated with GDF-6 (P>0.05) (*figure 6.6)*. Cell numbers were estimated at $7.14x10^5$ on day 1 with cell numbers significantly decreasing to $5.9x10^5$ on day 7 (**P<0.01). From day 7 to day 14 ($7.33x10^5$) there was a significant increase in cell number (***P<0.001). It has been hypothesised that NPCs may be able to 'sense' when cell density decreased significantly and respond by proliferating to restore original cell number (*figure 8.9*) [56]. Therefore if h-BMMSCs had undergone discogenic differentiation by day 7 then it was possible that cells entered a proliferative state to recover original cell density. The initial decrease in cell numbers from seeding to day 1, due to the basic nature of the culture environment, was comparable to *figure 6.5* and to bNPCs in SAPHs (*figure 5.10*). Reasons for cell death and methods to improve cell survival were discussed in *section 6.4.1*.

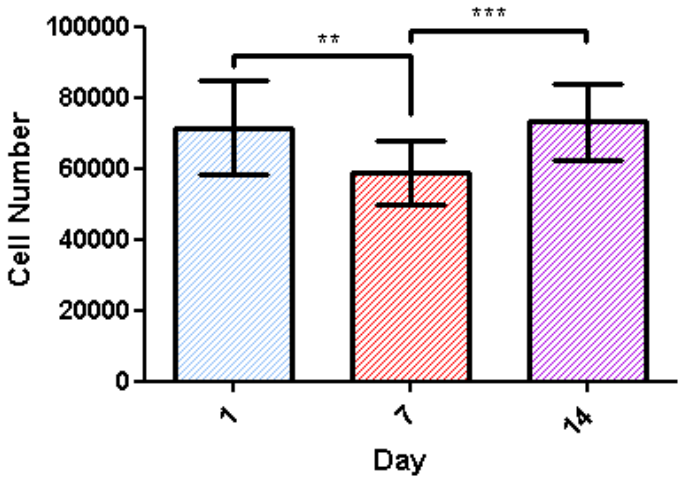

Figure 6.6. Cell numbers over 14 days *in vitro* culture for $1x10^6$ h-BMMSCs ml^{-1} in 30 mg ml^{-1} FEFEFKFK SAPH with 100 ng ml^{-1} GDF-6 stimulation. There was no significant changes in cell population on days 1 to 14 (P>0.05). However from days 1 to 7 and 7 to 14, there were significant changes in cell population (P<0.01, ***<0.001). Values expressed as mean±SD where n=5 from 2 experimental repeats. N.B. initial seeding amount $1.5x10^5$ h-BMMSCs.**

6.4.3. Comparison of non- and stimulated h-BMMSCs

There were no significant differences in population for any time point between culture condition (P>0.05) (*figure 6.7*) which demonstrated that GDF-6 had little effect on cell proliferation (*figure 6.3*). Gantenbein-Ritter *et al.* observed no significant difference in h-BMMSC number after culture in alginate hydrogels with GDF-5 and TGF-β stimulation compared to control samples without growth factor stimulation [48]. Stoyanov *et al.* determined that normoxic there were no significant differences in DNA content after culture with and without GDF-5 and TGF-β. Cell numbers for both control and stimulated samples decreased with culture length [5].

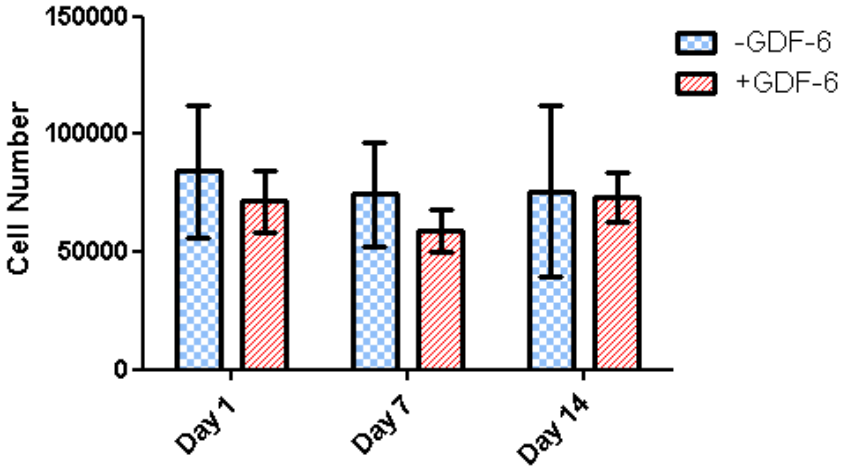

Figure 6.7. A comparison of cell numbers over 14 days *in vitro* culture for 1x10^6 h-BMMSCs ml^{-1} in 30 mg ml^{-1} FEFEFKFK SAPH cultured in absence of GDF-6 and cultured with 100 ng ml^{-1} GDF-6 stimulation. There was no significant difference between cell numbers at any time point between stimulated and non-stimulated samples (P>0.05) Values expressed as mean±SD where n=5 from 2 experimental repeats. N.B. initial seeding amount 1.5x10^5 h-BMMSCs.

6.4.4. Overview and further discussion

There was no significant difference in viable cell population on day 1 compared to day 14 for either h-BMMSC samples (*figures 6.5 & 6.6*) or bNPC samples (*figure 5.10*) In a healthy NP, the fundamental role of NPCs is to maintain and remodel the matrix [30]. NPCs have low proliferation potential so cell population remains stable in healthy native tissue [57]. NPCs will only significantly proliferate when under stress [58], when expanded in monolayer [59] or during DDD [60]. The stable bNPC population in the SAPH (*figure 5.10*) suggested that cells were behaving similarly to native NPCs, in terms of lack of proliferation, and therefore would be depositing ECM components which was confirmed by various assays (*sections 5.6-5.8*).

If h-BMMSCs had differentiated towards a NP-like phenotype, whether as a consequence of growth factor stimulation or the biomaterial effect, then the expectation would be that cell numbers would have remained stable (*figures 6.5 & 6.6)*. The lack of cell proliferation was not of particular concern as significant cell death was not recorded and cells in a proliferative state produce low amounts of ECM components.

The association between increased ECM production and absence of cell proliferation was demonstrated when Liu *et al.* cultured h-BMMSCs in PEG hydrogels incorporated with a collagen mimetic peptide. Population decreased significantly with time from around 95% viability on day 1 to 20 to 60% by day 30. Despite the high cell death, significant increases in aggrecan and type II collagen gene expression were recorded from days 1 to 12 [61]. Gantenbein-Ritter *et al.* determined that the DNA content significantly decreased from days 1 to 28 when h-BMMSCs were cultured in alginate gels with GDF-5 stimulation however a significant increase in GAG accumulation per sample was observed. Stoyanov *et al.* observed a significant decrease in DNA content over 28 days without GDF-5 stimulation whilst a non-significant increase in total GAG accumulation was recorded [5].

Scaffolds which stimulated a period of cell proliferation followed by maintenance of a stable cell population, to allow deposition of ECM components, would be ideal for NP tissue engineering [53]. Cell numbers are low in the native tissue [62] therefore an increase in cell numbers would lead to higher accumulation of ECM components [41] (*section 5.7.1*). A drawback of high proliferation is that inappropriate ECM components such as type I collagen would likely be deposited [58, 63]. Other potential disadvantages of high cellular proliferation rates include de-differentiation, loss of re-differentiation capacity and cellular senescence [3]. Therefore cell phenotype and ECM component production need to be assessed when utilising biomaterials that stimulate cellular proliferation to ensure that cells are still suitable for NP tissue engineering applications.

To summarise, there were no significant differences in cell numbers when comparing days 1 and 14 for samples cultured with and without GDF-6 stimulation (*figures 6.5 & 6.6*). The absence of proliferation was not of concern as significant proliferation by NPCs leads to a reduction in ECM deposition rate. Also NPC and h-BMMSC proliferation is associated with extracellular deposition of type I collagen which accelerates DDD.

6.5. DETERMINING CELL PHENOTYPE USING QUANTITATIVE POLYMERASE CHAIN REACTION

Quantitative RT-PCR was used to determine which genes were being up- and downregulated by h-BMMSCs after culture in SAPHs with and without GDF-6 stimulation. Genes of interest were the 'traditional' discogenic and chondrogenic markers of *COL1A2*, *COL2A1*, *ACAN* and *SOX9* [17, 64]. Recently identified NP-specific markers [65] of *KRT8*, *KRT18*, *KRT19*, *FOXF1* and *CA12* were also tested to differentiate the chondrogenic and discogenic phenotypes [64].

6.5.1. Gene expression for individual 'traditional' NPC markers

For h-BMMSCs cultured in absence of GDF-6, *COL1A2* relative gene expression normalised to *GAPDH* values remained consistently low (day 1; 0.72±0.19, day 7; 0.38±0.18 and day 14; 1.3±0.14) (P>0.05) (*figure 6.8*). For stimulated h-BMMSCs, *COL1A2* relative gene expression normalised to *GAPDH* values significantly decreased with culture period (day 1; 2.76±1.18, day 7; 0.59±0.35 and day 14; 0.14±0.076) (**P<0.01) (*figure 6.8*). By day 14, COL1A2 expression for GDF-6 stimulated samples was significantly lower that non-stimulated samples (**P<0.01).

Type I collagen is highly deposited by undifferentiated BMMSCs (*section 6.6.1 & 6.6.2*) [65] whilst in the native tissue, type I collagen is produced by NPCs in small amounts [66]. Significant production is strongly associated with DDD and de-differentiation of the NP phenotype. During DDD, NPCs switch from producing type II collagen to type I collagen and the stronger fibrils forms a more fibrous tissue which accelerates the condition [67]. The culture of bNPCs in SAPHs (*figure 5.12*) had comparable low *COL1A2* expression profile to *figure 6.8*. Most NP tissue engineering studies use low *COL1A2* expression in comparison to other traditional and novel NP marker genes, as evidence for upregulation of a healthy NPC phenotype [5, 6, 69].

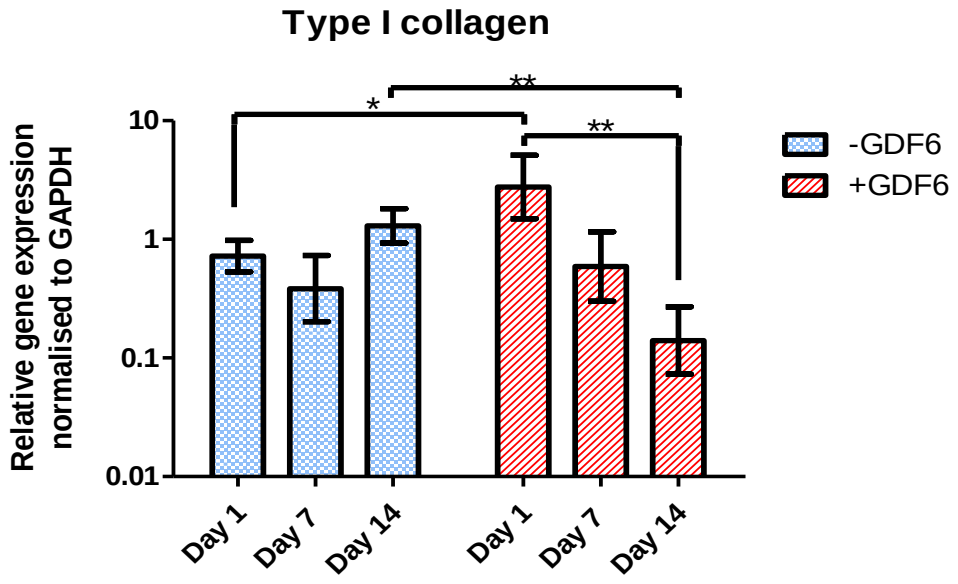

Figure 6.8. *COL1A2* relative expression for 1x10^{6} h-BMMSCs ml^{-1} cultured with and without 100 ng ml^{-1} GDF-6 in 30 mg ml^{-1} FEFEFKFK SAPHs. Gene expression normalised to *GAPDH*. (P>0.05, *P<0.05, **P<0.01). Values expressed as mean±SE where day 1 and 14; n=4, day 7; n=5 from 2 experimental repeats.

When h-BMMSCs were cultured in absence of GDF-6, relative gene expression for *SOX9* normalised to *GAPDH* values remained consistently low (day 1; 0.9±0.66, day 7; 1.58±3.56, day 14; 1.13±1.84) (P>0.05) (*figure 6.9*). When h-BMMSCs were stimulated with GDF-6, *SOX9* relative gene expression normalised to *GAPDH* values significantly decreased with time point (day 1; 14.71±32.06, day 7; 9.16±7.41, day 14; 0.23±0.099) (**P<0.01, ***P<0.001) (*figure 6.9*).

The trend in *SOX9* expression for cells without GDF-6 stimulation was comparable to the culture of h-BMMSCs in alginate beads with GDF-5 induction medium [5, 48] or after cells had undergone GDF-5 gene transfer by electroporation [71]. These studies observed that *SOX9* expression remained at consistently low levels with no changes over time period [5, 48, 70] and after further gene analysis it was concluded that MSCs had differentiated towards a NP-like phenotype. The significant decrease in *SOX9* expression observed for GDF-6 stimulated h-BMMSCs was not expected for NP-like cells as *SOX9* is typically upregulated or expressed at consistent levels [5, 6]. The decrease in both *SOX9* and *COL2A1* expression (*figure 6.10*) was likely related as *SOX9* is the main regulator of the chondrogenic phenotype and is a promoter of the *COL2A1* [71, 72]. When bNPCs were cultured in SAPHs, a significant increase in both *SOX9* and *COL2A1* expression was observed (*figures 5.14 & 5.15*).

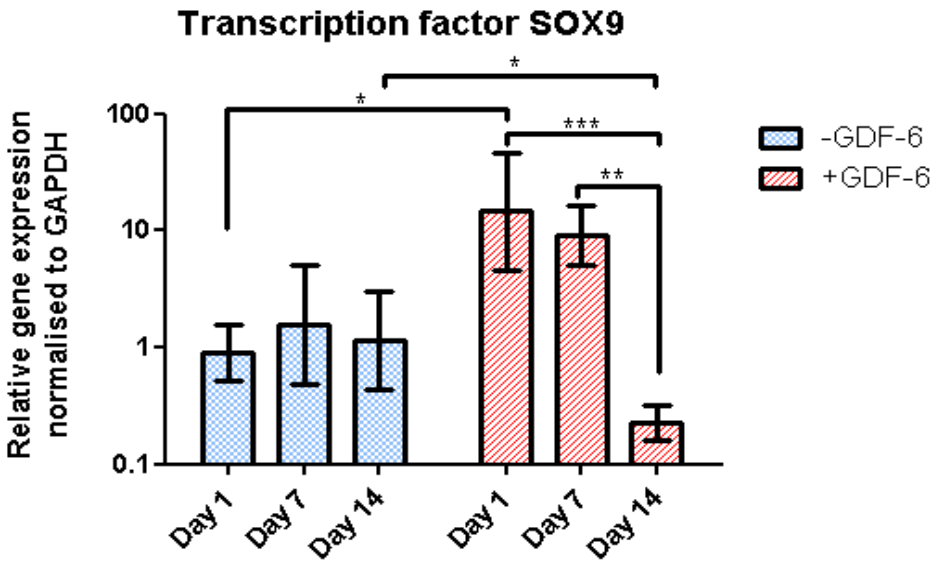

Figure 6.9. *SOX9* relative expression for 1x10^{6} h-BMMSCs ml^{-1} cultured with and without 100 ng ml^{-1} GDF-6 in 30 mg ml^{-1} FEFEFKFK SAPHs. Gene expression normalised to GAPDH. (P>0.05, *P<0.05, **P<0.01, ***P,0.001). Values expressed as mean±SE where day 1 and 14; n=4, day 7; n=5 from 2 experimental repeats.

When h-BMMSCs were cultured in absence of GDF-6, *COL2A1* relative gene expression normalised to *GAPDH* value remained consistently low (day 1; 0.0029 and day 14; 0.05±0.06) (P>0.05) (*figure 6.10*). When h-BMMSCs were stimulated with GDF-6, *COL2A1* relative gene expression normalised to *GAPDH* value significantly decreased from days 1 (16.64) to day 7 (1.09) (**P<0.01) and there was a non-significant decrease to day 14 (0.043±0.024) (*figure 6.10*). Some of the relative gene expression values were undetermined which explained the lack of error bars and values which would suggest that *COL2A1* expression levels were too low to be detectable. However an increase in number of samples with detectable levels was observed with increasing *in vitro* culture length which suggested that sufficient time was required before widespread protein gene expression occurred.

The expectation was that *COL2A1* expression would have increased over culture period as observed for bNPCs in SAPHs (*figure 5.14*). Type II collagen has an important mechanical role in the NP [49] therefore after discogenic differentiation of h-BMMSCs, corresponding gene expression should have increased as cells deposited ECM components and remodelled the matrix. Low *COL2A1* expression is associated with degenerated IVDs [17]. Other MSC NP tissue engineering studies that used GDF-5 or TGF-β culture medium observed significant increases in *COL2A1* expression over culture period which was attributed to upregulation of a NP-like phenotype [5, 18, 73].

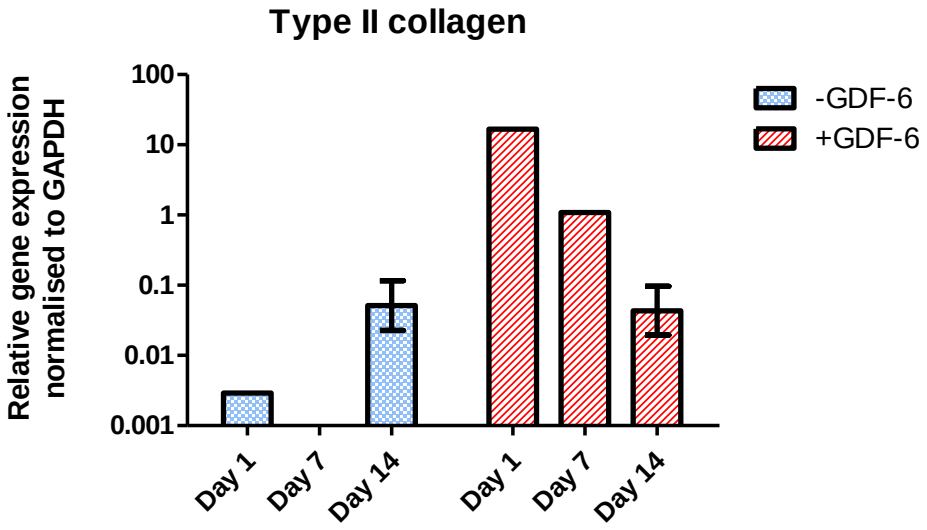

Figure 6.10. *COL2A1* relative expression 1x10^{6} h-BMMSCs ml^{-1} cultured with and without 100 ng ml^{-1} GDF-6 in 30 mg ml^{-1} FEFEFKFK SAPHs. Gene expression normalised to *GAPDH*. (P>0.05). Values expressed as mean±SE where day 1 and 14; n=4, day 7; n=5 from 2 experimental repeats.

When h-BMMSCs were cultured in absence of GDF-6, *ACAN* relative gene expression normalised to *GAPDH* values significantly increased with time point (day 1; 0.09±0.23, day 7; 9.88±11.27, day 14; 25.52±18.89) (*P<0.05) (*figure 6.11*). When h-BMMSCs were cultured with GDF-6 stimulation, *ACAN* relative gene expression normalised to *GAPDH* values significantly decreased with time point (day 1; 75.85±6.38, day 7; 11.64±3.07, day 14; 0.74±0.21) (***P<0.001) (*figure 6.11*).

Aggrecan is responsible for maintaining NP hydration [50] therefore high *ACAN* expression, as observed for bNPCs in SAPHs (*figure 5.13*), is crucial for NP tissue engineering [41, 54]. The *ACAN* expression profile for non-stimulated cells suggested that protein deposition by h-BMMSCs would increase with culture period. For samples stimulated with GDF-6, the significant decrease in *ACAN* expression was not expected as GDF-6 has been proven to increase expression [6] and downregulation is typically associated with loss of NP phenotype [74]. It was possible that day 1 gene expression levels were artificially high therefore downregulation occurred to return to normal levels. This did not explain the significant difference in *ACAN* expression on day 14 between the stimulated and non-stimulated samples (**P<0.01) which suggested that non-stimulated h-BMMSCs would deposit more protein [49, 75]. However, *ACAN* downregulation does not necessarily mean loss of NPC phenotype as cells do not constantly deposit ECM components. Cells will produce aggrecan to equilibrium then gene expression will be reduced if sufficient ECM components were present in the matrix. Other studies recorded significant increases in *ACAN* expression over culture period which was used as evidence of upregulation of NP-like phenotype [5, 53, 73]

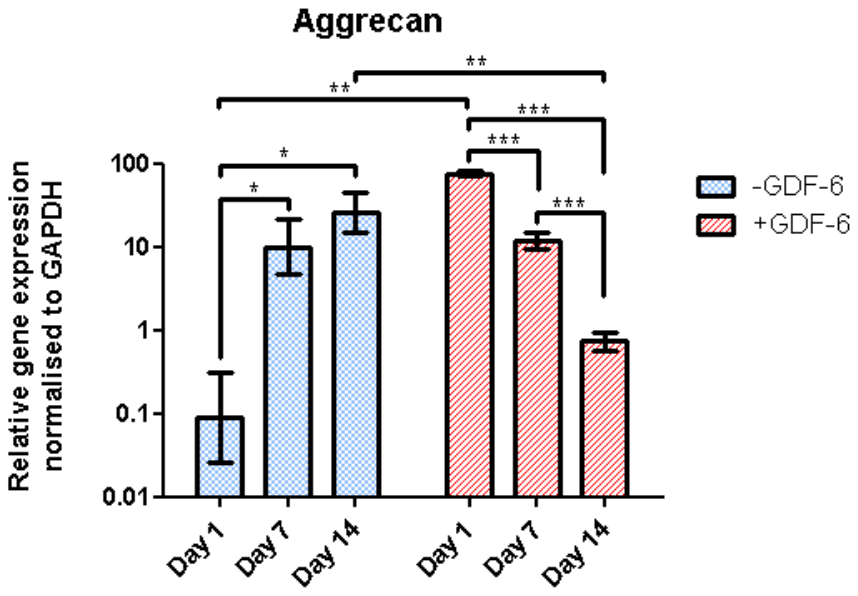

Figure 6.11. *ACAN* relative expression 1x10^6 h-BMMSCs ml^{-1} cultured with and without 100 ng ml^{-1} GDF-6 in 30 mg ml^{-1} FEFEFKFK SAPHs. Gene expression normalised to *GAPDH*. (P>0.05, *P<0.05, **P<0.01, ***P,0.001). Values expressed as mean±SE where day 1 and 14; n=4, day 7; n=5 from 2 experimental repeats.

6.5.2. Gene expression for individual 'novel' NPC markers

KRT8 is an intermediate filament protein present in the cytoplasm of epithelial cells [65]. It has been identified as a bovine and murine NPC phenotype marker although not for human NPCs [58, 70]. When h-BMMSCs were cultured in absence of GDF-6, *KRT8* relative gene expression normalised to *GAPDH* values significantly increased with time point for day 1 was 0.3±0.43, day 7 was 35.54±27.39 and day 14 was 98.39±70 (***P<0.001) (*figure 6.12*). *KRT8* expression levels for stimulated h-BMMSCs were high with relative gene expression normalised to *GAPDH* values recorded as 4.68±5.84 for day 1, 27.1±30.83 for day 7 and 15.23±5.69 for day 14 (P>0.05) (*figure 6.12*).

KRT8 expression is decreased in degenerated human NPCs [65] therefore the high *KRT8* expression in comparison to most other tested genes observed for both culture conditions (*figure 6.12*) would indicate that encapsulated cells behaved unlike NPCs from degenerated IVDs. Support for this hypothesis was observed in bovine IVDs where cells that expressed *KRT8* produced a more gelatinous matrix [76]. MSCs do not express *KRT8* therefore upregulation of the gene strongly suggested that differentiation had occurred [77]. Despite previous studies indicating that *KRT8* was not significantly expressed by human NPCs [59], the significant increase in gene expression for non-stimulated h-BMMSCs and high expression of *KRT8* by stimulated h-BMMSCs suggested that it might be considered as a novel human NPC marker (*figure 6.13*).

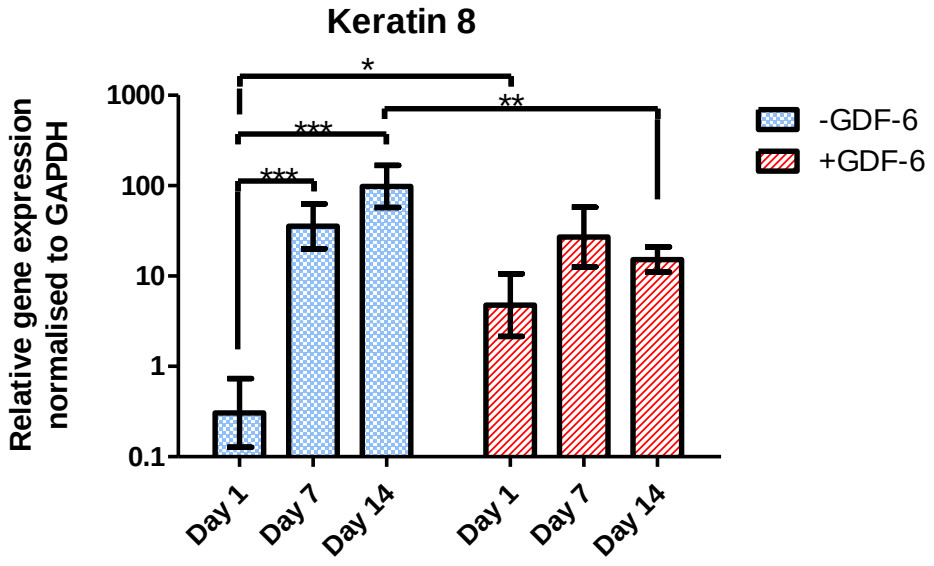

Figure 6.12. *KRT8* relative expression for 1x10^{6} h-BMMSCs ml^{-1} cultured with and without 100 ng ml^{-1} GDF-6 in 30 mg ml^{-1} FEFEFKFK SAPHs. Gene expression normalised to *GAPDH*. (P>0.05, *P<0.05, **P<0.01, ***P,0.001). Values expressed as mean±SE where day 1 and 14; n=4, day 7; n=5 from 2 experimental repeats.

KRT18 is an intermediate filament protein that is strongly expressed by notochordal cells [78] and is a canine, bovine and human NPC phenotype marker [64]. When h-BMMSCs were cultured in absence of GDF-6, *KRT18* relative expression normalised to *GAPDH* values significantly increased with time point (day 1; 0.39±0.68, day 7; 4.51±4.66 and day 14; 11.06±17.04) (*P<0.05) (*figure 6.13*). When h-BMMSCs were stimulated with GDF-6, *KRT18* relative expression normalised to GAPDH values remained stable from days 1 (1.52±3.63) to day 14 (1.81±0.81) (P>0.05) (*figure 6.13*).

KRT18 positive cells are thought to have differentiated from notochordal cells which are prevalent in the juvenile NP [79]. *KRT18* expression is downregulated in degenerated NPs [34, 65] therefore the gene profiles for both samples (*figure 6.13*) suggested that cells were behaving unlike NPCs from degenerated tissue. It has been hypothesised that *KRT18* may be a marker of a 'healthier' NP phenotype that is lost during DDD [64]. Accordingly, the significant increase in *KRT18* expression observed for h-BMMSCs cultured in absence of GDF-6 and the high expression for stimulated h-BMMSCs might indicate that a healthy NPC phenotype was present after culture in SAPHs. The gene expression profile for non-stimulated samples was comparable to the significant increase in *KRT18* expression observed after the culture of bNPCs in SAPHs (*figure 5.17*).

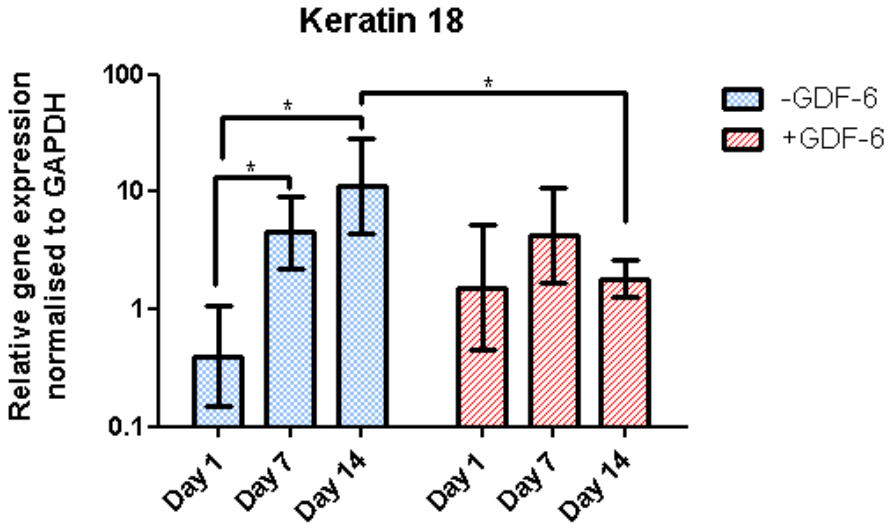

Figure 6.13. *KRT18* relative expression 1x10^6 h-BMMSCs ml^{-1} cultured with and without 100 ng ml^{-1} GDF-6 in 30 mg ml^{-1} FEFEFKFK SAPHs. Gene expression normalised to *GAPDH*. (P>0.05 *P<0.05). Values expressed as mean±SE where day 1 and 14; n=4, day 7; n=5 from 2 experimental repeats.

KRT19 is an intermediate filament protein present in epithelial cells that has been identified as a NPC marker gene for murine, bovine and human species [64]. When h-BMMSCs were cultured in absence of GDF-6, *KRT19* relative expression normalised to *GAPDH* values remained consistent with time point (day 1; 0.58±0.59, day 7; 0.81±1.11, day 14; 0.26±0.25) (P>0.05) (*figure 6.14*). When h-BMMSCs were cultured with 100 ng ml^{-1} GDF-6, *KRT19* relative expression normalised to GAPDH values significantly decreased with time point (day 1; 25.59±5.33, day 7; 1.17±1.04, day 14; 0.035±0.018) (**P<0.01, ***P<0.001) (*figure 6.14*).

KRT19 expression is low in human NPs [80] which likely explained the gene profiles observed in *figure 6.14*. Gantenbein-Ritter *et al.* observed consistently low levels of *KRT19* expression over *in vitro* culture (>0.3 relative gene expression compared to control) after h-BMMSC culture in alginate beads with GDF-5 or TGF-β stimulation, [48]. NPC *KRT19* expression decreases with age [81] therefore high expression could indicate presence of a more primitive cell phenotype. It was hypothesised that cells reduce *KRT19* expression with increasing *in vitro* culture period [48] as supported by GDF-6 stimulated samples where day 1 *KRT19* expression was significantly higher than day 14 *KRT19* expression (*figure 6.14*).

There is a clear link between IVD age and *KRT8*, *KRT18* and *KRT19* expression by NPCs. Weiler *et al.* determined that the large majority of cells positively labelled for *KRT8*, *KRT18* and *KRT19* (80 to 100%) from subjects less than 30 years old. In comparison, cells from subjects who were older than 30 contained fewer labelled nuclei (16-25%) and were associated with matrix defects [34]. *KRT8*, *KRT18* and *KRT19* are expressed by tissues that

are exposed to a fluid or semi-fluid environment [82] which suggests that they might play a physiological role in ECM homeostasis in the NP [65]. Therefore *KRT8*, *KRT18* and *KRT19* expression (*figures 6.12-6.14*) suggested that a NP-like phenotype was present and a NP-like matrix was being deposited.

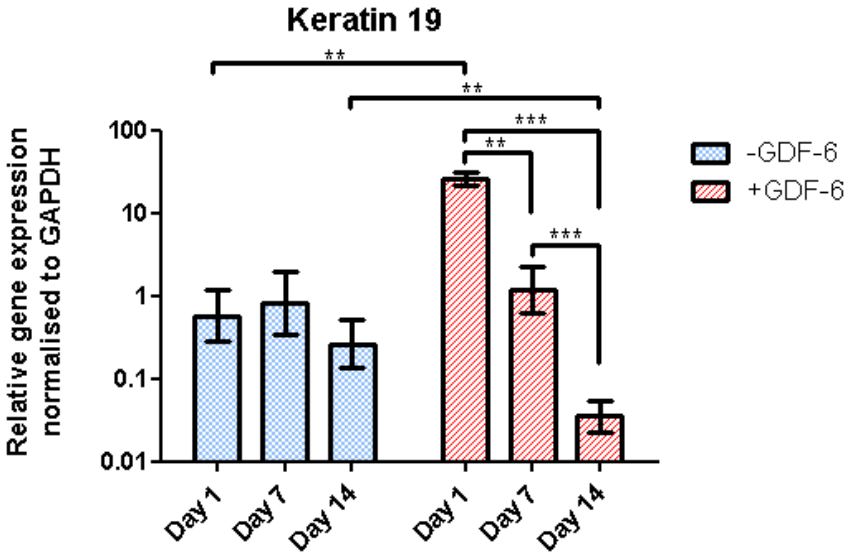

Figure 6.14. *KRT19* relative expression for 1x10^{6} h-BMMSCs ml^{-1} cultured with and without 100 ng ml^{-1} GDF-6 in 30 mg ml^{-1} FEFEFKFK SAPHs. Gene expression normalised to *GAPDH*. (P>0.05, **P<0.01, ***P<0.001). Values expressed as mean±SE where day 1 and 14; n=4, day 7; n=5 from 2 experimental repeats.

For h-BMMSCs cultured in absence of GDF-6, the general trend was a non-significant increase in *FOXF1* relative expression normalised to *GAPDH* (day 1; 0.082±0.23, day 7; 1.22±1.79, day 14; 6.94) (P>0.05) (*figure 6.15*). For h-BMMSCs cultured with 100 ng ml^{-1} GDF-6, the general trend was a non-significant decrease in *FOXF1* relative expression normalised to *GAPDH* (day 1; 11.037±12.13, day 7; 3.37±1.75, day 14; 0.37) (P>0.05) (*figure 6.15*).

FOXF1 is a mesenchyme-specific marker that plays a role in organ development and repair as well as MSC migration [83, 84]. Upregulation of *FOXF1* is associated with cell growth, proliferation and increased life expectancy [80, 85]. Therefore the gene profile for h-BMMSCs cultured in absence of GDF-6 suggested that cells had a healthy physiology which was supported by high cell viability over the culture period (*section 6.3*) however no proliferation was detected from days 1 to 14 (*figure 6.7*). The increasing gene profile was comparable to bNPCs *FOXF1* expression after culture in SAPHs (figure 5.18). As *FOXF1* expression decreases with aging [71], the decreased *FOXF1* expression by h-BMMSCs cultured with GDF-6 can be interpreted as cells behaving more akin to cells from an aged NP than cells from a juvenile NP which could explain the downregulation or low expression of some NP marker genes (*figures 6.10, 6.11, 6.14*). When comparing the relative gene expression with

the literature [65, 85], *FOXF1* expression for both non-stimulated and stimulated samples was high therefore could be interpreted as presence of the NP phenotype.

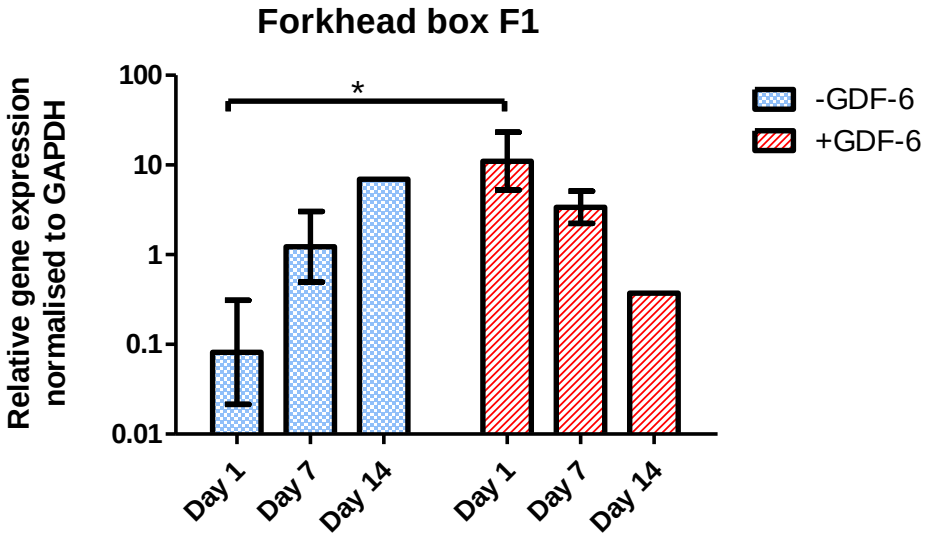

Figure 6.15. *FOXF1* relative expression for 1x10^{6} h-BMMSCs ml^{-1} cultured with and without 100 ng ml^{-1} GDF-6 in 30 mg ml^{-1} FEFEFKFK SAPHs. Gene expression normalised to *GAPDH*. (P>0.05, *P<0.05). Values expressed as mean±SE where day 1 and 14; n=4, day 7; n=5 from 2 experimental repeats.

When h-BMMSCs were cultured in absence of GDF-6, the general trend was a non-significant increase in *CA12* relative expression normalised to *GAPDH* (day 1; 4.01±3.02, day 7; 6.45±19.43, day 14; 13.99±21.03) (P>0.05) (*figure 6.16*). For h-BMMSCs cultured with 100 ng ml^{-1} GDF-6, the general trend was a significant decrease in *CA12* relative expression normalised to *GAPDH* (day 1; 40.36±88.13, day 7; 9.62±25.29, day 14; 0.61±0.73) (*P<0.05, **P<0.01) (*figure 6.16*).

CA12 is thought to play a role in counteracting increased NP acidity that arises following lactic acid accumulation from glucose metabolism and ineffective waste product removal. In juvenile NPs, high levels of CA12 are expressed to regulate cellular pH during high metabolic activity [86]. Cells from young NPs have higher metabolic activities [45] due to production of increased amounts of appropriate ECM components in comparison to cells from old or degenerated IVDs [87]. In severely degenerated discs there is intense protein expression of CA12 which might be a response to injury as cells attempt to repair the tissue by increasing metabolic activity [64, 86]. The significant decrease in *CA12* expression from days 1 to 14 when h-BMMSCs were stimulated with GDF-6 (***P<0.001) suggested that cells were behaving more like cells from degenerated IVDs than juvenile NPCs. Finally, it has been hypothesised that CA12 may play a role in maintaining intracellular pH regulation under low oxygen tension and low pH levels to ensure conservation of suitable IVD homeostasis [2]. Therefore as the SAPH pH

remained at approximately physiological levels throughout *in vitro* culture, high *CA12* expression would not be expected.

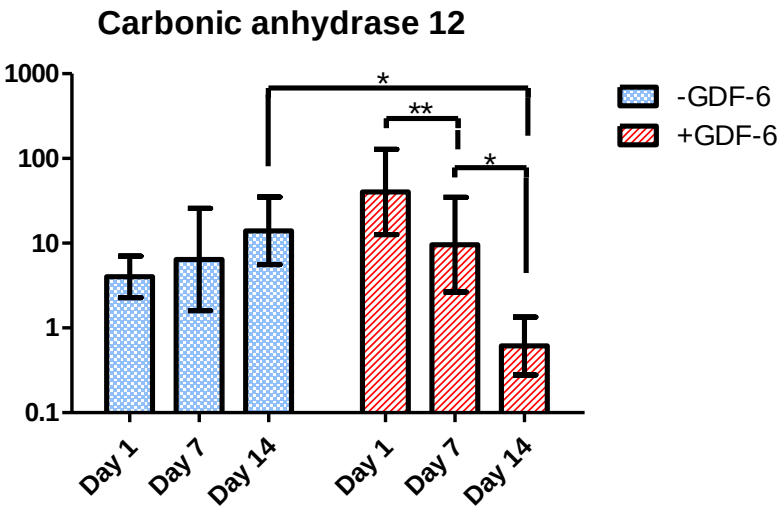

Figure 6.16. *CA12* relative expression for 1x10^{6} h-BMMSCs ml^{-1} cultured with and without 100 ng ml^{-1} GDF-6 in 30 mg ml^{-1} FEFEFKFK SAPHs. Gene expression normalised to *GAPDH*. (P>0.05, *P<0.05, **P<0.01). Values expressed as mean±SE where day 1 and 14; n=4, day 7; n=5 from 2 experimental repeats.

6.5.3. Overall gene expression profiles by day

Overall day 1 gene expression results demonstrated that h-BMMSCs cultured with GDF-6 stimulation had significantly higher gene expression than non-stimulated cells for the entire panel of NP marker genes (*P<0.05, **P<0.01, ***P<0.001) apart from *KRT18* and *CA12* (P>0.05) (*figure 6.17*). Due to the documented effect of GDF-6 stimulated h-BMMSCs expressing NP markers significantly higher than other NP-associated induction growth factors (TGF-β and GDF-5) [6], the overall gene profile was expected. Non-stimulated samples had no exogenous stimulation to direct differentiation towards a NP-like phenotype however it was encouraging to note that some NP-specific markers (*KRT8*, *KRT18*, *KRT19* and *CA12*) were expressed by non-stimulated cells. *ACAN* was the most highly expressed for GDF-6 treated cells whilst *KRT18* had the lowest expression (*figure 6.17*). For h-BMMSCs cultured without GDF-6, *CA12* had the highest expression whilst *COL2A1* had the lowest expression (*figure 6.17*). It was possible that the GDF-6 had a near immediate effect on h-BMMSCs to induce discogenic differentiation.

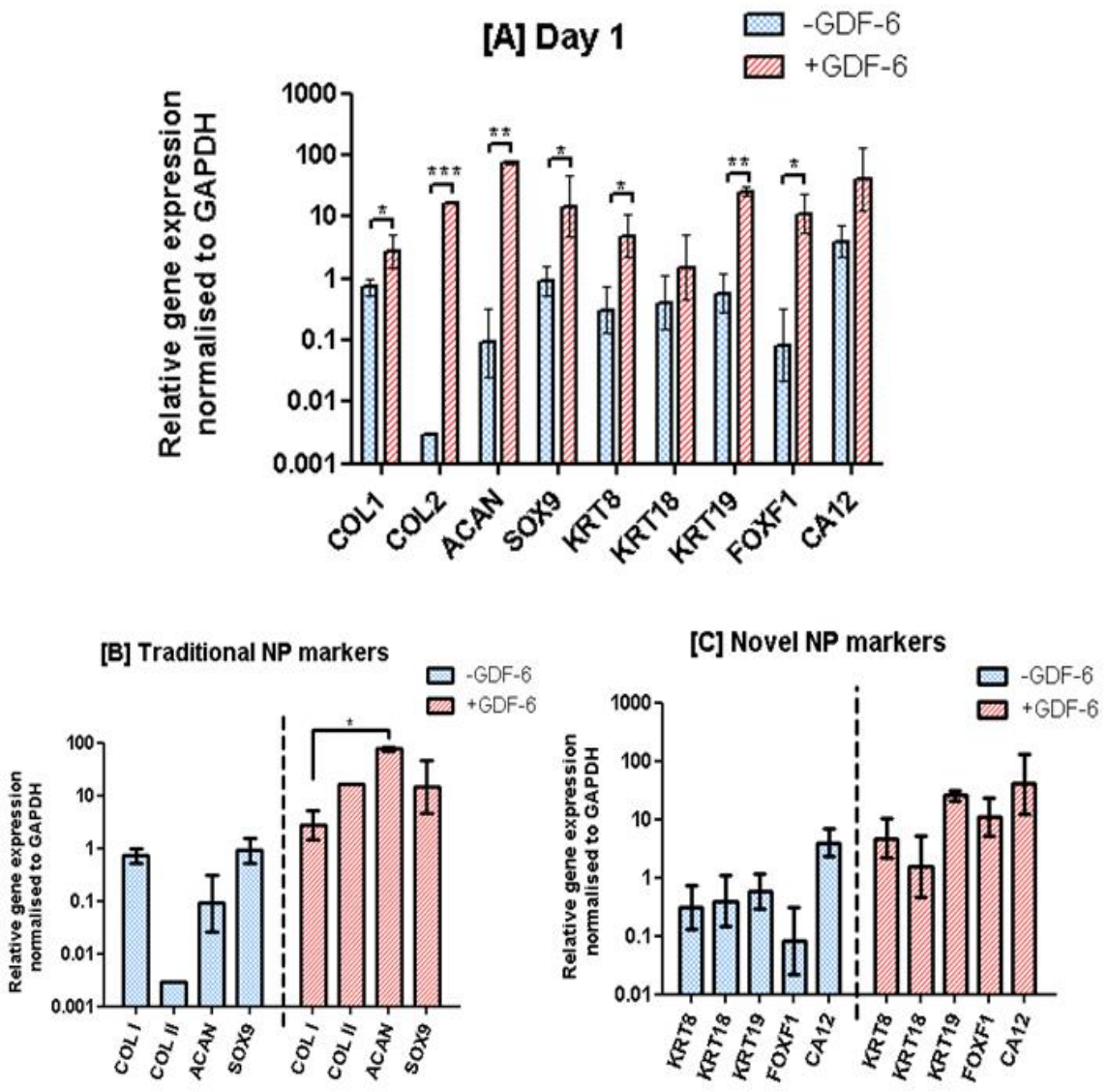

Figure 6.17. The relative gene expression for 1x10^{6} h-BMMSCs ml^{-1} cultured with and without 100 ng ml^{-1} GDF-6 in 30 mg ml^{-1} FEFEFKFK SAPHs on day 1. [A] Overall gene expression for 'novel' and 'traditional' NPC markers. [B] Gene expression for 'traditional' NPC markers. [C] Gene expression for 'novel' NPC markers. Gene expression normalised to *GAPDH*. (P>0.05, *P<0.05, **P<0.01, ***P<0.001). Values expressed as mean±SE where n=4 from 2 experimental repeats.

On day 7 (*figure 6.18*), the overall gene expression profile had altered from day 1 (*figure 6.17*) with no significant differences (P>0.05) between any NPC markers for h-BMMSCs that had been cultured with and without GDF-6. Gene expression profiles strongly suggested that cells in both stimulated and non-stimulated samples had a NP-like phenotype due to the upregulation of 'traditional' and 'novel' NP markers. *KRT8* was the most highly expressed gene for GDF-6 stimulated cells whilst *COL1A2* displayed the lowest expression (*figure 6.18*). For h-BMMSCs cultured in absence of GDF-6, *KRT8* displayed highest gene expression whilst *COL2A1* was the lowest expressed gene (*figure 6.18*).

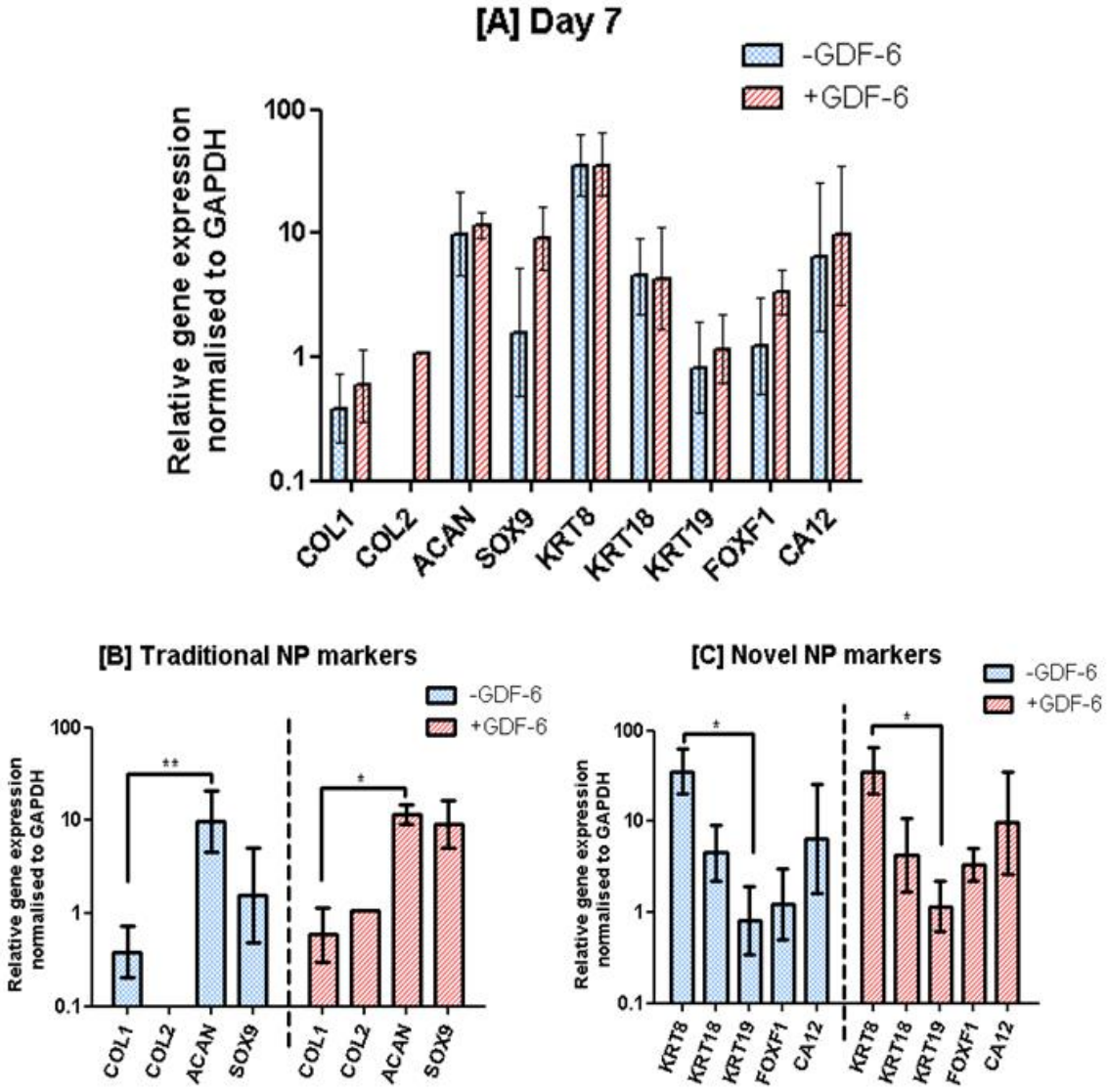

Figure 6.18. The relative gene expression for 1x10^{6} h-BMMSCs ml^{-1} cultured with and without 100 ng ml^{-1} GDF-6 in 30 mg ml^{-1} FEFEFKFK SAPHs on day 7. [A] Overall gene expression for 'novel' and 'traditional' NPC markers. [B] Gene expression for 'traditional' NPC markers. [C] Gene expression for 'novel' NPC markers. Gene expression normalised to GAPDH. (P>0.05, *P<0.05, **P<0.01, ***P<0.001). Values expressed as mean±SE where n=4 from 2 experimental repeats.

The overall day 14 gene profile demonstrated that surprisingly, h-BMMSCs cultured in absence of GDF-6 displayed significantly higher gene expression for all genes compared to h-BMMSCs that had been stimulated with GDF-6 (*P<0.05, **P<0.01) apart from *COL2A1*, *KRT19* and *FOXF1* (P>0.05) (*figure 6.19*). Possible explanations for the observed gene profiles were discussed in *sections 6.5.4 and 6.5.6*. *KRT8* was the most highly expressed gene for GDF-6 stimulated cells whilst *KRT19* displayed the lowest expression (*figure 6.19*). For h-BMMSCs cultured in absence of GDF-6, *KRT8* displayed highest gene expression whilst *COL2A1* was the lowest expressed gene (*figure 6.19*).

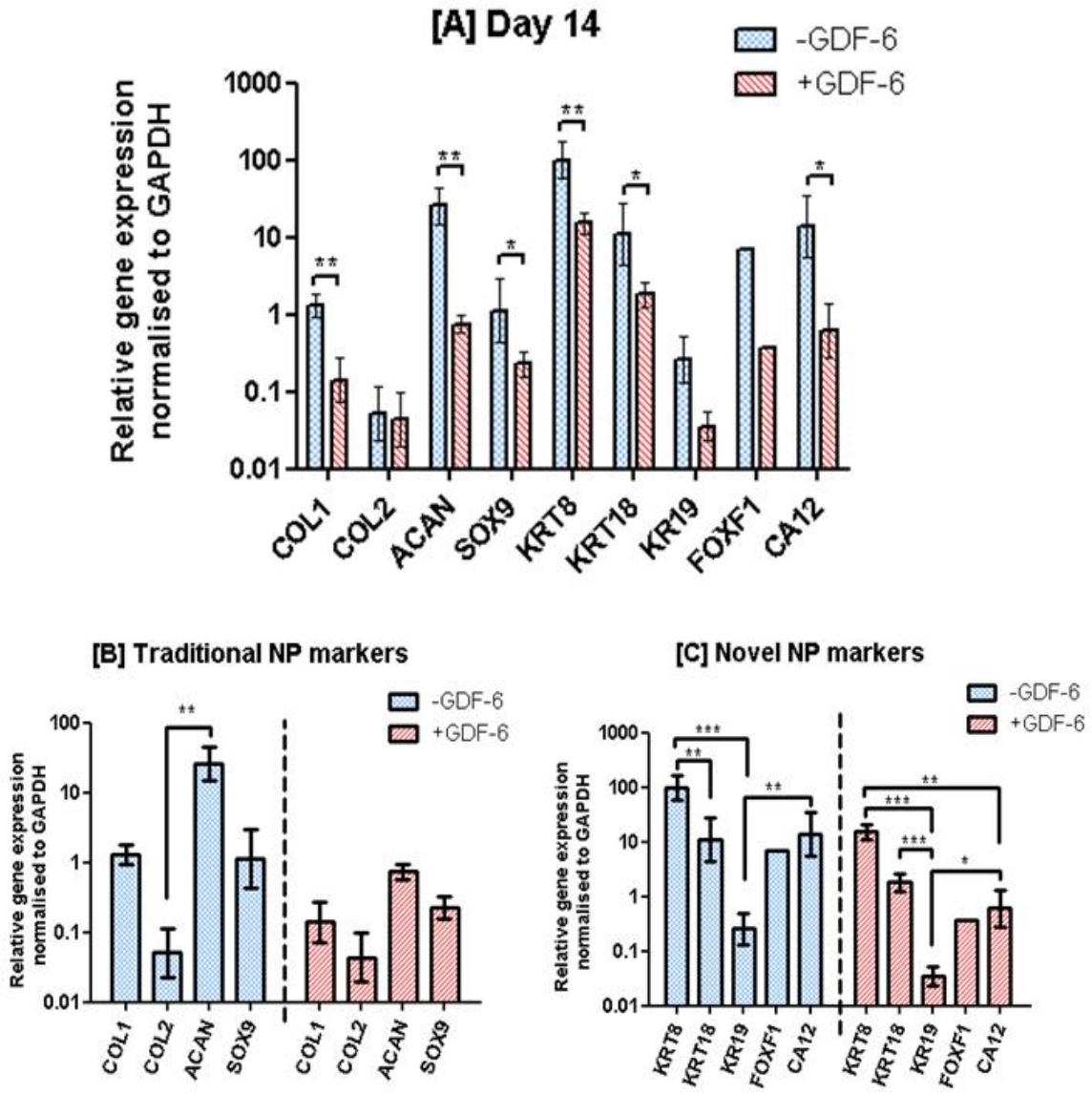

Figure 6.19. The relative gene expression for 1x10^{6} h-BMMSCs ml^{-1} cultured with and without 100 ng ml^{-1} GDF-6 in 30 mg ml^{-1} FEFEFKFK SAPHs on day 14. [A] Overall gene expression for 'novel' and 'traditional' NPC markers. [B] Gene expression for 'traditional' NPC markers. [C] Gene expression for 'novel' NPC markers. Gene expression normalised to *GAPDH*. (P>0.05, *P<0.05, **P<0.01, ***P<0.001). Values expressed as mean±SE where n=4 from 2 experimental repeats.

6.5.4. NP-like phenotype for h-BMMSCs cultured without GDF-6 stimulation

To the knowledge of the author, all studies investigating MSCs as a NP tissue engineering cell source required a stimulating factor, whether it was addition of exogenous growth factors [6, 5, 48, 51] or functionalisation of the scaffold with a bioactive motif [23, 53], to direct differentiation towards a discogenic phenotype. Therefore it was highly interesting to note that without exogenous growth factors or a functionalised scaffold to induce differentiation, h-BMMSCs cultured in SAPHs displayed a NP-like phenotype due to a number of 'traditional' and 'novel' NP markers being highly expressed (*figures 6.17-6.19*). Growth factor treatment and

production is costly [12] whilst rapid deterioration of growth factors *in vivo* means that long-term bioactivity is a problem [88] so a system that could spontaneously induce discogenic differentiation would be preferential.

We hypothesised that the SAPH played a crucial role in determining stem cell fate. In the characterisation chapter (*chapter 4*) it was determined that the SAPH consisted of a nanofibrous network with features that were of similar scale to type II collagen fibrils of the native NP (*section 4.3.2*). Oscillatory rheology demonstrated that the SAPH could be optimised so the stiffness of the system closely resembled the native tissue (*section 4.4.4*). In chapter 5, it was determined that the SAPH could restore and preserve the NP phenotype after de-differentiation following monolayer culture and stimulate NP associated ECM production. Scaffold stiffness, elasticity [11] and presented ECM components [30] can determine stem cell fate therefore the SAPH microenvironment and mechanical properties might have been mimicking the NP matrix and could have induced differentiation towards a NP-like phenotype.

Dexamethasone has been demonstrated to induce chondrogenic differentiation as a study determined that cartilaginous matrix was deposited by 25% of cells [95]. *KRT19* expression was higher than for cells cultured with only GDF-5 ($P>0.05$) when h-BMMSCs were cultured with GDF-5 and dexamethasone. The *ACAN* to *COL2A1* ratio was highest for GDF-5 and dexamethasone treated samples which suggested that a discogenic phenotype was present [48]. For this study, dexamethasone was present in both stimulated and non-stimulated culture medium (*section 3.3.2.4)* therefore could have played a role in inducing differentiation. Due to upregulation of a number of NP-specific markers (*figures 6.17-6.19*); gene expression results strongly suggested that a discogenic phenotype was present rather than a cartilaginous phenotype.

6.5.5. Aggrecan to type II collagen ratio

The ratio of aggrecan to type II collagen deposition, which is directly linked to corresponding gene expression [48, 55], is a reliable indicator of discogenic or chondrogenic phenotype presence. A number of studies have used the ratio of *ACAN* to *COL2A1* as evidence for a NP-like phenotype [6, 48]. Minogue *et al.* determined the ratio of *ACAN* to *COL2A1* expression to be ~0.4 to ~0.063 respectively in the human NP [65]. In this study, for h-BMMSCs cultured without GDF-6 the ratio of *ACAN* to *COL2A1* expression was 31.4 to 1 on day 1 and for h-BMMSCs cultured with GDF-6 the ratio was 4.6 to 1 (*figure 6.20A*). By day 14, for h-BMMSCs cultured without GDF-6 the ratio of *ACAN* to *COL2A1* expression was 499.4 to 1 and for h-BMMSCs cultured with GDF-6 the ratio was 17.1 to 1 (*figure 6.20B*). Therefore the gene expression profiles for both culture conditions suggested that a matrix more akin to the native NP than articular cartilage was being produced.

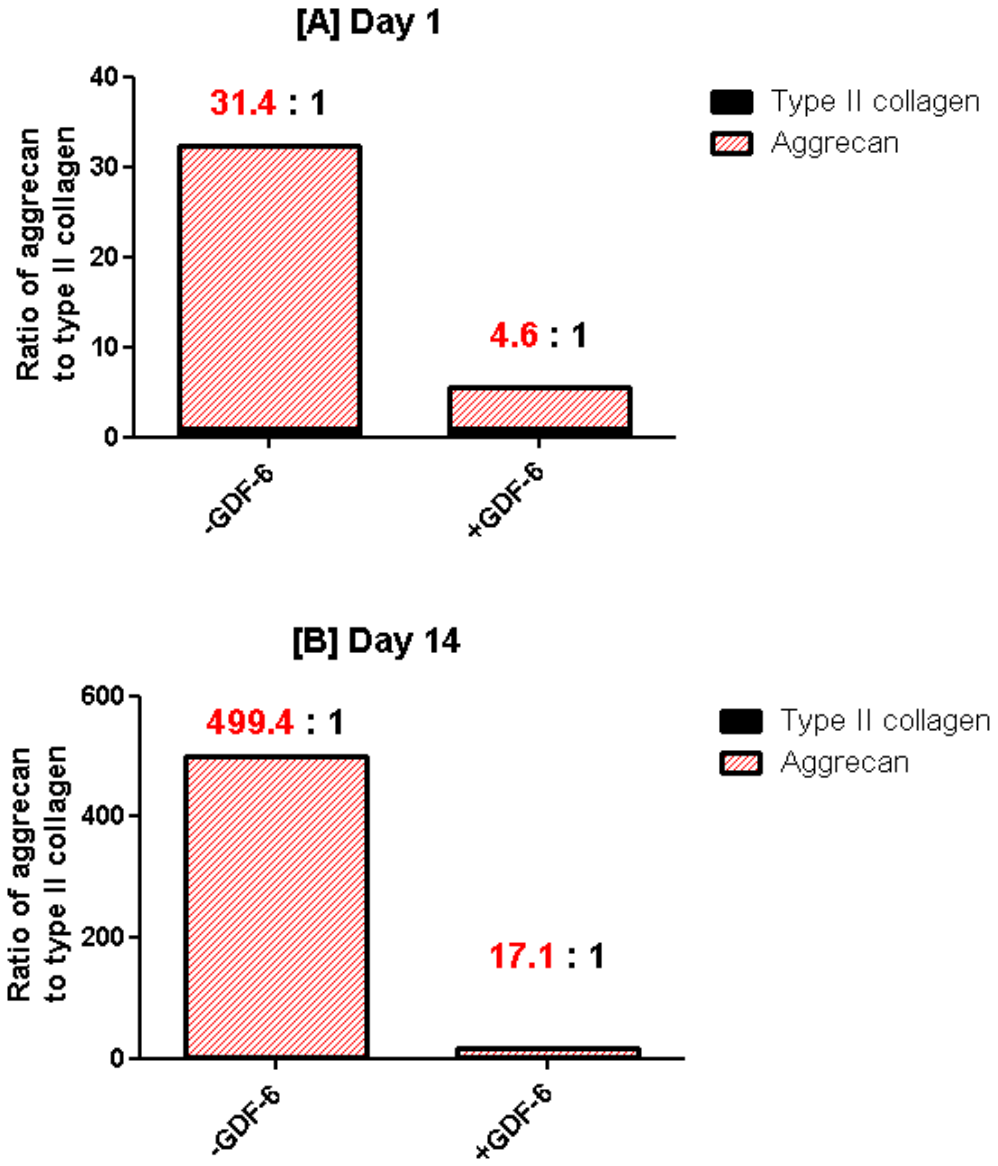

Figure 6.20. The ratio of *ACAN* to *COL2A1* for 1x10^6 h-BMMSCs ml^{-1} cultured with and without 100 ng ml^{-1} GDF-6 in 30 mg ml^{-1} FEFEFKFK SAPHs calculated from relative gene expression of the respective genes to *GAPDH*. [A] Ratio on day 1, -GDF-6 was more akin to native NP whilst +GDF-6 was more akin to articular cartilage. [B] Ratio on day 14, both culture conditions were more similar to the native NP ECM than articular cartilage.

Other studies determined the *ACAN* to *COL2A1* expression ratio for h-BMMSCs cultured in type II collagen-HA gels was around 1 to 1 with TGF-β1 stimulation [69], around 10 to 1 in alginate gels with GDF-5 stimulation [5] and around 1 to 1 in LN-NS SAPHs [53].

6.5.6. Overview and further discussion

There is evidence that GDF-6 might be the best current growth factor for induction of a discogenic phenotype [6] therefore the expectation was that h-BMMSCs cultured with GDF-6

would express ‘traditional’ and ‘novel’ NP marker genes significantly higher that the non-stimulated h-BMMSCs. GDF-6 is expressed in healthy and degenerate IVDs together with its receptor BMP RII suggesting that it is involved in normal matrix homeostasis [21]. The growth factor activates the alterative Smad 1/5/8 pathway which leads to distinct signalling pathways and downstream events [6] involving the recruitment and activation of Receptor-associated-Smad signalling molecules to propagate the GDF receptor signals to the cell nucleus via binding to specific DNA sequences. This promotes gene expression and likely determines stem cell fate [26, 27].

However overall gene expression profiles (*figures 6.8-6.19*) demonstrated that GDF-6 did not have the same degree of discogenic differentiation stimulating effect on the culture of h-BMMSCs in SAPHs as results demonstrated in Clarke *et al.* (*section 6.1.4*) [6]. For example non-stimulated samples had significantly higher *ACAN* expression in comparison to stimulated samples on day 14 (**P<0.01). Similarly, for the novel NP markers of *KRT8* (*figure 6.13*) and *KRT18* (*figure 6.14*), by day 14, gene expression was significantly higher than h-BMMSCs stimulated with GDF-6 (*KRT8*; *P<0.05, *KRT18*; **P<0.01). The unexpected gene expression results could be a consequence of constant growth factor stimulation as fresh media containing GDF-6 was added to samples every 2 days. If cells had undergone discogenic differentiation, as suggested by the high levels of NP marker gene expression on day 1 (*figure 6.17*) then continued growth factor stimulation could have caused downregulation of NP markers. To test this hypothesis, samples should be dosed with GDF-6 only at the beginning of *in vitro* culture to determine whether similar gene expression profiles were produced to *figures 6.17-6.19*. However addition of fresh GDF-6 to samples every 2 days was the protocol used by Clarke *et al.* where NP marker gene expression was significantly higher than samples cultured without GDF-6 [6].

Another explanation could be the difference in culture systems; FEFEFKFK SAPHs were highly hydrated, displayed comparable mechanical properties and architecture to the native NP (*section 4.3.2 & 4.4.4*), and became mechanically unstable after 14 days (*figure 4.8).* In comparison, type I collagen gels used in Clarke *et al.* were stiffer, fibrous scaffolds with microscaled fibres [6, 91]. Cell seeding density was $4x10^6$ cells ml^{-1} in collagen gels [6] in comparison to $1x10^6$ cells ml^{-1} for SAPHs. As type I collagen gels contracted over time [91] this further increased cell density and the number of cell to cell interactions which could have promoted differentiation in the system [6]. Future work should involve investigating the effect of h-BMMSC seeding density on gene expression. Finally, the interactions between GDF-6 and the SAPH nanofibrous architecture were unknown. As SAPHs mimic the porosity and gross structure of the ECM it has been speculated that growth factors diffuse very slowly in and out of the system [92] which could mean that the GDF-6 did not penetrate the system to stimulate all cells. However, day 1 overall gene expression (*figure 6.17*) suggested that cells had undergone discogenic differentiation due to significant upregulation of all NPC marker genes. The SAPH had 97% H_2O content and cells could migrate freely through the scaffold

(*section 5.3.3*) which would suggest that growth factors could migrate throughout. There is evidence that growth factors can induce differentiation even if they interact with scaffold architecture [91]. If the growth factor could not influence the majority of cells then the expectation would be that no significant differences for overall gene profiles between non-stimulated and stimulated samples would be observed (*figures 6.17-19*). The culture of MSCs stimulated with GDF-6 has only been investigated in type I collagen gels and SAPHs therefore the interactions of the growth factor with various biomaterials is not well documented.

To the knowledge of the author, this is the first study to demonstrate expression of NP marker genes by non-stimulated samples as high or superior to growth factor treated samples [5, 6, 48]. Similarly, h-BMMSCs cultured in functionalised scaffolds with discogenic or chondrogenic factors always express NPC marker genes significantly higher than cells cultured in scaffolds without functionalisation [29, 53]. No NP tissue engineering studies have investigated as extensive a panel of NP markers to determine MSC phenotype as this study. Typically *COL2A1*, *COL1A2* and *ACAN* were tested by other studies [53, 69] which can make it difficult to distinguish between the chondrogenic and discogenic phenotype [65, 80]. Investigations that tested a number of 'traditional' and 'novel' markers focused on determining the effects of various growth factors on the upregulation of NPC associated genes rather than determining suitability of scaffolds for NP tissue engineering applications [5, 6, 48].

In summary, gene expression results suggested that a NP-like phenotype was present after culture in the SAPHs stimulated with GDF-6 (*figures 6.17-6.19*). *ACAN* and *KRT8* were highly expressed by day 14 with NP-specific markers *FOXF1* and *CA12* also expressed. Despite *COL2A1* and *SOX9* expression profiles not producing expected results, when comparing the overall panel of genes it could be stated that discogenic differentiation likely occurred and a NP-like phenotype was present for encapsulated cells throughout *in vitro* cell culture.

Interestingly, when h-BMMSCs were cultured in absence of GDF-6, a discogenic phenotype was present (*figures 6.17-6.19*). The gene profile suggested that h-BMMSCs had spontaneously differentiated to a NP-like phenotype without use of an exogenous induction factor or bioactive motif. By day 14, non-stimulated cells expressed the majority of NP marker genes (*ACAN*, *KRT8*, *KRT18 FOXF1* and *CA12*) significantly higher than GDF-6 stimulated cells (*figures 6.9-6.18*). The exact reason behind the discrepancy in gene expression for the two culture conditions was unknown however it was possible that constant GDF-6 stimulation after discogenic stimulation caused some genes to be downregulated. Due to the disadvantages of using growth factor treatment, alternative methods for differentiating MSCs towards an NP-like phenotype would be preferable. A system that spontaneously induced h-BMMSCs towards a discogenic phenotype in absence of growth factors, as demonstrated by the FEFEFKFK SAPH (*figures 6.17-6.19*) would show significant potential for NP tissue engineering applications.

6.6. VISUALISING THE DEPOSITION OF EXTRACELLULAR MATRIX COMPONENTS USING IMMUNOCYTOCHEMISTRY

Production of appropriate NP ECM components is crucial for NP tissue engineering [1, 3, 41]. ICC was used to stain for types I and II collagen and aggrecan on day 7 intra- and extracellularly.

6.6.1. Human BMMSCs cultured without GDF-6 stimulation

Human BMMSCs cultured in SAPHs without GDF-6 stimulation produced little positive staining for type I collagen on day 7 (*figure 6.21A*), comparable to type I collagen staining for bNPCs on day 7 (*figure 5.25A*). Human BMMSCs cultured in monolayer deposited high amounts of type I collagen intra- and extracellularly. Undifferentiated BMMSCs [66] and NPCs [93] (*figure 5.25B*) deposit high amounts of type I collagen in monolayer.

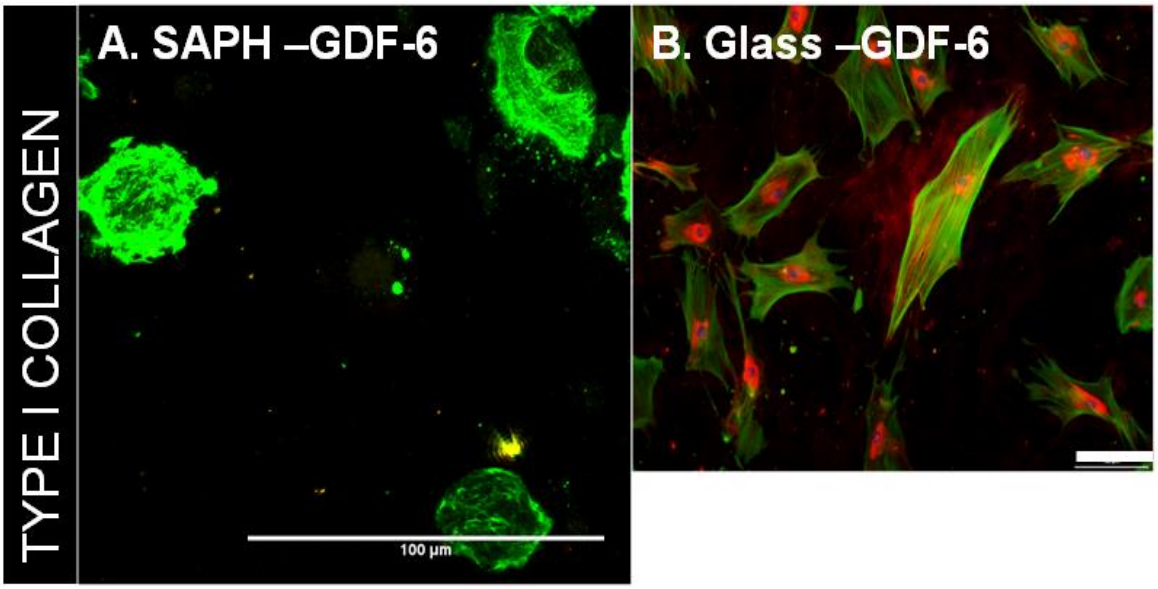

Figure 6.21. Fluorescence micrographs showing type I collagen ICC staining for 1x10^6 h-BMMSCs ml^{-1} on day 7 without GDF-6 stimulation. [A] Human BMMSCs cultured in 30 mg ml^{-1} SAPH showed little positive staining for type I collagen. [B] Human BMMSCs cultured on glass showed positive staining for type I collagen. Type I collagen was stained red, F-actin was stained green and nuclei were stained blue. Scale bar represents 100 µm.

High amounts of intense extracellular type II collagen staining was present on day 7 for h-BMMSCs cultured without GDF-6 stimulation, (*figure 6.22A*). Distribution of type II collagen was comparable to corresponding protein deposition by bNPCs in SAPHs on day 7 (*figure 5.27A*). Undifferentiated h-BMMSCs do not produce significant amounts of type II collagen [66,

94] which would strongly suggest that cells had differentiated in SAPHs. In contrast to 3D culture, h-BMMSCs cultured in monolayer did not produce significant amounts of type II collagen. Micrographs were comparable to the culture of bNPCs in monolayer (*figure 5.27B*).

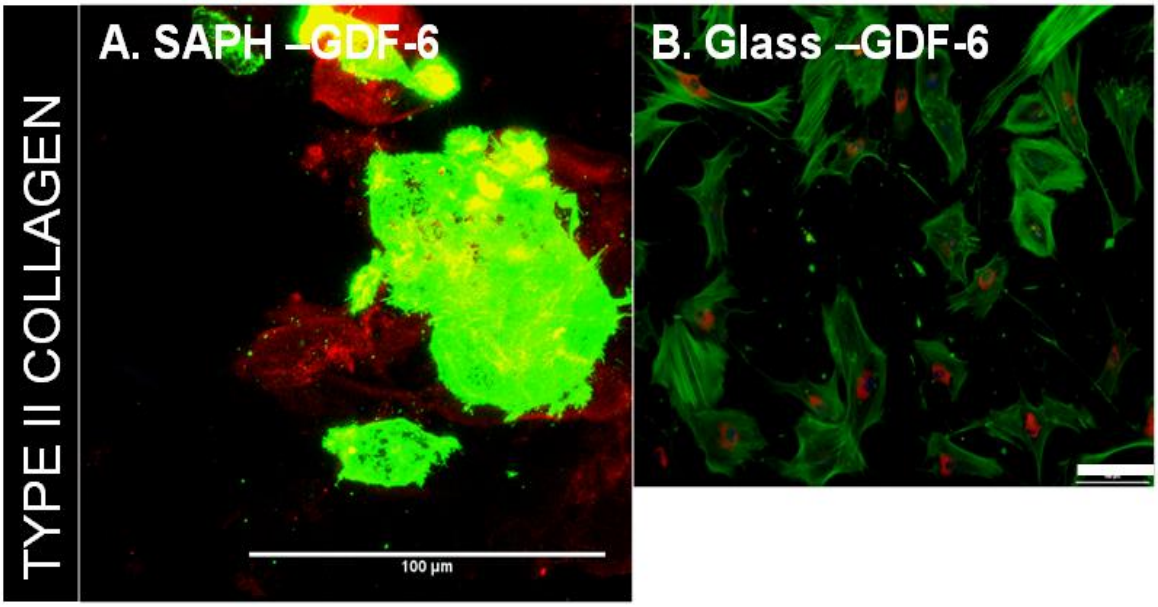

Figure 6.22. Fluorescence micrographs showing type II collagen ICC staining for $1x10^6$ h-BMMSCs ml^{-1} on day 7 without GDF-6 stimulation. [A] Human BMMSCs cultured in 30 mg ml^{-1} SAPH demonstrated intense extracellular staining for type II collagen. [B] Human BMMSCs cultured on glass demonstrated some positive intracellular staining for type II collagen. Type II collagen was stained red, F-actin was stained green and nuclei were stained blue. Scale bar represents 100 µm.

When h-BMMSCs were cultured in absence of GDF-6, there was evidence of intense pericellular aggrecan staining around some cells (*figure 6.23A, denoted by white arrows*). Undifferentiated h-BMMSCs do not produce aggrecan (*figure 6.23B & 6.28B*) [94] therefore production of the protein by specific encapsulated cells strongly suggested that h-BMMSCs had undergone differentiation. Aggrecan staining was comparable to micrographs for bNPCs cultured in SAPHs (*figure 5.29A*) although not as extensive. In contrast, h-BMMSCs cultured in monolayer did not stain for aggrecan intra- or extracellularly which was in agreement with NPCs cultured on glass (*figure 5.29B*) and the literature [51, 63].

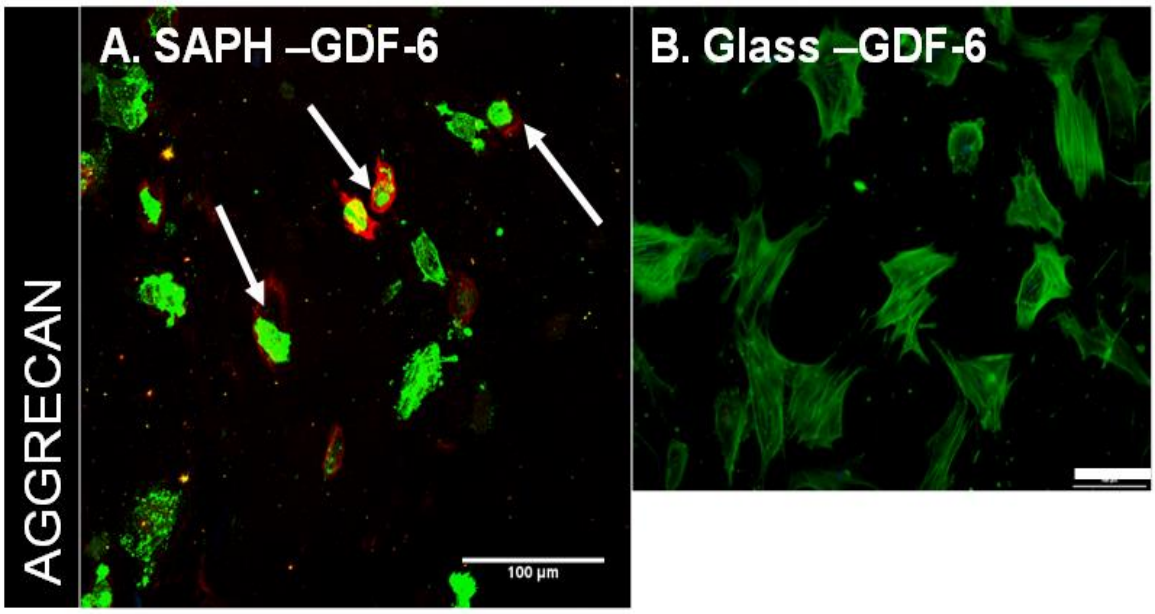

Figure 6.23. Fluorescence micrographs showing aggrecan ICC staining for 1x10^{6} h-BMMSCs ml^{-1} on day 7 without GDF-6 stimulation. [A] Human BMMSCs cultured in 30 mg ml^{-1} SAPH demonstrated intense extracellular positive staining for aggrecan around some cells (*denoted by white arrows*). [B] Human BMMSCs cultured on glass demonstrated no positive staining present for aggrecan. Aggrecan was stained red, F-actin was stained green and nuclei were stained blue. Scale bar represents 100 µm.

Rounded morphology is typical of chondrogenic [95], discogenic [36] or adipogenic [39] differentiation. Neither type II collagen nor aggrecan is produced by adipocytes [96]. The gene expression profiles (*figures 6.17-19*) strongly suggested that discogenic differentiation occurred without use of exogenous growth factor whilst extracellular deposition of both type II collagen (*figure 6.22*) and aggrecan (*figure 6.23*) supported this hypothesis as the production of ECM components was typical of native NPCs. Kumar *et al.* produced comparable ICC micrographs for type II collagen and aggrecan staining when h-BMMSCs were cultured with hMSC media without growth factors in a polymer hydrogel. The reasoning given was that a combination of hypoxic conditions and hydrogel environment could have induced chondrogenic differentiation. The study also observed extracellular staining for type II collagen and aggrecan was also produced for cells grown in monolayer [51] which is not typical for the NPC phenotype [63] (*figures 5.26B-5.29B)* or undifferentiated BMMSCs [66] (*figures 6.21B-6.26B*).

6.6.2. Human BMMSCs cultured with GDF-6 stimulation

It was determined in *section 6.1.3* that h-BMMSCs cultured with GDF-6 stimulated media upregulated ‘traditional’ and ‘novel’ NP markers. Therefore if h-BMMSCs had been differentiated towards a discogenic phenotype after exogenous growth factor stimulation then

deposition of low amounts of type I collagen and significant amounts of type II collagen and aggrecan extracellularly would occur.

On day 7 (*figure 6.24A*), dim extracellular type I collagen staining was present pericellularly for some cells which was expected as gene expression for type I collagen was low on day 7 (*figure 6.8*). Low amounts of type I collagen production is typical for NPCs in the native tissue [67]. High deposition or increased production of type I collagen would indicate that h-BMMSCs had not undergone discogenic differentiation. In monolayer culture there was intra- and extracellular type I collagen staining (*figure 6.24B*) which was in agreement with micrographs for non-stimulated samples (*figure 6.21B*). Undifferentiated BMMSCs [66] and NPCs in monolayer [63, 93] (*figure 5.25B*) deposit high amounts of type I collagen.

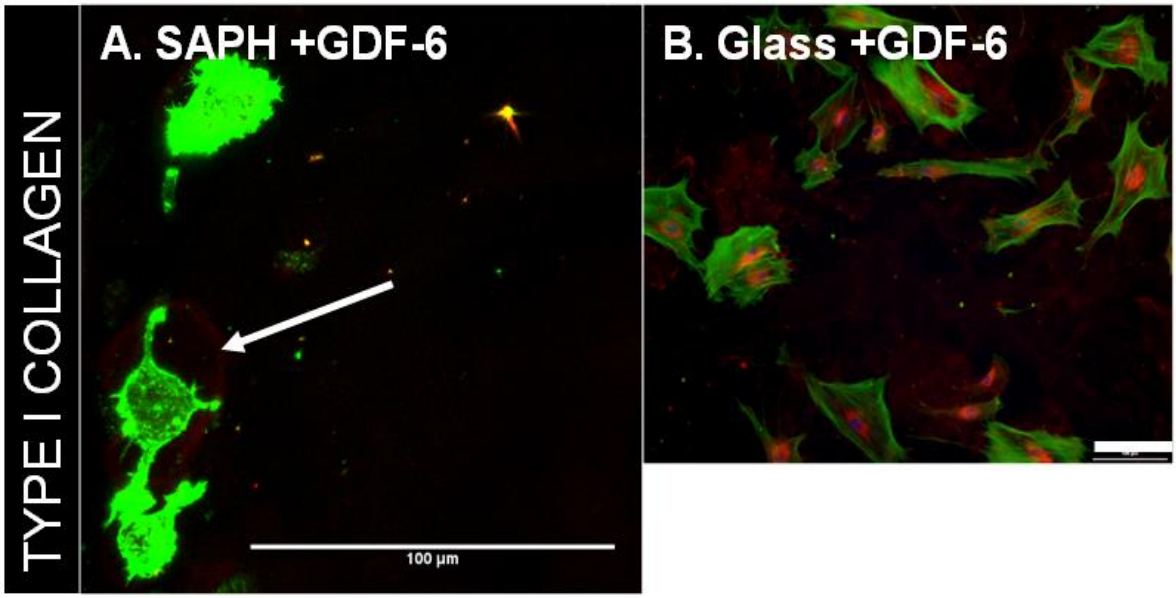

Figure 6.24. Fluorescence micrographs showing type I collagen ICC staining for 1x10^{6} h-BMMSCs ml^{-1} on day 7 with 100 ng ml^{-1} GDF-6 stimulation. [A] Human BMMSCs cultured in 30 mg ml^{-1} SAPH demonstrated some positive staining for type I collagen. [B] Human BMMSCs cultured on glass. Positive staining was present for 2D culture. Type I collagen was stained red, F-actin was stained green and nuclei were stained blue. Scale bar represents 100 µm.

There was intense staining for type II collagen intra- and extracellularly on day 7 after h-BMMSCs were cultured in SAPHs (*figure 6.25A*). Staining was brightest outside the cell membrane, which was denoted by F-actin staining [97] with type II collagen extending into the matrix and appearing fibrillar in distribution. The deposition of type II collagen was comparable to ICC micrographs for h-BMMSCs cultured without GDF-6 stimulation (*figure 6.22A*), NPCs in SAPHs (*figure 5.27A*) and the published literature [29, 51]. Due to the documented effect of GDF-6 differentiating h-BMMSCs towards a discogenic phenotype, the distribution and amount of type II collagen staining was expected. For h-BMMSCs cultured in monolayer, there

was little positive staining for type II collagen on day 7 (*figure 6.25B*). Some cells demonstrated dim positive staining intracellularly, distributed around the cell nuclei, however type II collagen staining made up only a small percentage of the total cellular architecture with the cytoskeleton denoted by F-actin staining [99].

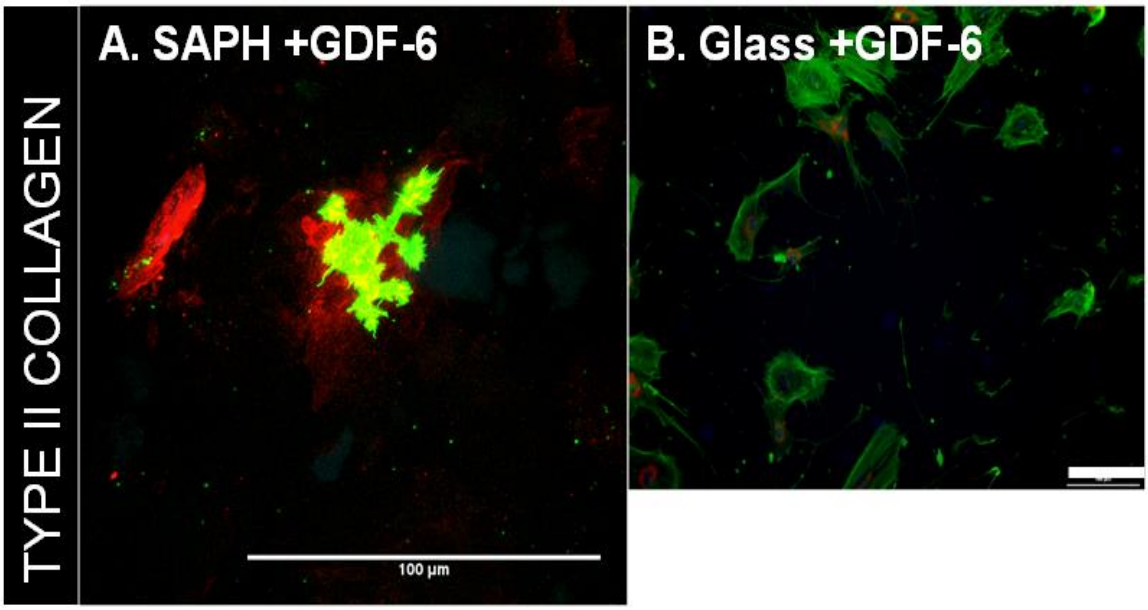

Figure 6.25. Fluorescence micrographs showing type II collagen ICC staining for $1x10^6$ h-BMMSCs ml^{-1} on day 7 with 100 ng ml^{-1} GDF-6 stimulation. [A] Human BMMSCs cultured in 30 mg ml^{-1} SAPH demonstrated intense extracellular positive staining for type II collagen [B] Human BMMSCs cultured on glass showed little positive staining for type II collagen. Type II collagen was stained red, F-actin was stained green and nuclei were stained blue. Scale bar represents 100 µm.

On day 7, there was extensive extracellular aggrecan deposition by some cells (*figure 6.26A*). Aggrecan staining was most intense pericellularly with aggrecan extending well into the SAPH. Objectively, aggrecan appeared more prevalent than type II collagen (*figure 6.26A*) which was supported by the ratio of aggrecan to type II collagen gene expression on day 7 (*figure 6.18)*. The deposition of aggrecan in *figure 6.26A* was comparable to NPC aggrecan deposition after culture in SAPHs (*figure 5.29A*) and more extensive than non-stimulated samples (*figure 6.23A*). In monolayer (*figure 6.26B*), there was no positive aggrecan staining on day 7 which was in agreement with the literature as undifferentiated h-BMMSCs do not produce aggrecan (*figure 6.23B & 6.26B*) [95] nor do NPCs in monolayer culture [63, 93].

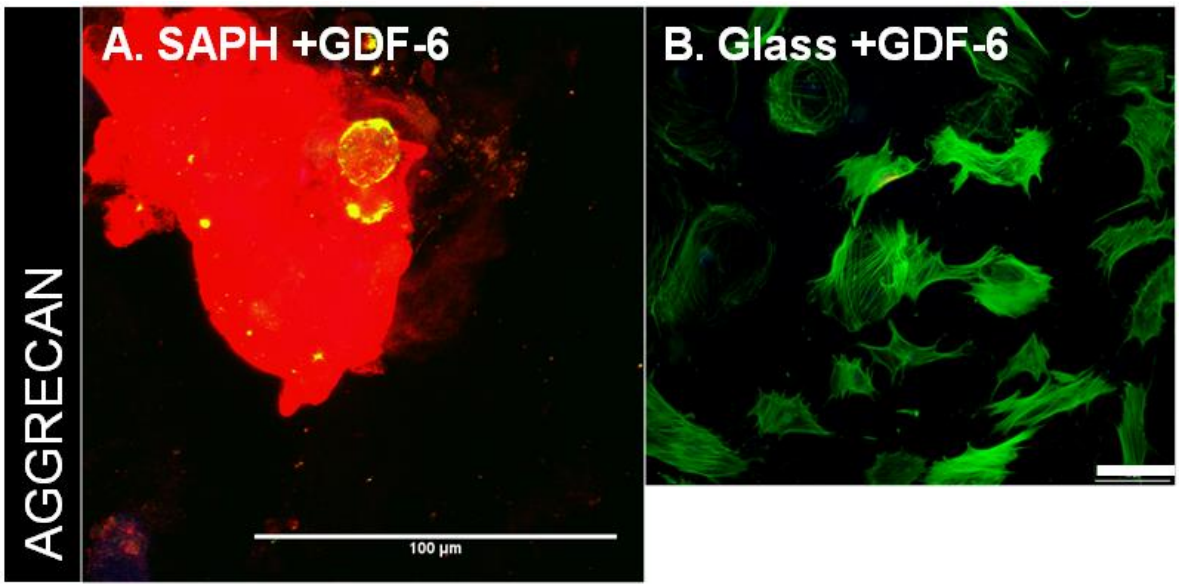

Figure 6.26. Fluorescence micrographs showing aggrecan ICC staining for 1x10^{6} h-BMMSCs ml^{-1} on day 7 with 100 ng ml^{-1} GDF-6 stimulation. [A] Human BMMSCs cultured in 30 mg ml^{-1} SAPH demonstrated intense extracellular positive staining for aggrecan. [B] Human BMMSCs cultured on glass demonstrated no positive aggrecan staining present. Aggrecan was stained red, F-actin was stained green and nuclei were stained blue. Scale bar represents 100 µm.

To summarise, the deposition of type I collagen, type II collagen and aggrecan by h-BMMSCs cultured in SAPHs (*section 6.6.2*) were as expected due to GDF-6 stimulated MSCs undergoing discogenic differentiation [6]. Type II collagen is the main structural component of the NP whilst aggrecan is the principal matrix component responsible for maintaining tissue hydration therefore extracellular deposition of both proteins was typical of native NPCs and supported the discogenic induction effect of GDF-6.

6.6.3. Overview and further discussion

The difference in ECM component production by h-BMMSCs after 3D culture in SAPHs and after 2D culture on glass, emphasised the importance and influence of culture microenvironment on the expression of appropriate ECM components. It was evident from ICC micrographs that 3D culture was required for h-BMMSCs to undergo discogenic differentiation and to produce NP associated ECM components [59, 63]. Reasoning behind the different cellular responses to 2D and 3D culture was discussed in *section 2.1.2* and *section 5.2*. The type and distribution of ECM component production by GDF-6 treated h-BMMSCs in monolayer strongly suggested that the growth factor could not stimulate production of NP-associated ECM components for 2D culture (*figure 6.22B-6.26B*).

Objectively (*figures 6.21A-6.26A)* it appeared that there was higher aggrecan deposition by h-BMMSCs in SAPHs, in comparison to type I and type II collagen. Day 7 gene expression

results (*figure 6.18*) supported the hypothesis that aggrecan was the prevalent ECM component for both GDF-6 stimulated and non-stimulated samples. Objectively, it appeared that h-BMMSCs cultured with GDF-6 deposited greater amounts of aggrecan than samples cultured in absence of GDF-6 (*figures 6.23A & 6.26A)* which was expected due to the known discogenic differentiation effect of the growth factor [6]. Deposition of aggrecan is directly related to corresponding gene expression levels [55, 74] however there was no significant difference in day 7 *ACAN* expression (*figure 6.18*) between stimulated and non-stimulated h-BMMSCs ($P>0.05$). *COL2A1* expression for both culture conditions (*figure 6.10*) suggested that corresponding protein deposition would have been low which is in contrast to ICC micrographs (figures *6.22 & 6.25*). Discrepancies in protein deposition and gene expression may be attributed to differences in detection limits between mRNA and protein expression, instability of mRNA, short protein half-life or inhibition at the transitional level [81]. A probable explanation for the difference in gene expression and corresponding protein deposition was that ICC micrographs only imaged a small area of the total sample. Therefore micrographs only showed a fraction of overall cells so ICC was not an accurate method for quantifying the total amount of ECM component in samples. ICC did allow visualisation of the type of ECM component and how it was deposited.

The vast majority of cells adopted a rounded morphology after culture in the SAPHs (*figures 6.21A-6.26A*) which was in agreement with LIVE/DEAD® assay micrographs (*section 6.3)*, bNPC morphology after encapsulation in SAPHs (*section 5.6*) and reported morphology of native NPCs [35]. At high magnifications, some cells had thin processes extending into the matrix from the main rounded body (*figure 6.27*, denoted with white arrows) when cultured with and without GDF-6. NPCs with long processes have been identified in healthy and degenerate human IVDs [99, 100]. It was discussed in *section 5.6.4* that the processes might be involved in cell mechanotransduction pathways as NPCs need to be able to respond to the loading that IVDs are subjected to [36]. MSCs also use focal adhesions and actin-myosin contractions as force transmission pathways to ‘feel’ their microenvironment which has been hypothesised to play a role in determining stem cell fate [9, 11]. Variations in matrix stiffness have been shown to influence focal-adhesion structure and cytoskeleton [11]. Therefore MSC focal adhesions were likely to have played a role in sensing the SAPH nanofibrous architecture (*section 4.3*) and comparable mechanical properties of the system to the native tissue (*section 4.4.4*) leading to discogenic differentiation. F-actin staining for h-BMMSCs cultured in monolayer displayed a highly organised cytoskeleton with high amounts of stress fibres. The distribution of F-actin was typical for h-BMMSCs cultured in 2D on stiff substrates [97] (*figures 6.21B-6.26B*)

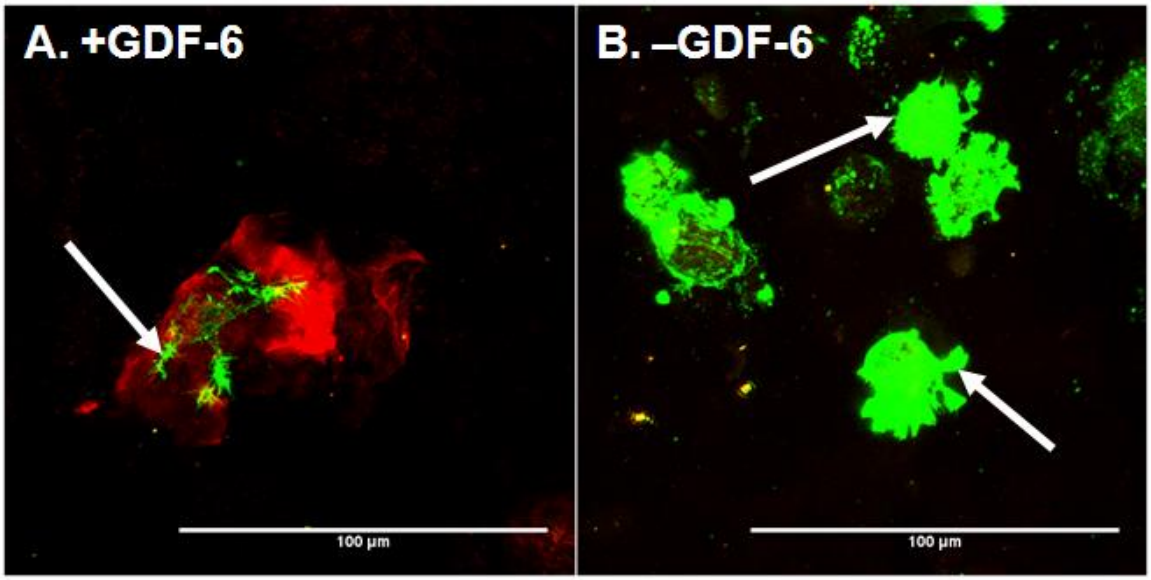

Figure 6.27. Fluorescence micrographs showing aggrecan ICC staining for 1x10^6 h-BMMSCs ml^{-1} on day 7 cultured in 30 mg ml^{-1} SAPH. [A] Human BMMSCs cultured with 100 ng ml^{-1} GDF-6 stimulation. [B] Human BMMSCs cultured in absence of GDF-6. Arrows denote cellular processes that have been hypothesised to be involved in mechanotransduction. Aggrecan was stained red, F-actin was stained green and nuclei were stained blue. Scale bar represents 100 µm.

Contemporary NP tissue engineering studies that utilised ICC to image ECM production by MSCs presented comparable micrographs to this study. Human BMMSCs cultured in synthetic polymer hydrogels (pHEMA-co-APMA) with chondrogenic medium produced intense staining for type II collagen and aggrecan intracellularly with some extracellular staining [51]. Type II collagen staining distribution was comparable to this study in PEG-HA hydrogels functionalised with the chondroinductive GAG pentosan polysulphate however intense extracellular staining for type I collagen was also observed [29, 63].

In most micrographs, cell nuclei were hard to distinguish due to background DAPI staining of the SAPH. Cell nuclei were large and filled the majority of the cell when visible (*figure 6.28, denoted with white arrows)*. NPs have been imaged as having large indented nuclei in the native tissue so encapsulated cells had comparable intracellular structure [100]. Samples were incubated with only sAB in the absence of pAB and analysis demonstrated that no unspecific binding occurred as only cell nuclei and F-actin visible (*figure 6.28*).

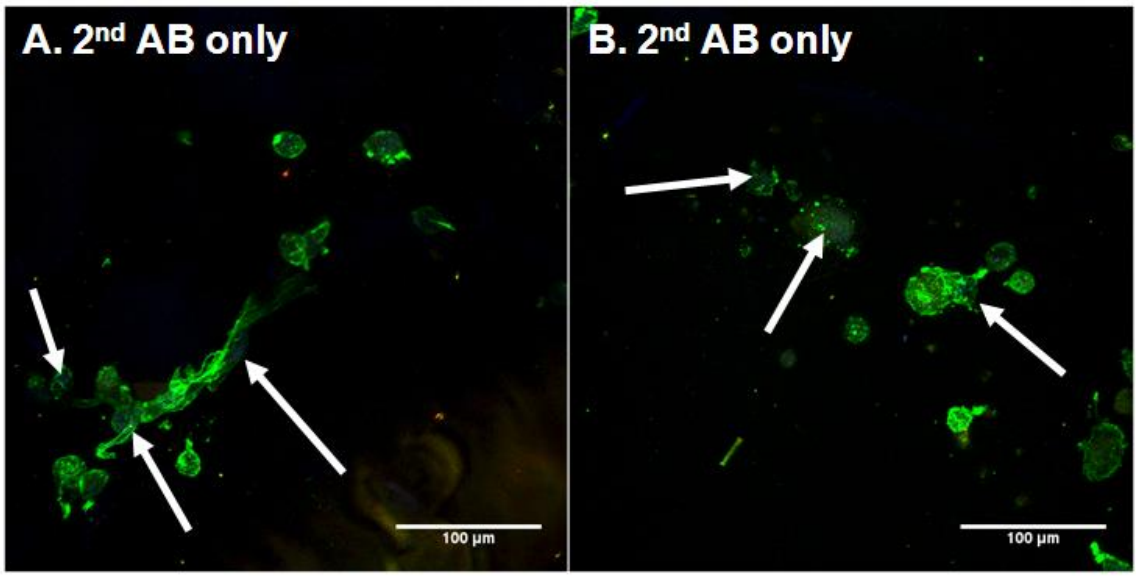

Figure 6.28. Fluorescence micrographs showing samples incubated with secondary AB only for 1x10^6 h-BMMSCs ml^{-1} on day 7 cultured in 30 mg ml^{-1} SAPH. [A] Secondary AB used for aggrecan, Alexa Fluor 568 goat anti-mouse IgG. [B] Secondary AB used for type I and II collagen, Alex Fluor 546 goat anti-rabbit IgG. No red staining was present which confirmed that no unspecific staining occurred. White arrows denote dim staining for cell nuclei using DAPI. F-actin was stained green and nuclei were stained blue. Scale bar represents 100 µm.

In conclusion, h-BMMSCs stimulated with GDF-6 deposited NP associated ECM components of type II collagen and aggrecan extracellularly when cultured in SAPHs. Type I collagen was also positively stained intracellularly. The rounded morphology of h-BMMSCs cultured in SAPHs was a marked alteration from the fibroblastic morphology of undifferentiated h-BMMSCs cultured in monolayer. Cells in 2D culture on glass with GDF-6 stimulation expressed significant amounts of type I collagen with little type II collagen or aggrecan deposition which demonstrated that GDF-6 could not stimulate production of NP associated ECM components if h-BMMSCs were cultured in monolayer. Protein synthesis for h-BMMSCs stimulated with GDF-6 was typical for NP-like cells.

For h-BMMSCs cultured in absence of GDF-6, there was extracellular production of type II collagen and aggrecan. Type I collagen staining was low for encapsulated cells. In monolayer, h-BMMSCs produced significant amounts of type I collagen and little type II collagen or aggrecan. When analysing ECM production in conjunction with the gene expression results for non-stimulated cells (*section 6.5*), results strongly suggested that h-BMMSCs spontaneously differentiated towards a NP-like phenotype without use of an exogenous growth factor.

6.7. QUANTIFYING THE PRODUCTION OF SULPHATED GLYCOSAMINOGLYCANS USING BLYSCAN™ s-GAG ASSAY

Blyscan™ sulphated GAG assay was used to determine total accumulated s-GAG content in SAPHs on days 1, 7 and 14 for human BMMSCs cultured with and without GDF-6 stimulation. Production of s-GAG was proportional to PG content, as s-GAGs are attached to the protein core via covalent bonds [103]. Total s-GAG accumulation was calculated from a standard curve that plotted absorbance against known cell number (*figure 8.4*).

6.7.1. Human BMMSCs cultured without GDF-6 stimulation

No significant differences in s-GAG accumulation with time point were detected (*figure 6.29A*) (P>0.05) when h-BMMSCs were cultured in absence of GDF-6. At day 1, total s-GAG was 0.63±0.11 µg, at day 7 total s-GAG was 0.51±0.06 µg and for day 14 s-GAG was 0.58±0.12 µg. When total sample s-GAG accumulation was normalised with viable cell number results demonstrated that there was no significant increases or decreases in s-GAG production per cell (P>0.05) (*figure 6.29B*). On day 1, s-GAG production per cell was 0.019±0.007 ng, on day 7 s-GAG production per cell was $4.96x10^{-3}$±$8x10^{-3}$ ng and for day 14 s-GAG production per cell was $6.46x10^{-3}$±$2.33x10^{-3}$ ng.

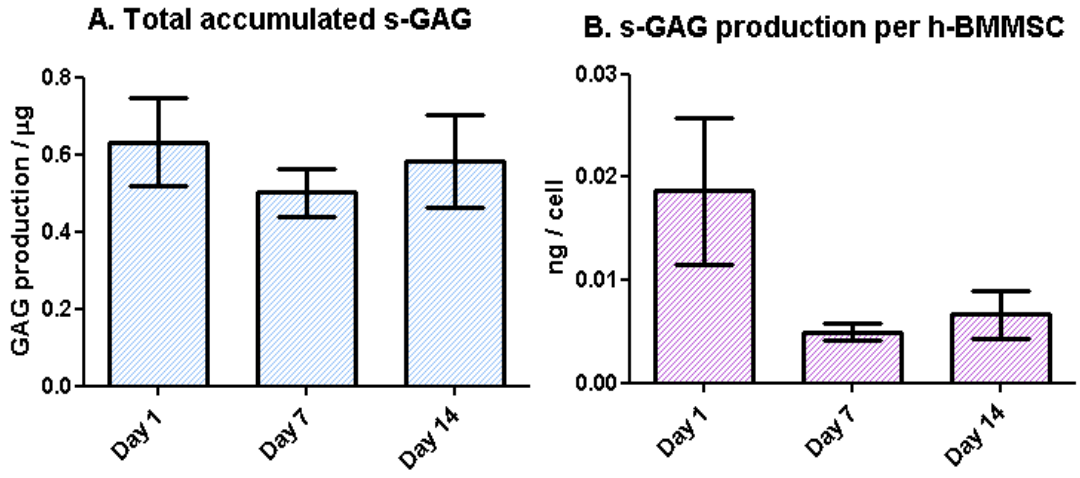

Figure 6.29. Sulphated-GAG production for $1x10^6$ h-BMMSCs ml^{-1} in 30 mg ml^{-1} FEFEFKFK SAPHs in absence of GDF-6. [A] Total accumulated s-GAG per sample. [B] Normalised results where total accumulated s-GAG was divided by viable cell number to estimate s-GAG production per h-BMMSC. (P>0.05). Values expressed as mean±SD where n=4 from 2 experimental repeats.

If h-BMMSCs had differentiated towards a NP-like phenotype as strongly suggested by gene expression profiles (*section 6.5*) and ECM component deposition (*section 6.6*) then significant amounts of s-GAGs should have been accumulated.

Normalised results, where total accumulated s-GAG was divided by viable cells on corresponding timepoint, demonstrated that there were no significant differences in s-GAG production per cell (*figure 6.29B*) which could be explained by the absence of discogenic induction factor. Typically without the appropriate stimulation and signalling provided by differentiating growth factors, spontaneous differentiation of MSCs towards a NP-like phenotype was unlikely [1, 104]. However s-GAG accumulation did occur (*figure 6.29A*) and was supported significant upregulation of *ACAN* expression with time point (*P<0.05) (*figure 6.11*). Gene expression is directly linked to protein deposition [55, 74] therefore the expectation was that a corresponding increase in s-GAG production per cell would have occurred. ICC micrographs also demonstrated extracellular aggrecan deposition (*figure 6.23*) therefore it was likely that aggrecan deposition was occurring but not at high levels.

Stoyanov *et al.* detected little s-GAG when h-BMMSCs were cultured in alginate beads without GDF-5 [5]. Gantenbein-Ritter *et al.* detected s-GAG production by h-BMMSCs cultured without GDF-5 however, s-GAG levels on day 18 were not significantly higher than day 0 levels (P>0.05) [48]. Human BMMSCs cultured in type I collagen gels without induction media detected s-GAG accumulation in the constructs by Clarke *et al*. Total accumulated s-GAG for non-stimulated h-BMMSCs was significantly lower than cells cultured with TGF-β, GDF-5 or GDF-6 [6]. Therefore it was apparent that s-GAG could be produced by h-BMMSCs after encapsulation in an appropriate scaffold without growth factor stimulation however for significant s-GAG accumulation, a suitable discogenic differentiation growth factor was necessary.

6.7.2. Human BMMSCs cultured with GDF-6 stimulation

Total s-GAG accumulation in SAPHs was consistent with time point with GDF-6 stimulation (*figure 6.30A*). On day 1, total s-GAG was 0.64±0.12 µg, on day 7 total s-GAG was 0.73±0.16 µg and for day 14 s-GAG was 0.8±0.13 µg (P>0.05). When s-GAG production was normalised with viable cell number, results determined that there was no significant increases or decreases in s-GAG production per cell (P>0.05) (*figure 6.30B*). On day 1, s-GAG production per cell was $8.76x10^{-3}$±$2x10^{-3}$ ng, on day 7 s-GAG production per cell was $6.4x10^{-3}$±$2.5x10^{-3}$ ng and for day 14 s-GAG production per cell was 0.012±$4.4x10^{-3}$ ng.

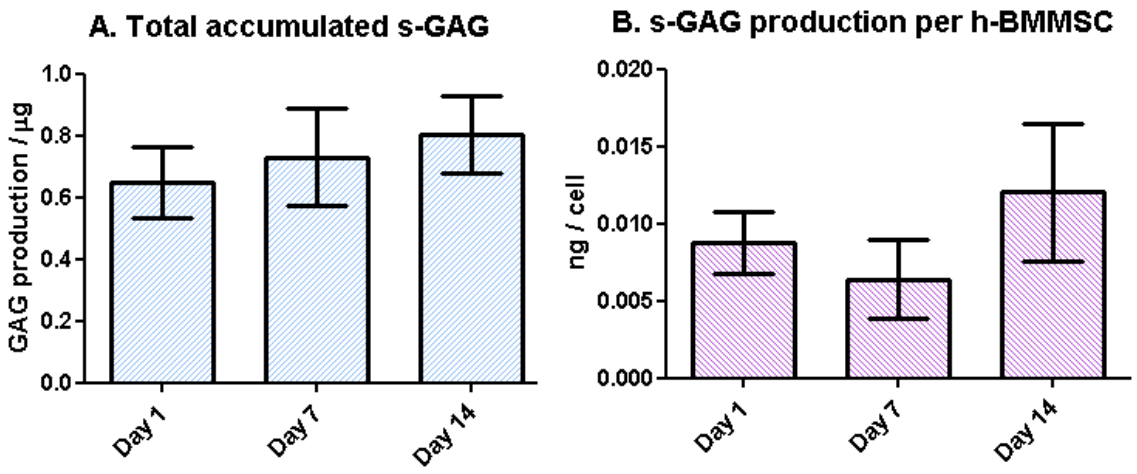

Figure 6.30. Sulphated-GAG production for 1x10^6 h-BMMSCs ml^{-1} in 30 mg ml^{-1} FEFEFKFK SAPHs with 100 ng ml^{-1} GDF-6 stimulation. [A] Total accumulated s-GAG per sample [B] Normalised results where total accumulated s-GAG was divided by viable cell number to estimate s-GAG production per h-BMMSC. (P>0.05) Values expressed as mean±SD where n=4 from 2 experimental repeats.

There was a significant increase in s-GAG production per bNPC (***P<0.001) from days 1 to 14 after culture in FEFEFKFK SAPH (*figure 5.33*). The effect that an appropriate culture environment had on supporting the rapid re-differentiation of NPCs after 2D culture [3, 21, 105] likely explained the s-GAG accumulation results for bNPCs. In monolayer, NPCs de-differentiated (*sections 5.2, 5.6-5.8*) [63] however after culture in FEFEFKFK SAPH, rapid re-differentiation and restoration of NP phenotype occurred with 'traditional' and 'novel' NP markers being upregulated on day 1 (*figure 5.20*). High *ACAN* expression was recorded as early as day 1 and production of aggrecan was stained and visualised intracellularly by day 3 with high amounts of intense extracellular positive staining by day 7 (*section 5.6.3*).

In comparison, h-BMMSCs required the stimulation of growth factors or the effect of the culture environment to induce differentiation. Accordingly most studies analysed the phenotype of encapsulated cells after day 7 to allow sufficient *in vitro* culture length for discogenic differentiation and stimulation of appropriate ECM components production [5, 6, 48]. *Figure 6.17* demonstrated that a discogenic phenotype was likely present on day 1. If the growth factor was having its intended effect then normalised data of s-GAG production per cell (*figure 6.30B*) should have increased with time point after stimulation with GDF-6. However a significant decrease in *ACAN* expression with time point was observed (*figure 6.11*) which likely explained the absence of increased s-GAG accumulation or s-GAG production per h-BMMSCs (*figure 6.30*).

No significant differences in GAG/DNA content over 21 day time period were detected when h-BMMSCs were transfixed with GDF-5 and cultured in alginate beads [70]. Similar results were detected by Gantenbein-Ritter *et al.* where no significant changes in s-GAG accumulation occurred after h-BMMSCs were cultured with 100 ng ml^{-1} GDF-5 in alginate beads [48]. In

contrast, a number of other h-BMMSC studies observed significant increases in normalised s-GAG/DNA after culture with various NPC differentiation growth factors (GDF-6, GDF-5 and TGF-β) in type I collagen [6], alginate [5] and poly(L-Lactide) [19] scaffolds.

6.7.3. Comparing non-stimulated and stimulated GDF-6 samples

The initial hypothesis (*section 6.1.4*) was GDF-6 treated samples would have accumulated significantly higher s-GAG than non-stimulated samples as observed in the literature [6]. However there were no significant differences in total s-GAG accumulation at any time point (P>0.05) (*figure 6.31*). Stoyanov *et al.* observed no significant differences in s-GAG accumulation for GDF-5 treated samples compared to the non-stimulated controls after culture in alginate beads under normoxic conditions [5].

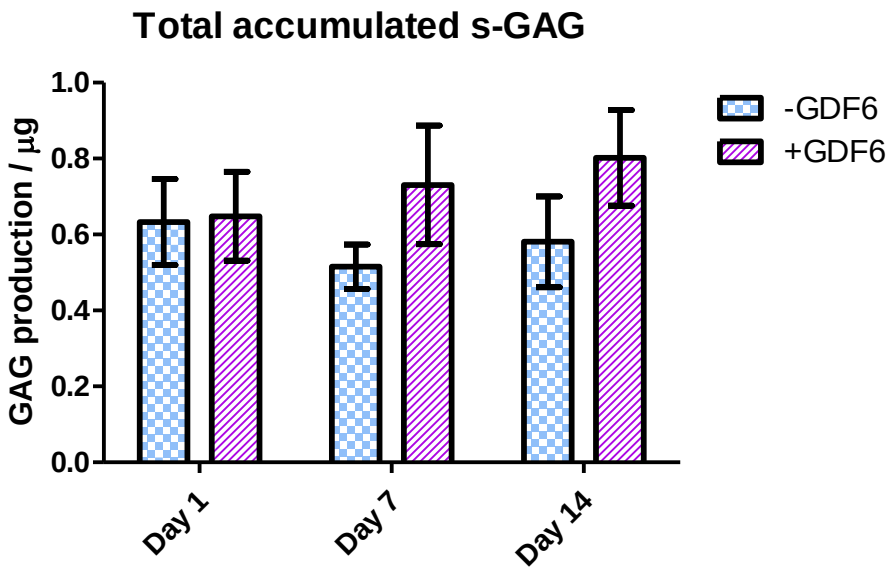

Figure 6.31. The total s-GAG accumulation for 1x10^6 h-BMMSCs ml^{-1} in 30 mg ml^{-1} FEFEFKFK SAPHs with and without 100 ng ml^{-1} GDF-6 stimulation. There was no significant differences in total s-GAG between culture conditions on any time point (P>0.05). Values expressed as mean±SD where n=4 from 2 experimental repeats.

There were no significant differences in s-GAG production per h-BMMSC for samples cultured with and without GDF-6 at any time point (P>0.05) which was unexpected as GDF-6 has been demonstrated to significantly increase s-GAG/DNA content compared to non-stimulated media controls [6]. Possible reasons for the unexpected s-GAG production results were discussed in *section 6.5.6*. Gantenbein-Ritter *et al.* demonstrated that the GAG/DNA content of h-BMMSCs treated with GDF-5 was lower than the GAG/DNA content of h-BMMSCs cultured in non-differentiation media [48].

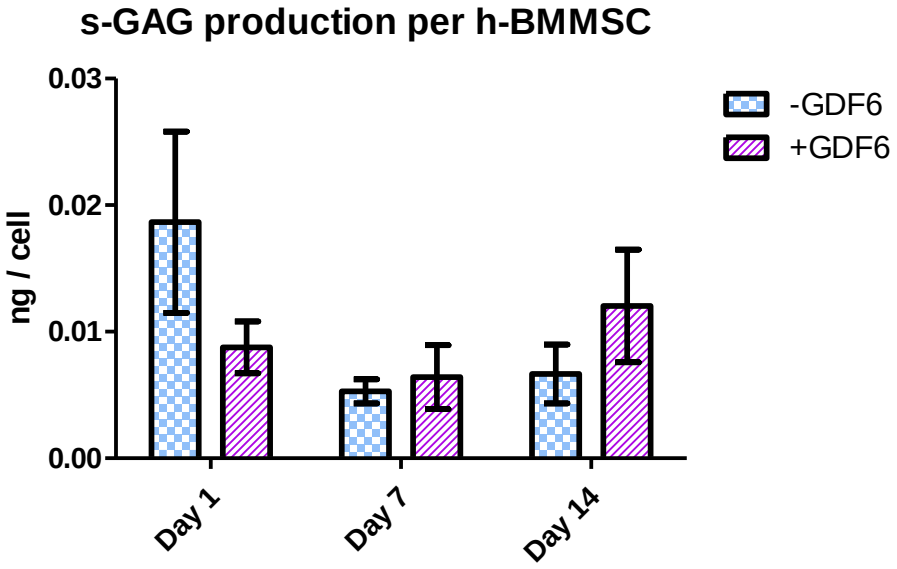

Figure 6.32. Normalised data of s-GAG production per h-BMMSC for 1x10^6 h-BMMSCs ml^{-1} in 30 mg ml^{-1} FEFEFKFK SAPHs with and without 100 ng ml^{-1} GDF-6 stimulation. There was no significant differences in s-GAG production per cell between culture conditions for any time point (P>0.05). Values expressed as mean±SD where n=4 from 2 experimental repeats.

6.7.4. Overview and further discussion

Insufficient *in vitro* culture length likely explained the lower than anticipated s-GAG accumulation and s-GAG production per cell results (*figures 6.31-6.32*) [91]. Experiments were concluded on day 14 (*figures 8.6 & 8.7*) as significant weakening and loss of volume was experienced by the system. Most comparable NP tissue engineering studies measured accumulated s-GAG after day 14 to allow adequate *in vitro* culture length for extensive aggrecan production [6, 19, 48] where it was determined that s-GAG production was time-dependent when h-BMMSCs were cultured with discogenic induction media in HA scaffolds [106], alginate beads [5] and photocrosslinked carboxymethylcellulose hydrogels [73]. Increased cell density has been demonstrated to increase total s-GAG accumulation (*section 5.7.1*) [41]. Therefore increasing initial cell seeding density (1x10^6 h-BMMSCs ml^{-1}) to amounts used by contemporary studies, ranging from 2x10^6 to 4x10^6 MSCs ml^{-1} [5, 6, 19, 48], should increase s-GAG accumulation. Finally, s-GAG content would be increased by carrying out *in vitro* cell culture under hypoxic conditions. The native NP has an oxygen level of around 2-3% [13] therefore hypoxic conditions have been demonstrated to stimulate higher s-GAG production compared to samples cultured in normoxic conditions [5, 19]. For future work, these factors are worthy of investigation to maximise s-GAG accumulation so levels approached that of the native tissue.

Cell culture medium from sample washes and media changes was collected and tested for presence of s-GAG. Results showed that no s-GAG was detected in the pooled media (*figures 8.11 & 8.12*) which suggested that the SAPH was effective in retaining the majority of the ECM component or that s-GAG released into the media was at a too low concentration for detection. In contrast, Clarke *et al.* determined that more s-GAG was released into the media than retained in the system when h-BMMSCs were cultured in type I collagen hydrogels with GDF-6 [6].

To summarise, it was determined that s-GAG was accumulated in FEFEFKFK SAPHs after h-BMMSC culture with and without GDF-6. However there were no significant differences in total s-GAG accumulation or for s-GAG production per cell over culture period. There were no significant differences for normalised s-GAG production between h-BMMSCs cultured with and without GDF-6 accumulation. The expectation was an increase in both total s-GAG detected and s-GAG production per cell with increasing time point would be detected as cells were expected to deposit increasing amounts of aggrecan after undergoing discogenic differentiation.

6.8. LIMITATIONS OF THE STUDY

Despite efforts to design a study that provided an accurate representation of how h-BMMSCs behaved after encapsulation in FEFEFKFK SAPHs there were a number of limitations. The main limitation was that human BMMSCs from only one source, a 27 year old female donor, were used. Cells from this patient were unlikely to be representative of the whole MSC population. To overcome this limitation, use of h-BMMSCs from a number of patients of various sexes and ages would allow a better understanding and overview of how h-BMMSCs behaved in the SAPHs. This increase in *n*-number would likely cause more variability in results as cells could respond differently to encapsulation in SAPHs but the findings would be more reliable due to use of a larger sample size.

In comparison to the literature [6], GDF-6 stimulated samples did not produce expected gene profiles or s-GAG accumulation results. As discussed in *section 6.5.6* it was possible that constant GDF-6 stimulation after discogenic differentiation caused a down-regulation of some NP marker genes. Therefore an experiment where h-BMMSCs were dosed with GDF-6 only at the beginning would determine if this hypothesis was correct.

The experimental length only allowed the behaviour of h-BMMSCs to be assessed over a relatively short period due to the system becoming mechanically unstable after 14 days. Longer term studies are required to better assess how h-BMMSCs behave after encapsulation which would require improving the degradation rate and mechanical stability of the FEFEFKFK SAPH.

6.9. CONCLUSION

There are a number of challenges faced when using MSCs for NP tissue engineering scaffolds including how best to differentiate cells towards a NP-like phenotype, whether to induce differentiation before encapsulation in a system or after culture in a system as well as preservation of the discogenic phenotype after seeding in the scaffold. *Chapter 5* provided evidence that bNPC phenotype could be restored and maintained after culture in SAPHs. Therefore if MSC could be differentiated towards a NP-like phenotype then the system should have be an appropriate microenvironment for cell survival, maintenance of NP phenotype and production of ECM components.

The ultimate aim of this study was to investigate whether FEFEFKFK SAPH could act as an effective cell delivery system and scaffold for NP tissue engineering. MSCs have been identified as a promising cell source for regeneration of degenerated NPs and GDF-6 has been established as potentially the most effective discogenic induction growth factor.

Cell behaviour analysis supported the hypothesis that the system could act as an effective MSC cell carrier and scaffold for NP tissue engineering applications. Cell population remained stable with high viability throughout culture, cells differentiated to a NP-like phenotype with high expression of a number of NPC markers and appropriate NP associated ECM components were produced after culture with and without GDF-6 in FEFEFKFK SAPHs.

Interestingly, results strongly suggested that h-BMMSCs were differentiated towards a discogenic phenotype without use of an exogenous growth factor. To the knowledge of the author, all published NP tissue engineering studies required either discogenic induction media containing various growth factors [5, 6] or a bioactive motif to differentiate MSCs towards a NP-like phenotype [29, 53]. A disadvantage of using growth factor treatment is the high cost associated with their production [12] and their rapid deterioration *in vivo* [88]. The hypothesis was that the nanofibrous architecture and the mechanical properties of the SAPH were mimicking the NP matrix. Microenvironment and the stem cell niche play a crucial role in determining stem cell fate therefore the SAPH biomaterial effect likely contributed to inducing discogenic differentiation of h-BMMSCs.

The aims set out at the beginning of the chapter were completed and results for h-BMMSC viability, gene expression and ECM production supported the hypothesis that FEFEFKFK SAPH holds great potential for NP tissue engineering applications and is deserving of further investigation.

6.10. REFERENCES

1. **Gilbert H, Hoyland J, Richardson S** '*Stem cell regeneration of degenerated intervertebral discs: Current status*' Curr Pain Headache Rep (2013); Vol.17 pp.1-9
2. **Sakai D, Mochida J, Iwashina T, Watanabe T, Nakai T, Ando K, Hotta T** '*Differentiation of mesenchymal stem cells transplanted into a rabbit degenerative disc model*' Spine (2005); Vol.30 No.21 pp.2379-2387
3. **Velikonja N, Urban J, Frohlich M, Wilke C, Kletas D, Potocar U, Turner S, Roberts S** '*Cell sources for nucleus pulposus regeneration*' Eur Spine J (2013); DOI 10.1007/s00586-013-3106-9
4. **Wang J, Liao L, Tan J** '*Mesenchymal stem cell based experimental and clinical trials: current status and open questions*' Expert Opin Biol Ther (2011); pp.893-909
5. **Stoyanov J, Gantenbein-Ritter B, Bertolo A, Aebli N, Baur M, Alini M, Grad S** '*Role of hypoxia and growth and differentiation factor-5 on differentiation of human mesenchymal stem cells towards intervertebral nucleus pulposus-like cells'* European Cells and Materials (2011); Vol. 21 pp.533-547
6. **Clarke L, McConnell J, Sherratt M, Derby B, Richardson S, Hoyland J** *'Growth differentiation factor 6 and transforming growth factor-beta differentially mediate mesenchymal stem cell differentiation, composition, and micromechanical properties of nucleus pulposus constructs'* Arthritis & Research (2014); Vol.16 pp.1-13
7. **Orozco L, Soler R, Morena C, Alberca M, Sanchez A, Sancho J** *'Intervertebral disc repair by autologous mesenchymal bone marrow cells: A pilot study'* Clinical and Translational Research (2011); Vol.92 pp.822-829
8. **Yoshikawa T, Ueda Y, Miyazaki K, Koizumi M, Takakura Y** *'Disc regeneration therapy using marrow mesenchymal stem cell transplantation'* Spine (2010); Vol.35 pp.475-480
9. **Bron J, Vonk L, Smit T, Koenderink G** *'Engineering alginate for intervertebral disc repair'* Journal of the mechanical behaviour of biomedical materials (2011); Vol.4 pp.1196-1205
10. **Breuls R, Jiya T, Smit T** *'Scaffold stiffness influences cell behaviour: Opportunities for skeletal tissue engineering'* The Open Orthopaedics Journal (2008); Vol.2 pp.103-109
11. **Engler A, Sen S, Sweeney H, Discher D** '*Matrix elasticity directs stem cell lineage specification'* Cell (2006); Vol.126 pp.677-689
12. **Chan S, Ganntenbein-Ritter B** *'Intervertebral disc regeneration or repair with biomaterials and stem cell therapy – feasible or fiction?'* European Journal of Medical Sciences (2012);
13. **Risbud M, Albert T, Guttapalli A, Vresilovic E, Hillibrand A, Vaccaro A, Shapiro I** '*Differentiation of mesenchymal stem cells towards a nucleus pulposus-like phenotype in vitro: Implications for cell based transplantation therapy*' Spine (2004); Vol.29 No.23 pp.2627-2632
14. **Walsh A, Bradford D, Lotz J** '*In vivo growth factor treatment of degenerated intervertebral discs*' Spine (2004); Vol.29 No.2 pp.156-163
15. **Steck E, Bertham H, Abel R, Chen B, Winter A, Richter W** '*Induction of intervertebral disc-like cells form adult mesenchymal stem cells*' Stem Cells (2005); Vol.23 pp.403-411
16. **Tuli R, Tuli S, Nandi S, Huang X, Manner P, Hozack W, Danielson K, Hall D, Tuan R** '*Transforming growth factor-β-mediated chondrogenesis of human mesenchymal progenitor cells involves N-cadherin and mitogen-activated protein kinase and Wnt signalling cross-talk*' J of Biological Chemistry (2003); Vol.278 No.42 pp.41227-41236
17. **Sive J, Baird P, Jeziorsk M, Watkins A, Hoyland J, Freemont A** '*Expression of chondrocyte markers by cells of normal and degenerate intervertebral discs*' J Clin Pathol: Mol Pathol (2002); Vol.55 pp.91-97
18. **Malzano C, Chan S, Kabiri A, Eglin D, Grad S, Bonel H, Benneker L, Gantenbein-Ritter B** '*A papain-induced disc degeneration model for the assessment of thermo-reversible hydrogel-cells therapeutic approach'* J of Tissue Engineering & Regenerative Medicine (2013); pp.1-20
19. **Feng G, Jin X, Hu J, Gupte M, Liu H, Ma P** '*Effects of hypoxia and scaffold architecture on rabbit mesenchymal stem cell differentiation towards a nucleus pulposus like phenotype*' Biomaterials (2011); Vol.32 pp.8182-8189
20. **Tassabehji M, Fang Z, Hilton E, McGaughran J, Zhao Z, de Bock CE, Howard E, Malass M, Donnai D, Diwan A, Manson F, Murrell D, Clarke R** *'Mutations in GDF6 are associated with vertebral segmentation defects in Klippel-Feil syndrome'* Hum Mutat (2008); Vol.29 pp.1017–1027
21. **LeMaitre C, Frain J, Sadler J, Fotheringham A, Freemont A, Hoyland J** '*Altered integrin mechanotransduction in human nucleus pulposus cells derived from degenerated discs*' Arthritis & Rheumatism (2009); Vol.60 pp.460-469
22. **Wei A, Williams L, Bhargav D, Shen B, Kishen T, Duffy N, Diwan A** '*BMP13 prevents the effect of annular injury in an ovine model*' International J of Biological Sciences (2008); Vol.5 pp.388-396

23. **Nohe A, Keating E, Knaus P, Petersen N** 'Signal transduction of bone morphogenic protein receptors' Cellular Signalling (2004); Vol.13 No.3 pp.291-299 [23]
24. **Yamashita H, Ten P, Heldin C, Miyazono K 'Bone morphogenic protein receptors' Bone (1996); Vol.19 No.6 pp.569-574**
25. **Miayzono K 'Signal transduction by bone morphogenic protein receptors: functional roles of Smad proteins' Bone (1999); Vol.25 No.1 pp.91-93**
26. **Von Bubnoff A, Cho K 'Intracellular BMP signalling regulation in vertebrates: pathway or network?' Dev Biol (2001); Vol.239 pp.1-14**
27. **Sakou T 'Bone morphogenic proteins from basic studies to clinical approaches' Bone (1998); Vol.22 Vol.6 pp.591-603**
28. **Williams L, Bhagrav D, Diwan A 'Unveling the BMP13 enigma: Redundant morphogen or crucial regulator?' Int J Biol Sci (2008); Vol.4 pp.318-329.**
29. **Frith J, Cameron A, Menzies D, Ghosh P, Whitehead D, Gronthos S, Zannettino A, White J** '*An injectable hydrogel incorporating mesenchymal precursor cells and pentosan polysulphate for intervertebral disc regeneration'* Biomaterials (2013); Vol.34 pp.9430-9440
30. **Shoukry M, Li J, Pei M** '*Reconstruction of an in vitro niche for the transition from intervertebral disc development to nucleus pulposus regeneration*' Stem Cells & Development (2013); Vol.22 No.8 pp.1-13
31. **Sekiya I, Larson B, Smith J, Pochampally R, Cui J, Prockop D** '*Expansion of human adult stem cells from bone marrow stroma: conditions that maximise the yields of early progenitors and evaluate their quality*' Stem Cells (2002); Vol.20 pp.530-541
32. **Zhang D, Kilian K** '*The effect of mesenchymal stem cell shape on the maintenance of multipotency*' Biomaterials (2013); Vol.34 pp.3962-3969
33. **Barry F, Murphy J** '*Mesenchymal stem cells: clinical applications and biological characterisation*' The International J of Biochemistry & Cell Biology (2004); Vol.36 pp.568-584
34. **Weiler C, Nerlich A, Schaaf R, Bachmeier B, Wuertz K, Boos N** *'Immunohistochemical identification of notochordal markers in cells in the aging human lumbar intervertebral disc*' Eur Spine J (2010); Vol.19 pp.1761-1770
35. **Trout J, Buckwalter J, Moore K** '*Ultrastructure of the human intervertebral disc III: cells of the nucleus pulposus*' The Anatomical Record (1982); Vol.204 pp.307-314
36. **Errington R, Puustjarvi K, White I, Roberts S, Urban J** '*Characterisation of cytoplasm-filled processes in cells of the intervertebral disc*' J Anat (1998); Vol.192 pp.369-378
37. **Saiani A, Mohammed A, Frielinghaus N, Collins R, Hodson N, Kielty C, Sherratt M, Miller A** *'Self-assembly and gelation properties of α-helix versus β-sheet forming peptides'* Soft Matter (2009); Vol.4 pp.193-202
38. **Ma H, Hung S, Lin S, Chen Y, Lo W** '*Chondrogenesis of human mesenchymal stem cells encapsulated in alginate beads*' J of Biomedical Materials Research (2002); pp.273-281
39. **MacQueen L, Sun Y, Simmons C** '*Mesenchymal stem cell mechanobiology and emerging experimental platforms*' J R C Soc Interface (2013); Vol.10 pp.1-16
40. **Iatridis J, Setton L, Weidenbaum M, Mow V** '*The viscoelastic behaviour of the non-degenerate human lumbar nucleus pulposus in shear'* J Biomechanics (1997); Vol.30 No.10 pp.1005-1013
41. **Kobayashi S, Meir A, Urban J** '*Effect of cell density on the rate of glycosaminoglycan accumulation by disc and cartilage cells in vitro*' J of Orthopaedic Research (2008); pp.493-504
42. **Georges P, Janmey P** '*Cell type-specific response to growth on soft materials*' J Appl Physiol (2005); Vol.98 pp.1547-1553
43. **Chou A, Nicoll S** *'Characterisation of photocrosslinked alginate hydrogels for nucleus pulposus cell encapsulation'* Wiley InterScience (2009) – pp.187-195
44. **Reza A, Nicoll S** '*Characterisation of novel photocrosslinked carboxymethylcellulose hydrogels for encapsulation of nucleus pulposus cells*' Acta Biomaterialia (2010); Vol.6 pp.179-186
45. **Zhang R, Ruan D, Zhang C** '*Effects of TGF-β1 and IGF-1 on proliferation of human nucleus pulposus cells in medium with different serum concentrations*' Journal of Orthopaedic Surgery and Research (2006); Vol.1 pp.1-11
46. **Baksh D, Yao R, Tuan R** '*Comparison of proliferative and multilineage differentiation potential of human mesenchymal stem cells derived from umbilical cord and bone marrow*' Stem Cells (2007); Vol.25 pp.1384-1392
47. **Liang H, Ma S, Feng G, Shen F, Li X '**Therapeutic effects of adenovirus-mediated growth and differentiation factor-5 in a mice disc degeneration model induced by annulus needle puncture' The Spin J (2010); Vol.10 pp.32-41
48. **Gantenbein-Ritter B, Benneker L, Alini M, Grad S** '*Differential response of human bone marrow stromal cells to either TGF-β1 or rhGDF-5*' Eur Spine J (2011); Vol.20 pp.962-971

49. **Aladin D, Cheung K, Ngan A, Chan D, Leung V, Lim C, Luk K, Lu W** *'Nanostructure of collagen fibrils in human nucleus pulposus and its correlation with macroscale tissue mechanics'* Journal of Orthapaedic Research (2010) – Vol. 28 Iss.4 pp.497-503
50. **Iatridis J, MacLean J, O'Brien M, Stokes I** '*Measurements of proteoglycan and water content distribution in human lumbar intervertebral discs'* Spine (2007); Vol.32 No.14 pp.1493-1497
51. **Kumar D, Gerges I, Tamplenizza M, Lenardi C, Forsyth N, Liu Y** '*Three-dimensional hypoxic culture of human mesenchymal stem cells encapsulated in a photocurable biodegradable polymer hydrogel: A potential injectable cellular product for nucleus pulposus regeneration*' Acta Biomater (2014); Vol.8 pp.3463-3474
52. **Guillaume O, Naqvi S, Lennon K, Buckley C** '*Enhancing cell migration in shape-memory alginate-collagen composite scaffolds: In vitro and ex vivo assessment for intervertebral disc repair*' J of Biomedical Applications (2014); DOI: 10.1177/0885328214557905
53. **Wang B, Sun C, Shao Z, Yang S, Che B, Wu Q, Liu J** '*Designer self-assembling peptide nanofibre scaffolds containing link protein N-terminal peptide induce chondrogenesis of rabbit bone marrow stromal cells*' BioMed Research International (2014); pp.1-11
54. **Ma K, Wu Y, Wang B, Yang S, Wei Y, Shao Z** *'Effect of a synthetic link N peptide nanofiber scaffold on the matrix deposition of aggrecan and type II collagen in rabbit notochordal cells'* J Mater Sci (2012); pp.1-11
55. **Wang B, Wu Y, Shao Z, Yang S, Che B, Sun C, Ma Z, Zhang Y** *'Functionalized self-assembling peptide nanofiber hydrogel as a scaffold for rabbit nucleus pulposus cells'* Journal of Biomedical Materials Research (2012); Vol.100 Iss.3 pp.643-653
56. **Stephan S, Johnson W, Roberts S** '*The influence of nutrient supply and cell density on the growth and survival of intervertebral disc cells in 3D culture*' European Cells and Materials (2011); Vol.22 pp.97-108
57. **Yamamoto Y, Mochida J, Sakai D, Nakai T, Nishimura K, Kawada H, Hotta *T*** *'Upregulation of the viability of nucleus pulposus cells by bone marrow-derived stromal cells'* Spine (2004); Vol.29 No.14 pp.1508-1515
58. **Sharp C, Roberts S, Evans H, Brown S** '*Disc cell clusters in pathological human intervertebral discs are associated with increased stress protein immunostaining*' Eur Spine J (2009); Vol.18 pp.1587-1594
59. **Kluba T, Niemeyer T, Gaissmaier C, Grunder T** '*Human annulus fibrosus and nucleus pulposus cells of the intervertebral disc'* Spine (2005); Vol.30 No.24 pp.2743-2748
60. **Johnson W, Eisenstein S, Roberts S** '*Cell cluster formation in degenerate lumbar intervertebral discs is associated with increased cell proliferation*' Connective Tissue Research (2001); Vol.42 pp.197-207
61. **Liu S, Tian Q, Hedrick J, Hui J, Ee P, Yang Y** *'Biomimetic hydrogels for chondrogenic differentiation of human mesenchymal stem cells to neocartilage*' Biomaterials (2010); Vol.31 pp.7298-7307
62. **Ludwinski F, Gnanalingham K, Richardson S, Hoyland J** '*Understanding the native nucleus pulposus cell phenotype has important implications for intervertebral disc regeneration strategies*' Regenerative Medicine (2013); Vol.8 pp.75-87
63. **Horner H, Roberts S, Bielby R, Menage J, Evans H, Urban J** '*Cells from different regions of the intervertebral disc'* Spine (2002); Vol.27 No.10 pp.1018-1028
64. **Rodrigues-Pinto R, Richardson S, Hoyland J** '*Identification of novel nucleus pulposus markers*' Bone Joint Res (2013); Vol.2 pp.169-178
65. **Minogue B, Richardson S, Zeef L, Freemont A, Hoyland J** '*Transcriptional profiling of bovine intervertebral disc cells: Implications for identification of normal and degenerate human intervertebral disc cell phenotypes*' Arthritis & Research (2010); Vol.12 pp.1-20
66. **Kollmer M, Keskar V, Hauk T, Collins J, Russell B, Gemeinhart R** '*Stem cell-derived extracellular matrix enables survival and multilineage differentiation within superporous hydrogels*' Biomacromolecules (2012); Vol.13 pp.963-973
67. **Melrose J, Smith S, Ghosh P** *'Assessment of the cellular heterogeneity of the ovine intervertebral disc: comparison with synovial fibroblasts and articular chondrocytes*' Eur Spine J (2003); Vol.12 pp.57-65
68. **Le Maitre C, Freemont A, Hoyland J** '*Expression of cartilage-derived morphogenetic protein in human intervertebral discs and its effect on matrix synthesis in degenerate human nucleus pulposus cells*' Arthritis Research & Therapy (2009); Vol.11 pp.1-10
69. **Calderon L, Collin E, Bayon D, Murphy M, O'Halloran D, Pandit A** '*Type II collagen-hyaluronan hydrogel – A step towards intervertebral disc tissue engineering*' Eur Cells & Materials (2010); Vol.20 pp.134-148

70. **Bucher C, Gazdhar A, Benneker L, Geiser T, Gantenbein-Ritter B** '*Nonviral gene delivery of growth and differentiation factor 5 to human mesenchymal stem cells injected into a 3D bovine intervertebral disc organ culture system*' Stem Cells (2013); pp.1-8
71. **Lefebvre V, Huang W, Harley V, Goodfellow P, de Crombrugghe B** '*SOX9 is a potent activator of the chondrocyte-specific enhancer of the pro alpha1 collagen gene*' Mol Cell Biol (1997); Vol.17 pp.2336-2346
72. **Zhao Q, Eberspaecher H, LeFebrve V, de Crombrugghe B** '*Parallel expression of SOX9 and COL2A1 in cells undergoing chondrogenesis*' Developmental Dynamics (1997); Vol.209 pp.377-386
73. **Gupta M, Nicoll S** '*Functional nucleus pulposus-like matrix assembly by human mesenchymal stromal cells is directed by macromer concentration in photocrosslinked carboxymethylcellulose hydrogels*' Cell Tissue Res (2014); Vol.358 pp.527-539
74. **Kim D, Martin J, Elliott D, Smith L, Mauck R** 'Phenotypic stability, matrix elaboration and functional maturation of nucleus pulposus cells encapsulated in photocrosslinkable hyaluronic acid hydrogels' Acta Biomaterialia (2015); Vol.12 pp.21-29
75. **Mwale F, Demers C, Petit A, Roughley P, Poole A, Steffen T, Aebi M, Antoniou J** '*A synthetic peptide of link protein stimulates the biosynthesis of collagens II, IX and proteoglycan by cells of the intervertebral disc*' J Chem Biochem (2003); Vol.88 pp.1202-1213
76. **Gilson A, Dreger M, Urban J** '*Differential expression level of cytokeratin 8 in cells of the bovine nucleus pulposus complicates the search for specific intervertebral disc cell markers*' Arthritis Research & Therapy (2010); Vol.12 pp.1-12
77. **Lv F, Leung V, Huang S, Huang Y, Sun Y, Cheung K** *'In search of nucleus pulposus-specific molecular markers*' Rheumatology (2013); pp.1-11
78. **Gotz W, Kasper M, Fischer G, Herken R '***Intermediate filament typing of the human embryonic and fetal notochord*' Cell & Tissue Research (1995); Vol.280 pp.455-462
79. **Hunter C, Matyas J, Duncan N** '*The notochordal cell in the nucleus pulposus: a review in the context of tissue engineering*' Tissue Engineering (2003); Vol.9 No.4 pp.667-677
80. **Minogue B, Richardson S, Zeef L, Freemont A, Hoyland J** '*Characterisation of the human nucleus pulposus cell phenotype and evaluation of novel marker gene expression to define adult stem cell differentiation*' Arthritis & Rheumatism (2010); Vol.62 pp.3695-3705
81. **Rutges J, Creemers L, Dhert W, Milz S, Sakai D, Mochida J, Alini M, Grad S** '*Variations in gene and protein expression in human nucleus pulposus in comparison with annulus fibrosus and cartilage cells: potential associations with aging and degeneration*' Osteoarthritis & Cartilage (2010); Vol.18 pp.416-423
82. **Omary M, Ku N, Liao J, Price D** '*Keratin modifications and solubility properties in epithelial cells and in vitro*' Sub-cellular Biochemistry (1998); Vol.31 pp.105-140
83. **Mahlapuu M, Pelto-Huikko M, Aitola M, Enerback S, Carlsson P** '*FREAC-1 contains a cell-type-specific transcriptional activation domain and is expressed in epithelial-mesenchymal interfaces*' Developmental Biology (1998); Vol.202 pp.183-195
84. **Malin D, Kim I, Boetticher E, Kalin T, Ramakrishna S, Meliton L, Ustiyan V, Zhu X, Kalinicheko V** '*Forkhead box F1 is essential for migration of mesenchymal cells and directly induces intergrin-beta3 expression*' Molecular Cell Biology (2007); Vol.27 pp.2486-2498
85. **Kalinichenko V, Zhou Y, Bhattacharyya D, Kim W, Shin B, Bambal K, Costa R** '*Haploinsufficiency of the mouse Forkhead Box f1 gene causes defects in gall bladder development'* J Biol Chem (2002); Vol.277 pp.12369-12374
86. **Power K, Grad S, Rutges J, Creemers L, van Rijen M, O'Gaora P, Wall J, Alini M, Pandit A, Gallagher W** '*Expression of Carbonic Anhydrase XII varies with age and degeneration*' Arthritis & Degeneration (2011); Vol.63 No.12 pp.3876-3886
87. **Singh K, Masuda K, Thonar E, Howard A, Szabo G** '*Age-related changes in the extracellular matrix of nucleus pulposus and annulus fibrosus of human intervertebral disc*' Spine (2009); Vol.34 pp.10-16
88. **Tao H, Zhang Y, Wang C, Zhang C, Wang X, Wang D, Bai X, Wen T, Xin H, Wu J, Liu Y, He Q, Ruan D** 'Biological evaluation of human degenerated nucleus pulposus cells in functionalised self-assembling peptide nanofibre hydrogel scaffold' Tissue Engineering (2014); Vol.20 pp.1621-1722
89. **Johnstone B, Hering T, Caplan A, Goldberg V, Yoo J** *'In vitro chondrogenesis of bone marrow – derived mesenchymal progenitor cells*' Exp Cell Res (1998); Vol.10 pp.265-272
90. **Mwale F, Roughley P, Antoniou J** '*Distinction between the extracellular matrix of the nucleus pulposus and hyaline cartilage: A requisite for tissue engineering of intervertebral disc*' European Cells and Materials (2004); Vol.8 pp.58-64
91. **Yuan M, Yeung C, Li Y, Diao H, Cheung K, Chan D, Cheah K, Chan P** *'Effects of nucleus pulposus cell-derived acellular matrix on the differentiation of mesenchymal stem cells*' Biomaterials (2013); Vol.34 pp.3948-3961

92. **Zhao X, Zhang S** '*Molecular designer self-assembling peptides*' Chemical Society Reviews (2006); Vol.35 pp.1105-1110
93. **Chou A, Reza A, Nicoll S** *'Distinct intervertebral disc cell populations adopt similar phenotype in three-dimensional culture'* Tissue Engineering (2008); Vol.14 No.12 pp.2079-2086
94. **Tremain N, Korkko J, Ibberson D, Kopen G, DiGirolamo C, Phinney D** '*MicroSAGE analysis of 2353 expressed genes in a single cell-derived colony of undifferentiated human mesenchymal stem cells reveals mRNAs of multiple cell lineages*' Stem Cells (2001); Vol.19 pp.408-418
95. **Mujeeb A, Miller A, Saiani A, Gough J** *'Self-assembled octapeptide scaffolds for in vitro chondrocyte culture'* Acta Biomaterialia (2012); Vol.9 Iss.1 pp.4609-4619
96. **Kubo Y, Kaidzu S, Nakajima I, Takenouchi K, Nakamura F** '*Organisation of extracellular matrix components during differentiation of adipocytes in long-term culture*' In Vitro Cell Dev Biol (1999); Vol.36 pp.38-44
97. **Yourek G, Hussain M, Mao J** '*Cytoskeletal changes of mesenchymal stem cells during differentiation'* Tissue Engineering (2007); pp.219-229
98. **Ballestrem C, Wehrle-Haller B, Imhof B** '*Actin dynamics in living mammalian cells*' J of Cell Science (1998); Vol.111 pp.1649-1658
99. **Johnson W, Roberts S** '*Human intervertebral disc morphology and cytoskeletal composition: a preliminary study of regional variations in health and disease*' J Anat (2003); Vol.203 pp.605-612
100. **Chen Y, Zhang Y, Zhang W, Luan G, Liu Z, Gao Y, Wan Z, Sun Z, Zhu S, Samartzis D, Wang C, H Wang, Luo Z** '*Insights into the hallmarks of human nucleus pulposus cells with particular reference to cell viability, phagocytic potential and long process formation*' Int J Med Sci (2013); Vol.10 pp.1805-1816
101. **Johnson W, Stephan S, Roberts S** *'The influence of serum, glucose and oxygen on intervertebral disc cell growth in vitro; Implications for degenerative disc disease*' Arthritis Research & Therapy (2008); Vol.10 pp.1-8
102. **Diaz L, Saiani A, Gough J, Miller A** '*Human osteoblasts within soft peptide hydrogels promote mineralisation in vitro*' J of Tissue Engineering (2014); Vol.5 pp.1-12
103. **Sztrolovics R, Alini M, Roughley P, Mort J** '*Aggrecan degradation in human intervertebral disc and articular cartilage*' Biochem J (1997); Vol.326 pp.235-241
104. **Luo W, Xiong W, Qiu M, Lv Y, Li Y, Li F** '*Differentiation of mesenchymal stem cells towards a nucleus pulposus-like phenotype utilizing simulated microgravity in vitro*' J Huazhong Univ Sci Technol (2011); Vol.31 No.2 pp.199-203
105. **Hegewald A, Enz A, Endres M, Sittinger M, Woiciechowsky C, Thome C, Kaps C** '*Engineering of polymer-based grafts with cells derived from human nucleus pulposus tissue of the lumbar spine*' J of Tissue Engineering and Regenerative Medicine (2011); Vol.5 pp.275-282
106. **Nesti L, Li W, Shanti R, Jiang Y, Jackson W, Freedman B, Kuklo T, Giuliana J, Tuan R** '*Intervertebral disc tissue engineering using a novel hyaluronic acid-nanofibrous scaffold amalgam*' Tissue Engineering (2008); Vol.14 No.9 pp.1527-1537

Chapter 7. *Conclusions & future work*

7.1. FUTURE WORK

There are a number of areas that further work should entail to progress research into the SAPH as a NP tissue engineering cell carrier and scaffold. Improving SAPH degradation rate and mechanically stability without significantly altering the mechanical properties would be an important area of research before *in vivo* work. Animal NPC (*chapter 5*) and human BMMSC (*chapter 6*) results strongly suggested that the current stiffness (*chapter 4*) was suitable for preserving NP phenotype and stimulating production of appropriate ECM components. It is possible that improved cell viability or higher ECM component production would occur with variations in SAPH mechanical properties however 30 mg ml^{-1} SAPHs most closely resembled the native tissue stiffness. Increasing the stability of the system would allow sufficient culture time for higher accumulation of ECM components and would likely improve SAPH structural stability after *in vivo* implantation.

From a cell biology standpoint, further research should include *in vitro* testing under hypoxic conditions to simulate the low oxygen environment of the native NP. There is evidence that hypoxic culture increases NP associated ECM production [1]. The native NP is subjected to constant loading therefore analysing the behaviour of encapsulated cells subjected to *in vivo* NP mechanical conditions would be worthwhile. Testing the culture of h-BMMSCs or h-AdMSCs from a variety of donors of different ages and sexes would allow better understanding of how MSCs behaved after SAPH encapsulation and determine whether results for *chapter 6* were reproducible. Further discussion into the limitations and future work of MSCs was reviewed in *section 6.8*.

Due to the promising initial *in vitro* results, after further testing with a larger pool of MSC donors under conditions designed to mimic the *in vivo* NP environment, animal studies would allow analysis of how the SAPH and encapsulated cells behaved *in vivo*.

7.2. CONCLUSION

Various natural and synthetic biomaterials have been investigated as cell carriers and scaffolds for NP tissue engineering (*tables 2.1 & 2.2*). The main challenges for potential NP scaffolds are replicating the native tissue mechanical properties *in vivo* [2], differentiating MSCs towards a discogenic phenotype [3, 4], preserving the NPC phenotype after encapsulation [5] and stimulating cellular production of appropriate ECM components to remodel the degenerated NP. Few studies have investigated both the rheological behaviour of systems and the behaviour of encapsulated cells in depth [6, 7]; typically either the material properties [2, 8] or cell culture aspect was focused on [9, 10]. Every study investigating MSCs as a NP tissue engineering cell source required a stimulating factor, whether it was addition of exogenous growth factors [1, 11] or functionalisation of the scaffold with a bioactive motif such as Link N protein [6, 12], to direct differentiation of MSCs towards a discogenic phenotype.

To the knowledge of the author this is the first study to investigate octapeptide SAPHs for NP tissue engineering applications and the first study to investigate the culture of NPCs and h-BMMSCs in octapeptide SAPHs. To date only one publication [11] has used GDF-6 as a discogenic induction factor for MSCs and only one publication has investigated the culture of MSCs in SAPHs for NP tissue engineering applications [6]. Therefore investigation into the mechanical properties of the SAPH as well as the culture of animal NPCs and human MSCs in the system for NP tissue engineering was determined to be novel.

For the system characterisation and optimisation work (*chapter 4*), FEFEFKFK SAPHs were demonstrated to form transparent self-supporting hydrogels simply by dissolving the peptide powder in *d*H_2O [13, 14]. SAPH gelation could be triggered by alterations in pH and ionic strength with stable hydrogels forming within minutes (*section 4.4*). It was established that by altering SAPH concentration and pH, the system could be optimised to closely replicate the native NP stiffness [2, 15] (*section 4.4.4*). Using AFM it was determined that SAPHs consisted of a nanofibrous network with the larger nanofibre assemblies closely resembling native NP type II collagen fibril diameter (*section 4.3.2*) [16]. It was hypothesised that the SAPH could potentially mimic the NP due to the comparable SAPH stiffness to the native tissue coupled with the nanofibre assemblies that resembled features of the NP ECM. A recovery cycle experiment, designed to replicate the injection process, demonstrated the shear thinning and self-healing properties of the SAPH (*section 4.5*) which confirmed that the system could be readily delivered into a degenerated NP via minimally invasive procedure.

For the investigation into the culture of animal cells (*chapter 5*), it was concluded that the FEFEFKFK SAPH could restore the NP phenotype following cellular de-differentiation as a result of monolayer culture. The NP phenotype was also preserved throughout *in vitro* culture. Cells displayed a rounded morphology and viability remained high (*section 5.3.2*). Gene expression profiles confirmed that encapsulated cells displayed a NP-like phenotype as high

expression of the 'traditional' NP markers (*ACAN* and *COL2A1*) (*section 5.5.1*) and upregulation of a number of 'novel' NP markers (*KRT8*, *KRT18* and *FOXF1*) (*section 5.5.2*) were recorded over the experimental period. Cell numbers remained stable throughout culture (*section 5.4*). Healthy native NPCs do not undergo significant proliferation as their main role is to remodel the matrix. Therefore it was hypothesised that, in terms of proliferation, cells cultured in SAPHs were behaving as they would in the native tissue. ICC micrographs visualised the increasing deposition of extracellular type II collagen (*section 5.6.2*) and aggrecan (*section 5.6.3*) with time point whilst s-GAG assay quantified that there was a time dependent significant increase in s-GAG production per cell (*section 5.7.2*). Ion exchange chromatography demonstrated that comparable to the native NP, mainly C-4-S and C-6-S were present in samples (*section 5.8*) with a small proportion of non-sulphated disaccharides. Results strongly supported the hypothesis that FEFEFKFK SAPH could act as an effective culture environment for NPCs.

For investigation into the culture of h-BMMSCs in FEFEFKFK SAPH (*chapter 6*), it was determined that GDF-6 induced h-BMMSCs to differentiate towards a NP-like phenotype. After encapsulation in the SAPHs, cell viability was high and cells adopted a rounded morphology (*section 6.3.2*). Population remained stable throughout *in vitro* culture (*figure 6.8*). Quantitative RT-PCR determined that 'traditional' NP markers were expressed (*COL2A1*, *ACAN*) although some genes were downregulated with timepoint (*section 6.5.1*). NP-specific markers (*KRT8*, *KRT18*, *KRT19*, *FOXF1* and *CA12*) were also expressed but similarly to *ACAN* and *SOX9*, *KRT19* and *CA12* were downregulated over culture period (*section 6.5.2*). The gene profiles did suggest that encapsulated cells had a NP-like phenotype however the downregulation of some NP marker genes was unexpected. It was possible that gene downregulation could have occurred after discogenic differentiation as a consequence of constant GDF-6 stimulation or due to the growth factor interacting with the SAPH architecture hindering its induction effect. Further investigation was required to better understand why GDF-6 was not stimulating NP gene expression as significantly in the SAPH as documented in the published literature [11]. ICC micrographs demonstrated intense extracellular staining for the two main NP associated ECM components of type II collagen and aggrecan (*section 6.6.2*). Sulphated-GAGs were accumulated in the SAPH however normalised results determined that there were no significant increases in s-GAG production per cell with time point (*figure 6.34*). Results suggested that the SAPH could maintain the culture of h-BMMSCs after discogenic differentiation however the downregulation of some NPC marker genes and the low ECM accumulation needed to be addressed and further investigated.

Similarly to GDF-6 stimulated samples and animal NPC samples, cells cultured in SAPHs in absence of GDF-6 adopted a rounded morphology, maintained high viability throughout culture (*section 6.3.1*) and the overall population remained stable (*figure 6.6*). Gene expression profiles demonstrated that a significant increase in gene expression for the 'traditional' NP marker *ACAN* (*figure 6.11*) and significant increases in gene expression for the

NP-specific markers of *KRT8*, *KRT18* and *FOXF1* with *in vitro* culture period were recorded. The novel NP markers of *KRT19* and *CA12* were also expressed (*section 6.5.2*). ICC (*section 6.6.1*) determined that extracellular type II collagen and aggrecan were being deposited by cells without growth factor stimulation. Sulphated-GAGs were accumulated in the SAPH (*section 6.7.3*) however, comparable to GDF-6 stimulated samples; normalised results determined that there were no significant increases in s-GAG production per cell with culture period. The gene expression profiles of encapsulated cells coupled with the morphology, stable population and type of ECM components deposited strongly suggested that a discogenic phenotype was present without use of exogenous growth factor stimulation. The hypothesis was that as the SAPH was optimised to have comparable mechanical properties to the native tissue, displayed high osmolarity and had nanofibrous assemblies of the similar scale to type II collagen fibrils in the NP it was possible that the system was replicating the NP microenvironment and inducing differentiation. It has been documented that an appropriate stem cell niche could direct differentiation towards a specific cell lineage whether by replicating mechanical properties [12, 17] or presenting appropriate ECM components [18, 19]. Therefore if the SAPH was mimicking the native NP environment, it is conceivable that the system induced discogenic differentiation of h-BMMSCs.

The overall take home message was that FEFEFKFK SAPH holds great potential for use as a scaffold and cell carrier for NP tissue engineering applications. This study produced useful information that acted as important groundwork for further investigation. The most exciting and novel finding was that unlike all other NP tissue engineering studies, it appeared that an exogenous differentiation factor was not required to induce a NP-like phenotype from MSCs after culture in SAPHs.

7.3. REFERENCES

1. **Stoyanov J, Gantenbein-Ritter B, Bertolo A, Aebli N, Baur M, Alini M, Grad S** '*Role of hypoxia and growth and differentiation factor-5 on differentiation of human mesenchymal stem cells towards intervertebral nucleus pulposus-like cells'* European Cells and Materials (2011); Vol. 21 pp.533-547
2. **Cloyd J, Malhotra N, Weng L, Chen W, Mauck R, Elliot D** '*Material properties in unconfined compression of human nucleus pulposus, injectable hyaluronic acid-based hydrogels and tissue engineering scaffolds*' Eur Spine J (2007); Vol.16 pp.1892
3. **Gilbert H, Hoyland J, Richardson S** '*Stem cell regeneration of degenerated intervertebral discs: Current status*' Curr Pain Headache Rep (2013); Vol.17 pp.1-9
4. **Gilbert H, Hoyland J, Richardson S** '*Stem cell regeneration of degenerated intervertebral discs: Current status*' Curr Pain Headache Rep (2013); Vol.17 pp.1-9
5. **Kandel R, Roberts S, Urban J** '*Tissue engineering and the intervertebral disc: the challenges*' Eur Spine J (2008); Vol.17 pp.480-491
6. **Wang B, Sun C, Shao Z, Yang S, Che B, Wu Q, Liu J** '*Designer self-assembling peptide nanofibre scaffolds containing link protein N-terminal peptide induce chondrogenesis of rabbit bone marrow stromal cells*' BioMed Research International (2014); pp.1-11
7. **Kim D, Martin J, Elliott D, Smith L, Mauck R** 'Phenotypic stability, matrix elaboration and functional maturation of nucleus pulposus cells encapsulated in photocrosslinkable hyaluronic acid hydrogels' Acta Biomaterialia (2015); Vol.12 pp.21-29
8. **Fraylich M, Liu R, Richardson S, Baird P, Hoyland J, Freemont A, Alexander C, Shaesheff K, Cellesi F, Saunders B** *'Thermally-triggered gelation of PLGA dispersions: Towards an injectable colloidal cell delivery system'* Journal of Colloid and Interface Science (2010) – Iss.344 pp.61-69
9. **Sun J, Zheng Q, Wu Y, Liu Y, Guo X, Wu W** *'Culture of nucleus pulposus cells from intervertebral disc on self-assembling KLD 12 peptide hydrogel scaffold'* Materials Science and Engineering (2010); Vol.30 pp975-980
10. **Tao H, Zhang Y, Wang C, Zhang C, Wang X, Wang D, Bai X, Wen T, Xin H, Wu J, Liu Y, He Q, Ruan D** 'Biological evaluation of human degenerated nucleus pulposus cells in functionalised self-assembling peptide nanofibre hydrogel scaffold' Tissue Engineering (2014); Vol.20 pp.1621-1722
11. **Clarke L, McConnell J, Sherratt M, Derby B, Richardson S, Hoyland J** *'Growth differentiation factor 6 and transforming growth factor-beta differentially mediate mesenchymal stem cell differentiation, composition, and micromechanical properties of nucleus pulposus constructs'* Arthritis & Research (2014); Vol.16 pp.1-13
12. **Frith J, Cameron A, Menzies D, Ghosh P, Whitehead D, Gronthos S, Zannettino A, White J** '*An injectable hydrogel incorporating mesenchymal precursor cells and pentosan polysulphate for intervertebral disc regeneration'* Biomaterials (2013); Vol.34 pp.9430-9440
13. **Mujeeb A, Miller A, Saiani A, Gough J** *'Self-assembled octapeptide scaffolds for in vitro chondrocyte culture'* Acta Biomaterialia (2012); Vol.9 Iss.1 pp.4609-4619
14. **Diaz L, Saiani A, Gough J, Miller A** '*Human osteoblasts within soft peptide hydrogels promote mineralisation in vitro*' J of Tissue Engineering (2014); Vol.5 pp.1-12
15. **Iatridis J, Setton L, Weidenbaum M, Mow V** '*The viscoelastic behaviour of the non-degenerate human lumbar nucleus pulposus in shear'* J Biomechanics (1997); Vol.30 No.10 pp.1005-1013
16. **Aladin D, Cheung K, Ngan A, Chan D, Leung V, Lim C, Luk K, Lu W** *'Nanostructure of collagen fibrils in human nucleus pulposus and its correlation with macroscale tissue mechanics'* Journal of Orthapaedic Research (2010) – Vol. 28 Iss.4 pp.497-503
17. **Engler A, Sen S, Sweeney H, Discher D** '*Matrix elasticity directs stem cell lineage specification'* Cell (2006); Vol.126 pp.677-689
18. **Yuan M, Yeung C, Li Y, Diao H, Cheung K, Chan D, Cheah K, Chan P** *'Effects of nucleus pulposus cell-derived acellular matrix on the differentiation of mesenchymal stem cells*' Biomaterials (2013); Vol.34 pp.3948-3961
19. **Shoukry M, Li J, Pei M** '*Reconstruction of an in vitro niche for the transition from intervertebral disc development to nucleus pulposus regeneration*' Stem Cells & Development (2013); Vol.22 No.8 pp.1-13

Chapter 8. *Appendix*

8.1. MATERIALS & METHODS

8.1.1. CytoTox 96® Cytotoxicity assay

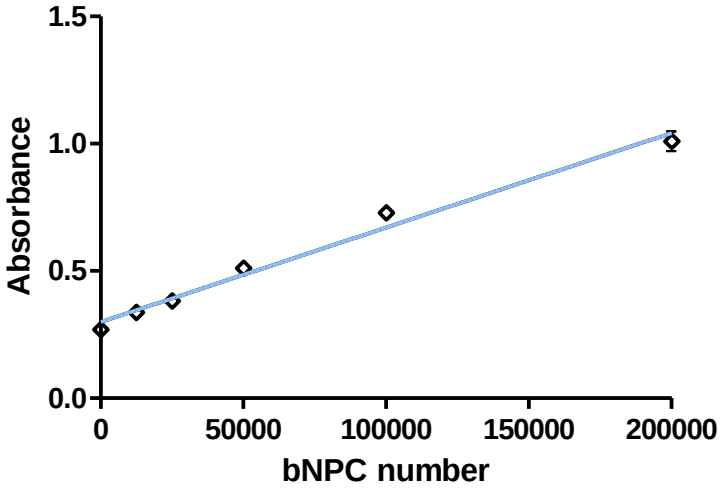

Figure 8.1. Standard curve plotting known bNPC number against absorbance (filter 450) following CytoTox 96® Cytotoxicity assay. Values expressed as mean±SD where n=4.

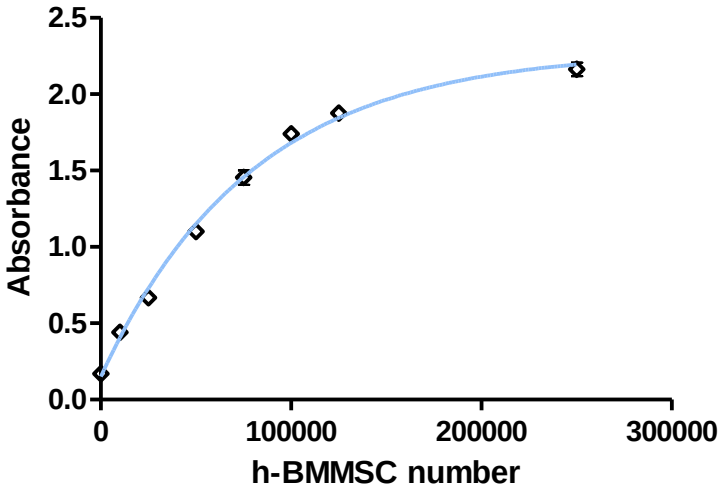

Figure 8.2. Standard curve plotting known h-BMMSC number against absorbance (filter 450) following CytoTox 96® Cytotoxicity assay. Values expressed as mean±SD where n=4.

8.1.2. Quant-iT™ PicoGreen® dsDNA assay

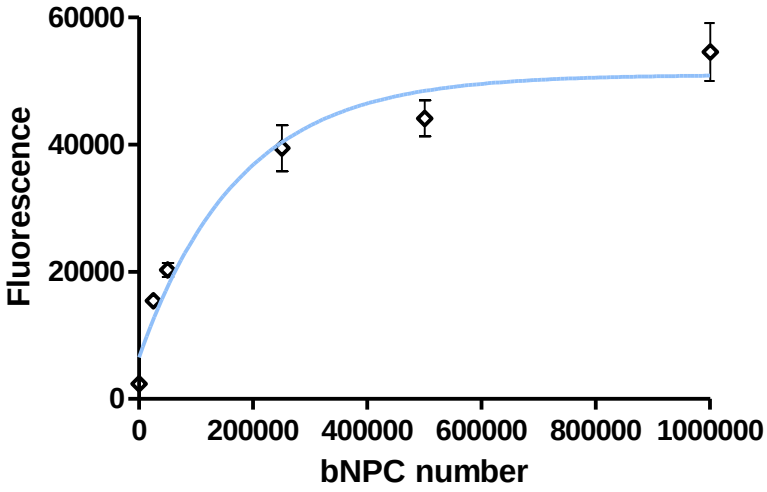

Figure 8.3. Standard curve plotting known bNPC number against fluorescence (filter 70, 485 nm excitation, 538 nm emission wavelength) following PicoGreen dsDNA assay. Values expressed as mean±SD where n=4.

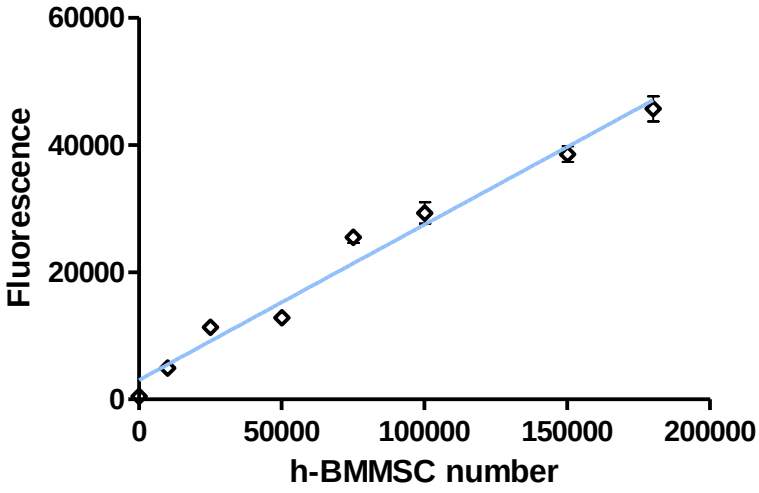

Figure 8.4. Standard curve plotting known h-BMMSC number against fluorescence (filter 70, 485 nm excitation, 538 nm emission wavelength) following PicoGreen dsDNA assay. Values expressed as mean±SD where n=4.

8.1.3. Blyscan™ sulphated glycosaminoglycan assay

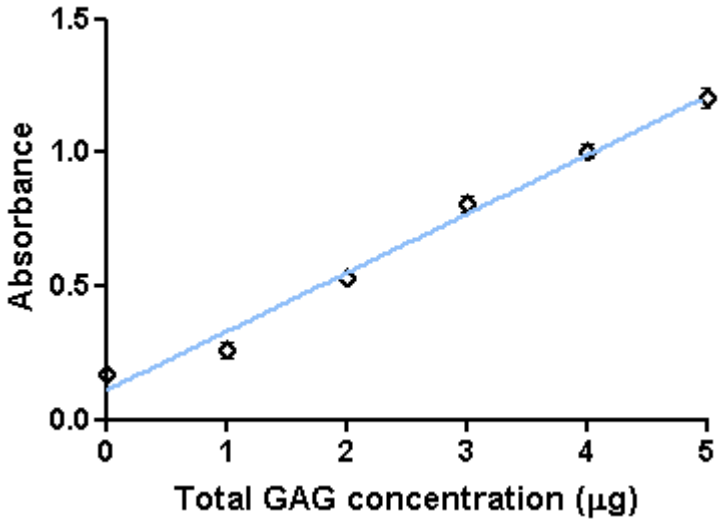

Figure 8.5. Calibration curve plotting known s-GAG concentrations against absorbance at 650nm. Values expressed as mean±SD where n=4.

8.2. CHARACTERISATION

8.2.1. Oscillatory rheology

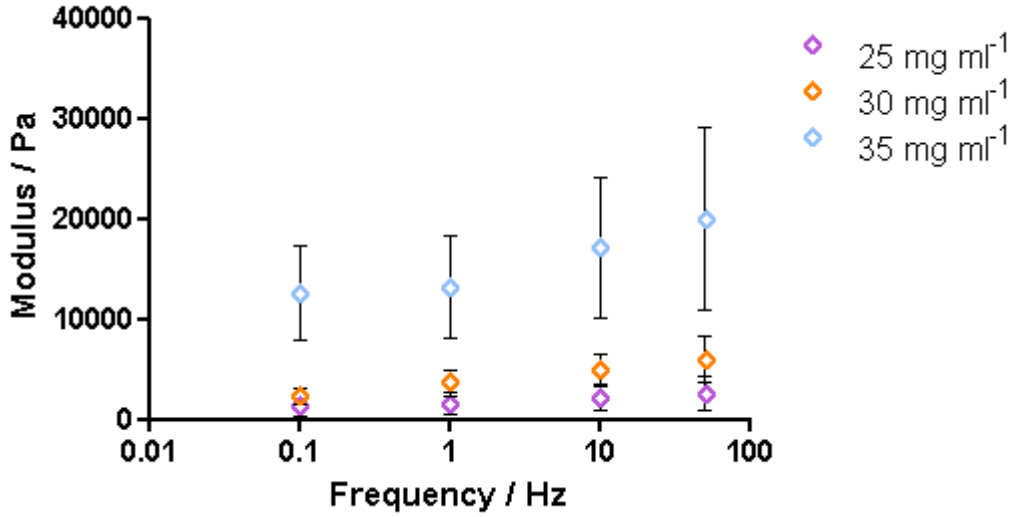

Figure 8.6. Frequency sweep G' values for various FEFEFKFK SAPH concentrations with $2x10^5$ bNPCs ml^{-1}. 25 mg ml^{-1}, 30 mg ml^{-1} and 35 mg ml^{-1} concentrations were tested. SAPHs were at a pH of 9.4 but following addition of cell suspension and media washes, the pH of the sample was reduced to the physiologically relevant pH 7.4. Values expressed as mean±SD where n=3.

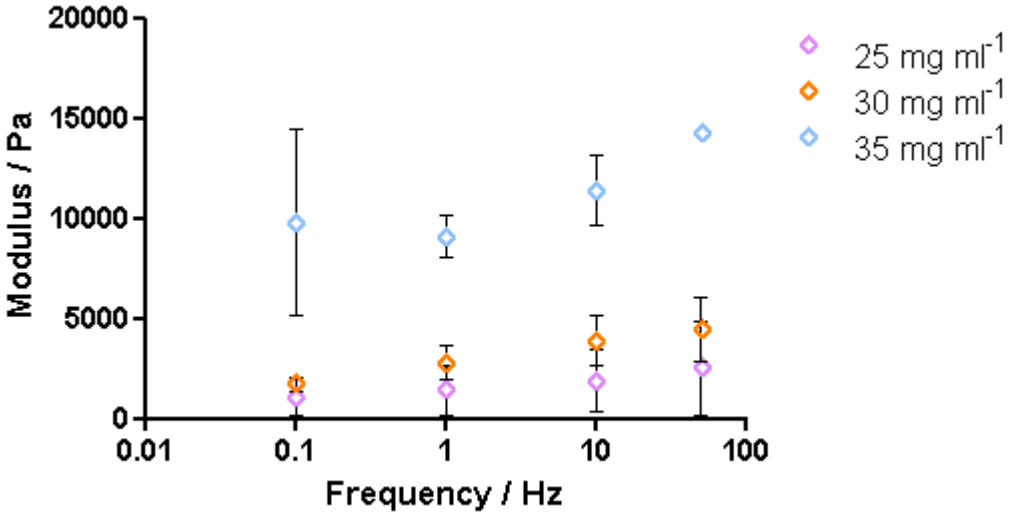

Figure 8.7. Frequency sweep G' values for various acellular FEFEFKFK SAPHs. 25 mg ml^{-1}, 30 mg ml^{-1} and 35 mg ml^{-1} concentrations were tested. SAPHs were at a pH of 9.4 but following addition of cell suspension and media washes, the pH of the sample was reduced to the physiologically relevant pH 7.4. Values expressed as mean±SD where n=3.

8.3. THE CULTURE OF BOVINE NUCLEUS PULPOSUS CELLS IN SAPHs

8.3.1. Cell viability

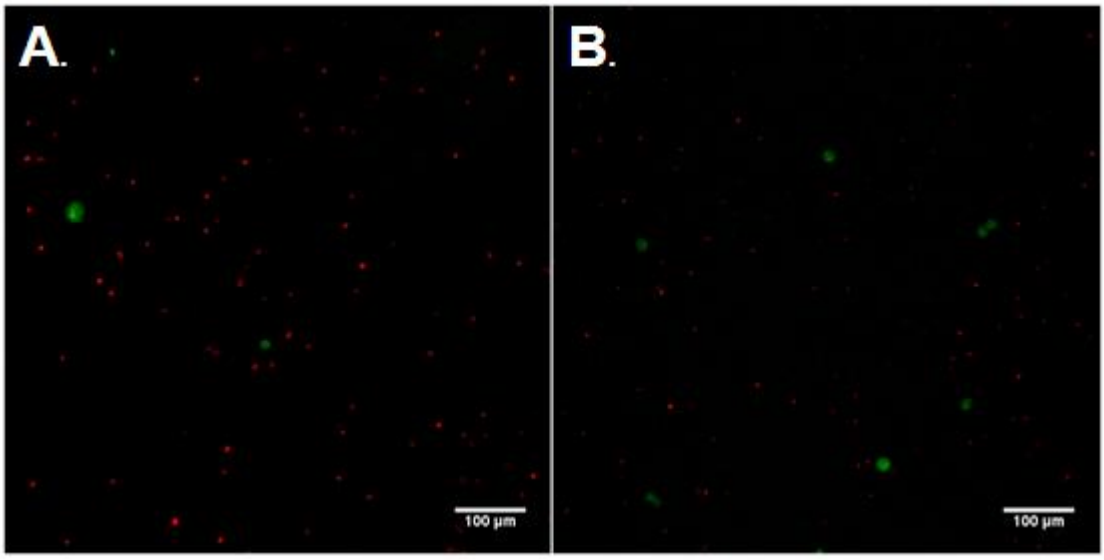

Figure 8.8. Fluorescence micrographs demonstrating cell viability of 2x10^{5} bNPCs ml^{-1} in FEFEFKFK SAPHs at 30 mg ml^{-1} after no media washes on [A] day 3 and [B] day 7. There was a majority dead cells present. Scale bar represents 100 µm.

8.3.2. LDH assay

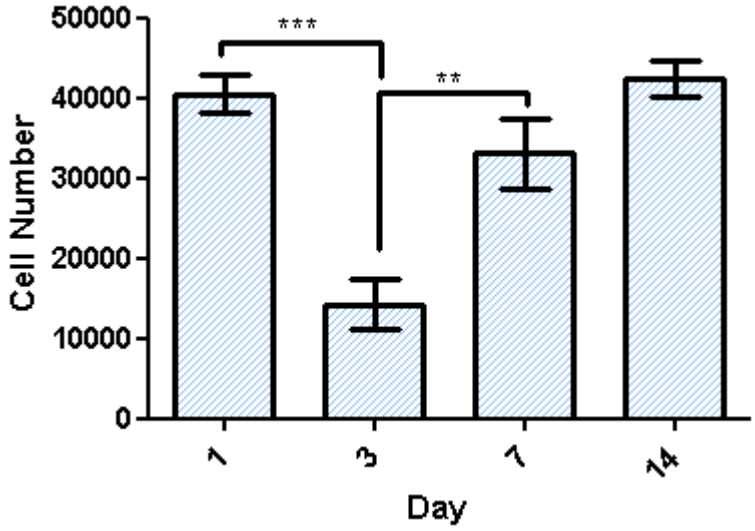

Figure 8.9. Cell numbers over 14 days *in vitro* culture for 2x10^5 bNPC ml^{-1} in 30 mg ml^{-1} FEFEFKFK SAPH. There was significant decrease in cell number from days 1 to 3 (*P<0.001) then an increase in cell numbers from days 3 to 7 (**P<0.01). Values expressed as mean±SD where n=4.**

8.3.3. DMMB assay

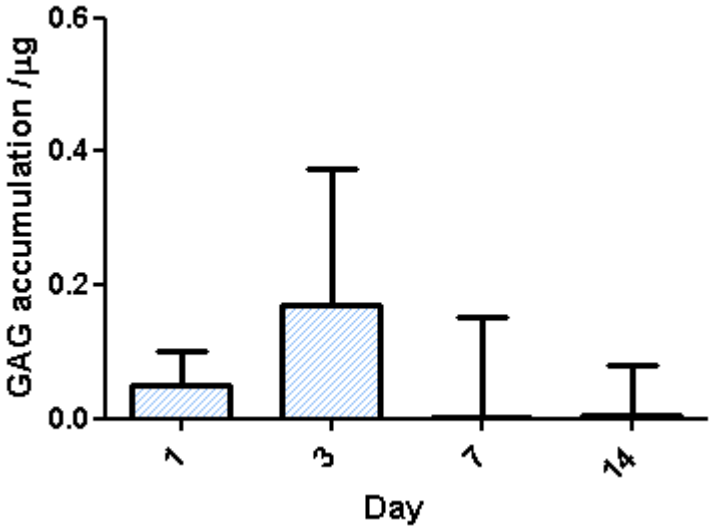

Figure 8.10. The total s-GAG released into media for 1.5x10^6 bNPC ml^{-1} in 30 mg ml^{-1} FEFEFKFK SAPHs. s-GAG accumulation was calculated from a standard graph plotting absorbance against standard s-GAG concentrations. (P>0.05). There was no significant difference comparing days 1 and 14 (P>0.05). Values expressed as mean±SD where n=4.

8.4. THE CULTURE OF HUMAN MESENCHYMAL BONE MARROW STEM CELLS IN SAPHs

8.4.1. DMMB assay

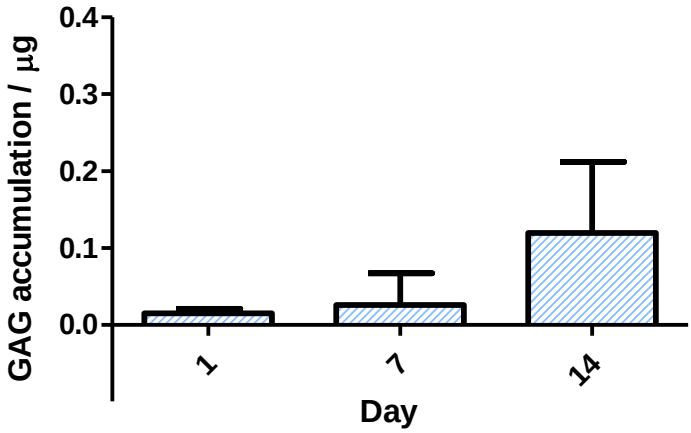

Figure 8.11. The total s-GAG released into the media for 1x10^6 h-BMMSCs ml^{-1} in 30 mg ml^{-1} FEFEFKFK SAPHs without stimulation. There was no significant differences in total s-GAG between culture conditions on any time point (P>0.05). Values expressed as mean±SD where n=4.

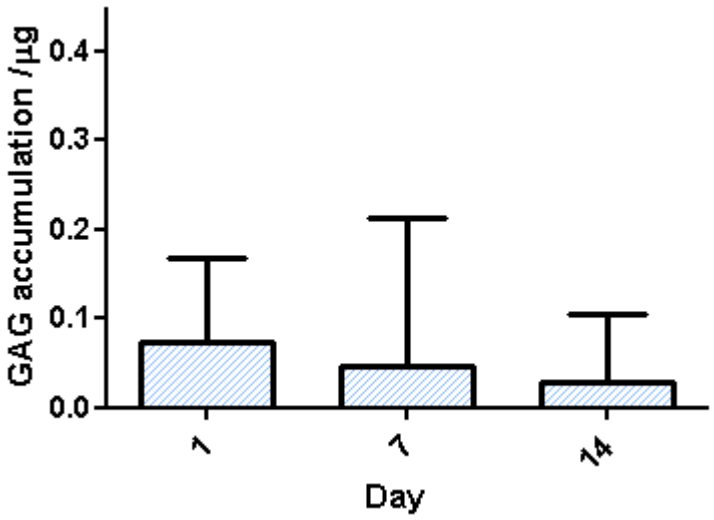

Figure 8.12. The total s-GAG released into the media for 1x10^6 h-BMMSCs ml^{-1} in 30 mg ml^{-1} FEFEFKFK SAPHs with and without 100 ng ml^{-1} GDF-6 stimulation. There was no significant differences in total s-GAG between culture conditions on any time point (P>0.05). Values expressed as mean±SD where n=4.